9950-297

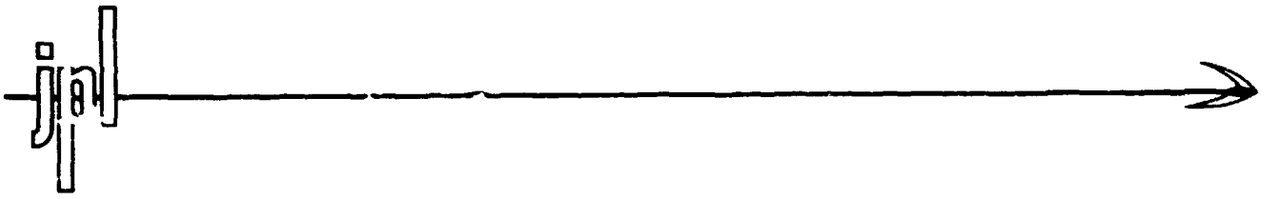

(NASA-CR-162870) AN ANALYTICAL STUDY OF ELECTRIC VEHICLE HANDLING DYNAMICS Final Report (MSA Research Corp.) 223 p
HC A10/MF A01 CSCL 13F G3/85

N80-23217
Unclas
19281

JET PROPULSION LABORATORY
CALIFORNIA INSTITUTE OF TECHNOLOGY
PASADENA, CALIFORNIA

JPL NO. 9950 – 297

MGA RESEARCH CORPORATION
Cambridge Square Building, 4245 Union Road
Buffalo, New York 14225 (716) 634-6950

AN ANALYTICAL STUDY OF ELECTRIC VEHICLE HANDLING DYNAMICS

BY
J. E. Greene and D. J. Segal

May 1979

FINAL REPORT

JPL Contract No. 955312
MGA Project No. G8-C06

This work was performed for the Jet Propulsion Laboratory, California Institute of Technology, sponsored by the National Aeronautics and Space Administration under Contract No. NAS7-100.

This report contains information prepared by MGA Research Corporation under JPL sub-contract. Its content is not necessarily endorsed by the Jet Propulsion Laboratory, California Institute of Technology, or the National Aeronautics and Space Administration.

ABSTRACT

Handling characteristics of hypothetical electric vehicle configurations were studied by applying available analytical methods. Elementary linearized models were used in addition to a highly sophisticated vehicle dynamics computer simulation technique. Physical properties of specific EV's were defined for various battery and powertrain packaging approaches applied to a subcompact base car. The group of configurations considered gave a wide range of weight distribution and inertial properties which characterize a generic class of EV's. Computer simulations of structured maneuvers were performed for predicting handling qualities in the normal driving range and during various extreme conditions related to accident avoidance. Results consistently indicate that an EV with forward weight bias will possess handling qualities superior to a comparable EV that is rear-heavy or equally balanced; the handling differences become more pronounced as yaw moment of inertia is increased. Rear-heavy EV's were found to be particularly susceptible to excessive sideslip, long response times and undesirable phase lags. Results also demonstrate the importance of properly matching tires, suspension systems and brake system front/rear torque proportioning to a given EV configuration during the design stage. The methodology employed in this study can provide valuable guidance for developing electric (and other) vehicles which have satisfactory handling qualities.

ACKNOWLEDGEMENTS

The authors gratefully acknowledge important technical contributions of several individuals. Mr. N. Balasubramanian, Assistant Mechanical Engineer, MGA Research Corporation, participated in nearly all aspects of the study and provided major assistance in software development, linear theory application and computer simulation. Mr. William F. Milliken, Jr., President, Milliken Research Associates, Inc., served as a technical consultant mainly in the areas of vehicle parameter deformation and handling performance evaluation. Inertial measurements of actual vehicles were performed by Dynamic Science, Inc., under the direction of Mr. Carroll Thatcher, Manager, Systems Measurement Department.

Mr. Herbert Fortgang was JPL's Technical Manager. We wish to especially thank Mr. Fortgang for his valuable technical guidance and enthusiastic interest in the project.

GLOSSARY

a_s	-	Portion of wheelbase from front axle to the longitudinal location of the sprung mass center of gravity
a_T	-	Portion of wheelbase from front axle to the longitudinal location of the total vehicle center of gravity
a_y	-	Lateral acceleration referenced to sprung mass center of gravity
b_s	-	Portion of wheelbase from rear axle to the longitudinal location of the sprung mass center of gravity
b_T	-	Portion of wheelbase from rear axle to the longitudinal location of the total vehicle center of gravity
C_α		Cornering stiffness, i.e., lateral force generated by a tire (or pair of tires) per unit slip angle
g	-	Gravitational constant (32.2 ft/sec^2)
h	-	Static margin, i.e., longitudinal location of resultant side force vector with respect to sprung mass c.g. for vehicle in steady-state turn
h_{cgs}	-	Vertical height above ground of sprung mass center of gravity
h_{cgT}	-	Vertical height above ground of total vehicle center of gravity
I_{xs}	-	Roll moment of inertia of sprung mass about c.g.
I_{xT}	-	Roll moment of inertia of total vehicle about c.g.
I_{ys}	-	Pitch moment of inertia of sprung mass about c.g.
I_{yT}	-	Pitch moment of inertia of total vehicle about c.g.

Note: For more complete and rigorous definitions, consult "Vehicle Dynamics Terminology," SAE J670e, Society of Automotive Engineers, June 1978.

I_{zs}	-	Yaw moment of inertia of sprung mass about c.g.
I_{zT}	-	Yaw moment of inertia of total vehicle about c.g.
I_{xzs}	-	Roll-yaw product of inertia of the sprung mass about its c.g.
ℓ	-	Wheelbase
R	-	Radius of path curvature
r	-	Yaw Rate (velocity)
V	-	Resultant speed of vehicle
W_s	-	Weight of sprung mass
W_T	-	Total weight of vehicle
x	-	Longitudinal axis of vehicle sprung mass
y	-	Lateral (transverse) axis of vehicle sprung mass
z	-	Vertical axis of vehicle sprung mass
α	-	Tire slip angle
β	-	Vehicle slip angle, i.e., angle between longitudinal axis and velocity vector
δ	-	Front wheel reference (input) steer angle, i.e., steering wheel angle divided by gearbox ratio
σ	-	Front wheel input steer angle normalized to a 10 ft. wheelbase (equal Ackermen angles)
ϕ	-	Roll angle of sprung mass with respect to ground-fixed axes
θ	-	Pitch angle of sprung mass with respect to ground-fixed axes
ψ	-	Yaw angle of sprung mass with respect to ground-fixed axes

TABLE OF CONTENTS

LIST OF FIGURES

LIST OF FIGURES (CONTD.)

LIST OF FIGURES (CONTD.)

LIST OF FIGURES (CONTD.)

LIST OF TABLES

1. INTRODUCTION

The objective of this study was to evaluate, through the use of a computer simulation program, the dynamic handling characteristics of a class of battery-powered passenger cars. Various battery packaging and driveline layout approaches were considered as possible derivatives of a subcompact base vehicle, which gave a wide range of mass distribution and inertia properties for analytical investigation. Results of this study are intended to provide information to electric vehicle designers and manufacturers on how battery placement and vehicle packaging can affect important physical properties of a vehicle (principally the weight distribution and yaw moment of inertia) and the resulting effects on handling qualities.

It is important to realize that vehicle handling qualities are largely subjective and qualitative in nature, and very little information exists which can be applied to determine whether a given vehicle handles "good" or "bad", except in a gross sense. Production passenger cars exhibit a wide range of dynamic characteristics, and the development of a vehicle requires many design compromises which include handling as one of many aspects of automotive engineering which must be addressed. Design and development of cars with consumer acceptable and "safe" handling properties is an art as well as a science.

With this in mind, we have approached the study by considering the predicted dynamic characteristics of hypothetical electric vehicle configurations relative to the corresponding characteristics of the selected base car--a 1979 Chevrolet Chevette. This production car certainly possesses reasonable handling qualities which are suitable for the general public and consistent with the control abilities and expectations of the "average" driver; but, it would not be expected to possess the ultimate in handling performance, if indeed such a vehicle is possible or definable. Nevertheless, tendencies produced by large changes in vehicle properties (when adding batteries and alternative drivetrain layouts) can be identified as generally helpful or

detrimental in most instances, and these trends are what we have endeavored to explore.

Electric vehicle handling has been largely ignored as a subject of research in the past mainly because other challenging problems must be overcome before introduction of large numbers of electric cars to the marketplace becomes a reality. The fundamental problem, of course, relates to battery energy density and the achievement of reasonable driving range without excessive onboard battery mass. However, one needs only to experience the ride and handling characteristics of many EV prototypes in existence to appreciate the importance of parallel research directed toward these engineering aspects of alternative-fueled passenger cars.

We view this study as an initial attempt to isolate some of the performance characteristics which can be adversely affected by the addition of batteries and correspondingly high moments of inertia applied to a passenger car with conventional chassis design and dimensions of the subcompact class, i.e., cars with a wheelbase in the neighborhood of 90-100 inches. We will deal with handling behavior in both the linear range (normal driving activity with lateral acceleration remaining below about 0.5 g) and the range of limit performance where tire side force capacity can be reached.

Linear range performance deals mainly with directional response to small steer angle changes characterized by lateral acceleration control gain and yaw velocity control gain and the sensitivities of other parameters such as sideslip angle and roll angle of the vehicle body to the magnitude of lateral acceleration. Linear performance theory will be reviewed in the Technical Discussion. Handling performance in this regime can be studied and evaluated somewhat more quantitatively than limit performance since guidelines are generally known for "acceptable" handling qualities in the "normal" driving regime of production cars.

Limit performance deals with stability and control in drastic maneuvers mainly related to accident avoidance. Examples are rapid lane

changes, sudden turning to evade an impending collision situation, and hard braking while negotiating a turn. Criteria for evaluating how well a vehicle handles in these kinds of situations relate to how quickly the intended maneuver can be performed, and if reasonable stability and control responsiveness exist during and immediately following the maneuver. Although some quantitative ways of evaluating vehicle handling and stability have b developed (primarily by the National Highway Traffic Safety Administration), this aspect of vehicle dynamics remains in an infant state and must be treated mainly in a subjective manner.

It should also be pointed out that performance in the linear range is, for the most part, limited to steady-state response, and moments of inertia therefore do not play a direct role in the vehicle's behavior; weight distribution and how well the suspension systems and tires are matched to physical properties of the vehicle are of prime importance in this regime. Moments of inertia become important when considering transient response, for instance in the limit maneuvers previously mentioned. But, mass distribution and moments of inertia are inter-related and we are in essence addressing the overall effects of mass (inertia) throughout this study.

In the following Technical Discussion, the electric vehicle packaging configurations are described which were selected for providing a range of physical properties for computer evaluation. The derivation procedure for obtaining these properti (necessary for input to the computer simulation) is also discussed and the resulting parameters are presented. This is followed by a review of linear handling theory. We then describe the specific maneuvers which were simulated with the computer model (HVOSM). Simulation results are then presented and evaluated, and conclusions and recommendations are summarized.

Appendices contain a brief overview of the Highway-Vehicle-Object Simulation Model (HVOSM) computer model, results of actual physical measurements made on three vehicles, a detailed list of computer program input parameters

for the base vehicle, and sample output plots for each of the general types of simulated maneuvers. Since approximately 200 computer simulations were performed within this study, the large amount of resulting information precludes complete documentation within this report; only the more important information is presented.

2. TECHNICAL DISCUSSION

This section presents technical results of the overall study. It is divided into nine sub-sections. The first describes specific electric vehicle configurations which were selected for analysis. This is followed by a review of how physical properties were developed to mathematically describe the EV's in a form required for the computer program input. We then give an overview of vehicle handling evaluation based on a linearized mathematical model; this gives an introduction to vehicle dynamics theory before discussing the computer simulation study (which treats significant non-linear vehicle properties). Next, the handling maneuvers that were simulated by the computer model are defined, i.e., trapezoidal steer, sinusoidal steer and braking-in-a-turn maneuvers. Results of these three simulated maneuvers are then presented for the base vehicle and EV configurations. The more significant results related to effects of weight distribution and yaw moment of inertia are then discussed. Finally, a brief exploratory study is described which was performed to give some preliminary insight as to how modification of suspension and tire properties can affect (and perhaps improve) handling performance.

2.1 Electric Vehicle Configurations

The first step in defining a group of electric vehicle configurations for this study was to select a reasonable base vehicle which could theoretically be converted to battery power. The base vehicle was to be in the subcompact size class with a curb weight of about 2000 lbs. A 1979 Chevrolet Chevette 2-door model was chosen as the base car because it met the size requirement, contains sufficient space for battery placement in the front and rear body areas, and information was available for mathematically representing most of the physical properties needed for the computer simulation program. Some published characteristics of the base car are listed below:

Curb Weight	-	2029 lbs.
Overall Length	-	159.7 in.
Overall Width	-	61.8 in.

Overall Height	-	52.3 in.
Wheelbase	-	94.3 in.
Track Width	-	51.2 in.

Measurements were made to define areas in the engine compartment and the luggage space behind the rear seat which could be used for battery and powerplant placements without requiring major body and chassis redesign. The intent was to indicate general available areas, but not to the extent of actually designing practical packaging layouts. Several hypothetical packaging schemes were then selected to provide a broad range of potential mass distribution and inertial properties for this size car conceptually converted to electric drive. The resulting configurations are described in the following paragraphs.

Conventional Drive, 50/50 Battery Split Over Axles

A front motor, rear drive configuration was packaged in the base car with 18 motive batteries equally split between the front and rear of the vehicle as shown in Figure 1(a), a plan view giving nominal dimensions. The front group of 9 batteries were centrally located over the front axle. The rear battery pack was positioned so as not to intrude into the rear seat area but as close to the rear axle as possible, given the available space. A side view of this electric drive system packaged in the base car, including the motor location, is given in Figure 2. Note that the individual batteries are 10.3" long, 7.0" wide and 10.3" high, approximately the size of the batteries used in the GE/Chrysler and AiResearch electric vehicle prototypes, which also contain 18 batteries.

Conventional Drive, 50/50 Battery Split, 10" Outboard

This configuration is the same as above except that the battery packs are moved 10" outboard, i.e., the front batteries are repositioned 10" forward and the rear batteries 10" rearward. This results in a larger yaw moment of inertia for the same battery mass, with the batteries located near the outermost boundaries of the available packaging areas as shown in Figure 3.

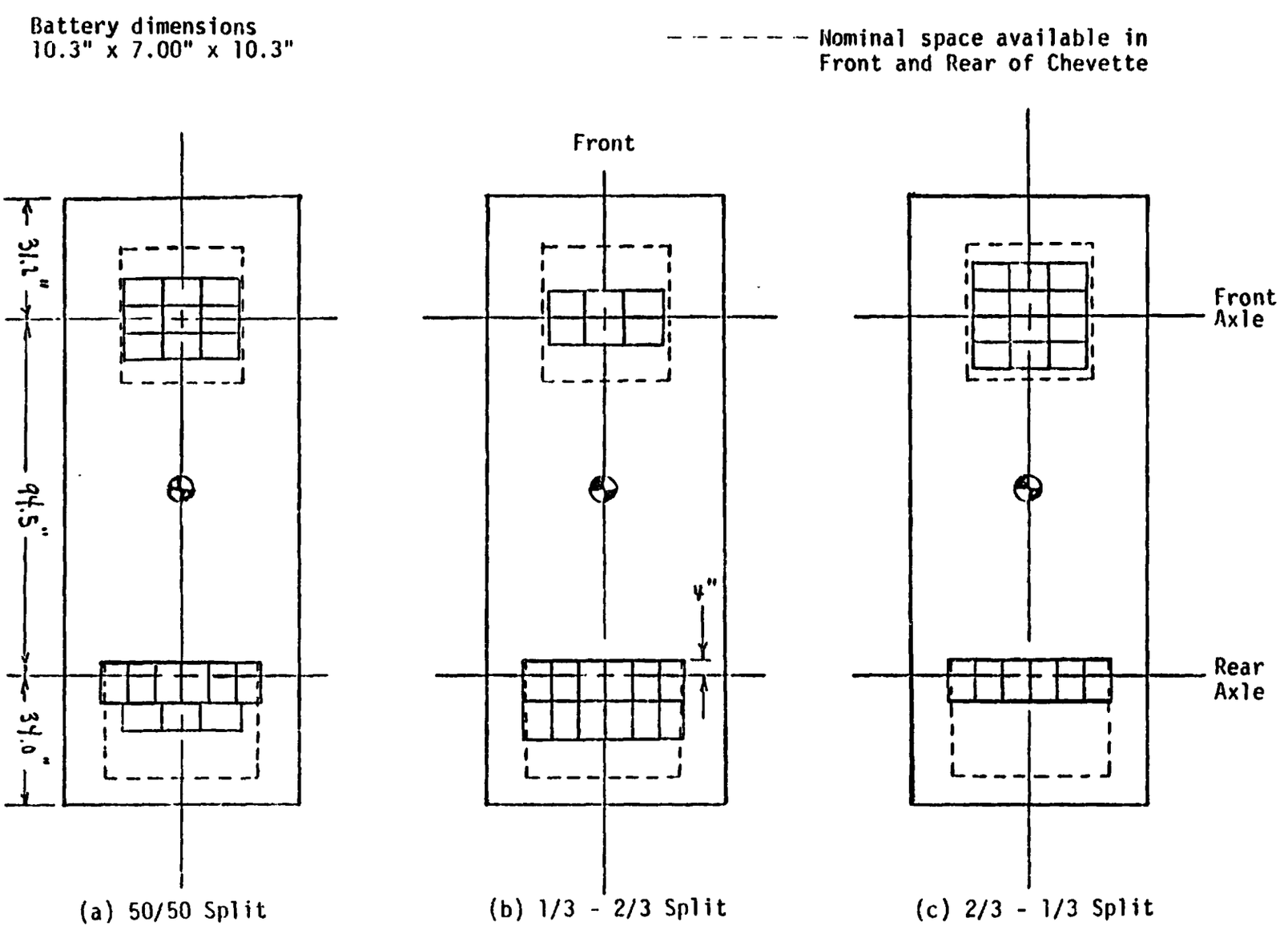

Figure 1 BATTERY PACKAGING IN CHEVETTE OVER THE AXLES

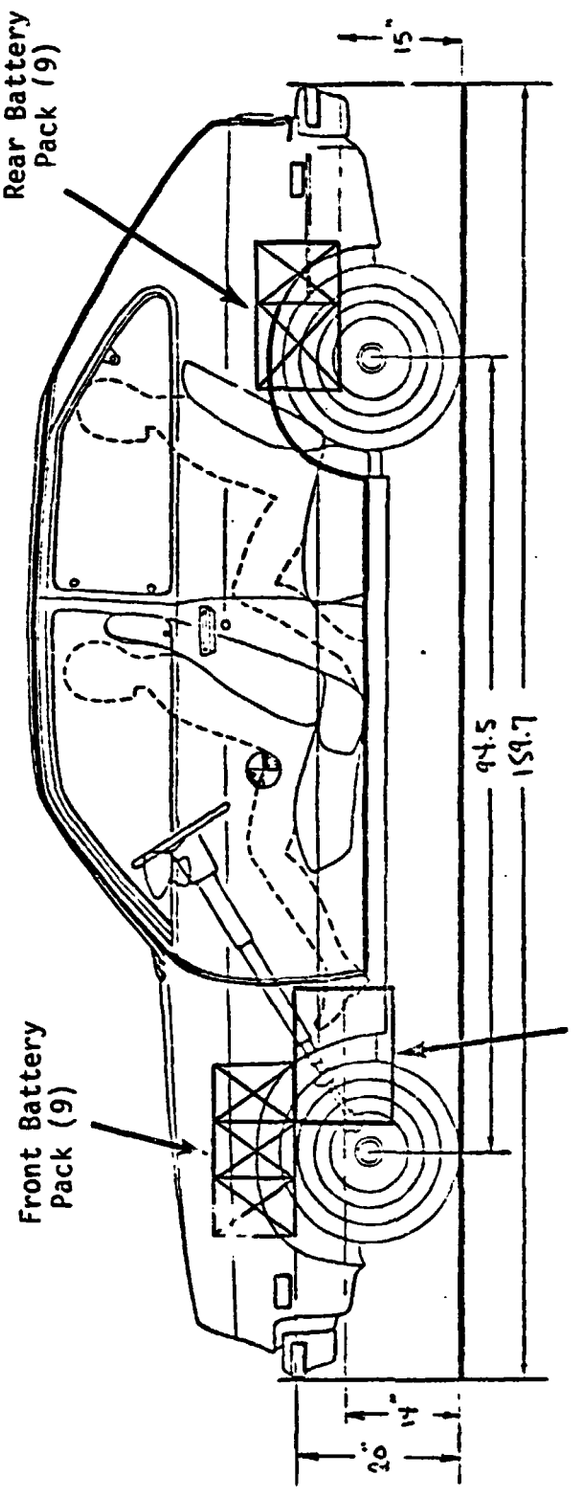

Figure 2 PACKAGING FOR 50/50 BATTERY SPLIT, CONVENTIONAL DRIVE LAYOUT

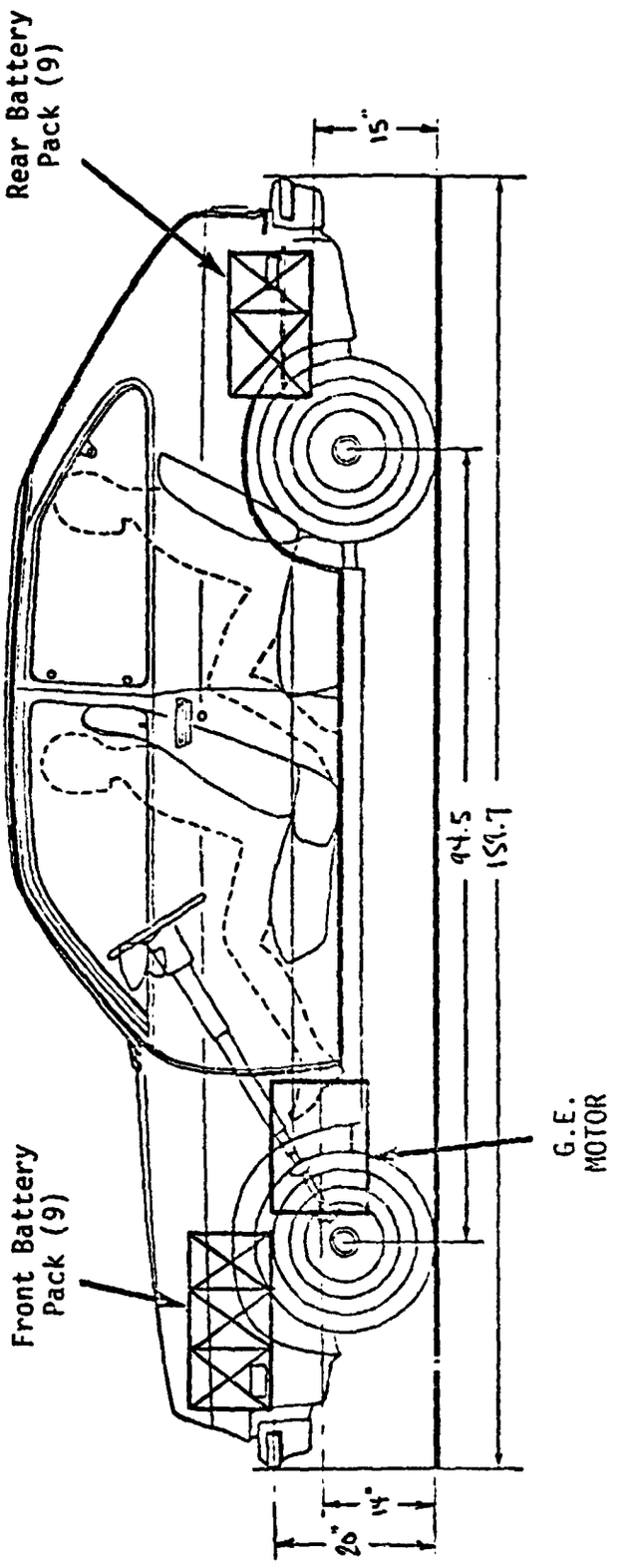

Figure 3 PACKAGING FOR 50/50 BATTERY SPLIT, 10" OUTBOARD, CONVENTIONAL DRIVE LAYOUT

GE Drive, 1/3 - 2/3 Battery Split Over Axles

A front motor, front drive confi_ ration was defined based on the drivetrain designed for the GE/Chrysler electric prototype.* To counterbalance the weight of the front drive system and due to space limitations in the front compartment, the batteries were split as shown in Figure 1(b), i.e., 6 were positioned in the front and 12 were placed in the rear. Figure 4 is a side view of this layout. Note that the motor is transversely oriented and placed at the same location as in the GE/Chrysler EV, with respect to the front axle, based on drawings provided by JPL. The front batteries were centrally located over the front axle and elevated to clear the motor and differential.

AiResearch Drive, 2/3 - 1/3 Battery Split Over Axles

In this case, the rear drive system contained in the AiResearch electric vehicle** was located in the rear of the base car in the same location relative to the rear axle. Figure 5 shows this configuration, which includes two motor/generators and a flywheel device. Batteries were split into a front package of 12 and a rear package of 6, as illustrated in Figure 1(c). Due to space limitations in the rear of the vehicle, it was necessary to slightly infringe on the rear seat space, but the resulting orientation is sufficient to provide approximate physical properties, although some redesign would obviously be necessary if this drive system was to be actually installed in the particular base car.

GE Drive, Tunnel Batteries

This configuration closely resembles the actual GE/Chrysler EV prototype in terms of battery and drive system layout. Batteries are placed in a central tunnel as illustrated in Figure 6(a). The motor and driveline are located in the front of the vehicle (refer again to Figure 4). The eighteen batteries are referenced to the rear axle equivalent to the

---

* Developed under Contract No. EY-76-C-03-1294

** Developed under Contract No. EY-76-C-03-1213

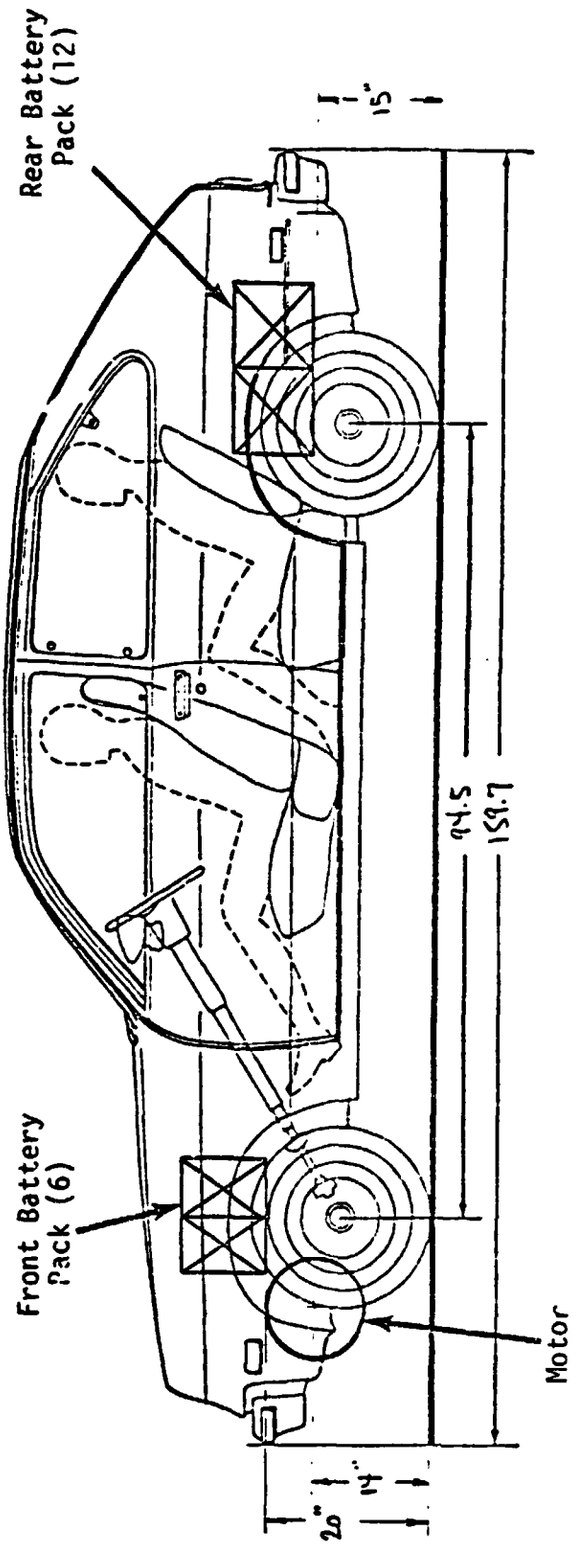

Figure 4 PACKAGING FOR $\frac{1}{3}$ - $\frac{2}{3}$ BATTERY SPLIT, GE/CHRYSLER POWERTRAIN

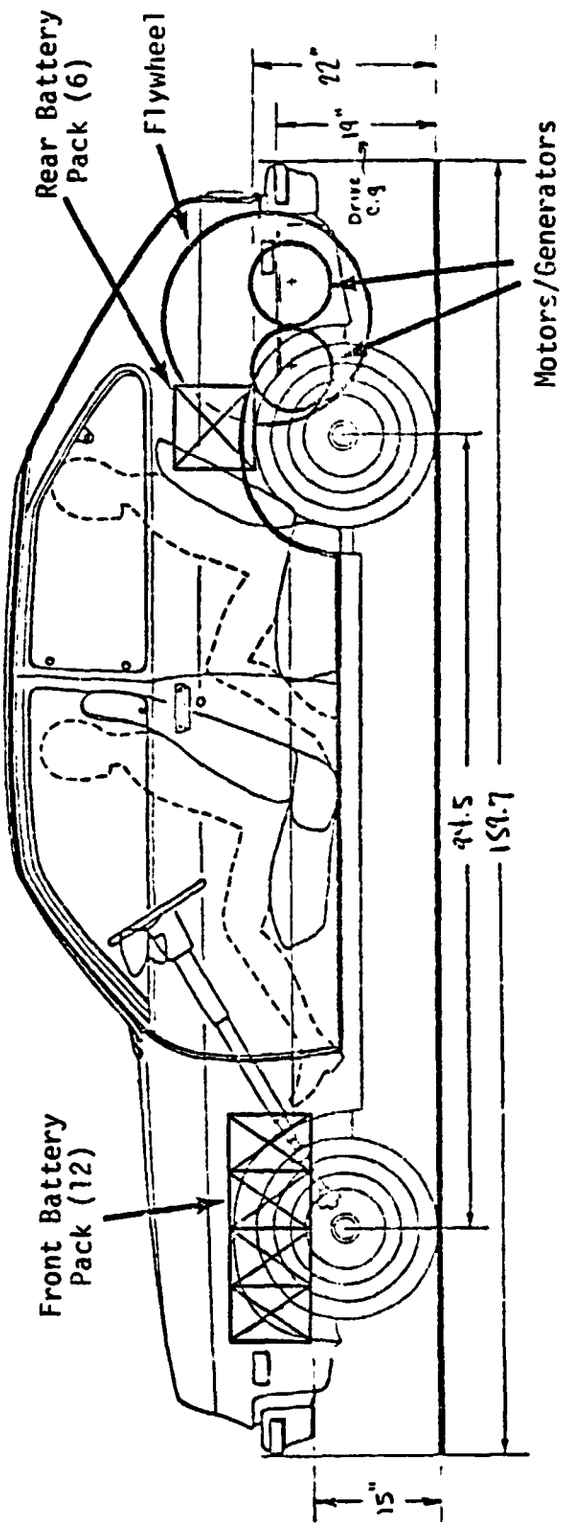

Figure 5 PACKAGING FOR $\frac{2}{3}$ - $\frac{1}{3}$ BATTERY SPLIT, AIRESEARCH POWERTRAIN

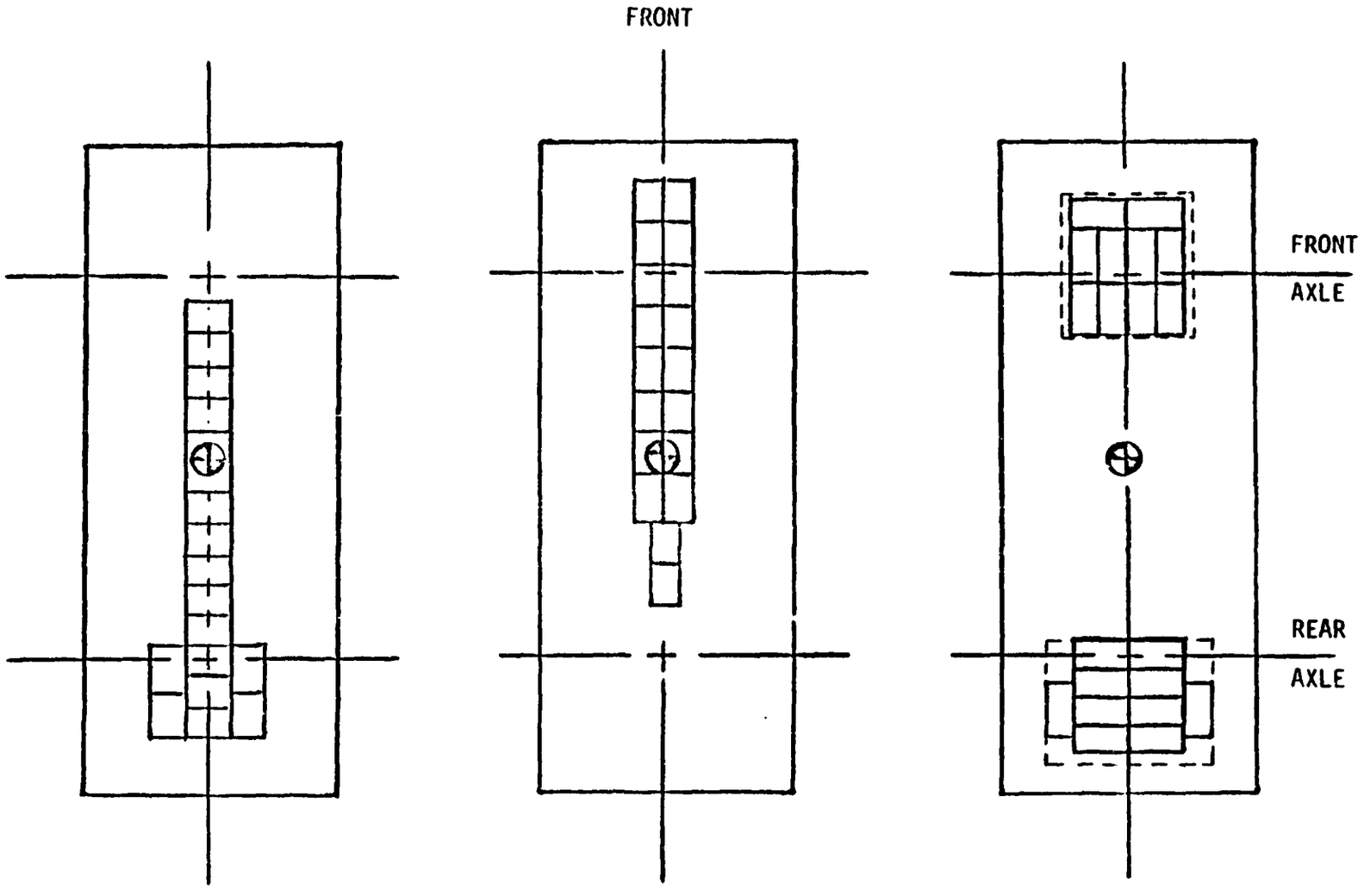

9950-297

Figure 6 BATTERY PACKAGING CONFIGURATIONS IN BASE VEHICLE

packaging approach taken by General Electric. A 10" ground clearance was assumed for the vertical battery location.

AiResearch Drive, Tunnel Batteries

A tunnel battery packaging layout comparable to that employed in the actual AiResearch EV was packaged in the base vehicle as shown in Figure 6(b). The rear drive system was retained as previously discussed (refer back to Figure 5). This approach also utilizes 18 batteries of the size considered for all the configurations described up to this point. A battery ground clearance of 10" was assumed.

Mars II Configuration

This configuration was derived from an actual electric vehicle, named the Mars II, which has been experimentally evaluated and found to be unacceptable with respect to handling performance (Ref. 1). It contained twenty heavy-duty batteries weighing 92 lbs. each, split equally between the front and rear, as shown in Figure 6(c) packaged in the base vehicle. The original Mars II was derived from a Renault R-10, which is approximately the same size as the Chevette base car. The electric motor was contained in the rear of the vehicle as illustrated by Figure 7. Simulating this configuration provides a basis for defining effects of high inertia which are known to be excessive and clearly unacceptable for a subcompact size car.

Front Heavy, High Inertia Configuration

The Mars II EV was rear heavy with approximately 55% of its weight supported by the rear axle. In order to take into account the effect of front/rear weight distribution for such a high inertia vehicle, a corresponding configuration was hypothesized that essentially turns the Mars II end-for-end. This gives a front-heavy configuration with the same inertial properties as the Mars II layout packaged in the base vehicle.

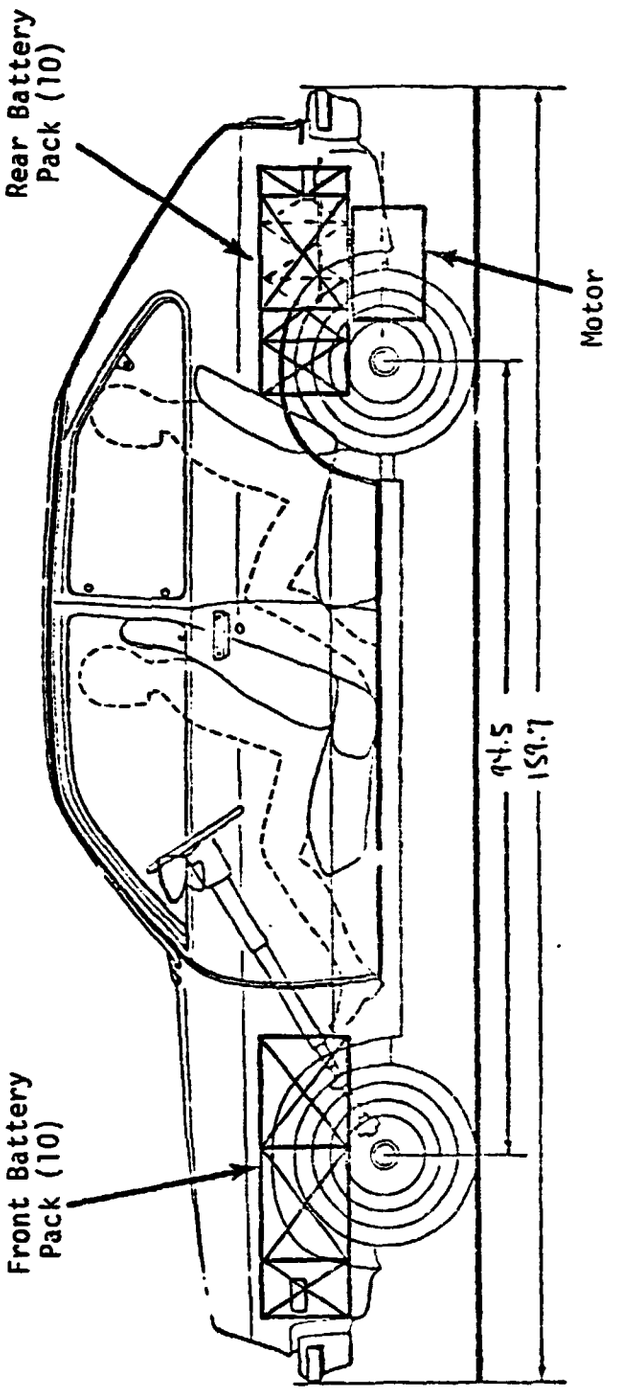

Figure 7 PACKAGING OF MARS II CONFIGURATION IN BASE VEHICLE

The eight electric vehicle configurations defined above are summarized in Table 1, along with the base car. In the next section, the physical properties of these configurations are given, e.g., the weight distributions and moments of inertia. It should be emphasized that all of these represent derivatives of the base vehicle and are therefore hypothetical vehicles. For instance, the suspension system properties of the base vehicle (except spring rates) were maintained constant for all EV's. It should not be assumed that these configurations represent their counterparts (GE, AiResearch, Mars II, etc.) in a strict sense, and can only be considered approximations of corresponding prototype EV's.

2.2 Physical Properties of Base Vehicle and EV Configurations

Various physical properties are required for input to the vehicle dynamics computer model to characterize a given configuration. These fall into the general categories of:

- Dimensions
- Masses and Moments of Inertia
- Suspension Characteristics
- Tire Properties

Many of the required parameters were available for the base car from various sources. It was particularly important to obtain an accurate representation of the base vehicle's weight distribution and moments of inertia. A 1979 Chevette 2-door was therefore obtained and appropriate measurements were made by Dynamic Science, Inc., Phoenix, Arizona. Their facility and procedures for measuring the desired parameters are described in Appendix A.

From this testing source, the following data were obtained for the base car at curb weight conditions:*

*See Glossary for definition of symbols.

Table 1

SELECTED CONFIGURATIONS FOR HANDLING PERFORMANCE EVALUATION

Configuration	Battery Packaging	Battery Distribution (Front/Rear)	Drivetrain Configuration	Motor Location	Drive Axle
Base Car	---	---	Std. ICE	Front	Rear
Conventional Drive EV	Over Axles	50/50	Conventional	Front	Rear
Conventional Drive EV	10" Outboard of Axles	50/50	Conventional	Front	Rear
G.E. Drivetrain	Ove Axles	$\frac{1}{3}$ / $\frac{2}{3}$	GE/Chrysler	Front	Front
AiResearch Drivetrain	Over Axles	$\frac{2}{3}$ / $\frac{1}{3}$	AiResearch	Rear	Rear
G.E. Drivetrain	Tunnel	---	GE/Chrysler	Front	Front
AiResearch Drivetrain	Tunnel	---	AiResearch	Rear	Rear
Mars II Configuration	Over Axles	50/50	Mars II	Rear	Rear
Front Heavy, High Inertia	Over Axles	50/50	Reversed Mars II	Front	Front

W_T - 2196 lbs.

a_T - 41.10 in.

b_T - 53.40 in.

h_{cgT} - 19.94 in.

I_{XT} - 3462 lb-in-sec^2

I_{YT} - 13,420 lb-in-sec^2

I_{ZT} - 13,820 lb-in-sec^2

These parameters are for the total vehicle treated as a single rigid body. The computer program, however, requires the corresponding parameters for the sprung mass uncoupled from the unsprung masses (suspension systems, wheels, tires, etc.). These parameters are traditionally obtained by analytically subtracting estimated masses and inertias of the unsprung components from the total vehicle. Based upon regression analyses of properties from a large number of passenger cars by Basso (Ref. 2), we have assumed the following values for the base vehicle:

W_f = 134 lbs. (total front unsprung weight)

W_r = 214 lbs. (total rear unsprung weight)

I_r = 185 lb-in-sec^2 (solid rear axle roll inertia)

Subtracting these weights and associated moments of inertia from the total vehicle, and accounting for translation of the center of gravity, results in the approximate sprung mass properties given below:

W_S = 1848 lbs.

a_S = 37.89"

b_S = 56.61"

h_{cgS} = 21.63",

$$I_{xS} = 2975 \text{ lb-in-sec}^2$$
$$I_{yS} = 11,124 \text{ lb-in-sec}^2$$
$$I_{zS} = 11,206 \text{ lb-in-sec}^2$$

The roll-yaw product of inertia for the sprung mass was calculated by assuming that the principal axis of the base vehicle is inclined about the pitch axis at -3°. This is believed to be a reasonable assumption for front engine cars, again based on Basso's study. The appropriate transformation relationship then gives a roll-yaw product of:

$$I_{xzS} = \frac{(I_{xS} - I_{zS}) \tan 2a}{2} = 433 \text{ lb-in-sec}^2$$

The other products of inertia are zero due to symmetry.

Since a two-passenger load was desired for all vehicles to be simulated, two 150 lb. masses were added to the base car at the front seating positions, which resulted in the following adjustments to the base vehicle properties:

	Curb Condition	Loaded Condition
W_s (lbs.)	1848	2148
a_s (in.)	37.89	39.20
b_s (in.)	56.61	55.30
h_{cgs} (in.)	21.65	22.33
I_{xS} (lb-in-sec^2)	2975	3104
I_{yS} (lb-in-sec^2)	11,124	11,199
I_{zS} (lb-in-sec^2)	11,206	11,376
I_{xzS} (lb-in-sec^2)	433	464

It is pointed out that the mathematical model used in this study (see Appendix B) requires on the order of fifty parameters to represent a given vehicle configuration. A complete description of these parameters goes beyond the scope of this report and the interested reader is referred to the HVOSM Users Manual developed by Segal (Ref. 3) for complete documentation. A complete set of input parameters for the base car is contained in Appendix C.

Most noteworthy is the very sophisticated suspension system representation treated by the computer program, which encompasses all important suspension properties of the base vehicle. These effects include ride-steer, lateral force compliance steer, aligning torque compliance steer, lateral force compliance camber, and aligning torque compliance camber. These compliance effects occur because suspension systems are intentionally designed with a certain amount of flexibility by the use of rubber bushings, for vibration control and other reasons. As will be discussed later in the report, these compliances play a very important role in the handling properties of a vehicle, and handling behavior can actually be modified by properly incorporating a certain amount of suspension system flexibility.

The standard tire for the 1979 Chevette is a P155/R13 metric radial (for 1978 models it is a P155/80D13 diagonal ply). We are not aware of published mechanical properties for these tire types. It was therefore decided to use properties for an A78-13 bias ply (load range B) with a relatively high cornering stiffness based upon tire test data obtained by Calspan (Ref. 4). Properties for this tire are given in Appendix C as input to HVOSM, and in Figure 8 in a carpet plot format. These properties are likely to be reasonably close to those of the standard Chevette tires. We also performed simulations with radial ply tires (BR78-13) on the base car, for direct comparison with the EV configurations.

With the above discussed information, the base vehicle is completely defined with respect to required HVOSM input data. The next step was to alter the mass distribution to represent the EV configurations considered for the simulation matrix.

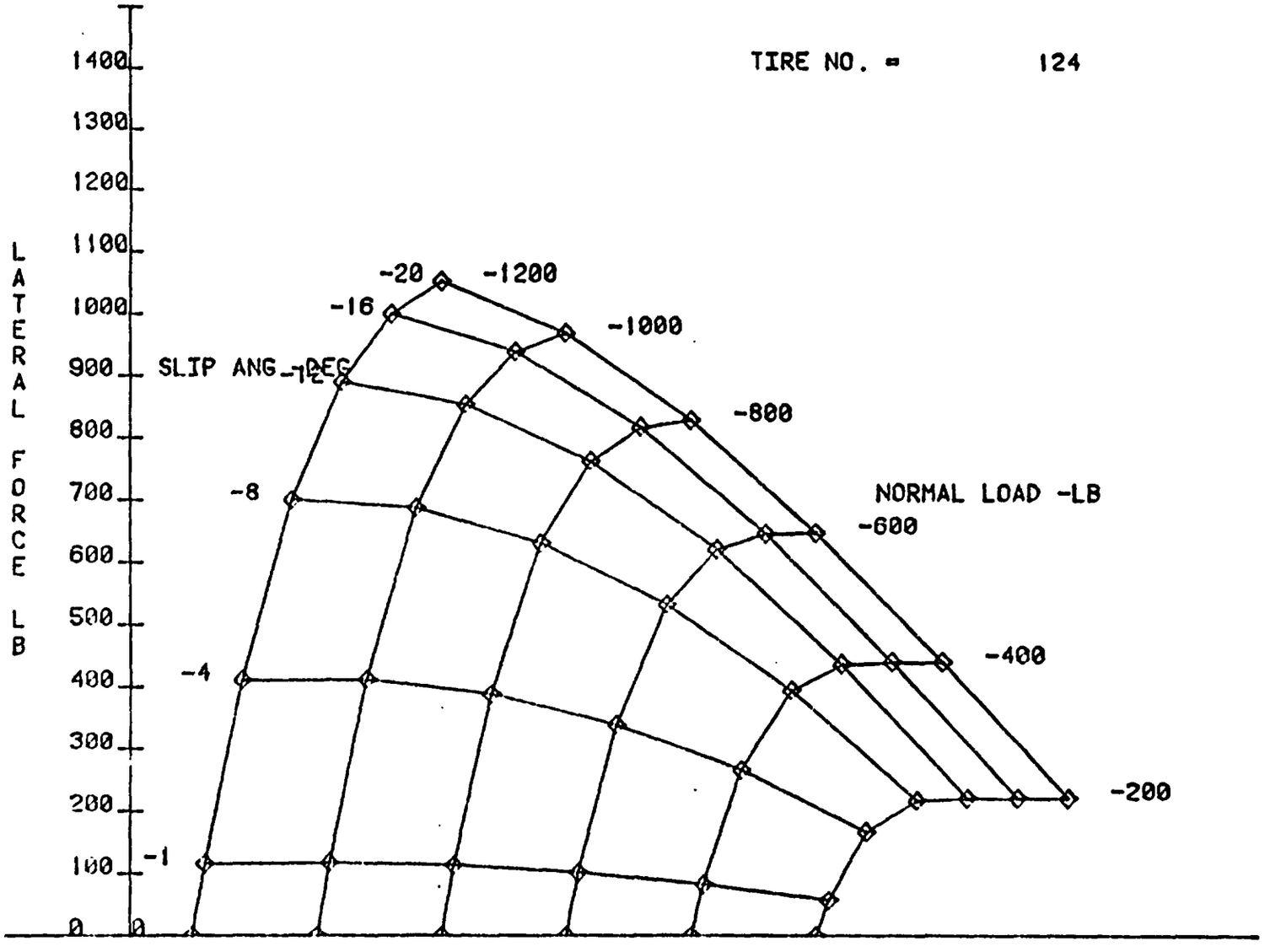

Figure 8 CORNERING STIFFNESS PROPERTIES OF SELECTED A78-13 TIRE FOR BASE VEHICLE

Before calculating inertial properties for these hypothetical EV conversions of the base car, the following components were analytically removed:

Component	Est. Weight (lbs.)
IC Engine	350
Transmission and Torque Conv.	100
Radiator and Coolant	50
Exhaust System	30
Full Fuel Tank (12.5 gal)	100
Driveshaft*	20
Differential*	40
	690

Based on approximate c.g. locations of the masses and their nominal overall dimensions, the appropriate IC engine components were subtracted from the base vehicle (with the two-passenger load maintained) using a computer program (INCAL) written for this purpose. Results are given below:

	Base Vehicle	Minus ICE Components
W_s (lbs.)	2148	1518
a_s (in.)	39.20	45.70
b_s (in.)	55.30	48.80
h_{cgs} (in.)	22.33	23.86
I_{xS} (lb-in-sec^2)	3104	2984
I_{yS} (lb-in-sec^2)	11,199	7659
I_{xS} (lb-in-sec^2)	11,376	7889
I_{xzS} (lb-in-sec^2)	464	399

*Subtracted from the rear unsprung mass, only for the GE/Chrysler and AiResearch powertrain configurations.

The final step in the EV inertia definition was to add the appropriate battery packages and powertrain components to the base vehicle stripped of its IC engine components. For this purpose, component weights for the GE/Chrysler and AiResearch electric prototypes were provided by JPL. Based on this information, the weights given below were used to calculate inertial properties for the EV configurations simulated.

Component	Conventional & GE/Chrysler Drives	AiResearch Drive
Motor	217	240
Transmission/Differential	48	90
Misc. Drive Components	20	47
Flywheel Assembly	--	173
Power Cond. Unit	97	86
Controller	8	12
On-board Charger	6	29
Misc. Power Comp.	14	33
Batteries (18 x 60#)	1080	1080
TOTAL (LBS.)	1490	1790

The EV design drawings also served to locate the various components relative to the drive axles for the GE and AiResearch approaches. Batteries were configured as previously discussed. Adding these components to the stripped base vehicle gives the weight distribution and inertial properties in Table 2.

Table 2 demonstrates that significant ranges of weight distribution and inertial properties are provided by the EV configurations selected. For instance, the 10" outboard shift of batteries for the 50/50 split causes about a 20% variation in yaw moment of inertia, while maintaining the same front/rear axle loadings. Conversely, the GE Drive and Conventional Drive (10" outboard) configurations have about the same yaw inertia, but a substantial difference in front/rear weight distribution (50/50 vs. 55/45).

Table 2

MASS DISTRIBUTION AND INERTIAL PROPERTIES

(Two Passenger Loadings)

Configuration	W_T lbs.	W_S lbs.	W_{SF} lbs.	W_{SR} lbs.	a_s in.	b_s in.	h_{cgs} in.	F/R %	I_{xs} lb-in-sec^2	I_{ys} lb-in-sec^2	I_{zs} lb-in-sec^2	I_{xzs} lb-in-sec^2
Base Car	2496	2148	1257	891	39.20	55.30	22.33	59/41	3104	11,199	11,376	464
Conv. Drive, 50/50 Battery Split	3356	3008	1650	1359	42.68	51.82	22.49	55/45	3397	15,696	16,108	236
Conv. Drive, 50/50 Battery 10" Outboard	3356	3008	1650	1359	42.68	51.82	22.49	55/45	3397	18,729	19,140	167
G.E. Drive 1/3 - 2/3 Battery Split	3296	3008	1515	1493	46.91	47.59	22.21	50/50	3476	18,010	18,505	368
A/R Drive, 2/3 - 1/3 Battery Split	3596	3308	1468	1840	52.56	41.94	22.44	44/56	3587	20,327	20,906	376

Table 2 (Contd.)

MASS DISTRIBUTION AND INERTIAL PROPERTIES

(Two Passenger Loadings)

Configuration	W_T lbs.	W_S lbs.	W_{SF} lbs.	W_{SR} lbs.	a_s in.	b_s in.	h_{cgs} in.	F/R %	I_{xs} lb-in-sec^2	I_{ys} lb-in-sec^2	I_{zs} lb-in-sec^2	I_{xzs} lb-in-sec^2
GE/Chrysler Tunnel Batteries	3296	3008	1481	1527	47.98	46.52	19.82	49/51	3275	15,034	15,172	265
AiResearch Tunnel Batteries	3596	3308	1554	1755	50.12	44.38	20.05	47/53	3412	17,751	18,019	487
Mars II Battery Configuration	4071	3783	1691	2092	52.27	42.23	21.18	45/55	3590	24,237	24,705	-115
Front Heavy, High Inertia Configuration	4071	3783	2092	1691	42.23	52.27	21.18	55/45	3590	24,237	24,705	115

Since axle loadings are substantially increased from the base car by the EV component additions, it is necessary to adjust the suspension spring rates accordingly. To maintain equal ride frequencies and ride heights, equal K/F ratios were incorporated in all vehicles, where K is the spring rate effective at the wheel for a particular suspension and F is the static vertical force (curb weight condition). For curb weight conditions, this gives spring rates for the EV's relative to the base car as listed below:

	SPRING RATES	
	Front Wheels (lb/in)	Rear Wheels (lb/in)
Base Vehicle (std. rates)	170	123
Conv. Drive, 50/50 Bat.	230	201
GE Drive, 1/3 - 2/3 Bat.	210	223
AiResearch, 2/3 - 1/3 Bat.	202	281
GE Drive, Tunnel Bat.	204	229
AiResearch Drive, Tunnel Bat.	216	266
Mars II Configuration	237	322
Front Heavy, High Inertia	298	256

Similarly, increased axle loadings necessitate selection of tires for the EV's with a higher load rating than for the base car tires. It is our understanding that the GE electric vehicle employs P175/75 Extra Load tires. No data are available for this type of tire in a form suitable for HVOSM input. We have therefore selected a BR78-13, which has a cornering stiffness significantly greater than the A78-13 tire used on the base car, tending to counteract effects of relatively high inertia in transient maneuvers. As will be discussed later, we also investigated the effect of using larger (14 inch) radial tires on the EV's.

These configurations give a spectrum of EV derivatives characterized by the weight-inertia relationship shown in Figure 9. The base car sprung

Figure 9 WEIGHT-INERTIA RANGE OF VEHICLE CONFIGURATIONS

mass has a yaw moment of inertia of about 11,000 lb-in-sec^2. There is then a group of EV's with a sprung weight in the 3000-3300 lb. range, with yaw moments of inertia between approximately 15,000 and 21,000 lb-in-sec^2; these are based on the various packaging layouts of 18 batteries (60 lbs. each) and compatible drivetrain designs. At the upper end of the spectrum lies the Mars II configuration containing 20 heavy-duty batteries (92 lbs. each), resulting in a sprung weight of 3800 lbs. and a yaw inertia of nearly 25,000 lb-in-sec^2.

In the next several sections, the handling properties of these configurations will be studied using computer simulations and linear theory for a simplified vehicle model. We will begin with a discussion of linear vehicle dynamics theory, which gives a foundation for understanding results of the handling simulations which follow.

2.3 Linear Vehicle Stability and Control Analysis

In order to provide a basis for more fully understanding the results obtained through simulating the various vehicle configurations with the HVOSM--a complex, nonlinear vehicle dynamics simulation--limited investigations have been conducted with simplified, linear automobile models. Such closed form analyses result in a better appreciation for the fundamental relationships between various physical parameters than can be obtained through simulation results alone. Although many independent vehicle dynamic analyses have been conducted through the years, the discussions contained below draw heavily on the work reported in References 5 and 6.

Consider the system shown in Figure 10, which illustrates geometric and kinematic variables for a two degree-of-freedom automobile. This schematic represents a vehicle in a steady turn of radius R with body slip angle (β), yaw rate (r), and front wheel steer angle (δ) held constant. The longitudinal and lateral components of the resultant velocity (V) in the body-fixed axes are u and v. Small angle assumptions are made for β, δ, and

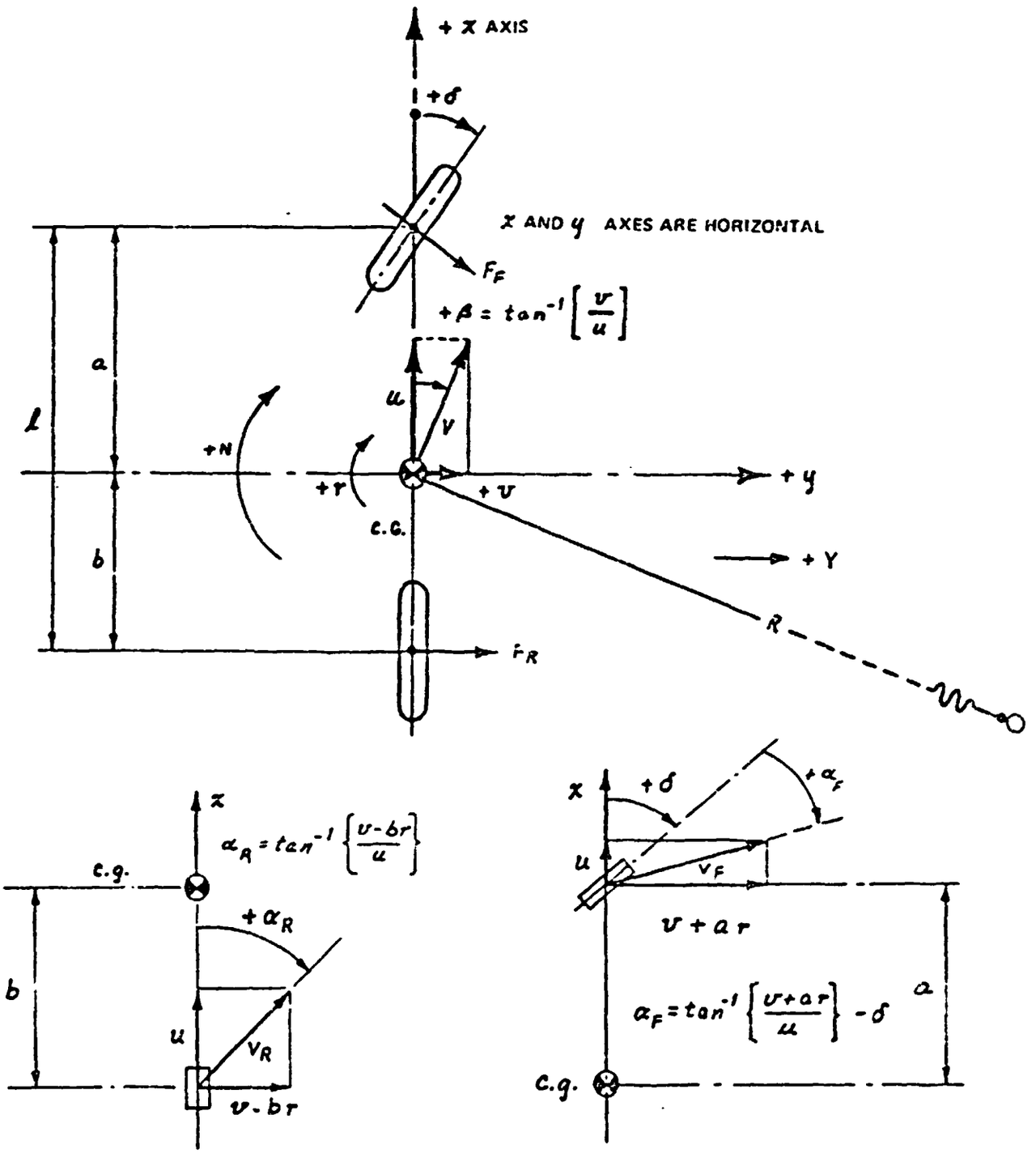

Figure 10 TWO DEGREE OF FREEDOM MODEL OF THE AUTOMOBILE

the front and rear slip angles (α_F and α_R), and longitudinal forces are neglected. The system is thus represented by a lateral force and a yaw moment equation:

$$Y = F_F + F_R$$

$$N = aF_F \cos \delta - bF_R \doteq aF_F - bF_R$$

Tire forces are assumed to be functions only of tire slip angle and, for small angles, can be represented as the product of the cornering stiffness and the slip angle:

$$F_F = C_{\alpha F}\, \alpha_F = C_{\alpha F} \tan^{-1} \left[\frac{v + ar}{u} - \delta\right]$$

$$F_R = C_{\alpha R}\, \alpha_R = C_{\alpha R} \tan^{-1} \left[\frac{v - br}{u}\right]$$

Applying the assumptions noted above we obtain:

$$F_F = C_{\alpha F} \left(\beta + \frac{ar}{V} - \delta\right)$$

$$F_R = C_{\alpha R} \left(\beta - \frac{br}{V}\right)$$

From these relationships, we can then obtain the side force and yaw moment equations as follows:

$$Y = \beta \left[C_{\alpha F} + C_{\alpha R}\right] + r\left[\frac{aC_{\alpha F} - bC_{\alpha R}}{V}\right] - \delta \left[C_{\alpha F}\right]$$

$$N = \beta \left[aC_{\alpha F} - bC_{\alpha R}\right] + r\left[\frac{a^2 C_{\alpha F} + b^2 C_{\alpha R}}{V}\right] - \delta \left[aC_{\alpha F}\right]$$

These equations define the total side force and yaw moment acting on an automobile subject to the validity of the assumptions made in the derivation. Note that the small angle and tire force assumptions result in linear equations in r and β, the yaw rate and side slip angle (for constant speed) and, thus, this representation is often referred to as the simple linear automobile model.* It is generally accepted that the overall linearity assumption is valid within the operating range from zero to approximately 0.3 g lateral acceleration.

If we now consider only steady-state turns, the resultant yaw moment (N) is zero and side force (Y) can be equated to mVr, the centrifugal force due to yaw rate r (or lateral acceleration $\frac{V^2}{R}$). With these further restrictions, the side force and yaw equations (with additional manipulation) become:

$$C_{\alpha F}\left[\beta + \frac{ar}{V} - \delta\right] + C_{\alpha R}\left[\beta - \frac{br}{V}\right] = mVr$$

$$aC_{\alpha F}\left[\beta + \frac{ar}{V} - \delta\right] - bC_{\alpha R}\left[\beta - \frac{br}{V}\right] = 0$$

Solution of these two equations for the front wheel steer angle (δ) results in:

$$\delta = \frac{\ell}{R} + \frac{mV^2}{\ell R}\left[\frac{aC_{\alpha F} - bC_{\alpha R}}{C_{\alpha F}C_{\alpha R}}\right]$$

The static margin h_o, is a particularly useful descriptor of the lateral-directional properties of the simple two degree of freedom (2df) model of Figure 10. It is defined (e.g., Ref. 5) as**

$$h_o = \frac{C_{\alpha R}}{C_{\alpha S}} - \frac{a}{\ell} = \frac{bC_{\alpha R} - aC_{\alpha F}}{C_{\alpha S}\ell}$$

---

* Later in this section we will discuss an improvement in certain relationships derived from this model which reflect an expansion of the physical factors considered, but maintaining the restriction of linearity.

** Note that $C_{\alpha S} \equiv C_{\alpha F} + C_{\alpha R}$

and is zero, positive, and negative for the neutral steer, understeer, and oversteer 2df car, respectively. In terms of the static margin, the steer angle equation becomes:

$$\delta = \frac{\ell}{R} - h_o \frac{mV^2}{R} \frac{C_{\alpha S}}{C_{\alpha F} C_{\alpha R}} = \frac{\ell}{R} - \frac{h_o}{C_o} \frac{V^2}{Rg}$$

which is the generalized steer angle expressed as a function of R, V, and vehicle physical constants where $\frac{C_{\alpha S} W}{C_{\alpha F} C_{\alpha R}}$ is defined as $\frac{1}{C_o}$.

This equation is often expressed as:

$$\delta = 57.3 \frac{\ell}{R} + K \frac{V^2}{Rg}$$

where K, in units of degrees per g, is referred to as the understeer factor or understeer gradient. Thus we have front wheel steer angle required for maintaining a given radius, R, (including the Ackerman angle, $\frac{\ell}{R}$) as a function of wheel base, ℓ, velocity, V, and understeer gradient, K.

Physically, C_o is always negative since tire cornering stiffness is always negative (a negative slip angle produces a positive side force). A positive static margin therefore requires an increase in steer angle in order to maintain a given radius as speed is increased. This is the understeering behavior to which drivers are most accustomed. The reverse is true for an oversteering car, that is, the steer angle must be reduced to maintain a constant radius as speed increases.

To this point, we have dealt only with a simplified automobile model whose steady-state steering characteristics are determined by weight distribution and tire cornering stiffnesses. In real automobiles there are many other factors which strongly influence a car's steering behavior in the linear realm of operation. These include tire self-aligning torques, tire camber effects, geometric roll steer, steer effects arising from steering and suspension compliances, lateral load transfer and aerodynamic effects.

Analyses conducted by Milliken, et al. (Ref. 7) have attempted to account for some of these additional factors (sometimes called "steer effects") in a rather unique fashion. Rather than including them directly into the equations of motion and dealing with attendant complex coupling terms, efforts have been made to isolate these "add-on" factors in an approximate manner by treating them one at a time. This approach ignores interactions (and the algebraic complexity) of an exact method, focusing on each factor individually and allowing one to compare the influence of different factors with relative ease.

This approach results in expressions for these factors in a manner that isolates their effects as an incremental change in the static margin, h_i, or an incremental change in the cornering stiffness parameter, C_i. For all of the analyzed effects, the steady-state steer equation then becomes:

$$\delta = \frac{\ell}{R} - \frac{h}{C} a_y$$

where:

$$h = h_o + \Sigma h_i$$

$$C = C_o + \Sigma C_i$$

and $K = \frac{h}{C}$ with appropriate factors applied to maintain consistent units.

Table 3 gives a list of the incremental changes in algebraic form for those steer effects that were considered (from Reference 7).

With regard to this study, it was felt that an understanding of the steady-state steering characteristics of the base vehicle and the hypothetical electric vehicle configurations was necessary. While the <u>total</u> vehicle understeer factor is available from the HVOSM output (as is discussed later), the linear analyses discussed in this section provide a breakdown of the contributions to understeer factor from many different sources.

Table 4 gives a breakdown of the contributions of the various steer effects to the total vehicle understeer factor for five of the vehicle configurations investigated. Note that static weight distribution and cornering

Table 3

SUMMARY OF STEER EFFECTS

FACTOR	H_i	C_i	REMARKS
RIGID BODY ALIGNING TORQUE DUE TO SLIP ANGLE	$h_{AT\alpha} = \dfrac{-2\,(N_{\alpha F} + N_{\alpha R})}{C_{\alpha S}\,\ell}$	$C_{AT\alpha} \cong \dfrac{2N_{\alpha F}C_{\alpha R} - 2\,N_{\alpha R}\,C_{\alpha F}}{W\ell\,C_{\alpha S}}$	
RIGID BODY ALIGNING TORQUE DUE TO CAMBER ANGLE	$h_{AT\gamma} = \dfrac{-2\,K_\phi\,(N_{\gamma F}\,\Gamma_F + N_{\gamma R}\,\Gamma_R)}{W\ell}$	$= 0$	
DEFLECTION STEER - SLIP ANGLE ALIGNING TORQUE	$h_{d\alpha} = \dfrac{C_o W\,(E_{\sigma F}\,N_{\alpha F} - E_{\sigma R}\,N_{\alpha R})}{(1 + E_{\sigma F}\,N_{\alpha F})\,C_{\alpha R} + (1 + E_{\sigma R}\,N_{\alpha R})\,C_{\alpha F}}$	$C_{d\alpha} = \dfrac{-C_o\,(C_{\alpha R}E_{\sigma F}\,N_{\alpha F} + C_{\alpha F}\,E_{\sigma R}\,N_{\alpha R})}{(1 + E_{\sigma F}\,N_{\alpha F})C_{\alpha R} + (1 + E_{\sigma R}\,N_{\alpha R})\,C_{\alpha F}}$	
DEFLECTION STEER - CAMBER ANGLE ALIGNING TORQUE	$h_{d\alpha} = C_o K_\phi\,(K_{\gamma R}\,\Gamma_R - K_{\gamma F}\,\Gamma_F)$	$= 0$	
DEFLECTION STEER - SLIP ANGLE LATERAL FORCE	$h_{f\alpha} = \dfrac{C_\alpha\,(E_{tF} - E_{tR})}{2\,(2 + C_\alpha\,(E_{tF} + E_{tR}))}$	$C_{f\alpha} = \dfrac{-C_\alpha^2\,(E_{tF} + E_{tR})}{W\,(2 + C_\alpha\,(E_{tF} + E_{tR}))}$	$C_{\alpha F} = C_{\alpha R} = 2\,C_\alpha$
DEFLECTION STEER - CAMBER ANGLE LATERAL FORCE	$h_{f\alpha} = -C_o K_\phi\,(K'_{\gamma R}\,\Gamma_R - K'_{\gamma F}\,\Gamma_F)$	$= 0$	
ROLL STEER	$h_\phi = -C_o K_\phi\,(E_{\phi R} - E_{\phi F})$	$= 0$	
ROLL CAMBER	$h_\gamma = \dfrac{-2\,\bar{C}_\gamma K_\phi\,(C_{\alpha R}\,\Gamma_F - C_{\alpha F}\,\Gamma_R)}{WC_{\alpha S}}$	$= 0$	$\bar{C}_{\gamma F} = \bar{C}_{\gamma R} = 2\bar{C}_\gamma$

$N_{\alpha F,R}$ = ALIGNING TORQUE PER UNIT SLIP ANGLE (USUALLY POSITIVE), ONE WHEEL — ft-# /rad

K_ϕ = BODY ROLL PER UNIT NORMALIZED LATERAL ACCELERATION (USUALLY NEGATIVE) — DIMENSIONLESS

$N_{\gamma F,R}$ = ALIGNING TORQUE PER UNIT CAMBER ANGLE (USUALLY POSITIVE), ONE WHEEL — ft # /rad

$\Gamma_{F,R}$ = WHEEL CAMBER PER UNIT ROLL OF THE SPRUNG MASS (USUALLY POSITIVE) — DIMENSIONLESS

$E_{\sigma F,R}$ = STEER PER UNIT APPLIED ALIGNING TORQUE, APPLIED SIMULTANEOUSLY TO BOTH WHEELS (USUALLY POSITIVE) — rad/ft #

$K_{\gamma F,R} = E_{\sigma F,R}\,N_{\gamma F,R}$ (USUALLY POSITIVE) — DIMENSIONLESS

$E_{tF,R}$ = STEER PER UNIT APPLIED LATERAL FORCE, APPLIED SIMULTANEOUSLY TO BOTH WHEELS (POSITIVE OR NEGATIVE) — rad/ #

$K'_{\gamma F,R} = E_{tF,R}\,C_{\gamma F,R}$ (POSITIVE OR NEGATIVE) — DIMENSIONLESS

$E_{\phi F,R}$ = STEER PER UNIT BODY ROLL (POSITIVE OR NEGATIVE) — DIMENSIONLESS

C_γ = SINGLE WHEEL LATERAL FORCE PER UNIT CAMBER (USUALLY POSITIVE), SEE REMARKS — # /rad

Table 4

ANALYTICALLY DERIVED STEER EFFECTS

STEER EFFECT	VEHICLE CONFIGURATION: Base Vehicle (A78x13 Tires) h	c	Base Vehicle (BR78x13 Tires) h	c	Conventional Drive, 50/50 Bat. Split h	c	GE Drive, 1/3-2/3 Bat. Split h	c	A/R Drive, 2/3-1/3 Bat. Split h	c
2 dof-weight distribution cornering stiffness (h_o,c_o)	.0616	-2.464	.0520	-2.507	.0338	-2.191	.0035	-2.217	-.031	-2.097
Rigid body aligning torque - slip angle	.0015	.0103	.0020	.013	.0026	.0087	.0026	0.0	.0028	-.0155
Rigid body aligning torque - camber angle	.0002	0.0	.0001	0.0	.0001	0.0	.0001	0.0	.0001	0.000
Deflection steer - slip angle aligning torque	.0410	.288	.0532	0.371	.0685	.4614	.0585	.445	.0480	.4394
Deflection steer - camber angle aligning torque	.0125	0.0	.0076	0.000	.0099	0.0	.0090	0.0	.0087	0.000
Lateral force deflection steer - slip angle	.0471	.261	.0480	0.271	.0551	.2714	.0548	.272	.0564	.2664
Lateral force deflection steer - camber angle	-.0089	0.0	-.0021	0.000	-.0032	0.0	-.0028	0.0	-.0026	0.000
Roll steer	.0086	0.0	.0088	0.00	.0089	0.0	.0088	0.0	.0088	0.000
Roll Camber	.0323	0.0	.0069	0.00	.0097	0.0	.0097	0.0	.0114	0.000
Total (h,c)	.1953	-1.903	.1807	-1.851	.1858	-1.449	.1442	-1.499	.1026	-1.407
Simple 2df K (= $-57.3 \frac{h_o}{c_o}$),o/g	1.431		1.188		0.884		0.090		-0.904	
Expanded model K (= $-57.3 \frac{h}{c}$),o/g	5.899		5.461		7.335		5.512		4.090	

stiffness provide only about 32% of the base vehicle's effective static margin.* The total of all deflection steer effects provides about 47% of the effective static margin. These deflection steer effects arise from compliances in the steering and suspension systems of a vehicle (i.e., steer angle changes induced by forces or moments) and, which taken into account in the design stage, not only provide for shock and vibration isolation but, as is illustrated here, have a substantial influence on a vehicle's steady-state steering characteristics.

It is particularly interesting to note that, even though the rear heavy (A/R Drive, 2/3 - 1/2 Bat. Split) electric vehicle listed in the table is an oversteering vehicle when considering weight distribution and cornering stiffness alone, when other effects are included it becomes a moderately understeering vehicle. This point is further illustrated by considering the steer characteristics of the remaining vehicle configurations shown in Table 5. Of these four vehicles, three are oversteer based on simple linear vehicle theory, while the expanded theory shows them to be all understeer.

From the point of view of electric vehicle design and construction, it is therefore significant to emphasize that even though other constraints (e.g., packaging) may require a rear-heavy vehicle layout, it is still possible to produce an understeering car in the linear range of operation by proper suspension design without resorting to undesirable practices such as tire pressure or size differentials.

In addition to steady-state response, linear theory can be used to predict transient response to various steer inputs. There are a number of different response times that can be used, and have been used in the past, to characterize transient response, both in terms of yaw rate and lateral

---

* Static margin can be thought of being the distance of the effective point of application of the tire side forces from the vehicle center-of-gravity, positive if ahead of the c.g. and negative if behind.

Table 5

ANALYTICALLY DERIVED STEER EFFECTS

STEER EFFECT	VEHICLE CONFIGURATION: GE Drive, Tunnel Bat.		A/R Drive, Tunnel Bat.		Mars II Configuration		Frt. Heavy High Inertia	
	h	c	h	c	h	c	h	c
2 dof-weight distribution, cornering stiffness (h_o,c_o)	-.0029	-2.216	-.0174	-2.108	-.0360	-1.942	.0376	-1.944
Rigid body aligning torque - slip angle	.0026	-0.002	.0028	-.008	.0032	-0.015	.0032	.013
Rigid body aligning torque - camber angle	.0001	0.0	.0001	0.0	.0001	0.0	.0004	0.0
Deflection steer - slip angle aligning torque	.0555	.440	.0552	.453	.0569	.465	.0879	.509
Deflection steer - camber ang. aligning torque	.0074	0.0	.0077	0.0	.0088	0.0	.030	0.0
Lateral force deflection steer - slip angle	.0548	.272	.0566	.268	.0588	.256	.0588	.257
Lateral force deflection steer - camber angle	-.0023	0.0	-.0024	0.0	-.0029	0.0	-.0110	0.0
Roll steer	.0074	0.0	.0074	0.0	.0078	0.0	.0217	0.0
Roll camber	.0082	0.0	.0093	0.0	.0116	0.0	.0299	0.0
Total (h,c)	.1307	-1.505	.1193	-1.395	.1082	-1.235	.2585	-1.164
Simple 2df K (= $-57.3 \frac{h_o}{c_o}$),o/g	-0.076		-0.472		-1.060		1.109	
Expanded model K (= $-57.3 \frac{h}{c}$),o/g	4.977		4.902		5.023		12.716	

acceleration. Such times can be measured with respect to the first crossover of the steady-state value (or 63% or 90% of this value) or to the peak value. Another response time that is typically used in experimental work is based on the time difference between the point where the steering input has reached 50% of its steady-state value and the point where the response (yaw rate or lateral acceleration) has reached 90% of its steady state value. This experimental procedure is based on the fact that (unlike analyses) pure step inputs are physically unrealizable. One additional effective time constant is determined by finding the frequency at which the yaw velocity lags the steer angle by 45° for a sinusoidal steer input. Within the simulation study, we have used the experimentally derived response time (50% of the input steer to 90% of the yaw rate steady state) as a metric. However, we will now illustrate the effects of certain vehicle parameters on a number of response times as determined from linear theory.

It is known that solution of the two degree-of-freedom linear equations of motion of an automobile leads to a second order damped system for yaw response. In general, this response can be underdamped, overdamped or critically damped depending on the physical properties of the particular automobile. Close inspection of the equations leads to the general conclusion that an understeering car will respond to a step steer input in an underdamped manner while an oversteering car will be overdamped. The oversteering vehicle will have a larger steady-state yaw rate gain but the understeer vehicle will reach a steady state sooner. While judgments as to the goodness or badness of vehicle handling is subjective and therefore difficult to quantify, it is widely believed that vehicles with smaller time constants (either in yaw or lateral acceleration response) are better handling vehicles than those with large time constants. This is supported by experimental studies reported in Reference 8, which result in a domain of acceptability for a vehicle's steady-state yaw rate vs. time constant response.

Yaw rate time constants were computed from a simplified two-degree-of-freedom automobile representation for a number of different vehicle configurations

that were also studied with the large scale HVOSM simulation. Included in Table 6 are both the simple and expanded two-degree-of-freedom understeer factors, the steady-state yaw rate gain, and three different time constants. These are the times at which the yaw response reaches the 63% and 90% steady-state level and the effective time constant determined from the frequency at which the yaw response lags a sinusoidal steering input by 45°. Also included in the table is the yaw moment of inertia for each configuration.

It should be noted that the model from which these time constants were obtained was based simply on weight distribution and cornering stiffness only. No compliances or roll effects are included as no known theory is available for a closed form solution to an expanded model. Consequently, the time constants listed in the table correspond to the simple two-degree-of-freedom understeer factors also shown.

A number of observations are apparent from study of Table 6. In general, the effective response times are close to the 63% response times (based on a perfect step steer) with the 90% times being considerably higher. Vehicles which are less understeer show increasing steady-state yaw velocity gain (degrees/second/degree of front wheel/steer angle). There is no obvious trend in response time when the base vehicle tires are changed from a bias ply construction to a larger sized radial tire. This should not be taken as a general conclusion since it is due to a pecularity of the particular radial tires used. The BR78x13 tires exhibited an unusually strong cornering stiffness fall-off with decreasing normal load and hence the total cornering stiffness did not increase significantly. However, the use of FR70x14 tires on the base vehicle did significantly increase cornering stiffness and reduce response times.

A significant relationship can be obtained from this data by plotting time constant as a function of yaw moment of inertia as is shown in Figure 11. Further, if the vehicle configurations are broken down into front heavy, rear heavy and balanced categories as is indicated in the figure, it becomes

Table 6

TIME CONSTANTS FROM LINEAR THEORY

Vehicle Configuration	Simple 2df Understeer Factor (deg/g)	Expanded 2df Understeer Factor (deg/g)	Steady-State Yaw Velocity Gain (deg/sec/deg)	63% Response Time (sec)	90% Response Time (sec)	Effective Response Time (45° Lag) (sec)	Yaw Moments of Inertia ($lb\text{-}in\text{-}sec^2$)
Base (A78x13)	1.43	5.64	5.56	.137	.276	.155	11376
Base (BR78x13)	1.19	5.34	5.81	.139	.280	.155	11376
Conventional E.V.	0.89	7.34	6.16	.169	.338	.179	16108
Conventional E.V. (10" OB)	0.89	7.34	6.16	.193	.397	.205	19140
GE Drive	0.09	5.52	7.29	.211	.477	.219	18505
A/R Drive	-0.91	4.14	9.48	.333	.858	.296	20906
GE (Tunnel)	- .08	4.98	7.59	.194	.456	.188	15172
A/R (Tunnel)	- .47	4.90	8.39	.250	.616	.228	18019
Mars II	-1.06	5.03	9.95	.395	.945	.349	24705
Front Heavy	1.11	10.50	5.90	.211	.420	.228	24705
Base (FR70x14)	0.69	4.19	6.41	.100	.217	.107	11376
Mars II (FR70x14)	- 53	5.14	8.53	.193	.477	.176	24705
Front Heavy (FR70x14)	0.57	8.94	6.56	.135	.299	.151	24705

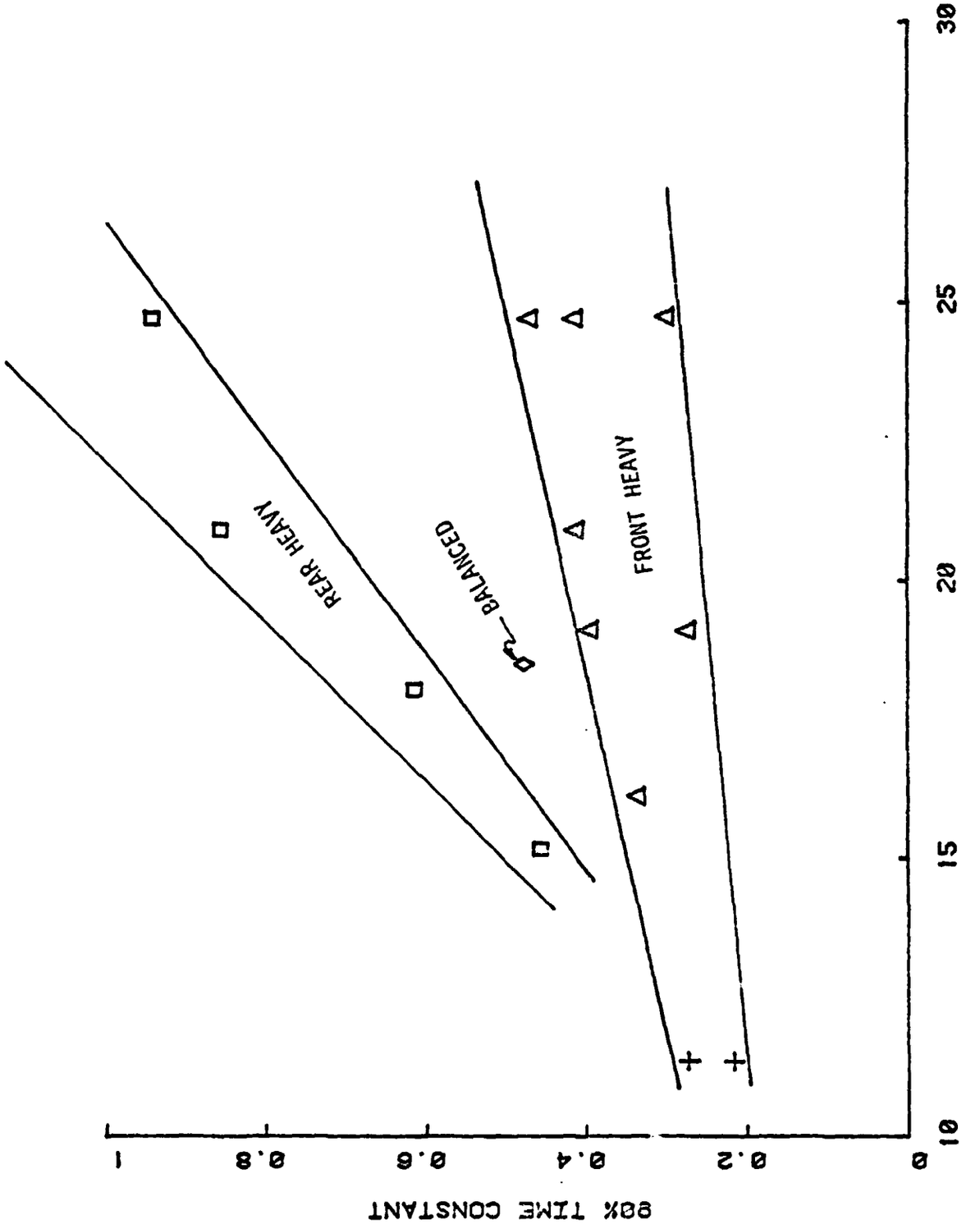

Figure 11 TIME CONSTANTS BASED ON LINEAR THEORY

appears that the rate of change of time constant for increasing inertia is significantly greater for rear heavy vehicles than for front heavy vehicles. This is an important observation since an inertia penalty will always be associated with electric vehicles. However, the response time penalty associated with this increase in inertia can be minimized by designing a front heavy vehicle. This conclusion, developed here from linear theory, will be confirmed in Section 2.8 from results of the HVOSM computer runs.

The handling maneuvers that were simulated are described next.

2.4 Handling Maneuvers Simulated

The main purpose of this study was to evaluate effects that mass distribution and moments of inertia have on directional control and braking stability, for various electric vehicle packaging configurations applied to the base car. Inertial properties directly affect vehicle transient response to control inputs, whereas mass (weight) distribution between the front and rear axles affects steady-state cornering behavior as well. Both steady-state and transient maneuvers were thus considered. The specific maneuvers simulated were:

- Trapezoidal Steer Response (including steady-state trim condition at a fixed steer angle input)
- Sinusoidal Steer Response
- Braking in a Turn

The trapezoidal and sinusoidal steer simulations were performed completely consistent with Vehicle Handling Test Procedures (VHTP's) No. 4 and 5, respectively, developed for the National Highway Traffic Safety Administration under contract with the University of Michigan (Ref. 9). The braking-in-a-turn simulation was consistent with VHTP No. 2, except for a

modification required because detailed brake system data were not available for the base vehicle. Each of these maneuvers is described in the remainder of this section.

Trapezoidal Steer Maneuver

An overview of this maneuver is given by the following excerpts from Reference 10.

> "This maneuver results in a J-turn trajectory which does not appear to be representative of any realistic highway maneuver but which does, nevertheless, provide the conditions appropriate for examination of the transition from straight-line motion to limit turning, such as may occur in the initial phase of an obstacle-avoidance maneuver. The effectiveness with which a vehicle performs an obstacle-avoidance task in an emergency, as a result of a steering input, would seem to be determined by the ability of the vehicle to achieve lateral displacement in a controllable manner. As a consequence of having nonsteerable rear wheels, the passenger vehicle achieves lateral displacement only by means of a curvilinear trajectory. It follows that a characterization of the curvilinear path produced by a rapid steering input can serve as a measure of the obstacle avoidance capability of a motor vehicle.
>
> For characterization of the curvilinear path response, a normalized path-curvature measure, $R_S\ (1/R)_{ave}$, is obtained by averaging the time history of path curvature over a 2 s period following the initiation of the trapezoidal steer input. As a result of this averaging process, the measure combines the dynamic delay in response together with the achieved quasi-static level of path curvature. The normalizing term, R_S, is the value of path curvature constituting a steady 1 g turn at 40 MPH, and is used simply to obtain a convenient scale. The path-curvature measure is plotted versus normalized steer angle to indicate the response trend as a function of the steer input level.
>
> Sideslip response to trapezoidal steer input is again seen as a driver challenge factor. Accordingly, the peak value of β, as observed within the first 2 s of the maneuver, is plotted versus steer input level as well as cross-plotted against the path-curvature measure. The cross plot is seen as indicating the "price" (in terms of sideslip angle) that is "paid" for the level of path curvature that is achieved. It is hypothesized that obstacle avoidance capability is maximized in those vehicles which produce a high path-curvature measure without exhibiting significant sideslip."

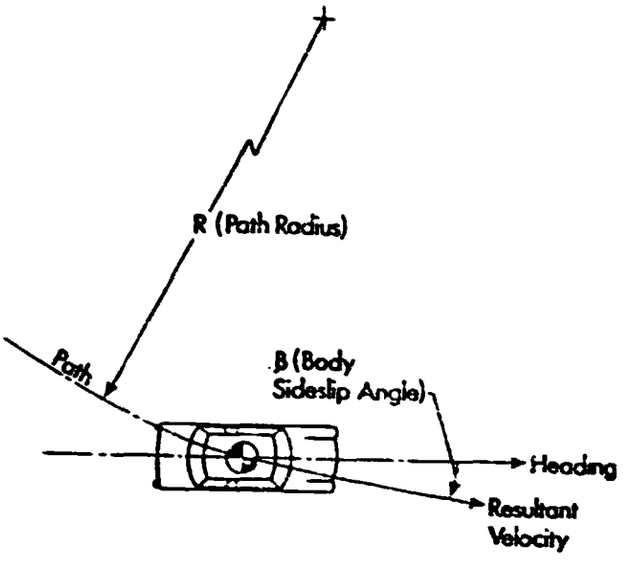

The sideslipping vehicle in a curved path

This maneuver therefore characterizes the transient response of a vehicle to a suddenly applied steer input. Th magnitude of steer angle is increased through a series of simulations until the limit of lateral adhesion is reached resulting in either a plowing condition (understeer), lateral drift (neutral steer), or spin-out (oversteer). Since the steering angle is held constant after the rapid steer input, this simulation also provides steady-state (trim condition) information after the transient motions damp out.

An initial velocity of 40 MPH is normally used, and the standard steering input angle (average angle of front wheels) time history is shown below:

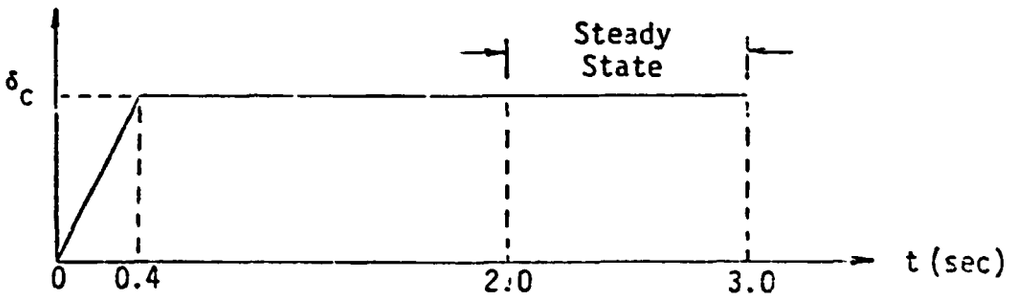

The constant steer angle (δ_c) is normalized for a given wheelbase (ℓ) and reference angle (σ) by:

$$\delta_c = \frac{\ell}{10} \sigma$$

Simulations were generally performed for the following range of reference angles:

$$\sigma = 2, 4, 8, 12, 16, 20, 24°$$

For the base car,

$$\ell = 7.86' \ (94.3")$$

This gives the actual front wheel command steering angles that were considered:

$$\delta_c = 1.57, 3.14, 6.29, 9.43, 12.58, 15.72, 18.86°$$

For this maneuver, the standard evaluation numerics are:

- Maximum lateral acceleration (a_{yp})
- Maximum yaw rate (r_p)
- Peak sideslip angle (β_p)
- Peak rate of change of sideslip angle ($\dot{\beta}_p$)
- Average path curvature ratio defined by:

$$R_s \left(\frac{1}{R}\right)_{ave}$$

where $$\left(\frac{1}{R}\right)_{ave} = \frac{1}{2} \int_{t=0}^{2} \left(\frac{1}{R}\right) dt$$

and R_s = radius for 1 g lateral @ 40 MPH = 106.9'

The most significant response numeric in the context of this study is the maximum sideslip angle, which is a measure of how closely a car points in the direction that it is traveling. It is universally agreed that a high sideslip angle is undesirable to an average driver because it can be disorienting and difficult to recover from in an effective and controlled manner. Another measure of vehicle responsiveness that can be determined from this maneuver is the time constant related to the transition from a steer angle input to a steady-state cornering (trim) condition. This response time is generally considered to be highly observable to a driver and, if excessively long, detrimental to vehicle handling.

As previously noted, trapezoidal steer maneuvers with relatively small steer angle inputs provide valuable information about the linear response properties of a given vehicle configuration, i.e., in the "normal" driving regime where lateral accelerations above 0.2 or 0.3 g are rarely experienced. This subject was discussed in Section 2.5.

Sinusoidal Steer

We again quote from Reference 10 to give an overall understanding of the intent of this handling maneuver:

> "The sinusoidal-steer test is designed to examine the effectiveness with which steering control can produce a lane change, in a limit sense. Whereas, in actual driving, the trajectories required during emergencies result from closure of the control loop by the driver, in this test the intent is to evaluate the resulting loop-closure challenge on the basis of findings obtained in an open-loop testing procedure. Implicit in the use of the sinusoidal steer input is the proposition that, in normal driving, symmetric steering inputs are found to be appropriate for producing a lane change. In an emergency it is hypothesized that the driver loop-closure burden is least when a lane change can be achieved in response to control inputs which are directly extrapolated from those employed in normal driving.
>
> The extent to which the vehicle's response trajectory approximates a lane change is assessed by way of the "lane-change-deviation" measure, Δ. This measure is defined as an

integral error term operating on the time history of lateral displacement, y(t), and is expressed by the following relationship:

$$\Delta = \frac{\int_0^{3.4} |12-y|\, dt}{3.4}$$

Note that the measure as defined has units of feet, representing an average deviation from a desired lateral displacement of 12 ft as determined over the computation time, 3.4 s. This measure is plotted as a function of the amplitude of the sinusoidal steer input to demonstrate the trend of trajectory responses over the range of input levels.

Peak sideslip angle is also computed in this test, and plotted versus steer input amplitude, as well as cross-plotted with the lane-change-deviation measure, Δ. It is hypothesized that driver loop-closure burden is monotonic with both of the variables on the cross-plot such that desirable performance is constituted by data points clustered near the origin."

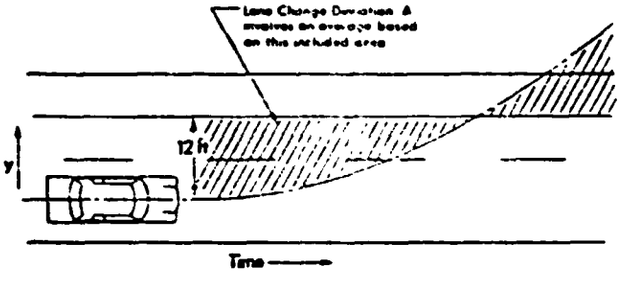

Open loop y(t) time history to sine steer input

This maneuver thus relates to the response of a vehicle to a rapid lane change type of steer input. An ideal response is one in which the steer input produces a lateral displacement of approximately 12 feet and a final heading direction parallel to the original direction. However, real vehicles tend to either "undercorrect" or "overcorrect" resulting in a heading angle deviation from the intended direction; the magnitude of this deviation is another measure of the vehicle's stability and controllability.

The initial speed is 45 MPH and the command steering input (at the front wheels) is defined as a sine wave with a period of 2 seconds and various amplitudes. As normally applied, the maneuver is terminated at 3.4 seconds. The general steer angle time history is illustrated below:

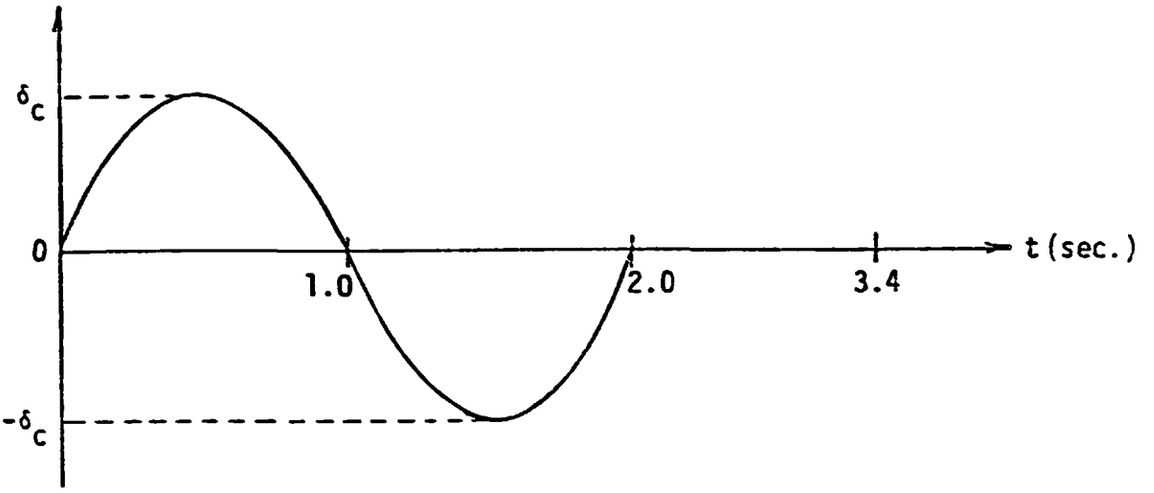

The amplitude of the sine wave (δ_c) is normalized with respect to wheelbase (ℓ) and a reference steer angle (σ) by:

$$\delta_c = \frac{\ell}{10} \quad \sigma$$

The following reference angles were used in the simulations:

$$\sigma = 4, 8, 16^\circ$$

Thus, since wheelbase is equal to 7.86 feet, the actual peak steer angles were:

$$\delta_c = 3.14, 6.29, 12.58^\circ$$

For this maneuver, the conventional evaluation numerics are as follows:

- Lane change deviation defined by

$$\Delta = \frac{1}{3.4} \int_{t=0}^{3.4} |y - 12| \, dt$$

where y is the lateral displacement of the vehicle c.g.

- Maximum sideslip angle (β_p)

- Heading angle at t = 3.4 sec ($\Delta\Psi$)

Braking-in-a-Turn

This maneuver measures the ability of a vehicle to maintain a constant path curvature and a controlled sideslip angle when brakes are applied during a steady-state turn. In an actual test, brake line pressure is monitored and pressures are applied in increments of 100 psi in successive runs until both wheels lock up on either the front or rear axle. However, since brake line pressure/wheel torque data were not available for the base vehicle, a modification to this procedure was employed for the computer simulations; this will be described later.

Reference 10 also provides a summary of this general kind of maneuver, from which we have excerpted the following:

> "The subject maneuver involves an initially curved path whose curvature can change as a result of braking. It is argued that drivers do not apply braking with the intention of affecting a change in directional response. Consequently, an interpretation scheme is needed which comprehensively describes the properties of a turn such that deviations from

the initial turn can be recognized and evaluated. Thus, the data presentation is structured to detect such changes from the initial turning state, which change drivers, in real life, would have to recognize and accompany with a steering correction.

An "ideal" directional response is defined for this maneuver to be a constant path radius (or curvature) trajectory, over which the vehicle maintains a zero or small value of sideslip angle. It is postulated that the "ideal turn," expressed in these terms, represents a comprehensive manner of viewing directional response in this or any turning maneuver.

The sideslip response, β, is felt to be of major safety significance. It seems likely that large sideslip angles, as often occurs under limit-maneuvering conditions, will disorient the driver with respect to the normal view of his vehicle's path, and, further, cause the vehicle to project a larger target for collision in the roadway. The rarity of emergency maneuvering events suggests that driver adaptability under such circumstances must derive from talents other than those attainable from learning (trial and error) experience. Thus, the analog or continuous measurement of sideslip angle and sideslip rate is viewed as representing an error quantity which imposes a monotonically increasing challenge to the human controller as he proceeds to close the loop. Note that the path-curvature measure provides a single quantity characterizing the curvilinear trajectory without introducing any ambiguities in the measure due to a simultaneous sideslip response.

Although the peak value of sideslip angle would be of interest in assessing braking-in-a-turn response, this variable was not computed in view of the poor accuracy that prevails as velocity goes to zero. Nevertheless, in this short-lived maneuver, it is felt that β and $\dot{\beta}$ each reflect the same phenomenon, with β being a substantially more sensitive measure. For example, the $\dot{\beta}$ measure will readily characterize the limit performance of vehicles which exhibit lockup of rear wheels prior to lockup of front wheels. Conversely, locking of front wheels prior to rear wheels is characterized by a loss of path curvature as indicated by a sharp decrease in 1/R. The "ideal" value of normalized path-curvature response, defined as the average value of path curvature ratioed to the initial steady turn value, would be 1.0 indicating that no directional adjustment would be required due to braking."

The initial vehicle condition for this maneuver is defined as a 0.5 g lateral acceleration steady-state turn at 40 MPH. For a given vehicle

configuration, the front wheel steer angle corresponding to this cornering condition was determined from results of the trapezoidal (steady state) steering simulations performed previously. We also obtained the body roll angle and slip angle for a 0.3 g turn at 40 MPH, from the previous simulations.

The general braking torque input time history is illustrated below:

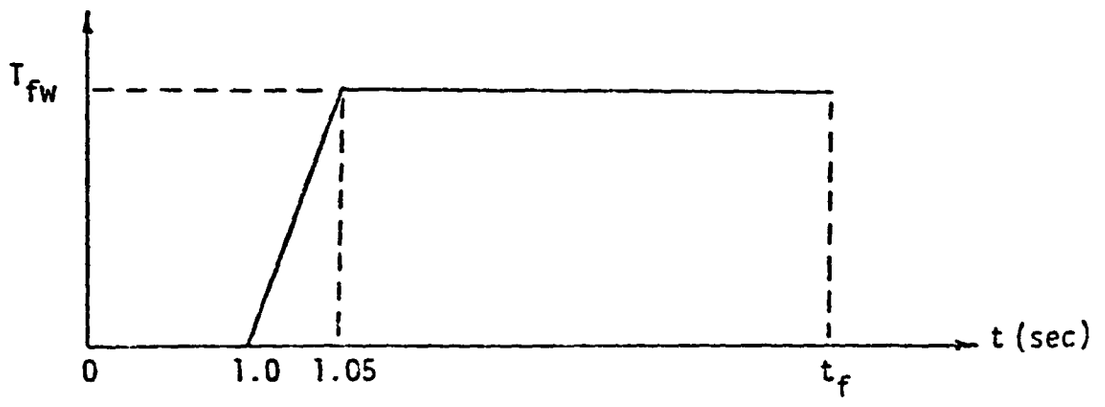

where a stabilizing interval from zero to 1.0 second is provided to insure that the vehicle is in equilibrium before the brakes are applied and:

T_{fw} = torque applied to the front wheels

t_f = time when the vehicle comes to a halt

To determine the magnitude of front wheel braking torque applied, we first assumed that the rear wheel torques were proportional to the front wheel torques as follows:

$$T_{rw} = \gamma T_{fw}$$

where γ is the proportioning constant of the base car braking system (0.67). From the steady-state steering simulations, the normal force was known for each wheel under the 0.3 g turn condition at 40 MPH. Also known were the

deflected tire radii. This allowed calculation (forward weight transfer was also considered) of the minimum wheel torque that causes lockup of the front and/or rear wheels, i.e.,

$$T_{fw} = \min \left\{ \mu F_1 R_1, \ \frac{\mu F_2 R_2}{\gamma} \right\}^*$$

where

γ = coefficient of friction (0.75 was used)

F_i = normal forces of each wheel

R_i = deflected tire radii

$$i = \begin{cases} 1 \text{ refers to the left front wheel}^* \\ 2 \text{ refers to the left rear wheel} \end{cases}$$

These simulation runs were made for each configuration. The first run was performed with the braking torques corresponding to the lockup condition at either the front or rear axle as discussed above. Subsequent runs were made at 75% of lockup torque and 50% of lockup torque.

The standard evaluation numerics for this maneuver are as follows:

- Average deceleration as defined by:

$$(a_x)_{ave} = \frac{1}{t_{10}-1} \int_{t=1}^{t_{10}} a_x \, dt$$

where

t_{10} is the time when forward speed reaches 10 MPH.

*Assuming a turn to the right, which increases loads on the left side wheels. Both wheels on an axle will generally lock if the outside wheel locks, due to the weight transfer.

- Average path curvature ratio as defined by:

$$R_o \left(\frac{1}{R} \right)_{ave}$$

where

$$\left(\frac{1}{R} \right)_{ave} = \int_{t=1}^{2} \left(\frac{1}{R} \right) dt$$

R_o = path curvature at t = 1 second

- Maximum absolute value of sideslip angle (β_p)
- Maximum absolute value of rate of change of sideslip angle ($\dot{\beta}_p$)

2.5 Results of Trapezoidal Steer Simulations

This maneuver was described in the previous section. Briefly, a steer angle is rapidly applied and held at a constant angle thereafter. This results in a sudden change from a stable forward motion to a cornering condition at varying degrees of severity. Normalized steer inputs ranging from 2° to 24° were applied to the front wheels at a speed of 40 MPH. The normalization approach relates the steer angle to a standardized vehicle with a 10' wheelbase; actual front wheel input steer angles ranged from 1.57° (σ = 2°) to 18.86° (σ = 24°). Figure 12 typifies trajectories that result from such control inputs for several representative steer angles, where sequential positions of the subject vehicle (at 0.5 sec. intervals) are shown in true perspective from an overhead "camera" in these computer-generated graphics.

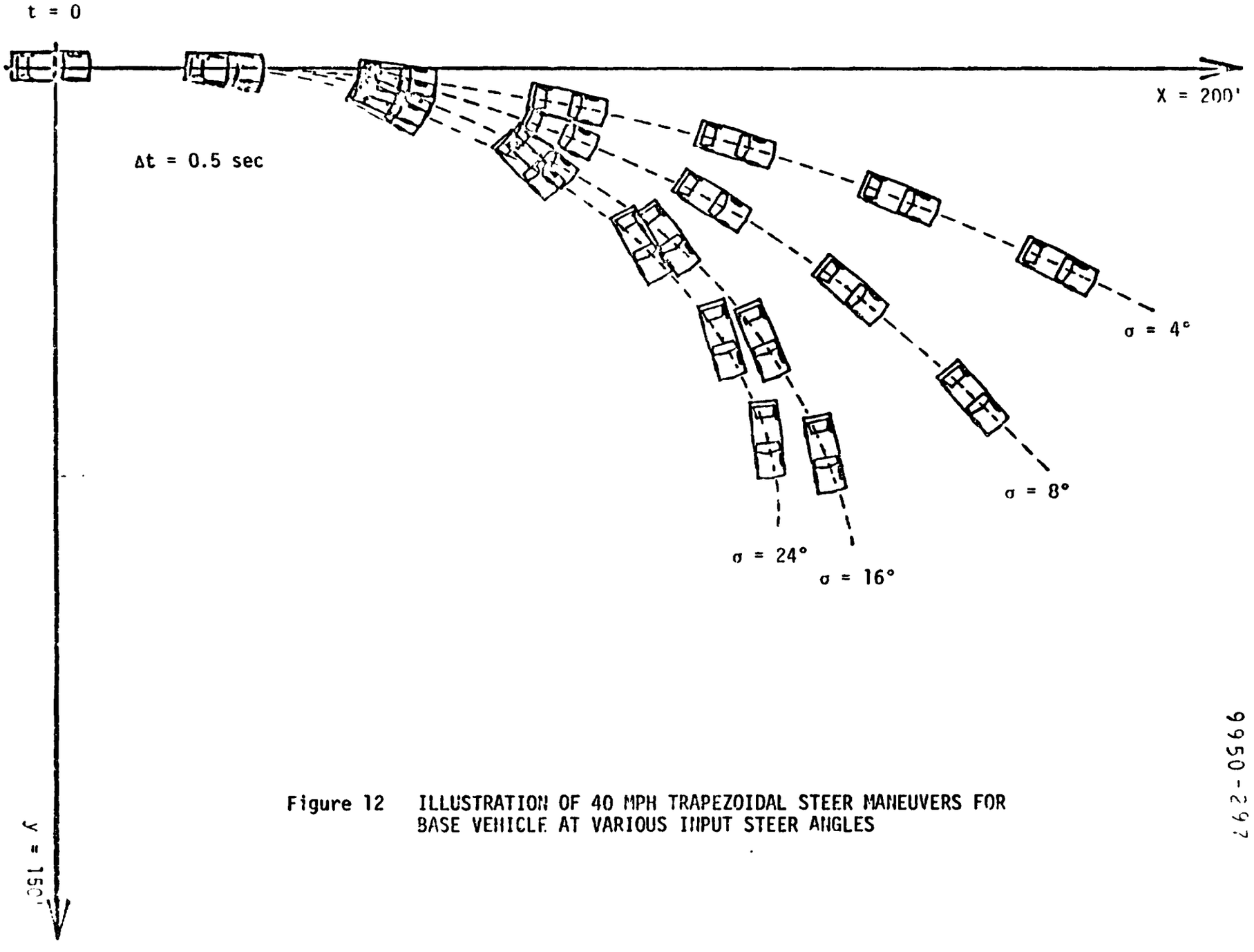

Figure 12 ILLUSTRATION OF 40 MPH TRAPEZOIDAL STEER MANEUVERS FOR BASE VEHICLE AT VARIOUS INPUT STEER ANGLES

Figures 13 through 20 show trajectory graphics for each of the electric vehicle configurations compared with the base vehicle responses for two normalized steer angle inputs, 4° and 16°. For these comparisons, the base car was equipped with the same radial tires as the EV's (BR78-13) for direct comparisons without potential differences due to tire property variations.

For the smaller steer angle (σ = 4°), the trajectories are very similar except, in some cases, where the EV's take a wider path. This is not particularly important, however, since a slightly higher steer angle would tighten up the EV trajectories (more curvature in steady-state turn).

A significant effect is apparent for the larger steer angle (σ = 16°) trajectories for several of the EV configurations. Note the extremely high sideslip angles corresponding to the AiResearch Drive, 2/3 - 1/3 Battery Split configuration (Figure 16), the GE Drive, Tunnel Battery configuration (Figure 17), the AiResearch Drive, Tunnel Battery configuration (Figure 18), and the Mars II configuration (Figure 19).

Maximum values of sideslip angle for each of the vehicle configurations are quantitatively given in Figures 21 and 22 as a function of the normalized steer angle. An interesting observation is that those configurations exhibiting the higher sideslip angles are all rear-heavy (refer back to Table 2). It is believed that sideslip angles for the vehicles noted above (in the 30° to 50° peak magnitude range) are excessive and clearly undesirable.

Figures 23 and 24 are plots of peak sideslip rate ($\dot{\beta}$) versus normalized path curvature ratio. The baseline performance boundary shown in the figure was defined from actual tests of a group of twelve real passenger cars with widely varying properties (Ref. 10). In view of this comparison, the EV configurations may not be particularly unusual, but nevertheless demonstrate undesirable behavior in the instances discussed above. Recall from Section 2.4 that this plot indicates the "price" (in terms of side slip angle) that is "paid" to achieve a given magnitude of path curvature.

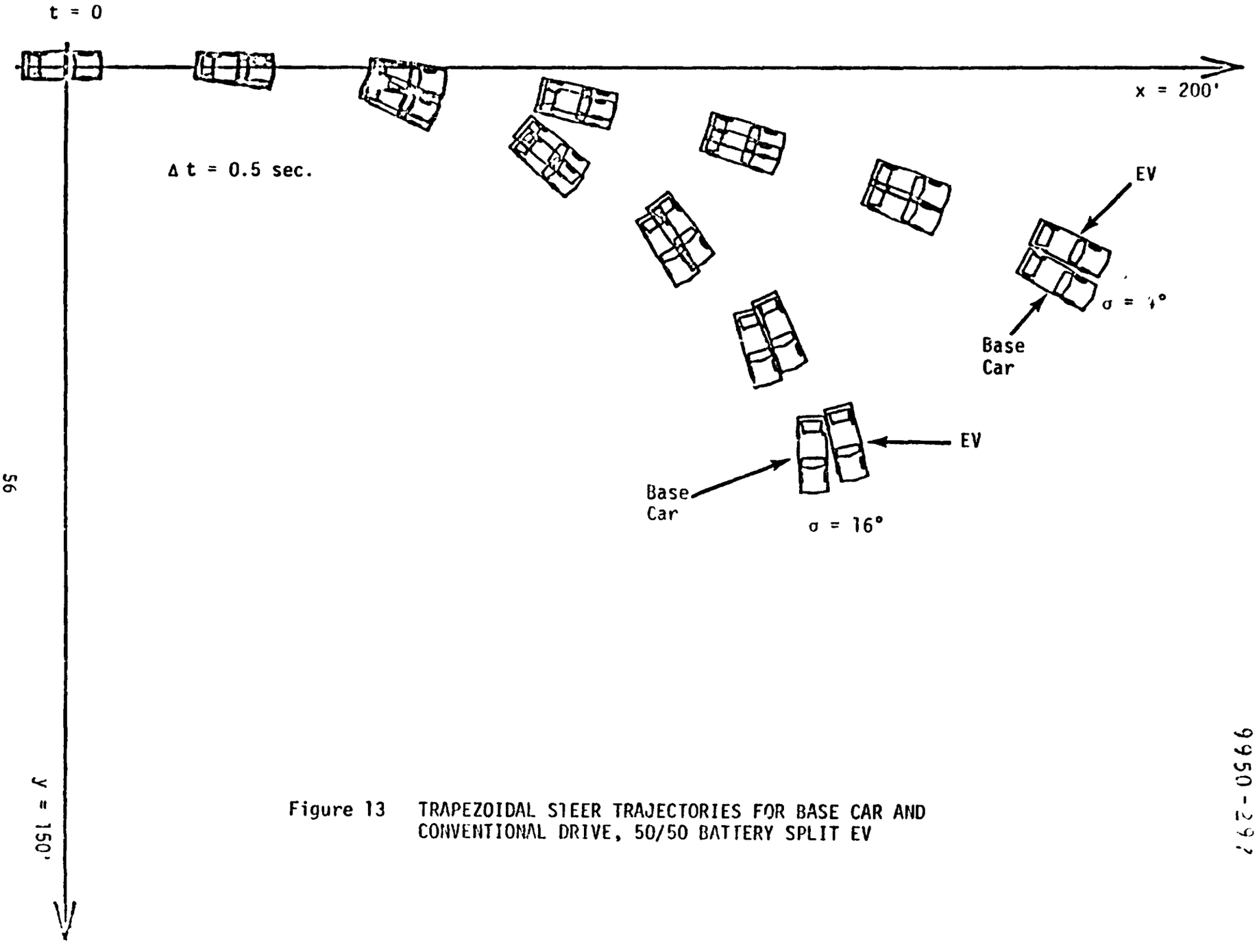

Figure 13 TRAPEZOIDAL STEER TRAJECTORIES FOR BASE CAR AND CONVENTIONAL DRIVE, 50/50 BATTERY SPLIT EV

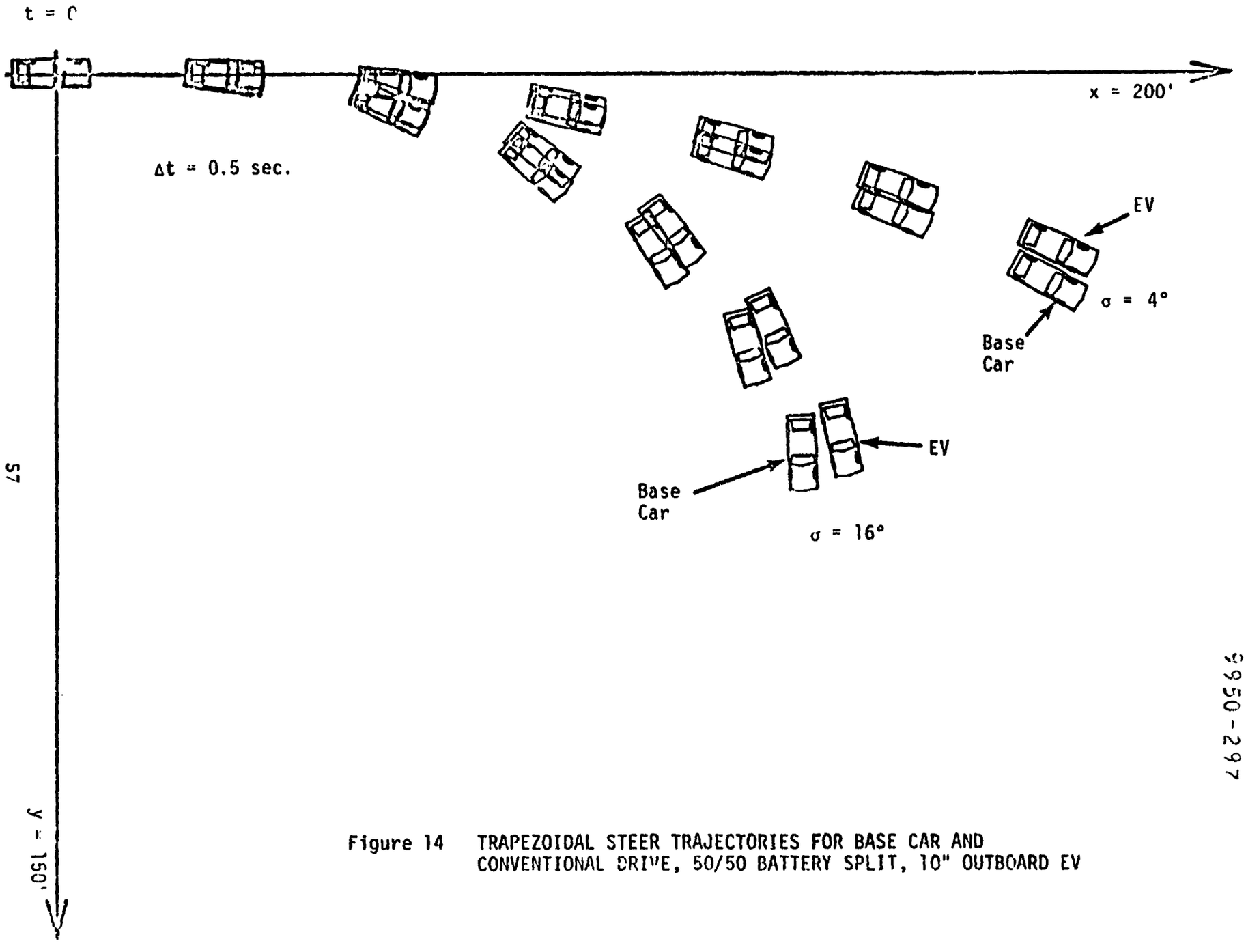

Figure 14 TRAPEZOIDAL STEER TRAJECTORIES FOR BASE CAR AND CONVENTIONAL DRIVE, 50/50 BATTERY SPLIT, 10" OUTBOARD EV

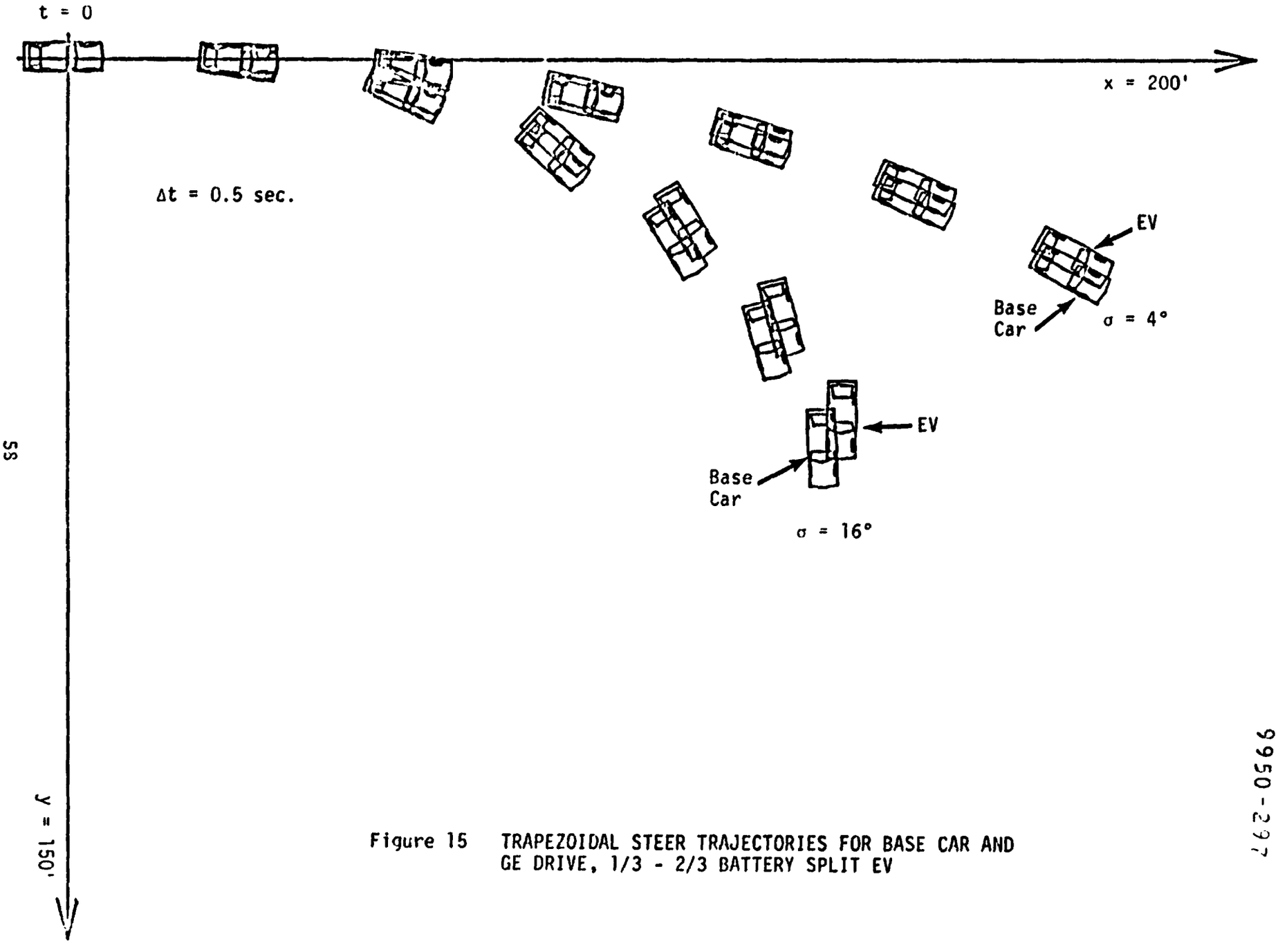

Figure 15 TRAPEZOIDAL STEER TRAJECTORIES FOR BASE CAR AND GE DRIVE, 1/3 - 2/3 BATTERY SPLIT EV

9950-297

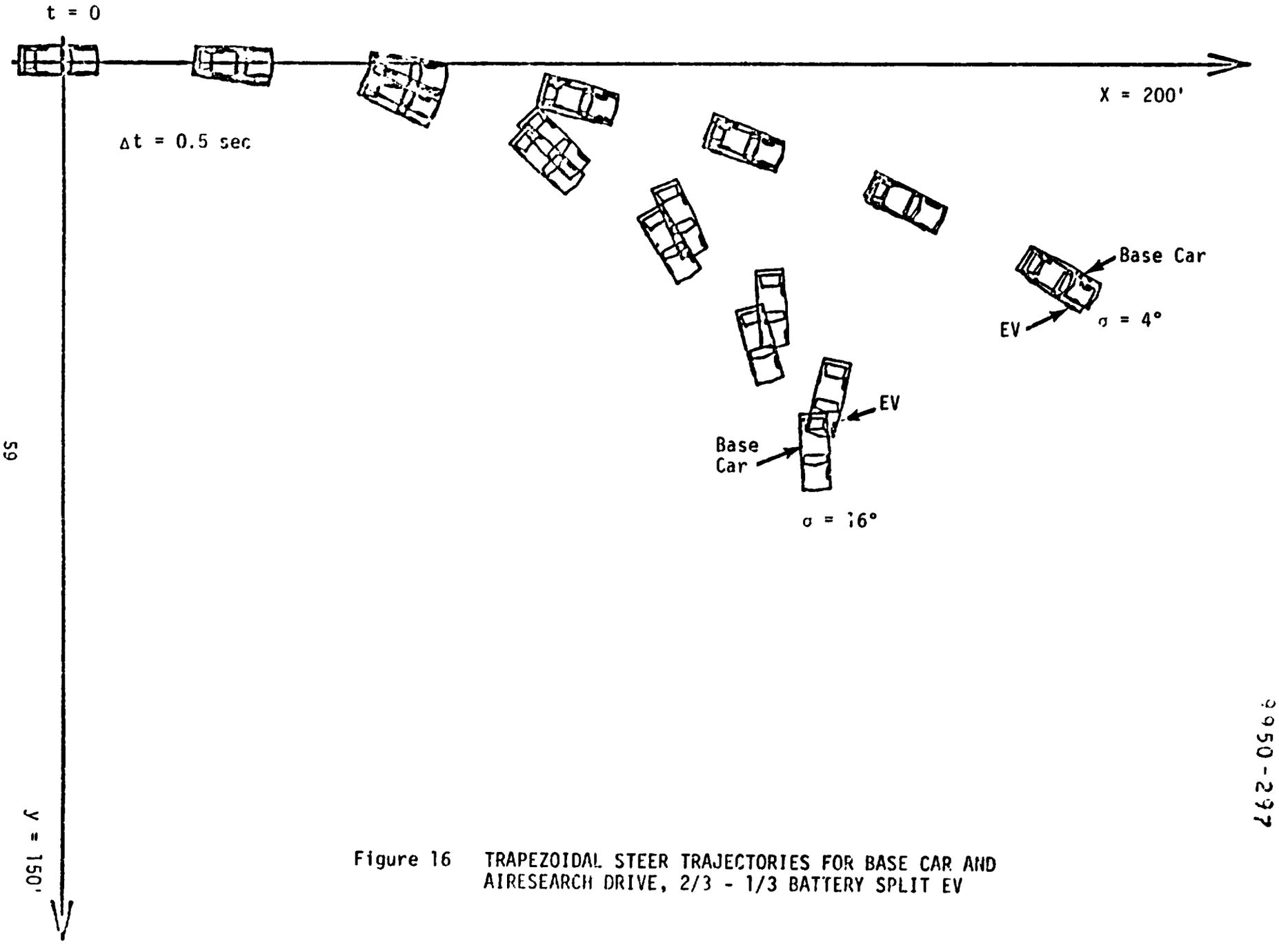

Figure 16 TRAPEZOIDAL STEER TRAJECTORIES FOR BASE CAR AND AIRESEARCH DRIVE, 2/3 - 1/3 BATTERY SPLIT EV

Figure 17 TRAPEZOIDAL STEER TRAJECTORIES FOR BASE CAR AND GE DRIVE, TUNNEL BATTERY EV

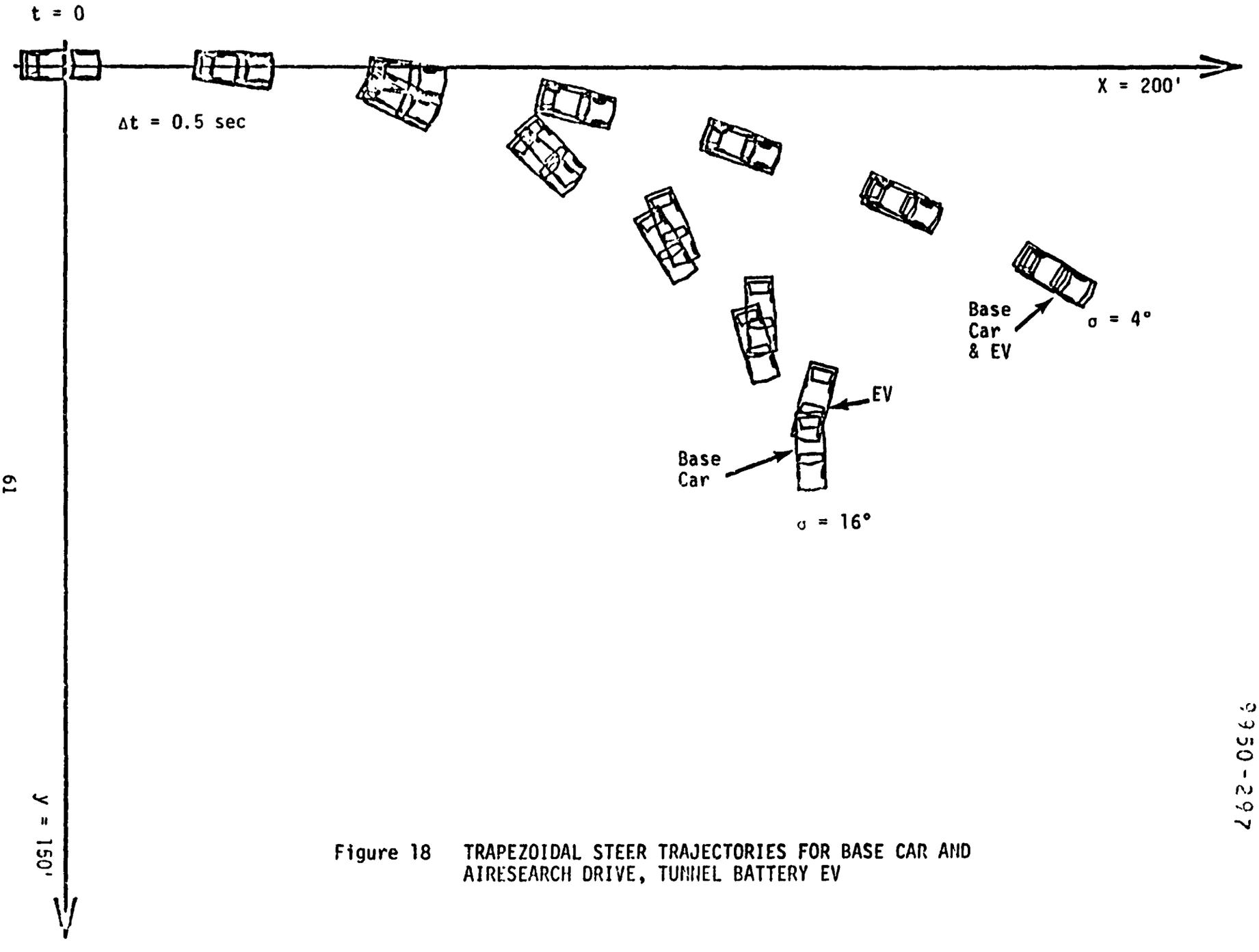

Figure 18 TRAPEZOIDAL STEER TRAJECTORIES FOR BASE CAR AND AIRESEARCH DRIVE, TUNNEL BATTERY EV

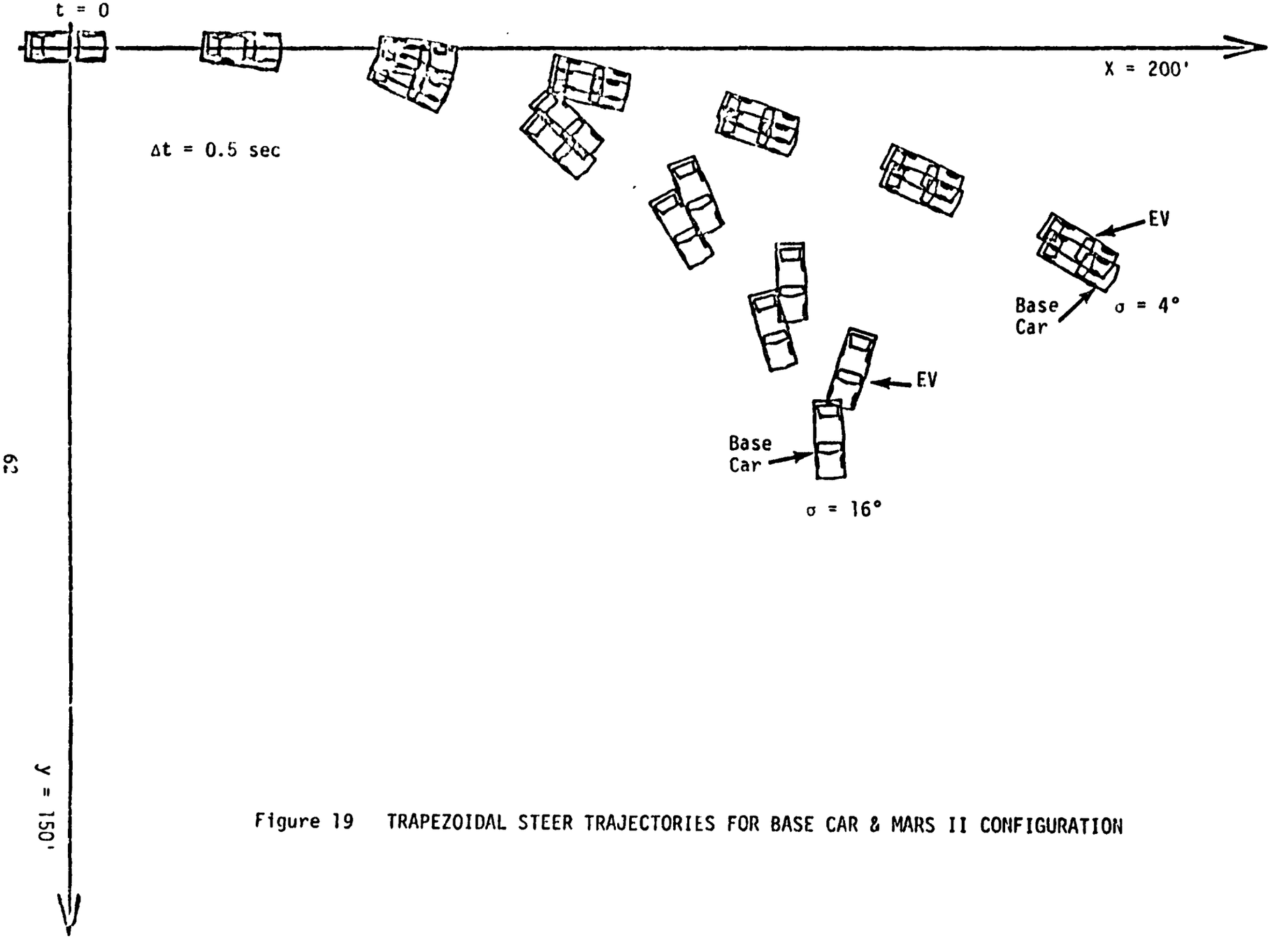

Figure 19 TRAPEZOIDAL STEER TRAJECTORIES FOR BASE CAR & MARS II CONFIGURATION

9950-297

Figure 20 TRAPEZOIDAL STEER TRAJECTORIES FOR BASE CAR AND FRONT HEAVY, HIGH INERTIA CONFIGURATION

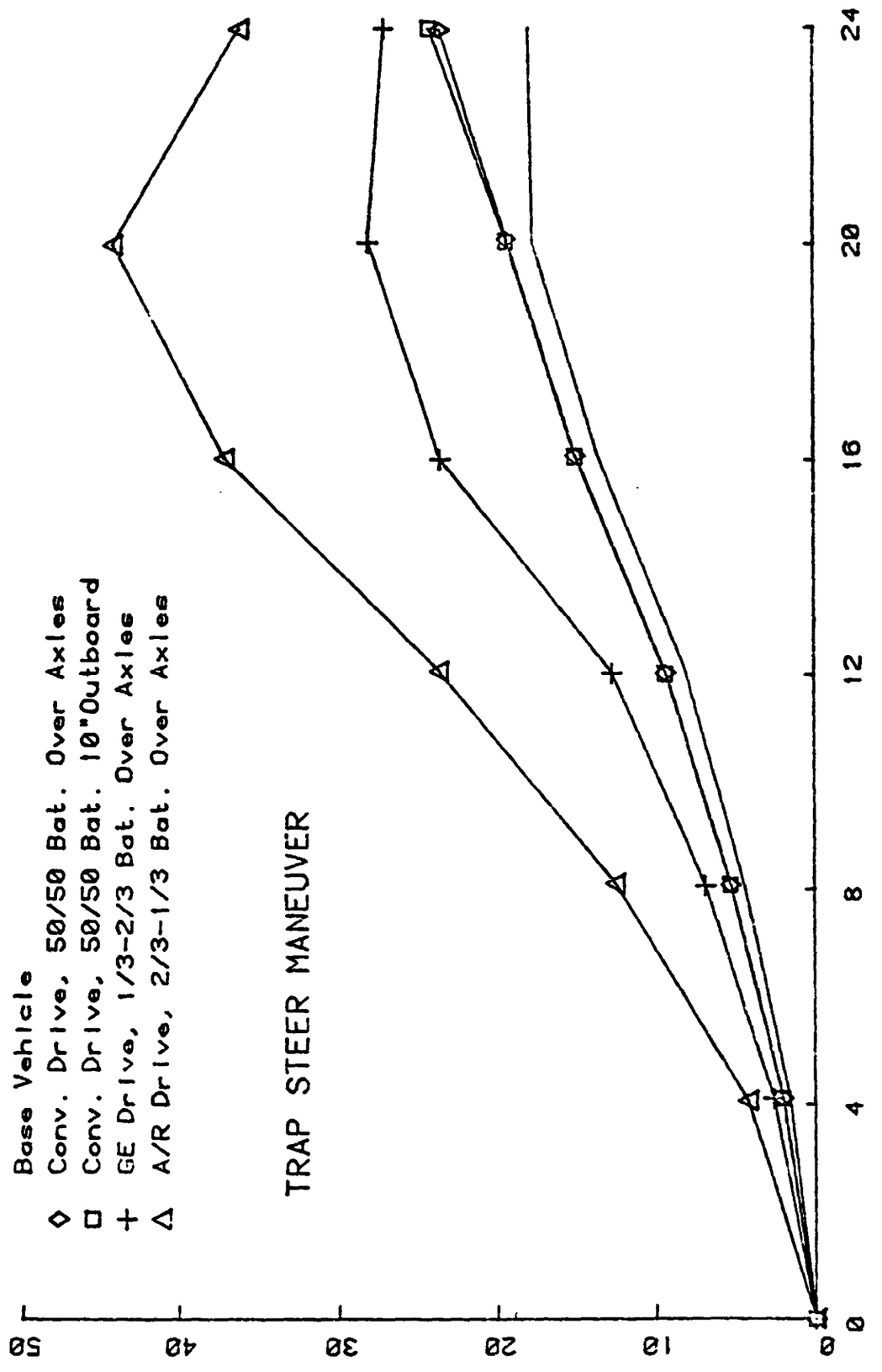

Figure 21 PEAK SIDESLIP ANGLES FOR TRAPEZOIDAL STEER MANEUVER

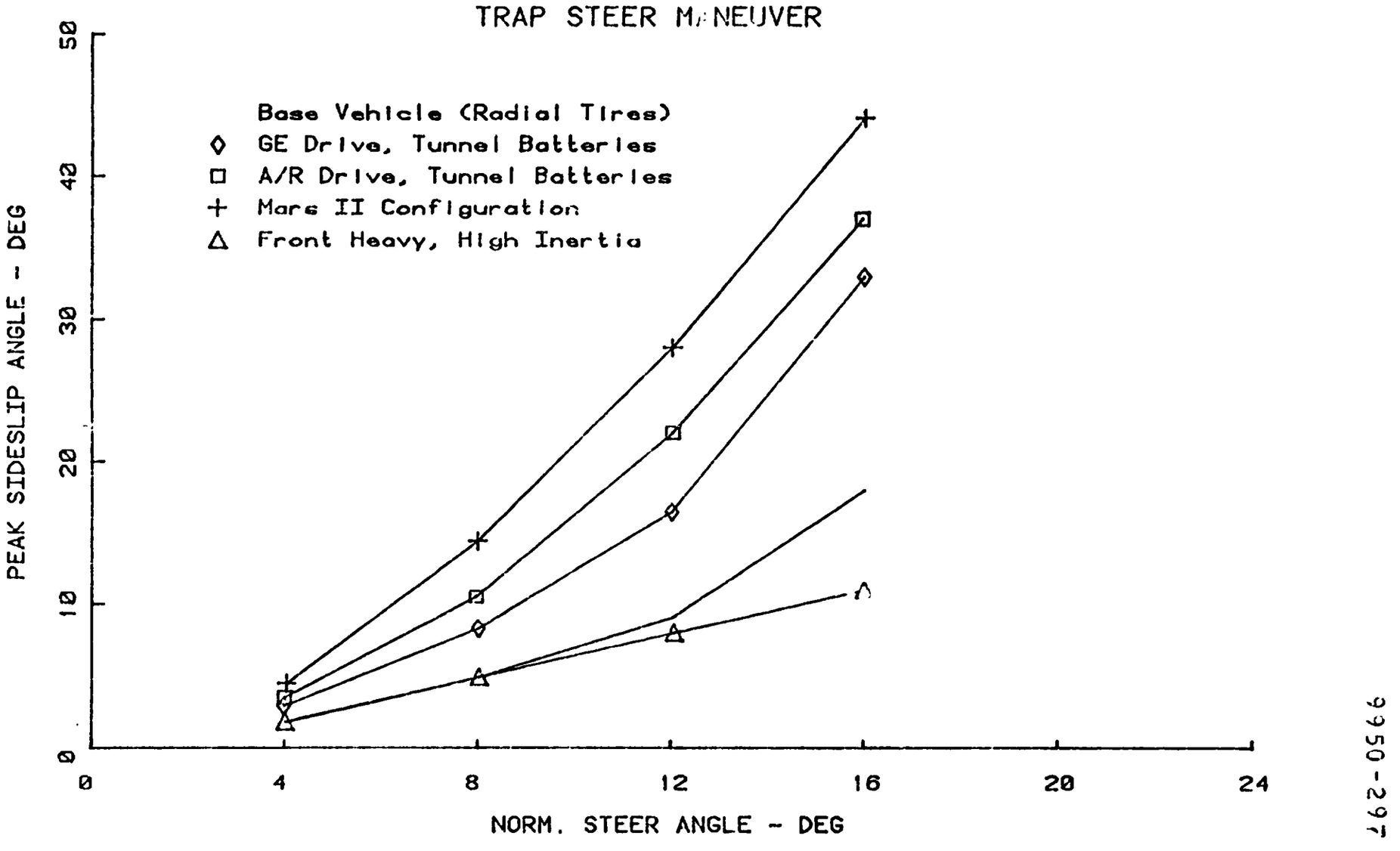

9950-297

Figure 22 PEAK SIDESLIP ANGLES FOR TRAPEZOIDAL STEER MANEUVERS

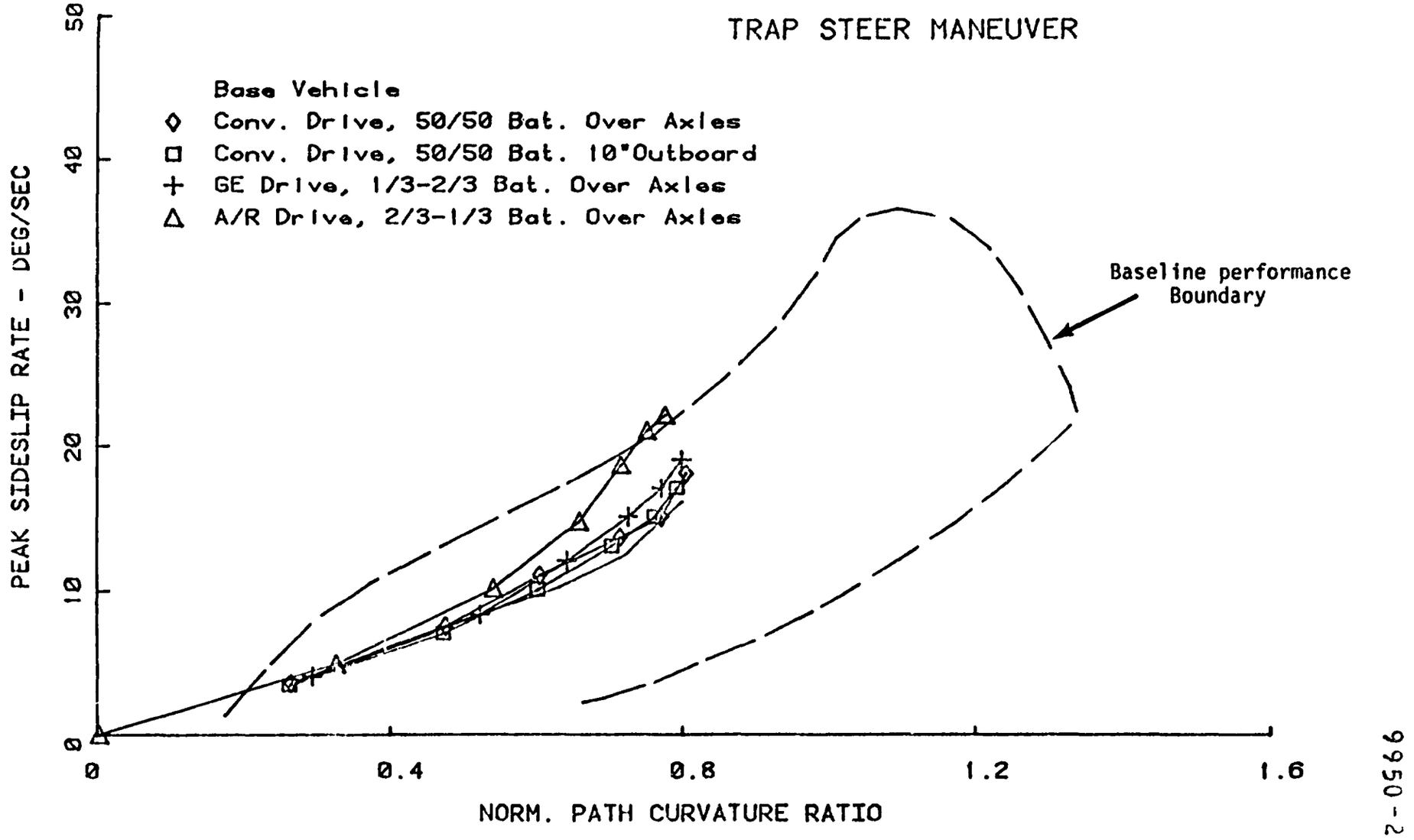

9950-297

Figure 23 COMPARISON OF TRAPEZOIDAL STEER RESULTS RELATED TO SIDESLIP RATE AND PATH CURVATURE

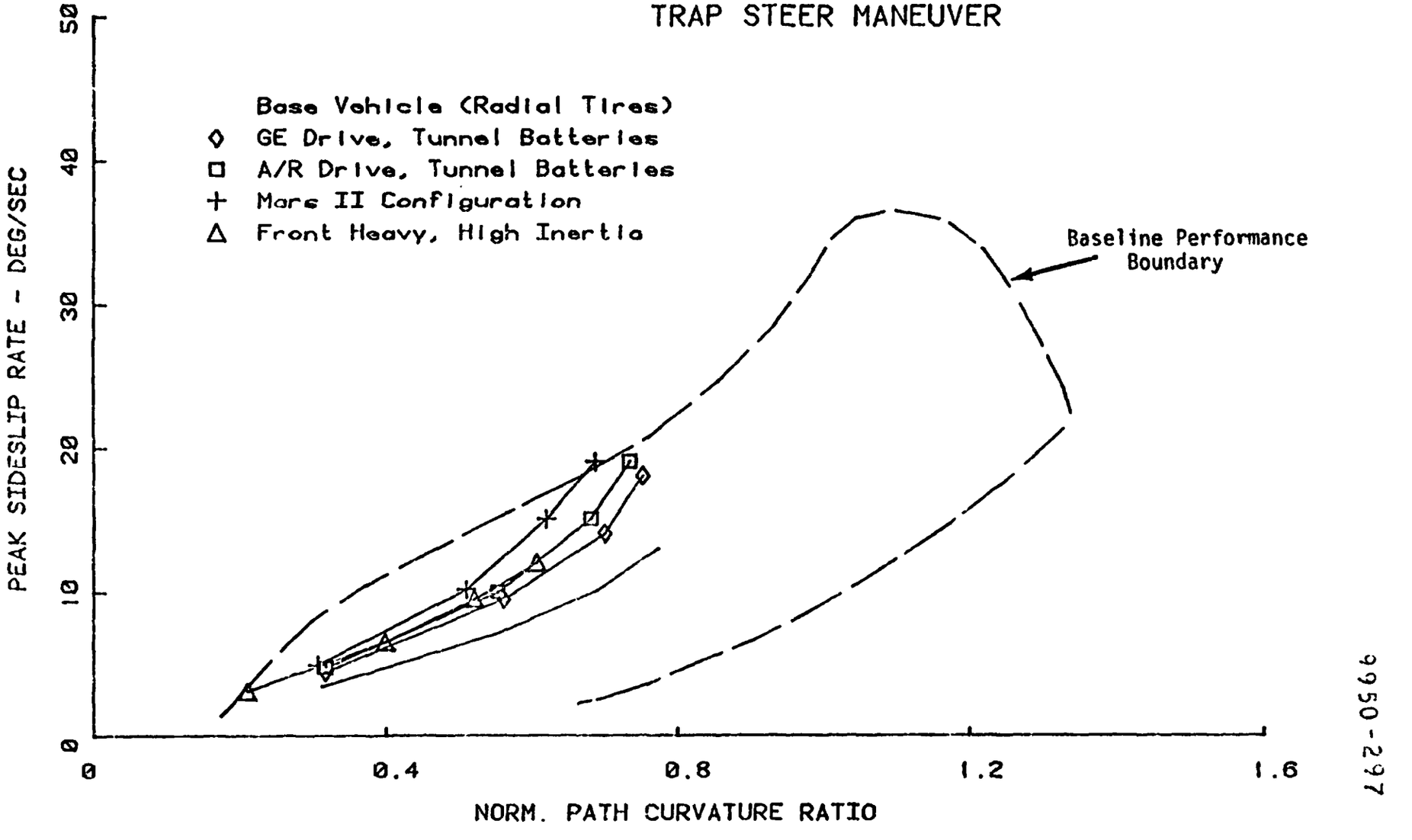

Figure 24 COMPARISON OF TRAPEZOIDAL STEER RESULTS RELATED TO SIDESLIP RATE AND PATH CURVATURE

A relatively high path curvature ratio (small radius) without excessive sideslip is clearly preferable. Vehicle configurations exhibiting curves in Figures 23 and 24 which approach (or cross) the upper boundary line therefore are likely to perform poorly in this maneuver. Again, these suspect configurations are all rear-heavy.

Another aspect of the trapezoidal steer maneuver that is particularly important relates to response time constants, i.e., yaw rate (velocity) response time (T_r) and lateral acceleration response time (T_a). These response measures were discussed in the section dealing with linear response theory of simplified vehicle models (Section 2.3). Yaw rate time constant is defined (as used in this study) in Figure 25, and pertains to the time duration between the mid-point of steer input and the point in time when 90% of the steady-state value of the response variable is reached. Lateral acceleration time constant is defined in the same manner.

Figures 26 and 27 are plots of yaw velocity time constants for all configurations as functions of steady-state lateral acceleration. Note that the base car exhibits the shortest yaw velocity response time (on the order of 0.2 sec). With a few exceptions in the high lateral acceleration range, the EV configurations generally produce longer duration response times. This is particularly true for the AiResearch Drive, 2/3 - 1/3 Battery Split and Mars II configurations, which are in the 0.35 sec. range.

Similar trends are evident for the EV's when lateral acceleration response time is considered in Figures 28 and 29. Note that these time constants are generally double the corresponding yaw response times. The Mars II configuration has a response time exceeding 0.8 sec; this is consistent with lateral acceleration response duration actually measured with this vehicle and found to be clearly excessive, resulting in sluggish response to steer inputs (Ref. 1). Although there is no known published information regarding subjective determination of the maximum acceptable values, it is doubtful that lateral acceleration response times longer than about 0.5 sec. would be found acceptable by most drivers. Thus, many of the EV's are likely

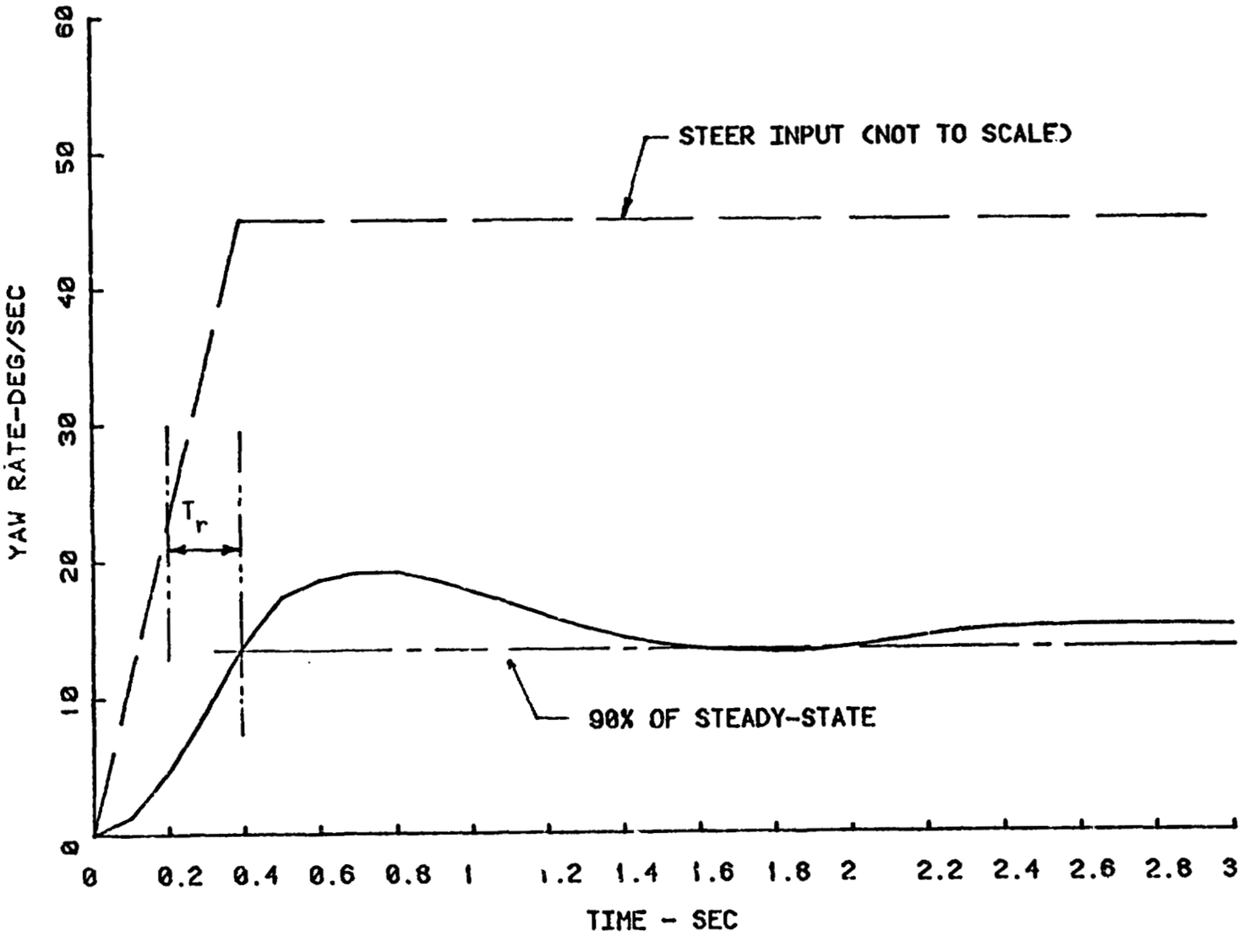

Figure 25 DEFINITION OF TIME CONSTANTS BASED ON SIMULATION RESULTS

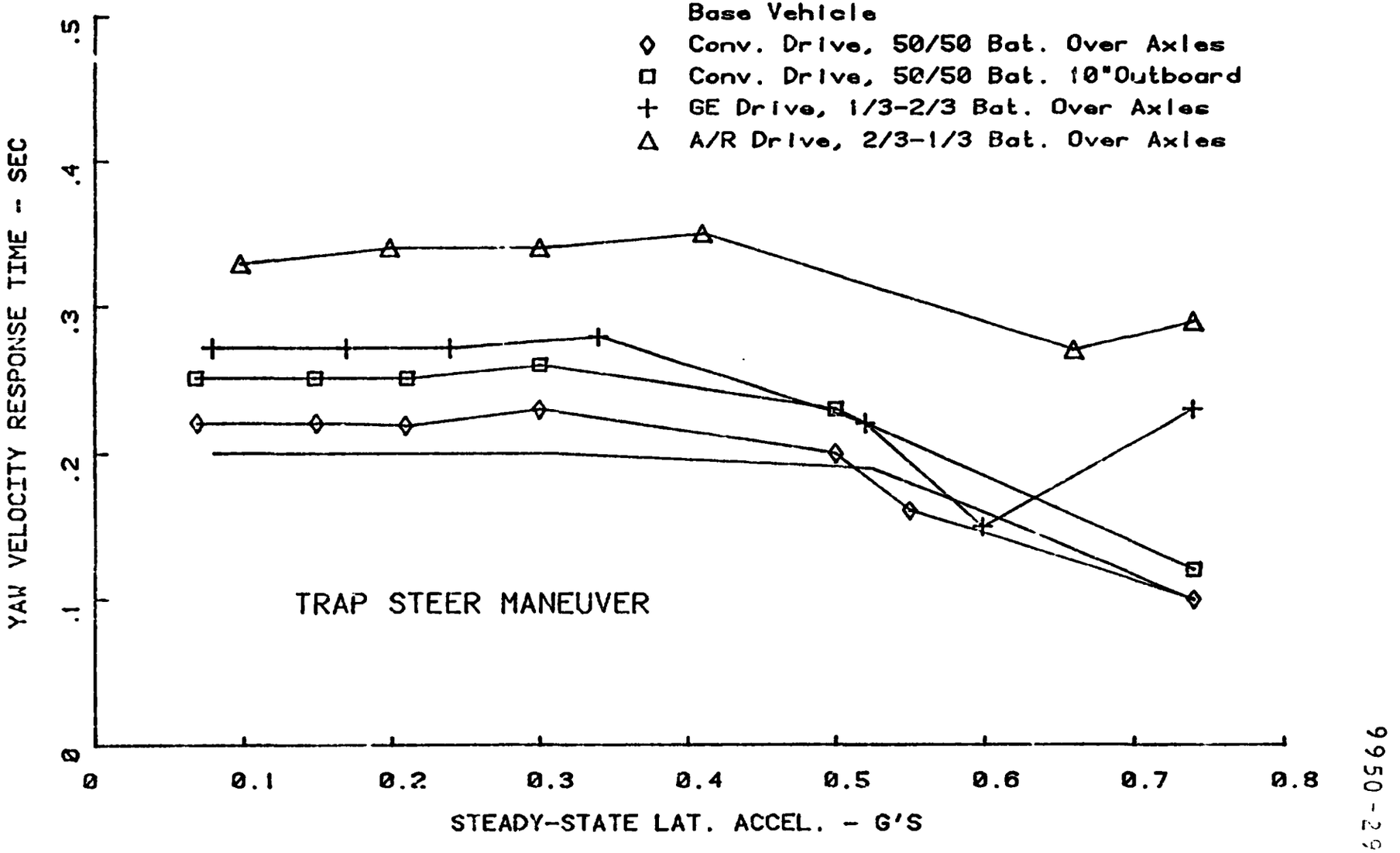

Figure 26 YAW VELOCITY TIME CONSTANTS

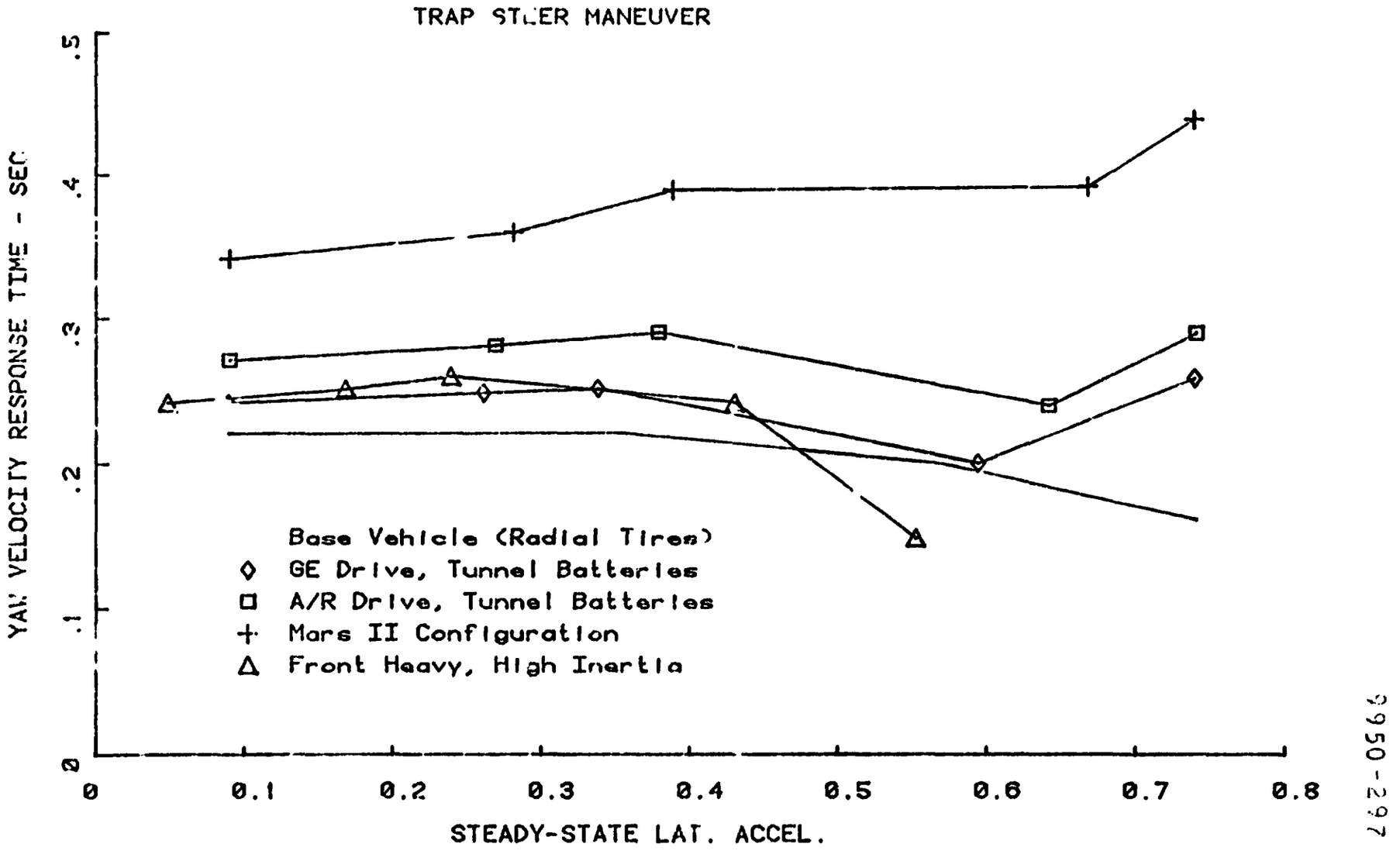

Figure 27 YAW VELOCITY TIME CONSTANTS

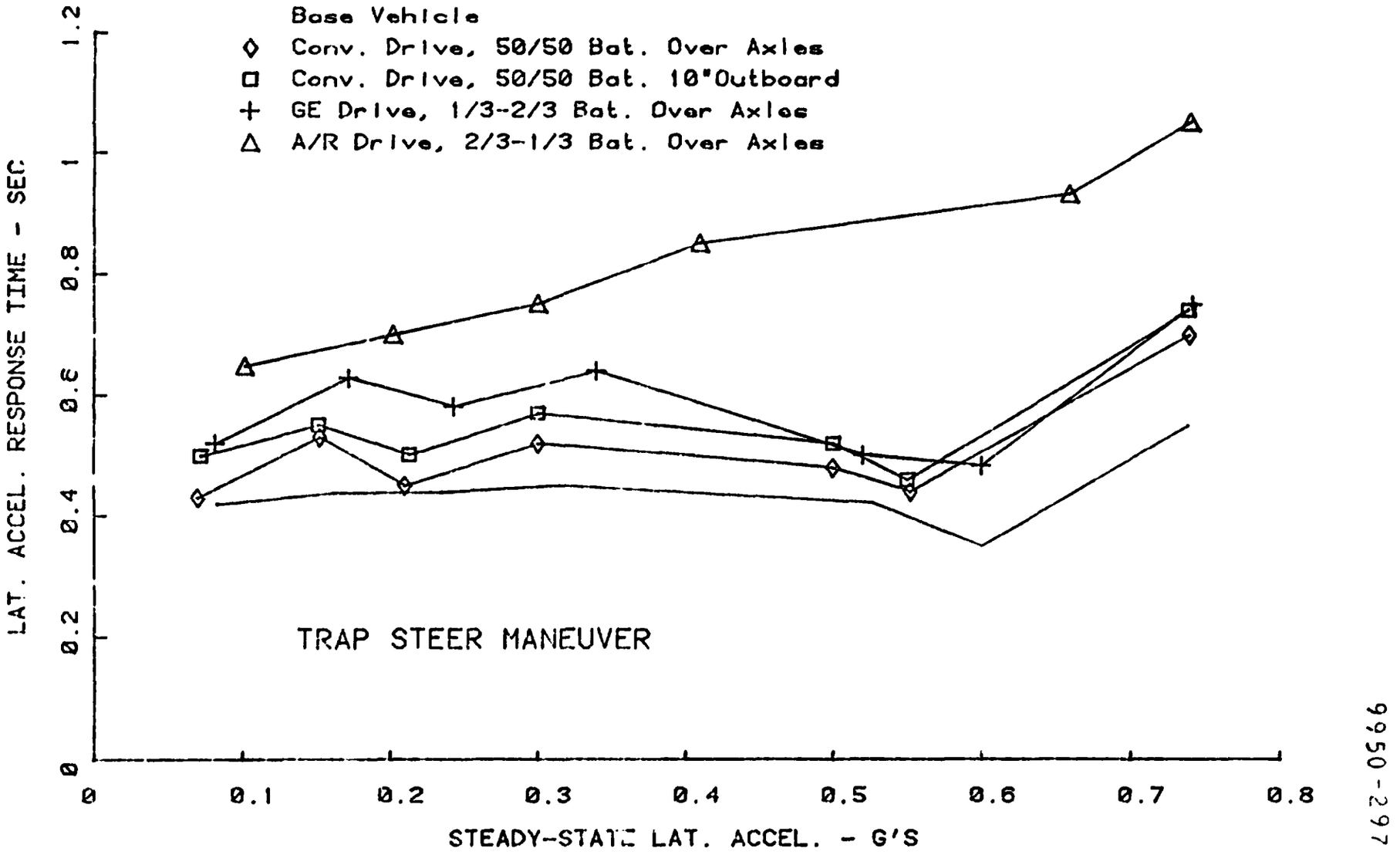

9950-297

Figure 28 LATERAL ACCELERATION TIME CONSTANTS

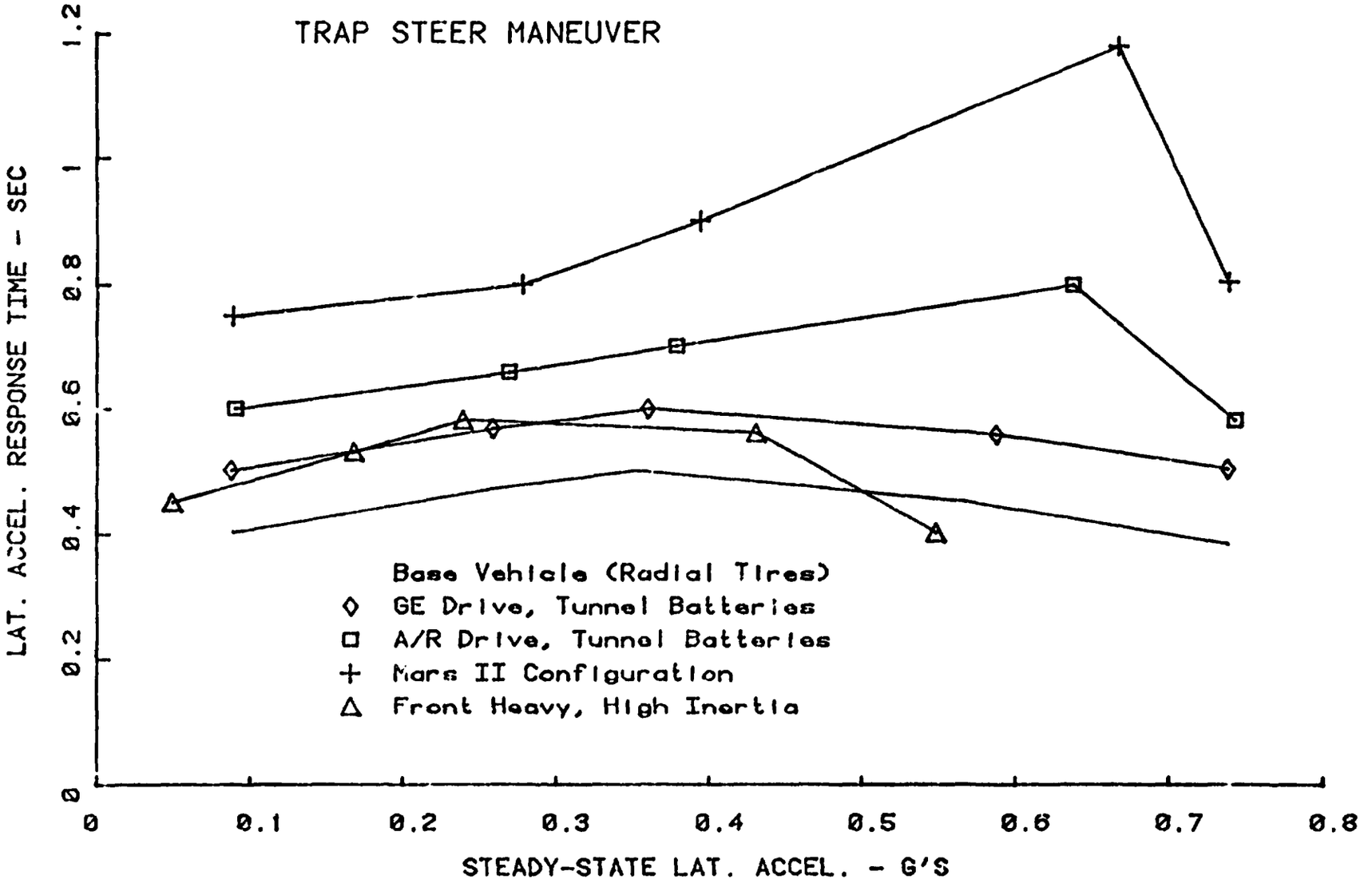

Figure 29 LATERAL ACCELERATION TIME CONSTANTS

to be poor responding configurations, particularly the two AiResearch Drive configurations, the GE Drive, 1/3 - 2/3 Battery Split configuration, and the Mars II. This finding will be explored more fully in Section 2.8.

As pointed out previously, results of the trapezoidal steer maneuver for low steer angles which result in steady-state lateral accelerations below about 0.3 g provide information relating to linear performance characteristics. Linear response theory was explored from a theoretical viewpoint (using rather simple mathematical models) in Section 2.3. Several numerics are of particular interest as listed below:

- K - Understeer gradient
- $\frac{\partial a_y}{\partial \delta}$ - Lateral acceleration gain
- $\frac{\partial r}{\partial \delta}$ - Yaw rate gain
- $\frac{\partial \Phi}{\partial a_y}$ - Body roll angle sensitivity
- $\frac{\partial \beta}{\partial a_y}$ - Body slip angle sensitivity
- T_r - Yaw rate time constant
- T_a - Lateral acceleration time constant

Table 7 contains values obtained for each of these linear properties for the vehicle configurations examined by computer simulation (HVOSM results). The understeer factor, lateral acceleration gain and yaw rate gain, as listed in the table, were calculated from the HVOSM output based on a reference steer angle. In this program, reference steer angle was defined as the steering wheel angle divided by the overall steering gear ratio.* This

*This definition is consistent with the SAE Reference Steer Angle.

Table 7

LINEAR PROPERTIES OF VEHICLES BASED ON SIMULATION RESULTS

No.	Vehicle Configuration	K (deg/g)	$\partial a_y/\partial \delta$ (g/deg)	$\partial r/\partial \delta$ (deg/sec/deg)	$\partial \phi/\partial a_y$ (deg/g)	$\partial \beta/\partial a_y$ (deg/g)	Tr (sec)	Ta (sec)
1	Base Car (bias-ply tires)	5.8	0.10	3.2	6.5	4.5	0.20	0.44
2	Base Car (radial tires)	4.9	0.11	3.5	6.5	4.1	0.23	0.45
3	Conv. Drive, 50/50 Batteries	6.9	0.09	2.9	7.8	6.2	0.22	0.48
4	Conv. Drive, 50/50, 10" Outboard	6.9	0.09	2.9	7.8	6.2	0.25	0.52
5	GE Drive, 1/3-2/3 Batteries	5.8	0.10	3.2	7.5	6.7	0.27	0.58
6	A/R Drive, 2/3-1/3 Batteries	3.5	0.13	4.2	8.0	8.2	0.34	0.70
7	GE Drive, Tunnel Batteries	4.9	0.11	3.5	6.5	6.7	0.25	0.53
8	A/R Drive, Tunnel Batteries	4.6	0.11	3.7	6.8	7.7	0.28	0.63
9	Mars II Configuration	4.2	0.12	3.8	7.8	9.3	0.35	0.75
10	Front Heavy, High Inertia	8.9	0.08	2.5	7.9	6.7	0.26	0.58

reference steer angle would equal the front wheel steer angles if no Ackerman geometry, ride steer or compliance steers were considered.

Note that the two Conventional Drive configurations, which have different yaw moments of inertia due to longitudinal battery location differences, have identical control gains and sensitivities. This points that inertial properties do not have a direct influence on these particular properties because they are based on steady-state behavior (no transient effects are considered). Response times are exceptions because these are functions of the duration of the time interval before a steady-state condition is attained; time constants given in Table 7 were computed by averaging times from two or three simulations of the trapezoidal steer maneuver in the linear response range (refer back to Figures 26 through 29 and note time constants for lateral acceleration below 0.3 g).

From the table, the understeer gradient (K) is seen to vary between 3.5 and 8.9; all values are positive indicating that all configurations are understeering vehicles in the linear range. Passenger cars generally have understeer gradients in the range from 2 to 10, and values exceeding 5 or 6 are generally considered to be somewhat high. Of primary importance, however, is that vehicles indeed be understeer ($K > 0$), as is the case for all the configurations considered. In addition, the amount of understeer can be tailored by making suspension and steering system adjustments. This will be explored further in Section 2.9.

Lateral acceleration gains ($\partial a_y/\partial\delta$) are about the same for all the vehicle considered. Similarly, yaw rate gains ($\partial r/\partial\delta$) are generally quite close for all configurations. Again, these properties can be adjusted by suspension and/or tire changes. Or they can be compensated for by selecting an appropriate steering ratio so that acceptable gains related to steering wheel input angle are obtained.

Roll angle sensitivity ($\partial\phi/\partial a_y$) is found to be essentially constant for all configurations. This is not surprising since c.g. heights do not

vary dramatically for the configurations defined. and spring rates were selected based upon axle loadings to give equivalent ride heights. In any event, these values are probably quite reasonable and comparable to many production passenger cars. High performance cars have somewhat higher roll stiffness and associated roll angle sensitivities in the 3 to 6 deg/g range.

Sideslip angle sensitivity is seen to vary widely between the various configurations, ranging from 4.1 deg/g for the base car (with radial tires) to 9.3 deg/g for the Mars II configuration. It is desirable to maintain sideslip angle sensitivity as low as possible; a value of about 2 deg/g is considered to be excellent by some handling experts. Magnitudes above 5 or 6 deg/g are probably quite excessive. Note that several of the EV configurations exceed this range.

Lateral acceleration response times range from 0.44 sec. to 0.75 sec. Values exceeding 0.5 sec. are believed to indicate particularly poor performance: a very responsive car would have a lateral acceleration response time on the order of 0.25 sec. It is therefore concluded that several of the EV configurations have excessive response times related to lateral acceleration as is apparent from Table 7

Yaw velocity response times range from 0.20 sec. for the base car to 0.35 sec. for the Mars II. A crisp handling car is believed to generally have a yaw velocity response time in the neighborhood of about 0.10 to 0.20 sec. Response times in excess of 0.25 sec. are believed to be undesirable. The Mars II was found to possess highly excessive response time based on experimental testing, and the value obtained from the simulation study is generally consistent with the experimental results. Note that the AiResearch Drive, 2/3 - 1/3 Battery Split configuration has a yaw velocity response time nearly as high as the Mars II (0.34 sec.) and must thus be considered to be equally unacceptable.

Some theoretical and experimental work has been done in an attempt to relate yaw velocity response time to subjective evaluation

of a vehicle's handling qualities (Ref. 8). Based on this work, a domain of acceptability has been established for yaw rate gain as a function of response time as was discussed and applied to vehicle configuration evaluation in Reference 11. However, it must be pointed out that this domain of acceptability is not strictly nor sharply defined -- the bounds represent gray areas where there is no clear consensus as to whether a vehicle handles acceptably or not. In fact, studies have shown that these bounds change with driver skill. Furthermore, there is some question as to the appropriate time constant to be used in this evaluation. Time constants that have been used in the past include calculations based on simplified linear theory relationships, fits of a simplified dynamics model to experimental results, and values based on a 45° phase lag between a sinusoidal steer input and yaw response output.

We have chosen to use the 90% yaw velocity time constant as previously defined and listed in Table 7 for use in this evaluation procedure because it is easily obtainable from experimental results and thus could provide a direct comparison should experimental electric vehicle handling programs be undertaken.

Results from Table 7 are indicated on Figure 30, and show the relationship of the various vehicle configurations considered with respect to each other and the bounds of acceptability. On this figure, the upper boundary has been adjusted to reflect a neutral steer yaw rate gain at 40 MPH for the base car wheelbase. Since all of the vehicle configurations investigated were understeer, they are well below this neutral steer condition. However, only four of the ten configurations are clearly within the right side boundary. These are:

- Two base car configurations
- Conventional drive EV
- GE drive, tunnel battery location

Two configurations are well beyond the right side boundary--the Mars II configuration and the Air Drive 2/3 - 1/3 battery configuration. Experience with the actual Mars II vehicle clearly proved that time constants of the

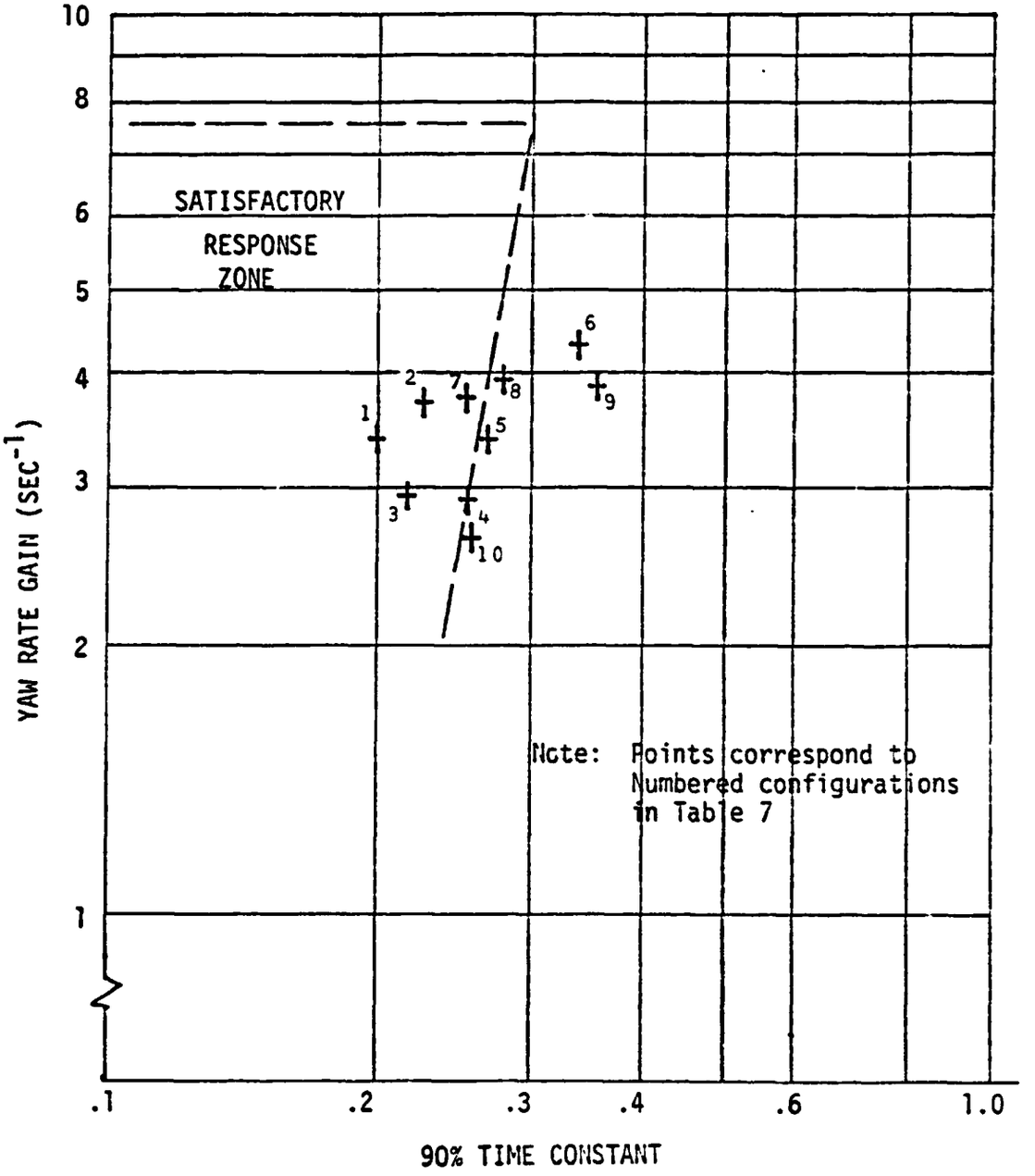

Figure 30 PERFORMANCE POINTS PREDICTED BY COMPUTER SIMULATION IN LINEAR RANGE

order indicated were unacceptable. The other four configurations are very close to the boundary, and owing to the vague nature of the boundary, would probably be marginally acceptable (but not necessarily desirable).

It is interesting to compare these results obtained from HVOSM simulation runs to similar results from simplified linear theory. As shown in Figure 31, linear theory predictions of yaw rate gain are considerably higher (that is, less understeer or even oversteer) than those from the HVOSM. This results from additional understeer effects (compliances, roll effects, etc.) included in the HVOSM vehicle representation which are not considered in simple linear theory. Also note that an effective time constant is used in the figure. This effective time constant was determined by finding the frequency at which the yaw response lags a sinusoidal steer response by 45° in a linear model. This time constant appears to be, in general, somewhat less than the 90% time constant determined from HVOSM results.

Results of the trapezoidal steer simulations will be evaluated further in Section 2.8, which deals with more general effects of weight distribution and moment of inertia instead of concentrating on specific design configurations.

2.6 Results of Sinusoidal Steer Simulations

As described in Section 2.4, this maneuver is generated by a steer input represented by a sine wave with a period of 2.0 sec. and various amplitudes; peak steer inputs (normalized to a 10' wheelbase) of 4, 8 and 16° were selected for the simulations. The "ideal" response to this control input is a lateral displacement (lane change) of 12' with final heading parallel with the initial travel direction.

Figures 32 through 36 are computer-generated graphics which show trajectories predicted by the computer simulations for the two extremes (σ = 4° and 16°). In all instances, a well-controlled lane change takes place at the smaller steer input. However, considerable variation in directional response is noted for the more drastic condition

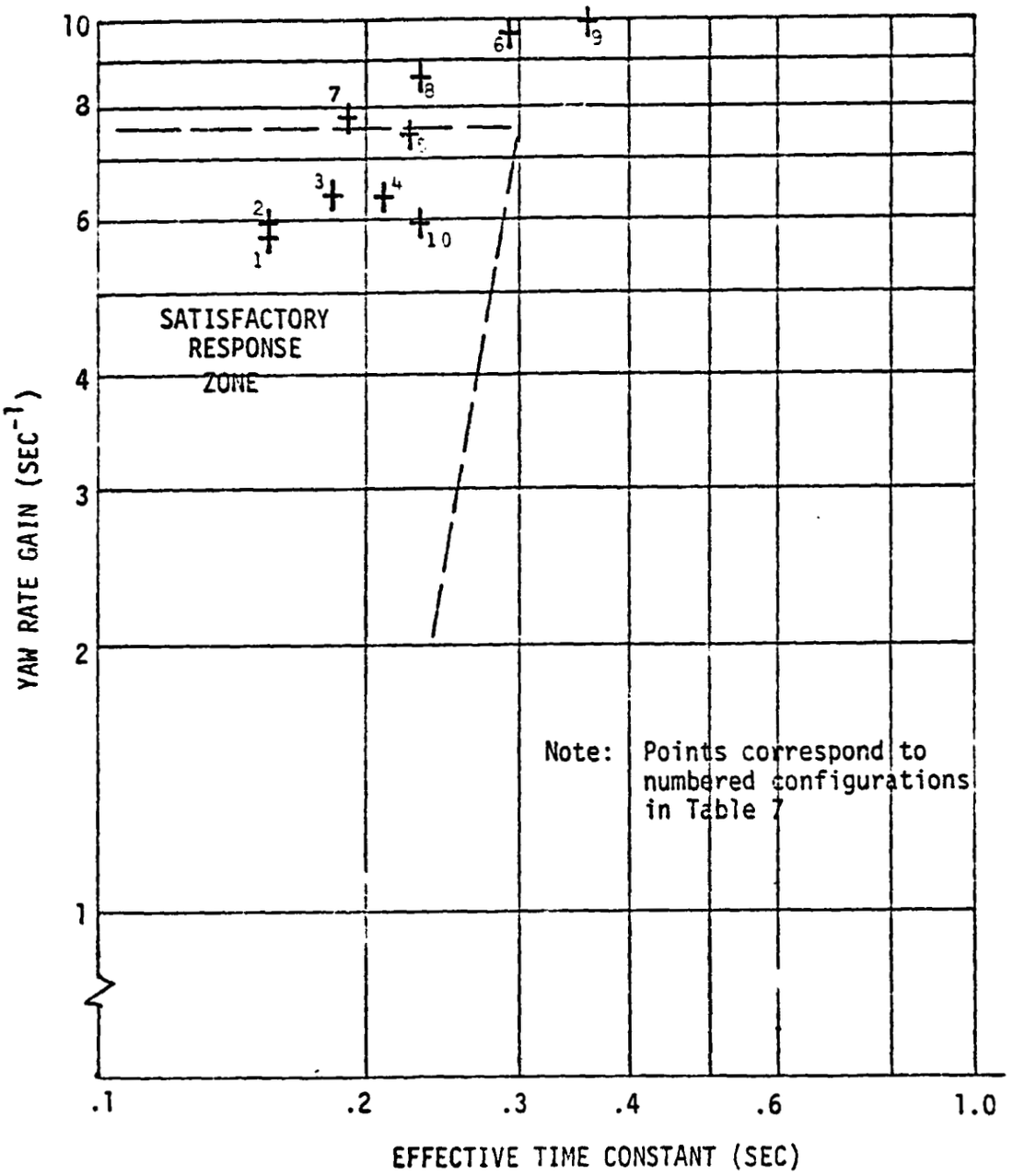

Figure 31 PERFORMANCE POINTS CALCULATED FROM SIMPLE LINEAR THEORY

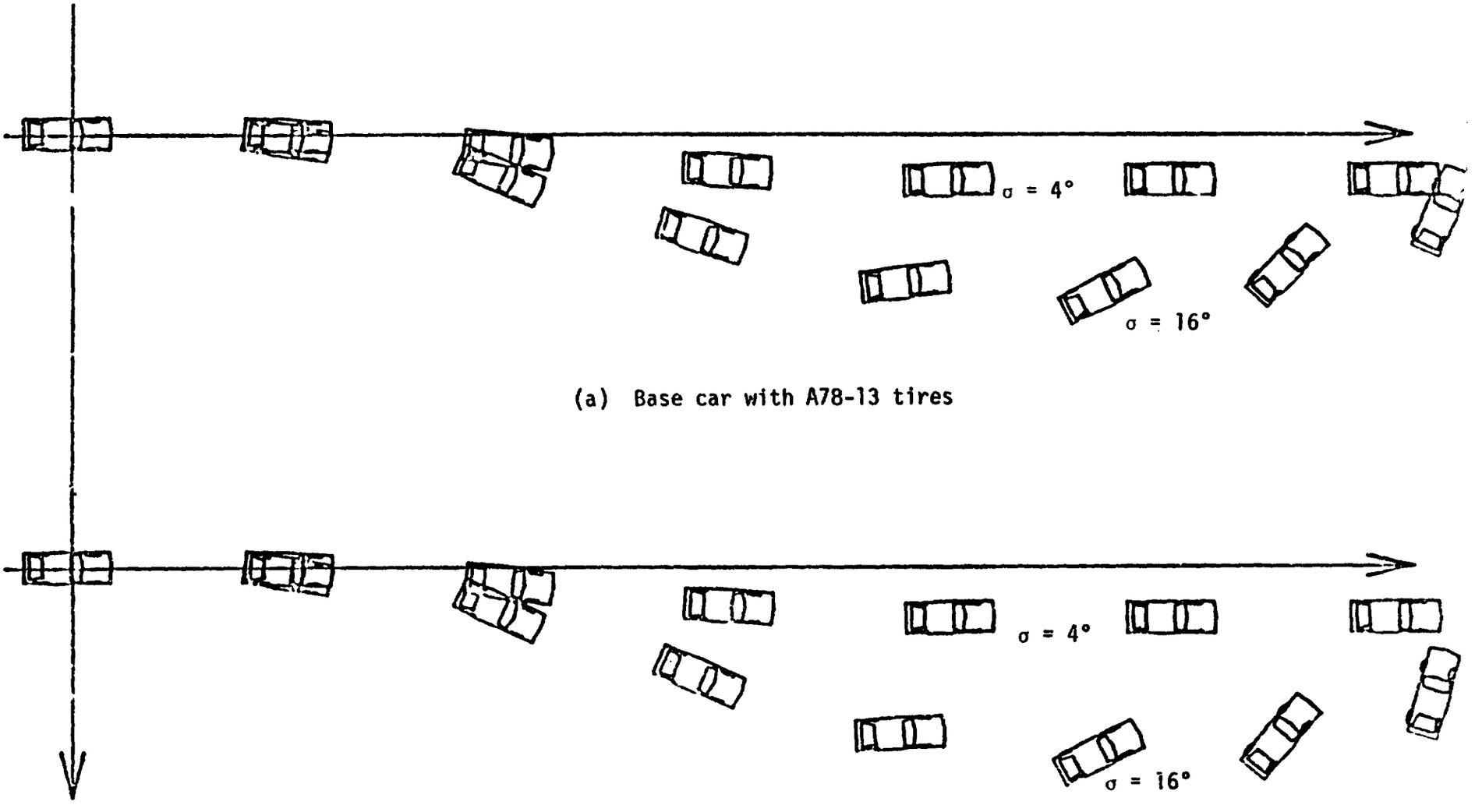

(a) Base car with A78-13 tires

(b) Base car with BR78-13 Tires

Figure 32 SINUSOIDAL STEER TRAJECTORIES FOR BASE VEHICLE

9950-297

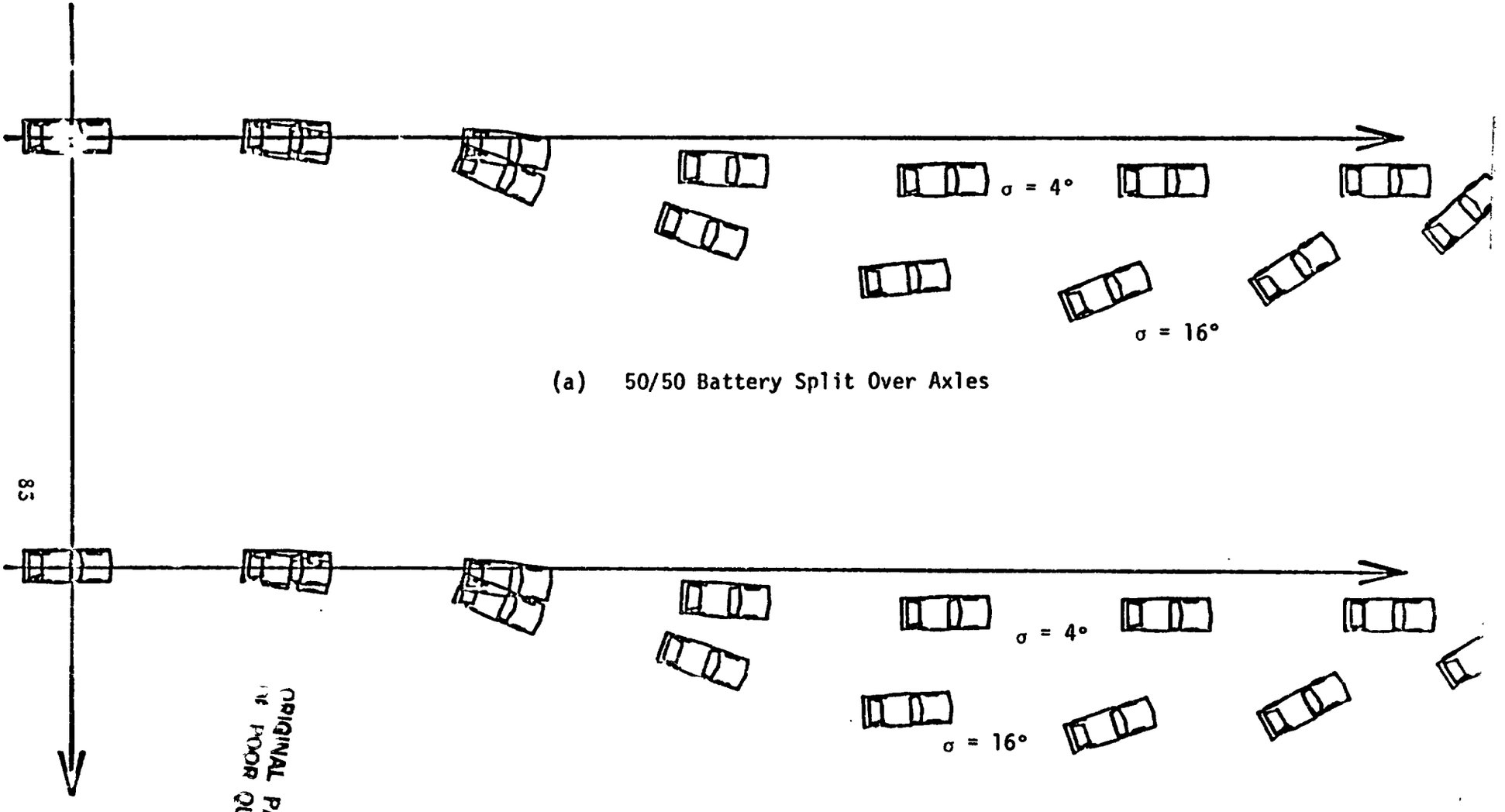

(a) 50/50 Battery Split Over Axles

(b) 50/50 Battery Split, 10" Outboard

Figure 33 SINUSOIDAL STEER TRAJECTORIES FOR CONVENTIONAL DRIVE EV's

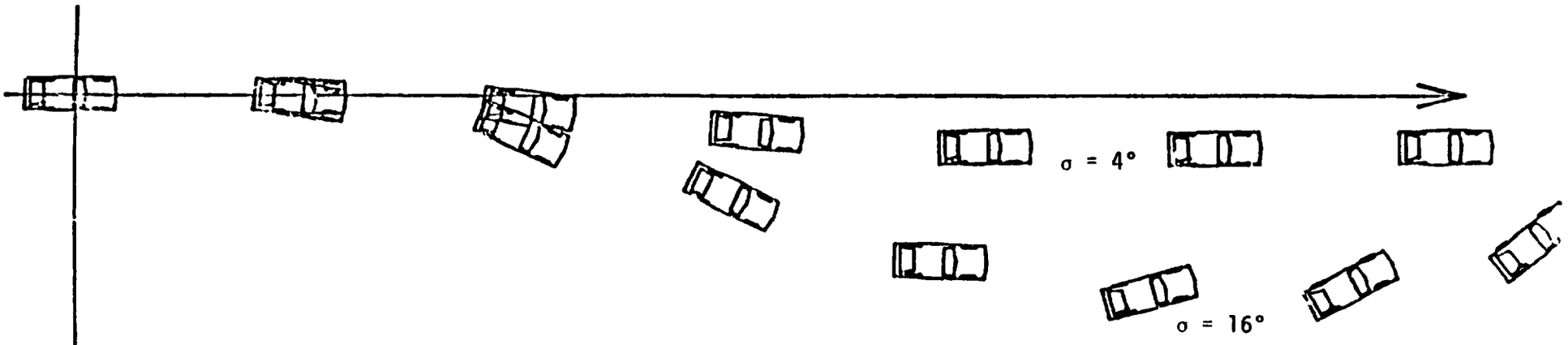

(a) 1/3 - 2/3 Battery Split Over Axles

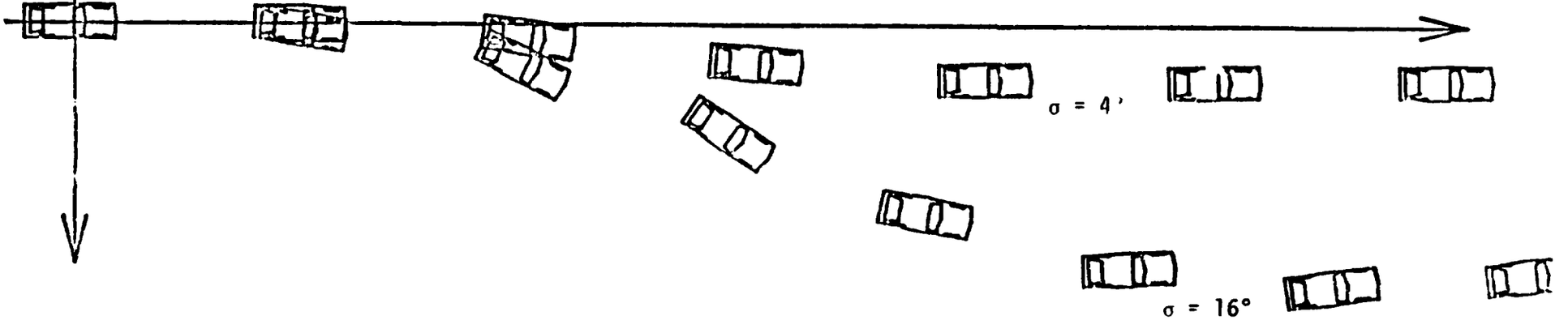

(b) Tunnel Batteries

Figure 34 SINUSOIDAL STEER TRAJECTORIES FOR GE DRIVETRAIN EV's

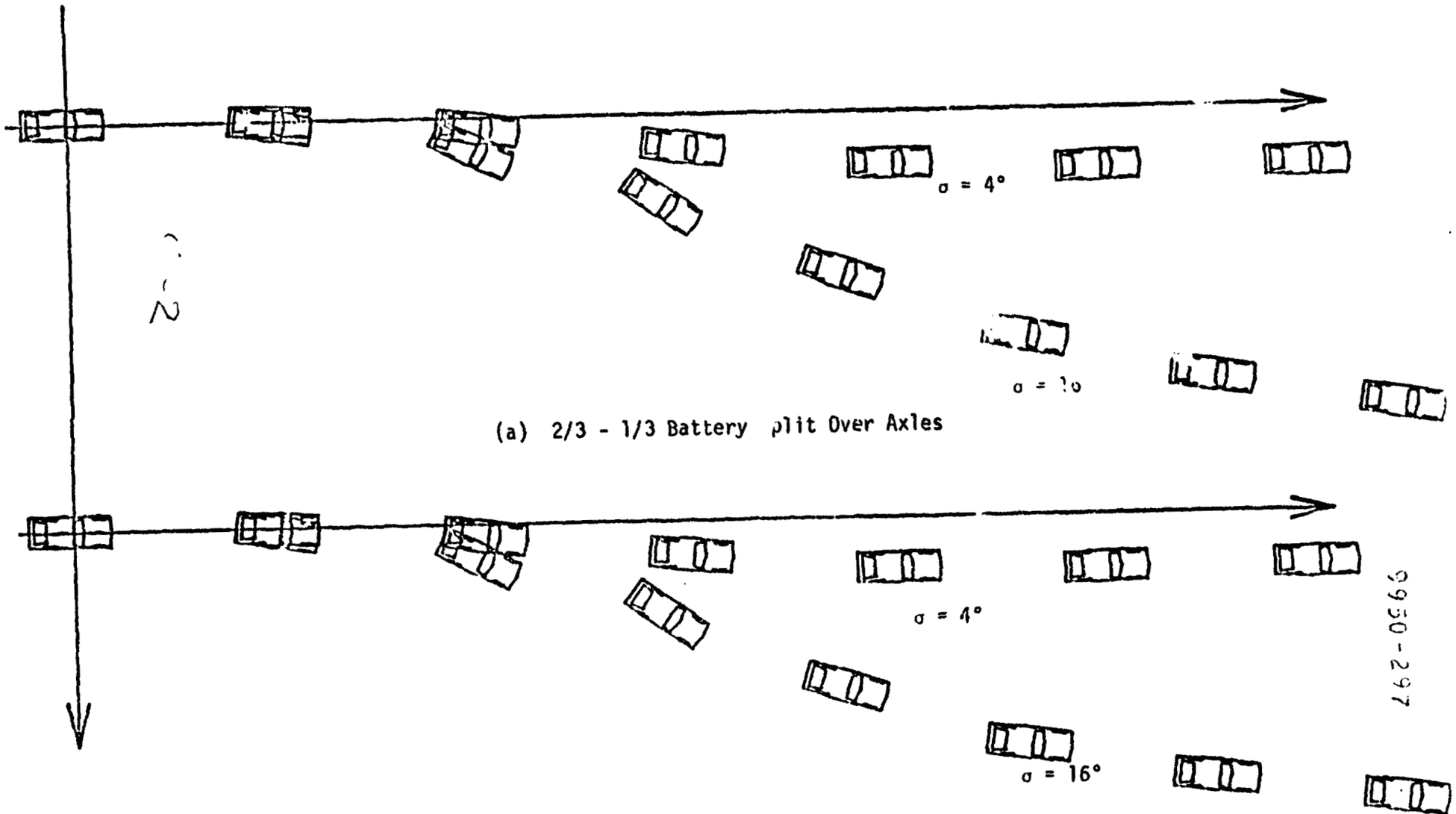

(a) 2/3 - 1/3 Battery Split Over Axles

(b) Tunnel Batteries

Figure 35 SINUSOIDAL STEER TRAJECTORIES FOR AIRESEARCH DRIVETRAIN EV's

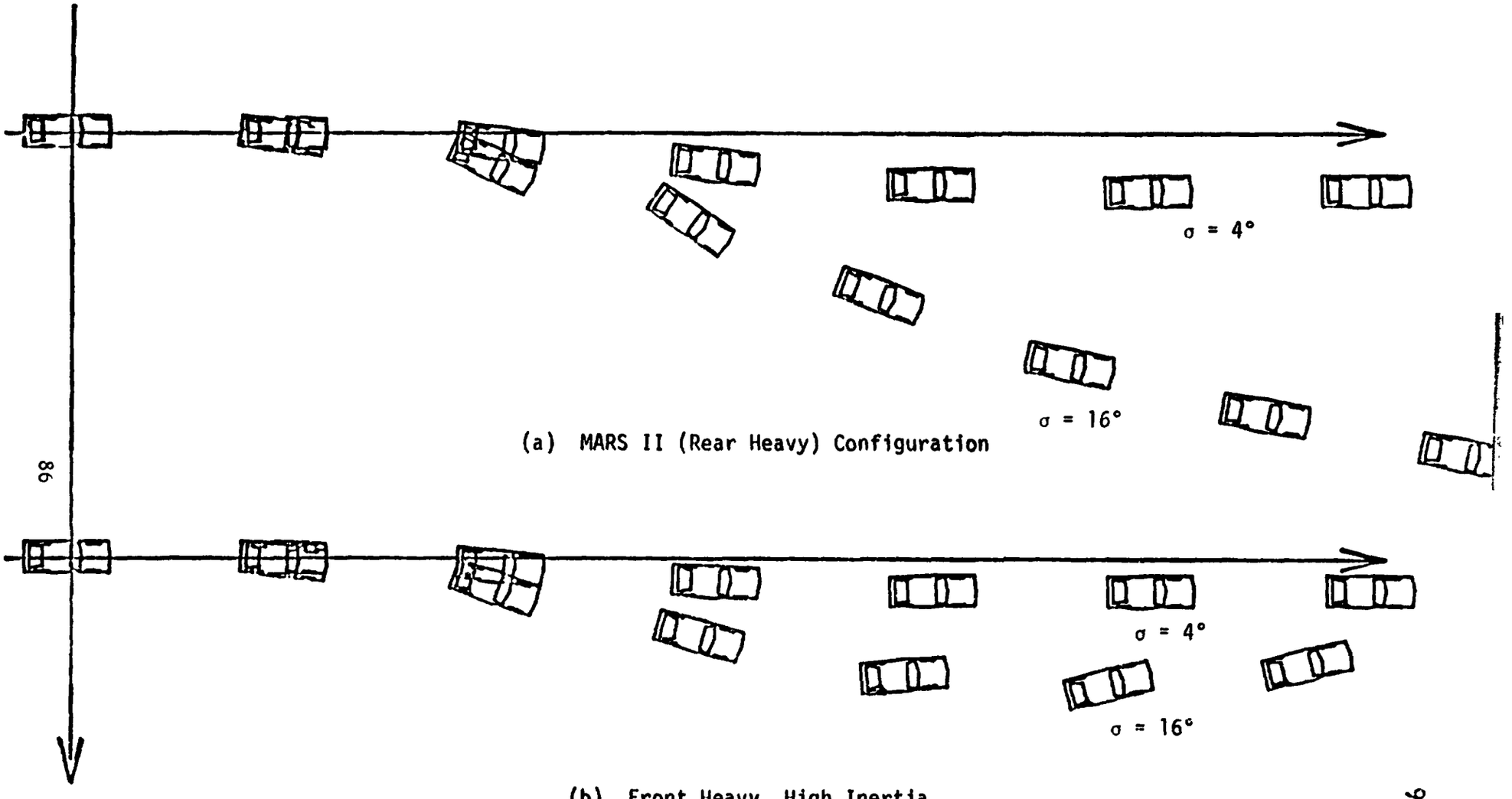

(a) MARS II (Rear Heavy) Configuration

(b) Front Heavy, High Inertia

Figure 36 . SINUSOIDAL STEER TRAJECTORIES FOR FRONT HEAVY AND REAR HEAVY HIGH INERTIA CONFIGURATIONS

Base vehicle responses are compared in Figure 32 for the two tires simulated, i.e., bias-ply (A78-13) and radials (BR78-13). The difference between these specific tires is seen to have a small effect on the response. In both cases, the car achieves very high sideslip angles after about 2 sec into the maneuver. The resultant speed is still approximately 40 MPH at the last position shown in the figure (t = 3.5 sec). The base car therefore exhibits unstable yaw response for the high sinusoidal steer input and may thus be difficult to control in similar, high level, maneuvers.

The Conventional Drive EV configurations (50/50 battery splits over the axles, and 10" outboard) also tend to generate high sideslip angles and an "overcorrecting" response for the higher steer input (Figure 33), but not to the extent predicted for the base car. Responses for the two battery placements (different yaw moments of inertia) are seen to be very similar. Recovery to a parallel heading direction would perhaps be possible if proper corrective action was taken by a driver, but this is speculative and dependent upon driver skill.

Figure 34 shows trajectories for the two GE Drive configurations (1/3 - 2/3 battery split and tunnel batteries). In this case, sideslip is much less severe for the configuration with lower moment of inertia (tunnel batteries). Lateral displacement is high for this configuration, however, which can also be undesirable.

The two configurations based upon the AiResearch Drive packaging approach, with either a 2/3 - 1/3 battery split or tunnel located batteries, are shown in Figure 35. A similar "undercorrecting" response is predicted by the computer simulation for these cases.

The two EV's with the highest moment of inertia exhibit very different responses (see Figure 36) depending on whether the weight distribution is front-heavy or rear-heavy (Mars II). This effect will be explored further in Section 2.8.

Quantitative results for all configurations are given in Figure 37 and 38 in the form of plots of peak sideslip angle versus lane change deviation. As pointed out in Section 2.4, excessive magnitudes of each of these measures are undesirable and, therefore, performance "points" are favorable when clustered near the origin of the graph, i.e., relatively low sideslip and lane change deviation. Also shown in these figures is a boundary of baseline performance generated from experimental testing of 12 actual passenger cars (Ref. 10). The base car is seen to exceed the boundary limit (in the direction of high sideslip angle) and may thus behave somewhat differently than the group of cars experimentally tested, at least for the more drastic (high steer input) conditions. Since all EV's fall within the boundary, these may not substantially depart from "real" vehicle behavior. But, in a relative sense, some of the configurations are clearly better performers than others. We will return to this subject in Section 2.8.

A measure of vehicle responsiveness and controllability that is not specifically addressed by the sinusoidal steer VHTP, but of particular significance in our opinion, is the amount of time lag that exists between the steer input and the directional response. Similar to the yaw rate and lateral acceleration time constants addressed for the trapezoidal steer maneuvers, a time constant (phase lag) was defined as given in Figure 39 for lateral acceleration response (yaw rate response time lag is defined in the same manner). This gives an indication of how much lag time exists at the mid-point of the control input, e.g., during the initial (evasive) phase of a rapid lane change prior to countersteering to straighten the vehicle back to the intended path.

Figures 40 and 41 are plots of the yaw velocity (rate) response time lag as a function of the peak input steer angle (normalized), for all the vehicle configurations. As is clear from the figure, response time varies considerably between EV's and generally exceeds the response time for the base car. The AiResearch Drive, 2/3 - 1/3 Battery Split and the Mars II configuration exhibit the longest time lags, which approach 0.5 sec. (90° out of phase) at the higher steer angle input.

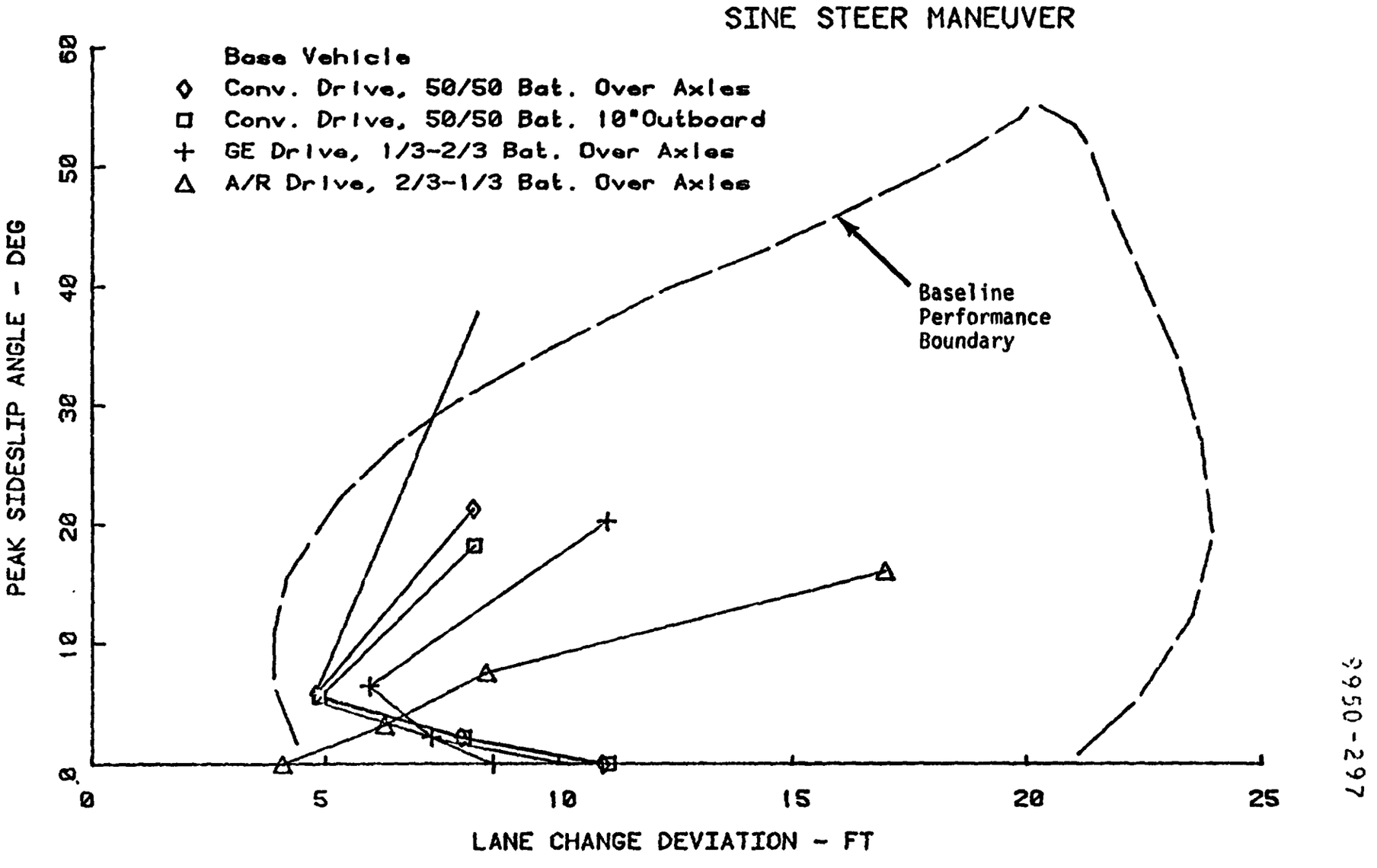

Figure 37 COMPARISON OF SINUSOIDAL STEER RESULTS RELATED TO SIDESLIP ANGLE AND LANE CHANGE DEVIATION

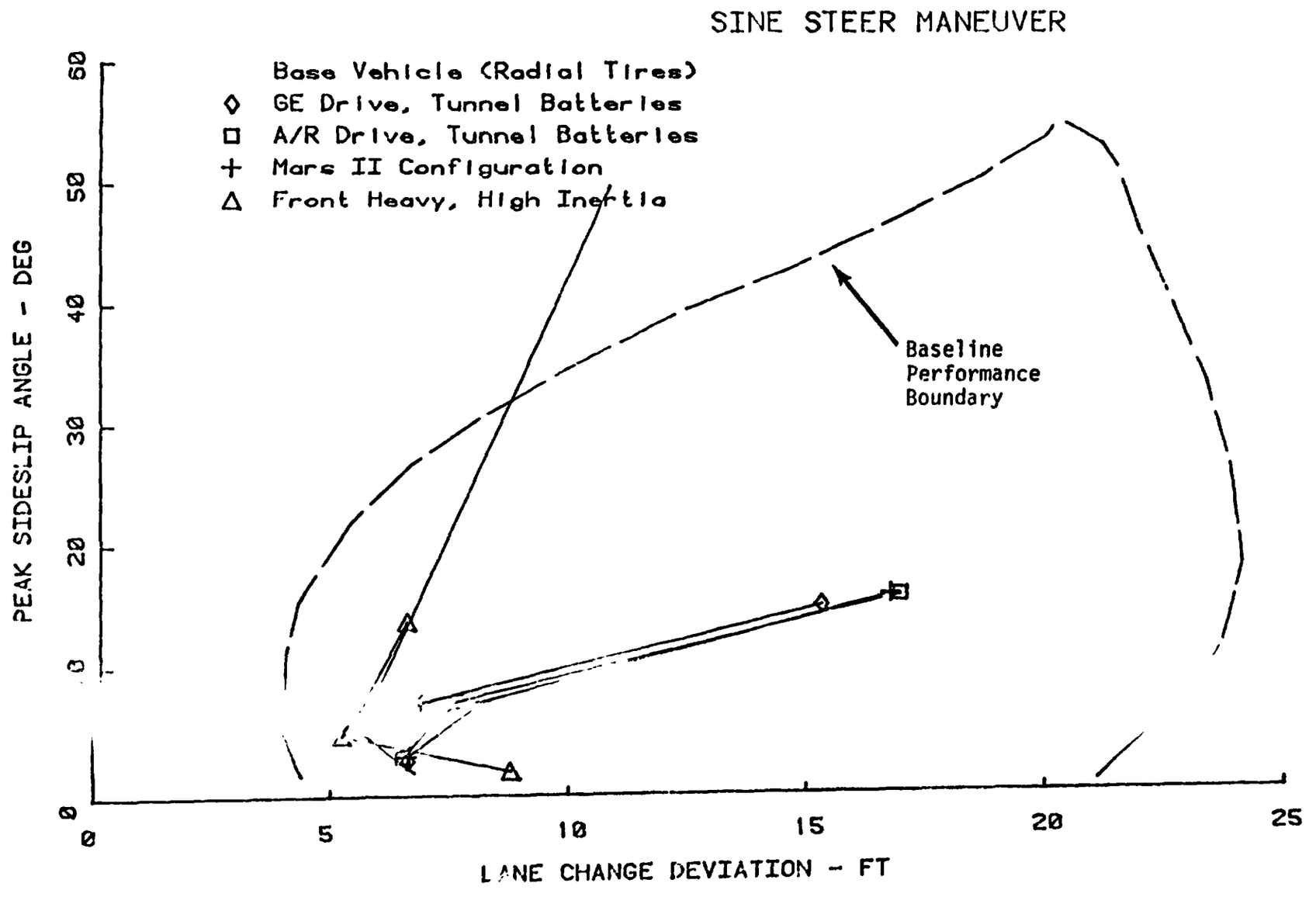

Figure 38 COMPARISON OF SINUSOIDAL STEER RESULTS RELATED TO SIDESLIP ANGLE AND LANE CHANGE DEVIATION

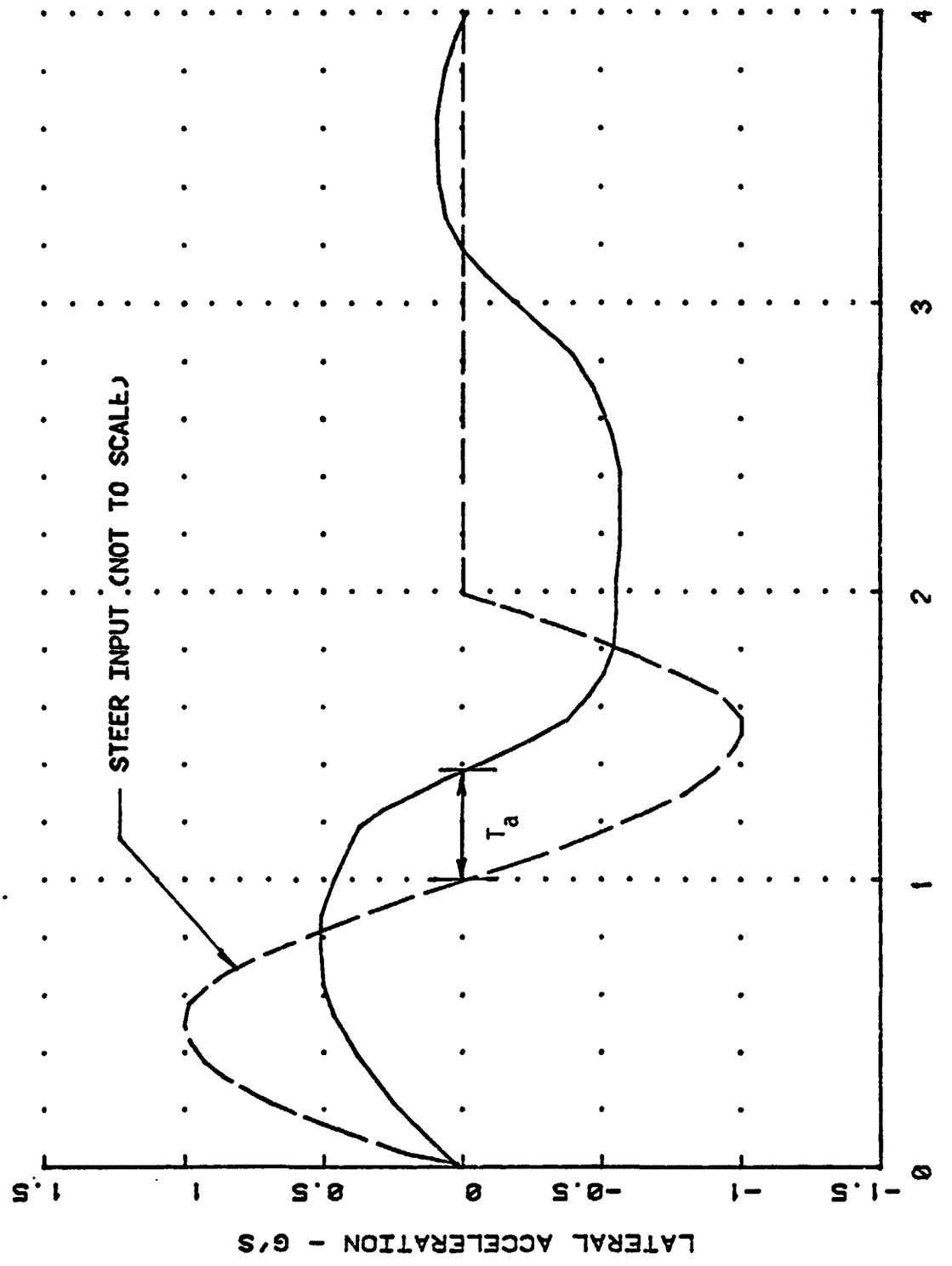

Figure 39 DEFINITION OF RESPONSE TIME LAGS BASED ON SIMULATION RESULTS

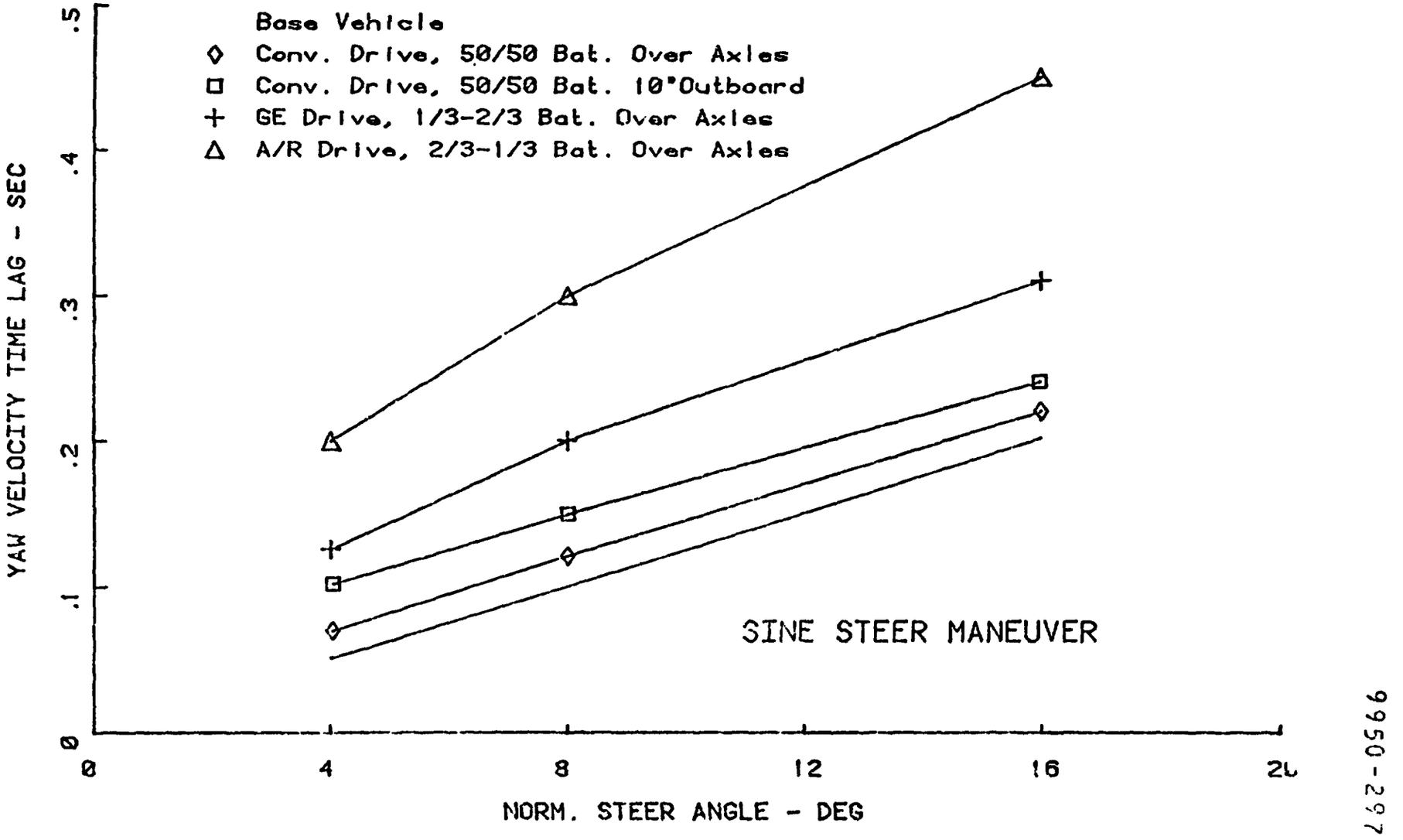

9950-297

Figure 40 COMPARISON OF YAW VELOCITY RESPONSE TIME LAGS

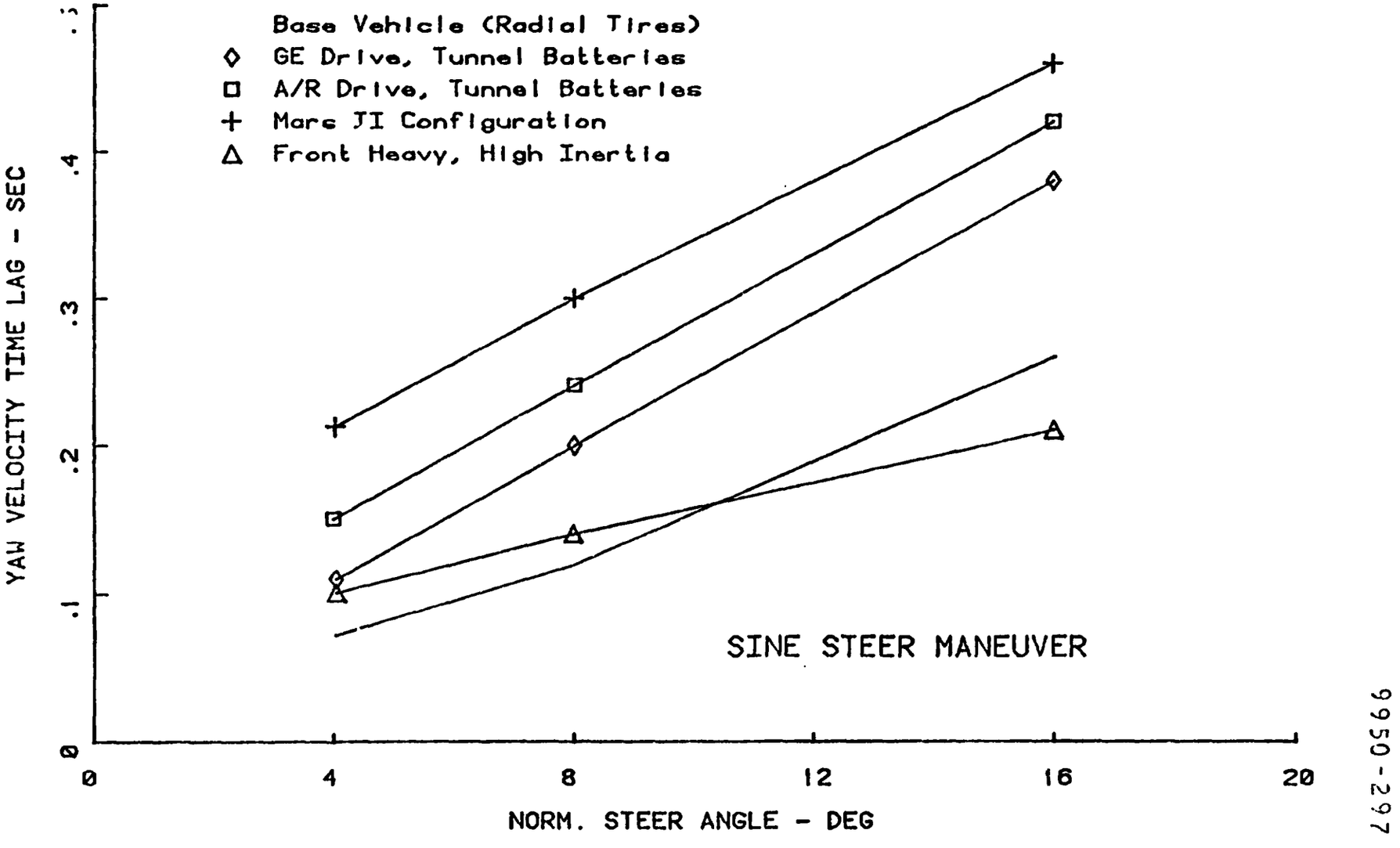

Figure 41 COMPARISON OF YAW VELOCITY RESPONSE TIME LAGS

Lateral acceleration time lags are given in Figures 42 and 43. These response measures show trends which are similar to the yaw velocity response, but at extreme lag times approaching 0.9 sec. for the worst cases. This amount of time corresponds to phase lags approaching 180°, which will certainly produce very poor handling qualities. This was found to be the case for the Mars II EV when evaluated experimentally (Ref. 1). Excessive phase lags are very apparant to a driver and result in reduced ability to control the direction of a vehicle in a precise and consistent manner.

It will be shown in Section 2.8 that weight distribution plays an important role in the response to this maneuver, as was also the case for the trapezoidal steer (and steady-state steering) behavior. The braking-in-a-turn maneuver will be considered next.

2.7 Results of Braking-in-a-Turn Simulations

The braking-in-a-turn test procedure is intended to provide a measure of the interaction between tire side and braking forces and their ultimate influence on safety. The interaction is a function of many variables--test surface characteristics, tire characteristics, vehicle braking system characteristics, etc. The relationship of the vehicle response to safety, although not definable in a quantitative sense, is apparent when one considers the possible vehicle responses--deviation from the intended path and/or yaw instability.

The test procedure calls for the application of braking forces while the test vehicle is negotiating a 0.3 g turn at an initial speed of 40 MPH. Once in the steady-state turn, brakes are applied at increments of 100 psi brake line pressure in successive runs until two wheels on one axle lock up at a speed above 10 MPH.

The ideal directional response to the braking-in-a-turn procedure is defined to be a constant radius (or curvature) trajectory over which the

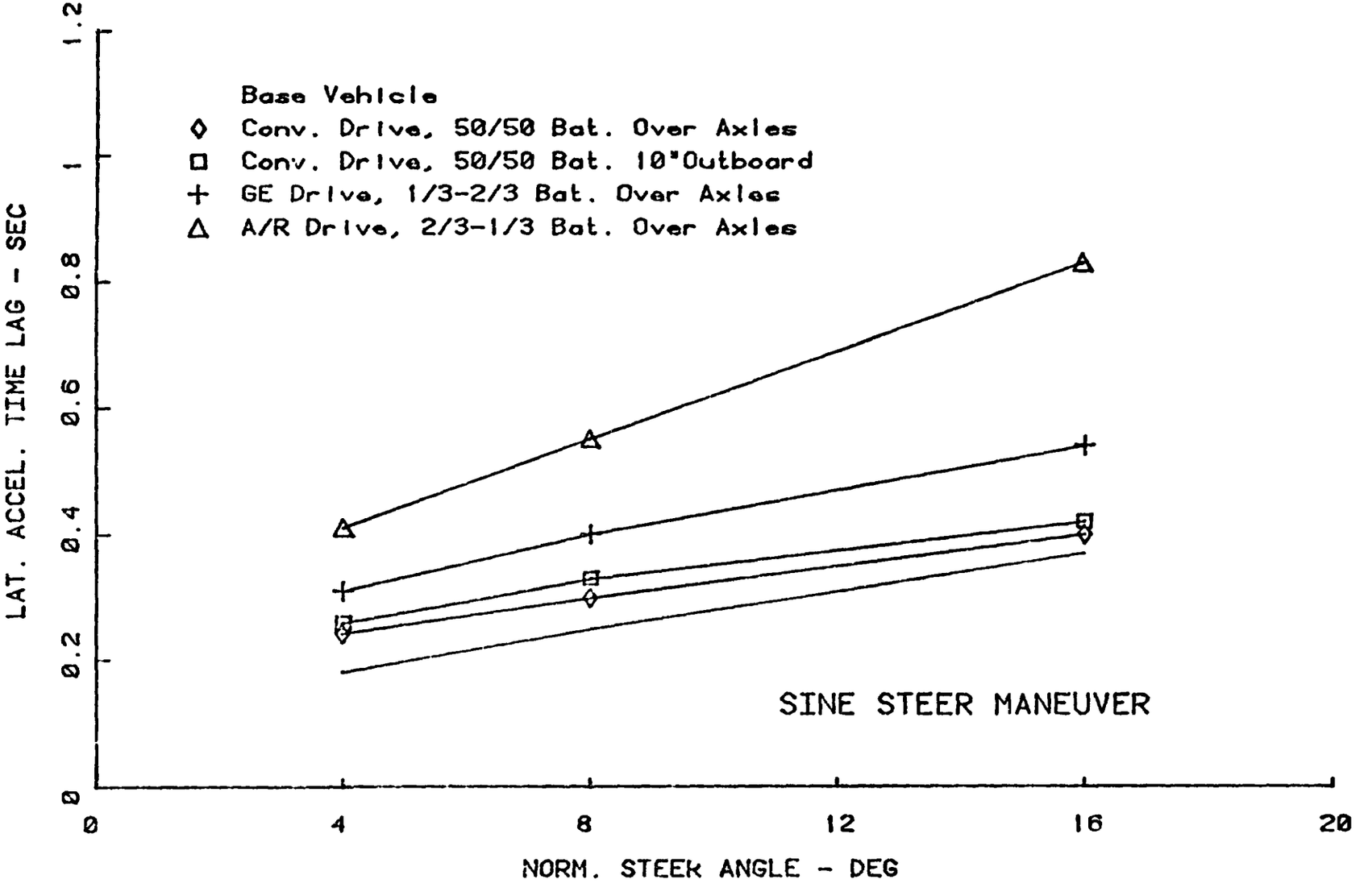

9950-207

Figure 42 COMPARISON OF LATERAL ACCELERATION RESPONSE TIME LAGS

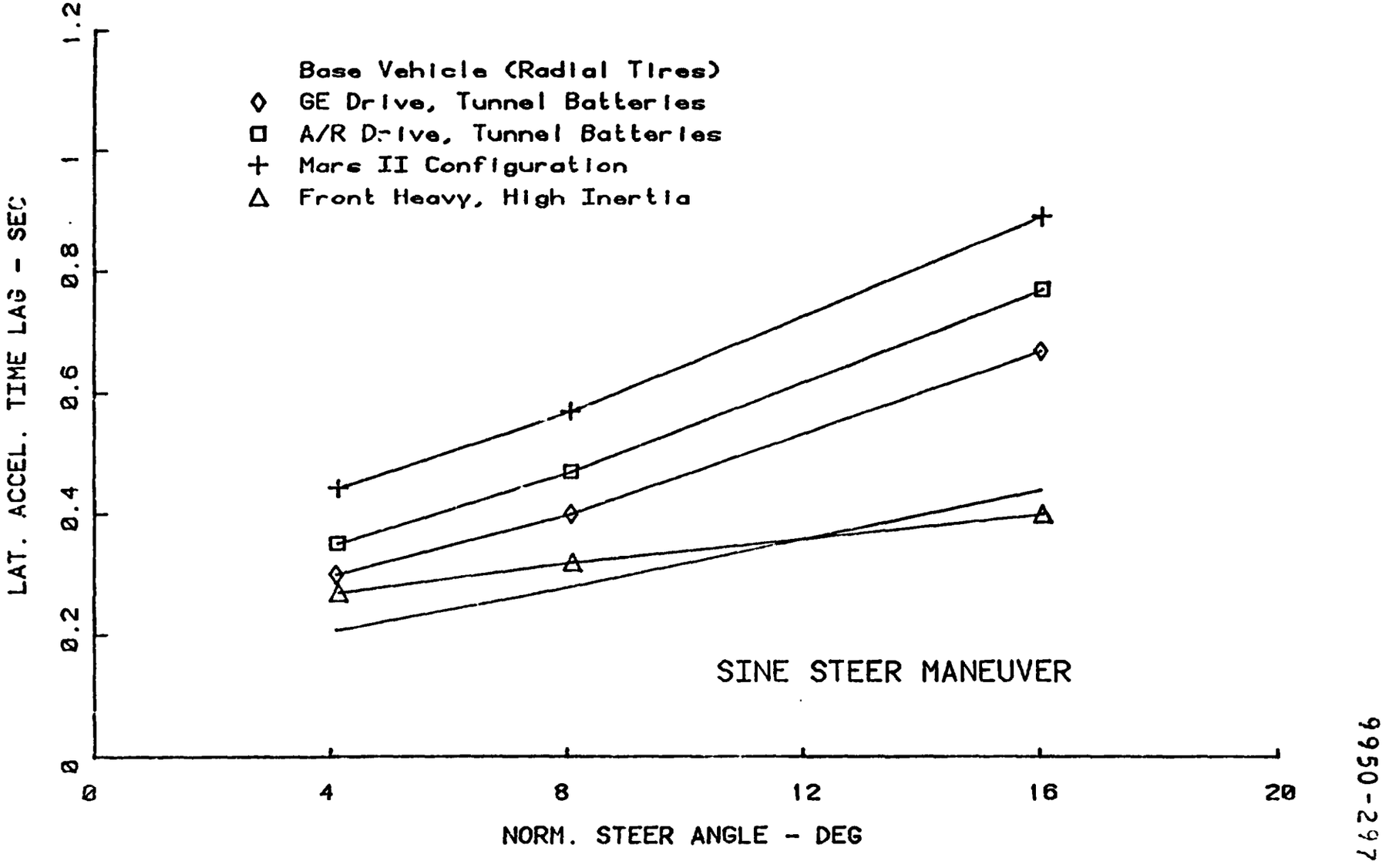

Figure 43 COMPARISON OF LATERAL ACCELERATION RESPONSE TIME LAGS

vehicle maintains a zero or small value of sideslip angle. Deviations from this ideal response occur primarily due to the sequence of axle lockup. That is, lockup of the tires on the rear axle is characterized by a sudden and large increase in β, the sideslip angle, and its time derivative. Conversely, lockup of the front axle tires is characterized by a sharp decrease in path curvature due to the loss of cornering power associated with the locked wheels.

This procedure, as applied to the simulation study, was modified somewhat in order to minimize the number of non-essential computer runs. The modified procedure consisted of analytically determining the brake torques required for lockup of one axle subject to the braking distribution constraint, then running the simulated maneuver with these torques, and subsequently 75% and 50% of their values.

Results obtained for the various vehicle configurations run with this maneuver are summarized in Figures 44 - 47, which illustrate peak sideslip rate achieved and the average path curvature ratio attained over a one second interval after brake application, both as functions of the average longitudinal deceleration. Also included on the figures are bounds obtained in [illegible]g 12 vehicles during development of these procedures. Note that the bounding conditions illustrated reflect the conditions of a specific skid pad on which the tests were made, which had a substantially higher skid number (or friction coefficient) than was simulated. The bounds are not then directly applicable to the simulated configuration but are presented for illustrative purposes.

Two opposite types of limit responses are illustrated in Figure 44. The peak sideslip rate attained by the A/R Drive configuration saturates at about 10°/sec. indicating front wheel lockup and subsequent driftout or plowing limit response with a loss of directional control capability. The other four configurations all exhibit limit spin-out response caused by rear wheel locking. Figure 46 illustrates loss of path curvature at the limit for both types of response (both limit responses produce a center of gravity trajectory that runs outside the intended path). The loss of path curvature is, however, greater with the limit plow response.

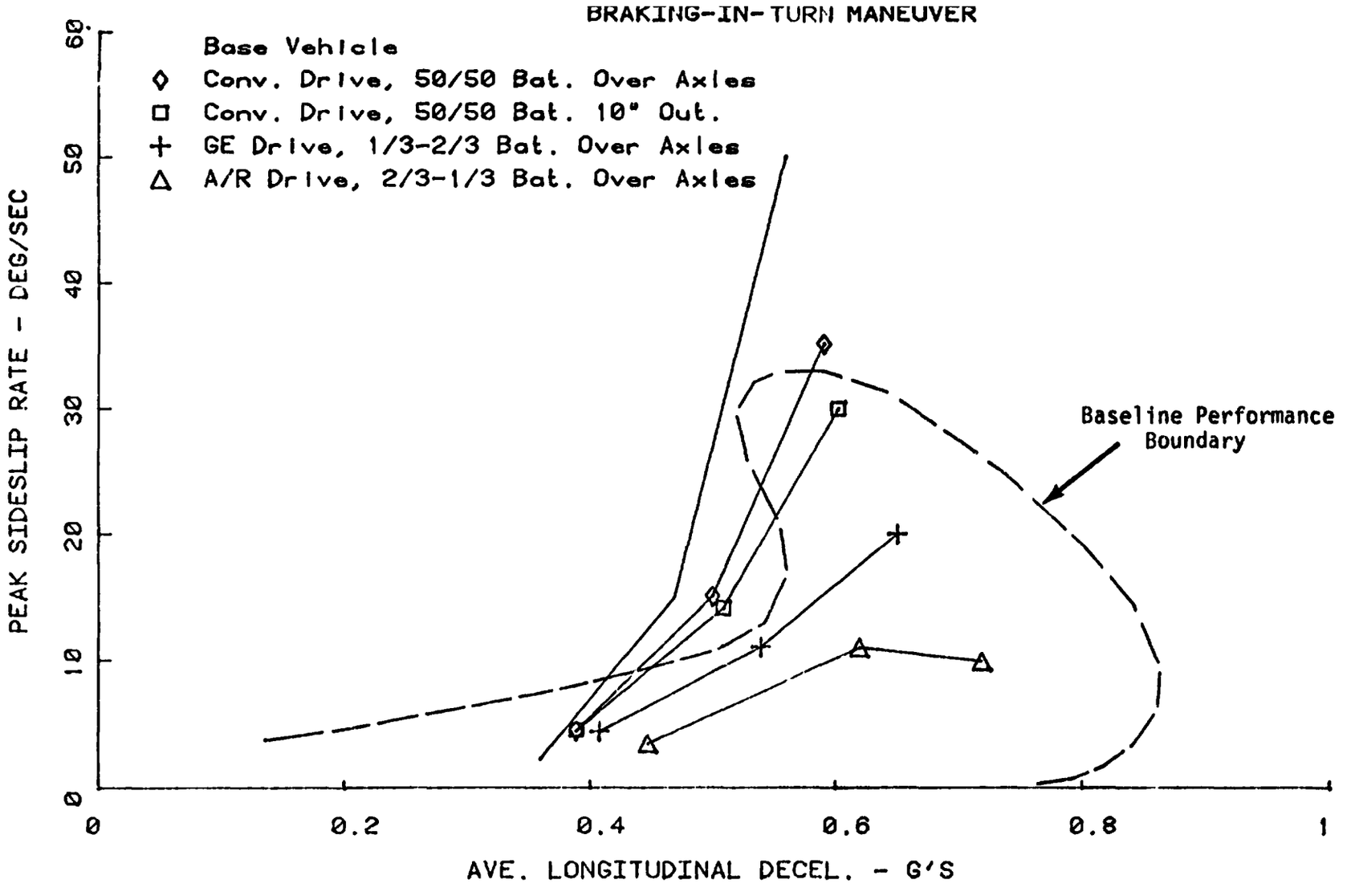

9950-297

Figure 44 COMPARISON OF SIDESLIP RATES FOR A RANGE OF VEHICLE DECELERATION

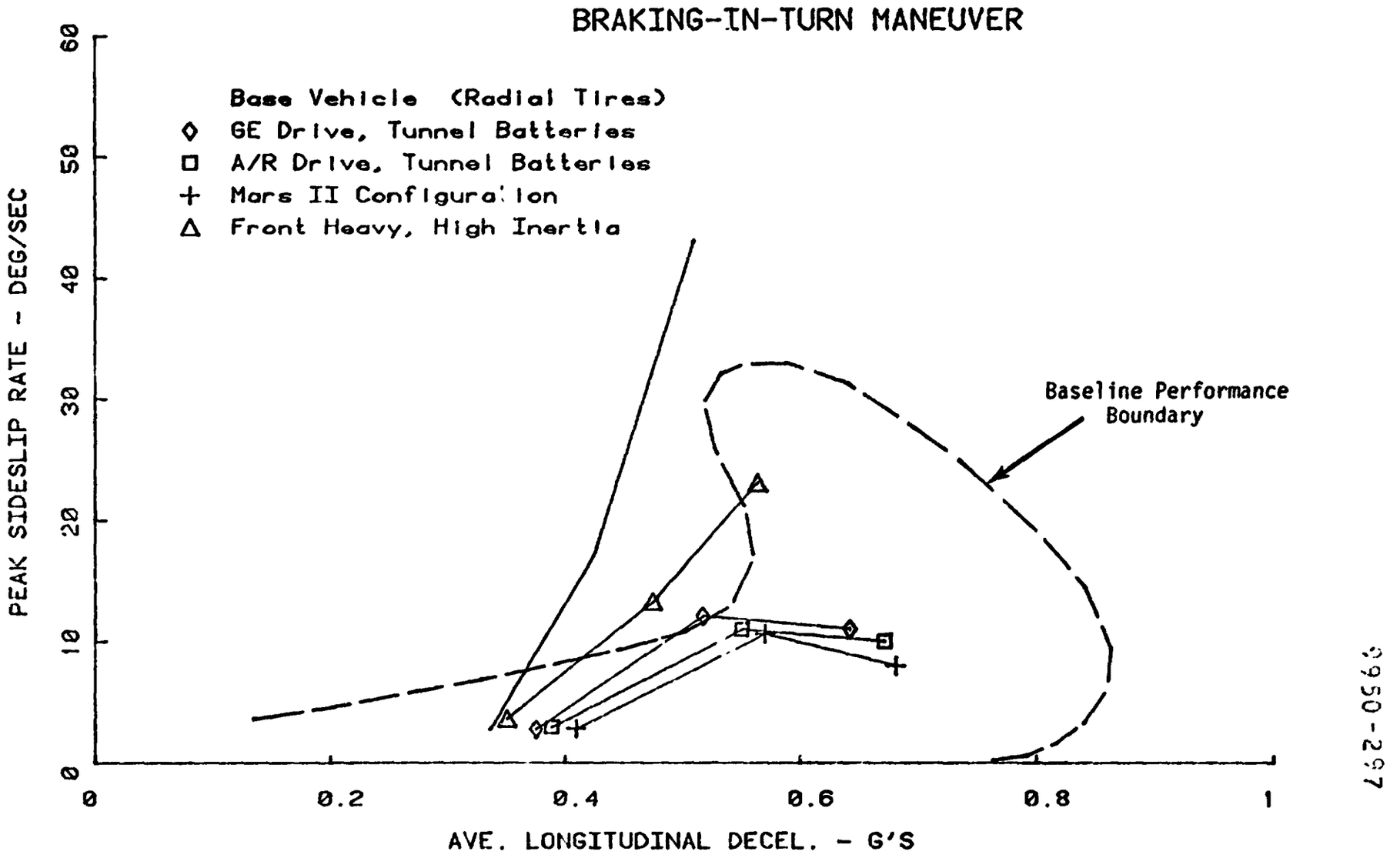

Figure 45 COMPARISON OF SIDESLIP RATES FOR A RANGE OF VEHICLE DECELERATION

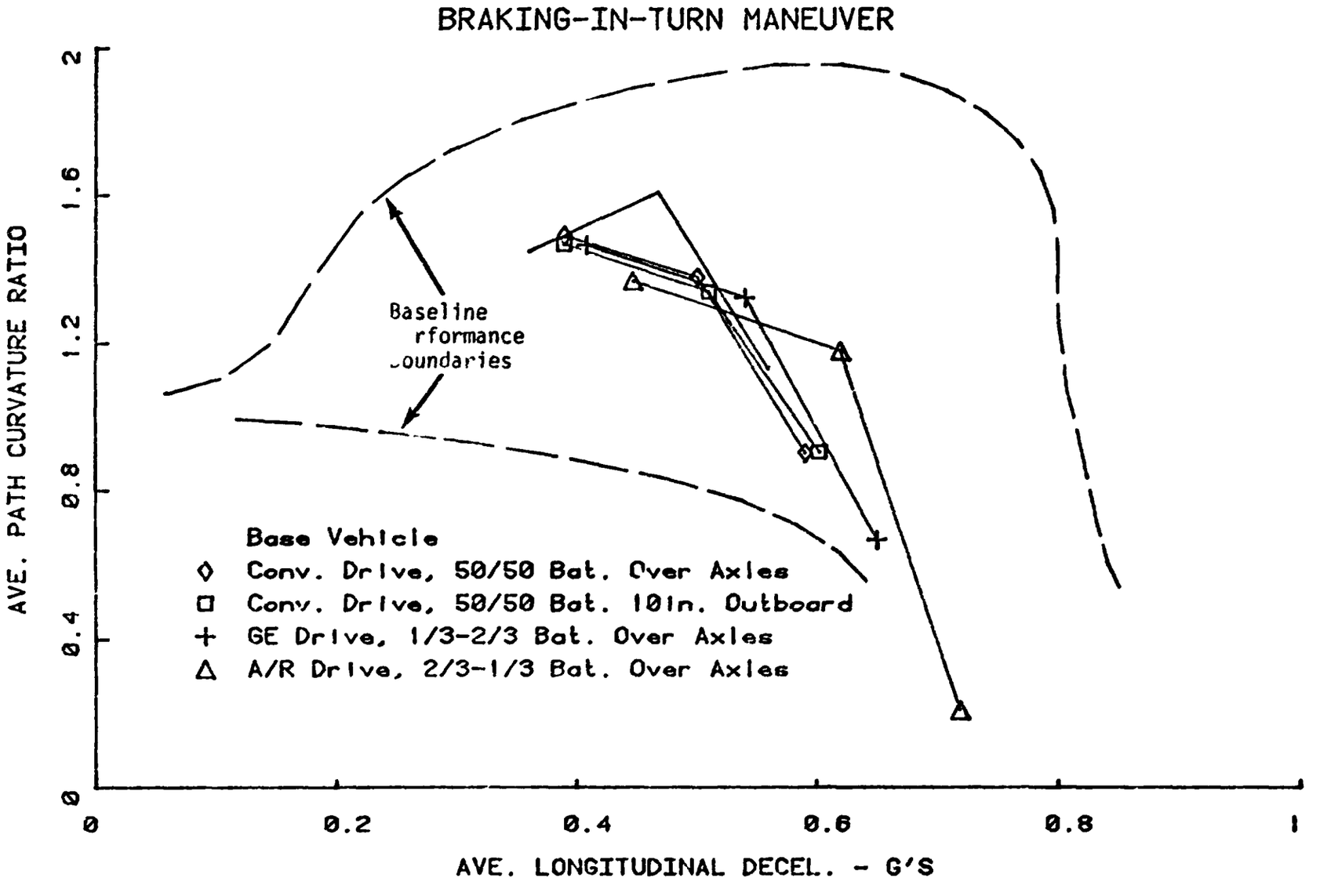

9950-237

Figure 46 COMPARISON OF PATH CURVATURE FOR A RANGE OF VEHICLE DECELERATION

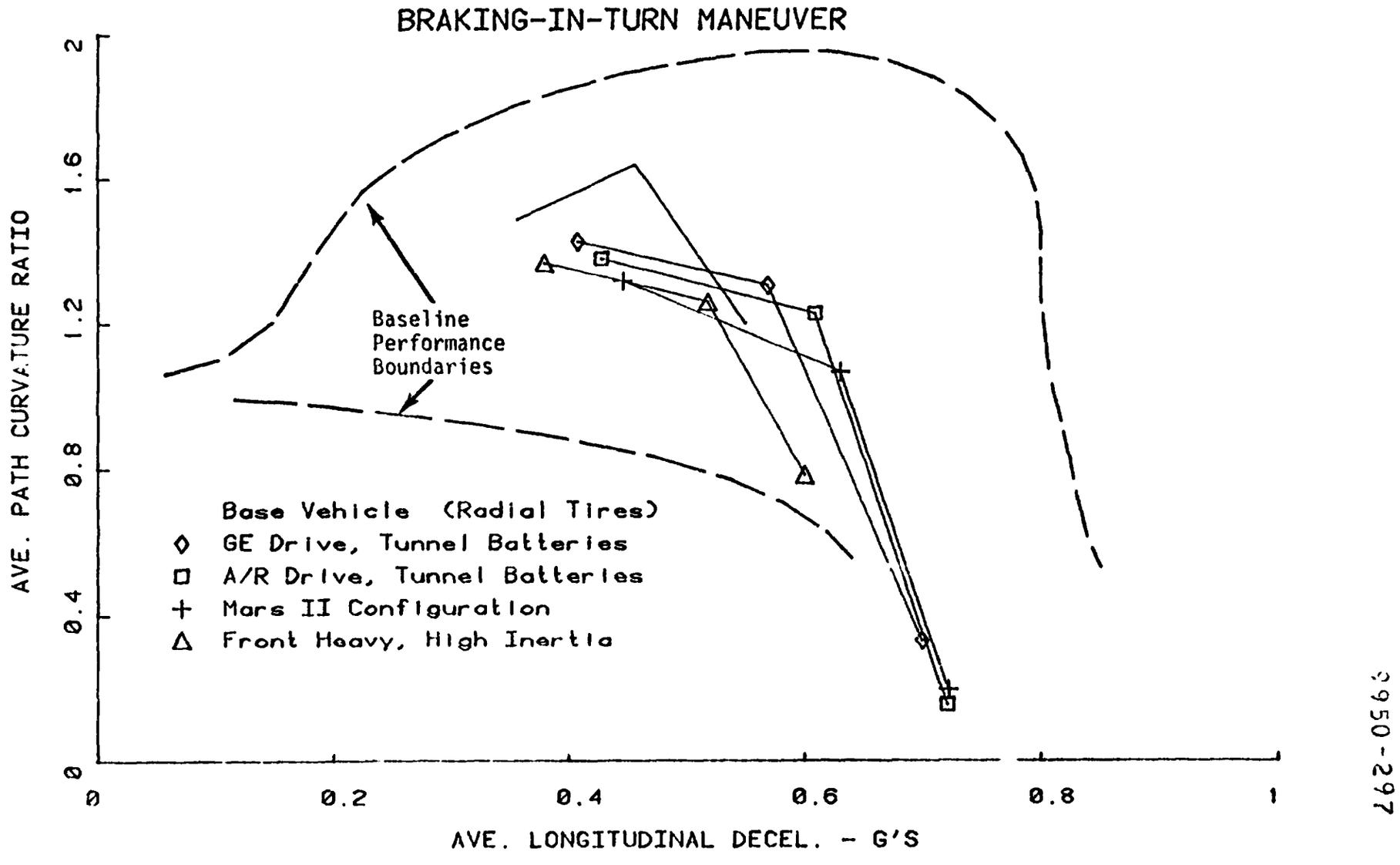

Figure 47 COMPARISON OF PATH CURVATURE FOR A RANGE OF VEHICLE DECELERATION

Figures 45 and 47 illustrate similar summaries for five additional vehicle configurations. In this case, however, only the base vehicle with radial tires and the front heavy, high inertia configurations exhibit limit spin response--the others plow at the limit. These two types of limit response are graphically illustrated in Figure 45.

The results shown above require some explanation as to the apparently better performance (assuming limit plowing is more desirable than limit spinning) of some of the EV configurations than is seen with the base car. The brake system proportioning for the base car is fixed at 60/40 according to available information. That is, 60% of the total braking torque is applied to the front wheels, while 40% is applied to the rear wheels. This is a typical braking effort distribution for automobiles. The reason for the front bias in braking effort derives from the forward weight transfer experienced under braking--the normal loads at the front axle increase and those at the rear axle decrease the extent depending on the vehicle center of gravity height and level of deceleration. This implies that the front tires can support more torque under braking than is indicated by the static weight distribution, rolling radius and tire/ground sliding friction coefficient without locking.

The specific configuration of the base vehicle, as simulated, resulted in a 59/41 front to rear weight distribution under static conditions. Consequently, any significant amount of weight transfer occurring as a result of braking results in a situation where more than 60% of the steady-state vehicle weight is at the front and less than 40% at the rear. As a result of this condition, the fixed 40% brake torque split to the rear axle causes the rear tires to lock before the fronts, ultimately resulting in the observed limit spin behavior. Conversely, vehicle configurations which are statically rear-heavy exhibit steady-state front to rear axle load conditions under braking which are less than the 60/40 brake torque split and therefore tend to lock the front tires first.

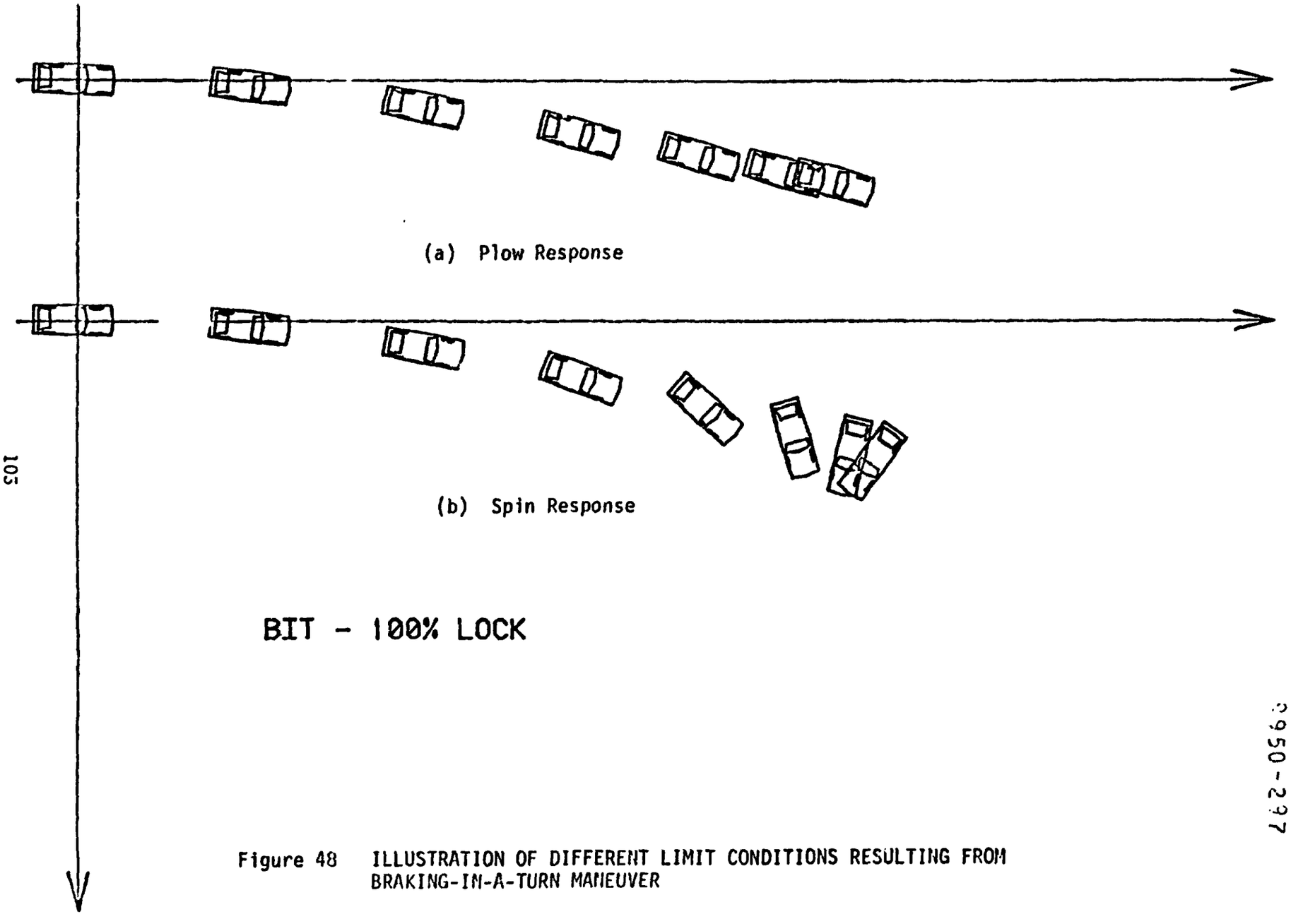

Figure 48 ILLUSTRATION OF DIFFERENT LIMIT CONDITIONS RESULTING FROM BRAKING-IN-A-TURN MANEUVER

We do not know why the fixed proportioning of 60/40 was (according to our information) designed into the brake system of the base vehicle, but a brief discussion of some of the potential trade-offs that go into the design process is in order. First, fixed proportioning can never produce optimum braking performance (i.e., front and rear wheels locking at the same level of deceleration) under all conditions. Variations in tire/surface sliding friction (as are commonly encountered due to road construction, tire characteristics or weather conditions) and variations in vehicle load conditions both affect brake system performance. Under low coefficient surface conditions, front brakes commonly lock before the rears due to decreased weig . transfer resulting from the lower deceleration capability of the surface. The opposite is true for fixed proportioning under very high coefficient surface conditions.

Variations in vehicle load conditions also affect optimum brake distribution. This is particularly true in small cars (as the subcompact base vehicle) since the load changes resulting from passengers and/or baggage can be a larger percentage of the total weight than with large cars. With this small car, any increase in load conditions would bias the static weight distribution toward the rear, thus resulting in improved braking performance (i.e., less of a tendency to lock the rear tires before the fronts).

With regard to electric vehicle design, it is important that due consideration be given to brake system performance. Whether a given EV results from a conventional vehicle modification or a "ground-up" vehicle, suspension and braking system components from existing production vehicles would likely be employed in the car. These components must be chosen or modified to consider the appropriate balance between braking-induced weight transfer, static weight distribution and braking torque distribution.

2.8 Evaluation of Weight Distribution and Inertia Effects

The preceding discussion of technical results has dealt with specific electric vehicle configurations and their response to various control inputs. We now wish to generalize the evaluation and consider overall effects of two primary parameters--weight distribution and yaw moment of inertia. The results obtained through computer simulation will thus be treated as representative of a generic group of vehicles having a wheelbase on the order of 95 inches.

Three categories of weight distribution will be addressed, i.e., front-heavy, balanced and rear-heavy. Referring back to Table 2, the front-heavy EV's all have front axle loadings of 55% of the sprung weight, and the rear-heavy configurations range between 44% and 49% front axle loading. The balanced configuration is split exactly 50/50 between the front and rear axles. The base car is front-heavy with sprung weight distribution of 59/41 front/rear. All of these distributions are for two-passenger load conditions.

Yaw moment of inertia varies between approximately 16,100 and 24,700 lb-in-sec^2 for the front-heavy EV's, and between 15,200 and 24,700 lb-in-sec^2 for the rear-heavy EV's. The ranges are thus very similar for these vehicle groups. The yaw moment of inertia for the single balanced configuration is 18,500 lb-in-sec^2. These values are for the sprung mass only. The corresponding value for the base car is 11,400 lb-in-sec^2.

We will now evaluate findings discussed previously in the context of these basic physical parameters. The evaluation will be divided into steady-state steering properties in the linear range, trapezoidal steer response, and sinusoidal steer behavior. Braking-in-a-turn will not be addressed here because we believe that achievement of effective braking performance is largely related to prudent design of the front/rear braking torque proportioning system, a topic which is beyond the scope of this study.

Steady-state Steering Performance (Linear Range)

For consistency with the remaining graphical presentations, steady-state properties will be evaluated as a function of yaw moment of inertia. This is not rigorously correct since moments of inertia will not directly affect steady-state behavior. But, moment of inertia essentially increases monotonically with mass (weight), so we are in essence considering the effect of vehicle mass throughout this section.

The most important numeric characterizing steady-state steering behavior is the understeer gradient (K). Figure 49 shows that the base car has an understeer gradient of about 5 or 6 deg/g, depending on whether bias-ply (A78-13) or radial (BR78-13) tires are used in the simulation.* Understeer gradient increases with mass for the front-heavy configurations and, conversely, decreases slightly with mass for the rear-heavy EV's. Since typical passenger cars are generally in the range from 2 to 10 deg/g, none of the configurations possess unusual steady-state steering properties. The important point is that they are all understeer, as opposed to oversteer ($K < 0$), which is undesirable for the average driver. Also recall from Section 2.3 that all of the rear-heavy configurations are understeer due to suspension and roll effects.

Lateral acceleration gain and yaw rate gain are shown in Figures 50 and 51, respectively. These results show that, for a given command (input) steer angle, the front-heavy configurations produce somewhat less path curvature (lower lateral acceleration and yaw rate) than the rear-heavy vehicles. The differences in directional control capability indicated by these numerics is not believed to be of great significance, since it essentially means only that more steer angle is required by the front-heavy

*Note that all figures in this section show simulation results for the base car with both of these types of tires.

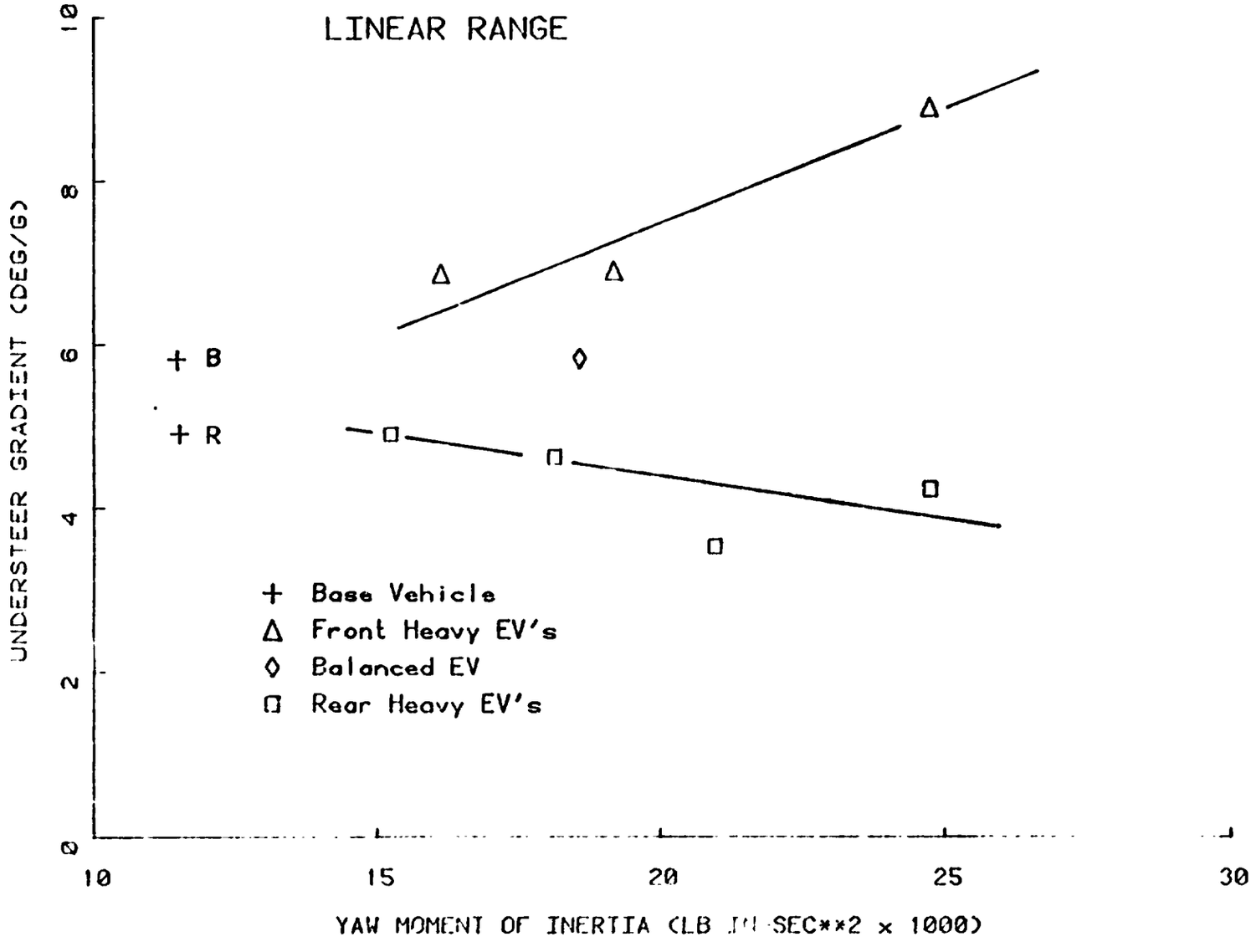

Figure 49 EFFECT OF INERTIA AND WEIGHT DISTRIBUTION ON UNDERSTEER GRADIENT

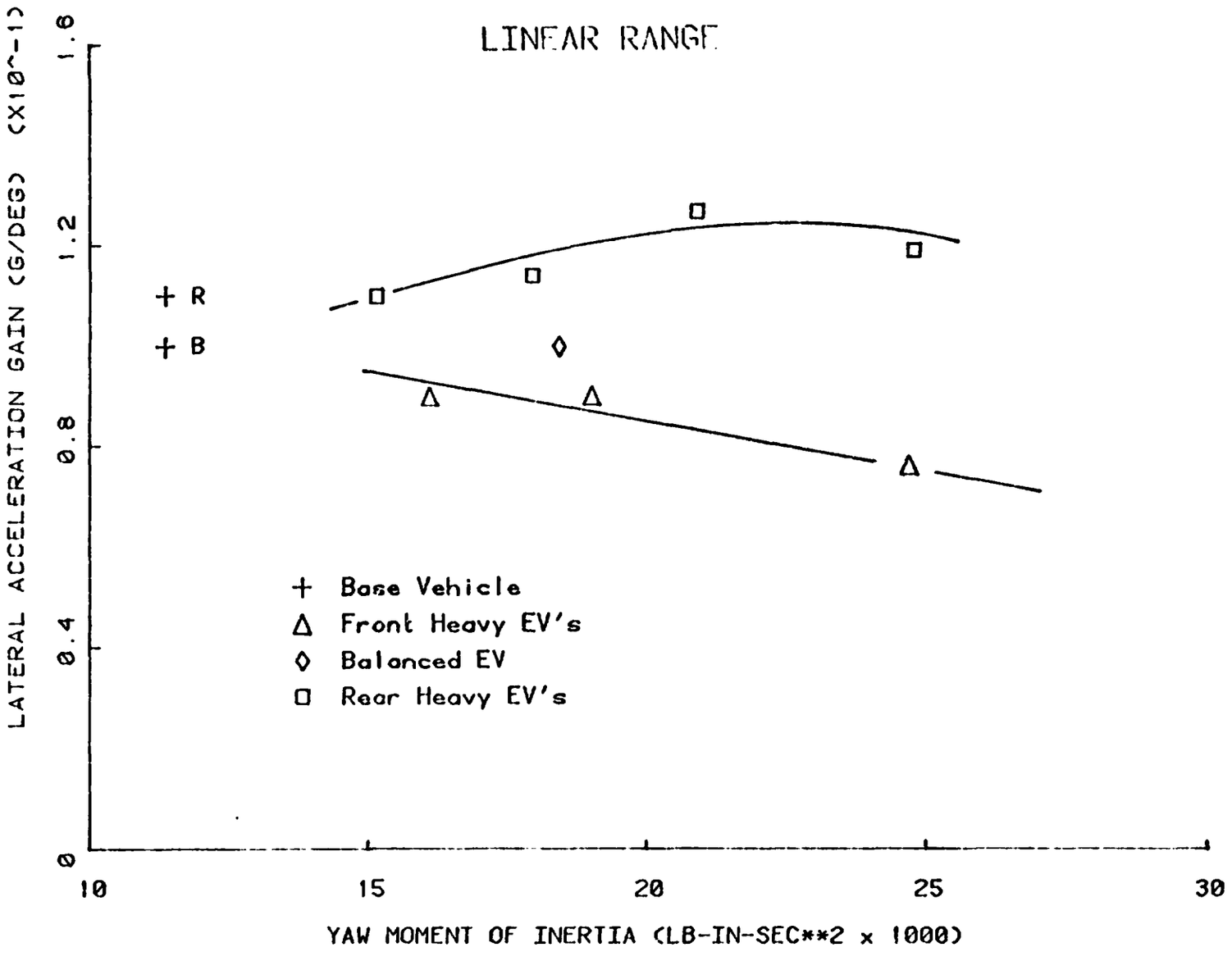

9950-297

Figure 50 EFFECT OF INERTIA AND WEIGHT DISTRIBUTION ON LATERAL ACCELERATION GAIN

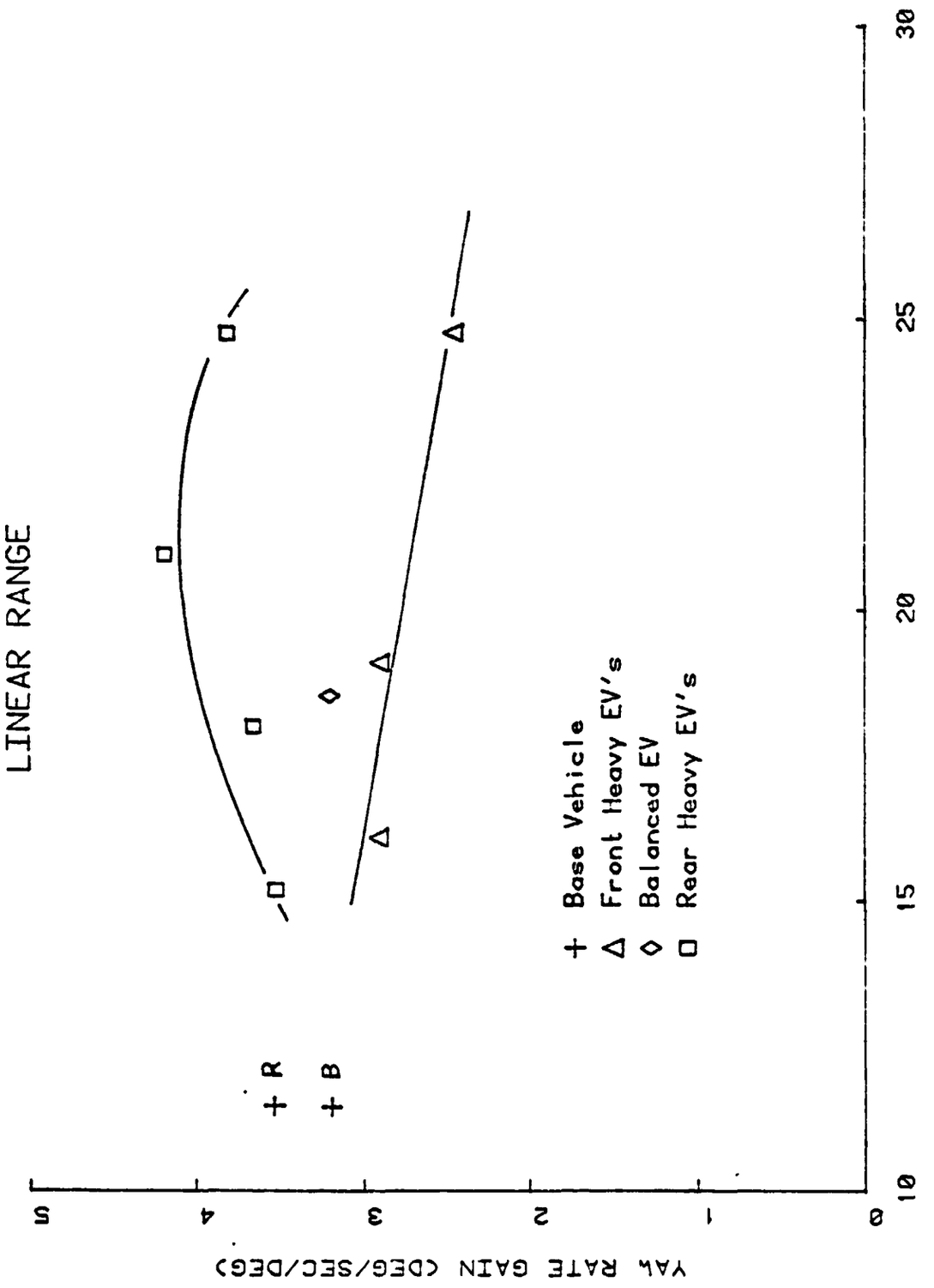

Figure 51 EFFECT OF INERTIA AND WEIGHT DISTRIBUTION ON YAW RATE GAIN

configurations to achieve a given cornering (equilibrium) condition relative to the rear-heavy configurations. This can easily be compensated for by adjustments in steering gearbox ratio or by other changes in suspension and/or tire properties.

Figure 52 illustrates a trend that is of more concern than the control gain magnitudes, i.e., the rapid increase in sideslip sensitivity for the rear-heavy EV's as mass (moment of inertia) becomes larger. For the front-heavy configurations, sideslip sensitivity is higher than for the base car but remains relatively constant as mass increases. Excessive sideslip sensitivity is clearly undesirable and disconcerting to an average driver. Although acceptable limits for this parameter are not precisely quantifiable, it is our understanding that magnitudes much above 5 or 6 deg/g are considered excessive by some handling experts. Therefore, the front-heavy EV configurations considered in this study are likely to be marginally acceptable, whereas the rear-heavy configurations having moments of inertia above approximately 20,000 lb-in-sec^2 probably exceed a reasonable range of sideslip sensitivity.

Similar trends are apparent when considering the yaw velocity (rate) and lateral acceleration time constants in Figures 53 and 54. Again, quantitative upper bounds of acceptability are not precisely known for these response measures. However, based on the work of Systems Technology, Inc. (Ref. 8) and from sources within the automotive industry, a conservative estimate is that yaw response time constants in excess of about 0.25 sec. would be highly objectionable, as would lateral acceleration time constants above approximately 0.5 second. Results in Figures 53 and 54 therefore suggest that front-heavy configurations can accommodate a high moment of inertia without radically affecting time constants. This is not the case for the rear-heavy configurations, which exhibit time constants which would likely be troublesome particularly when yaw moments of inertia on the order of 20,000 lb-in-sec^2 are approached or exceeded.

Figure 55 shows the region of acceptability defined by STI related to yaw rate gain plotted versus 90% time constant (adapted from Ref. 8).

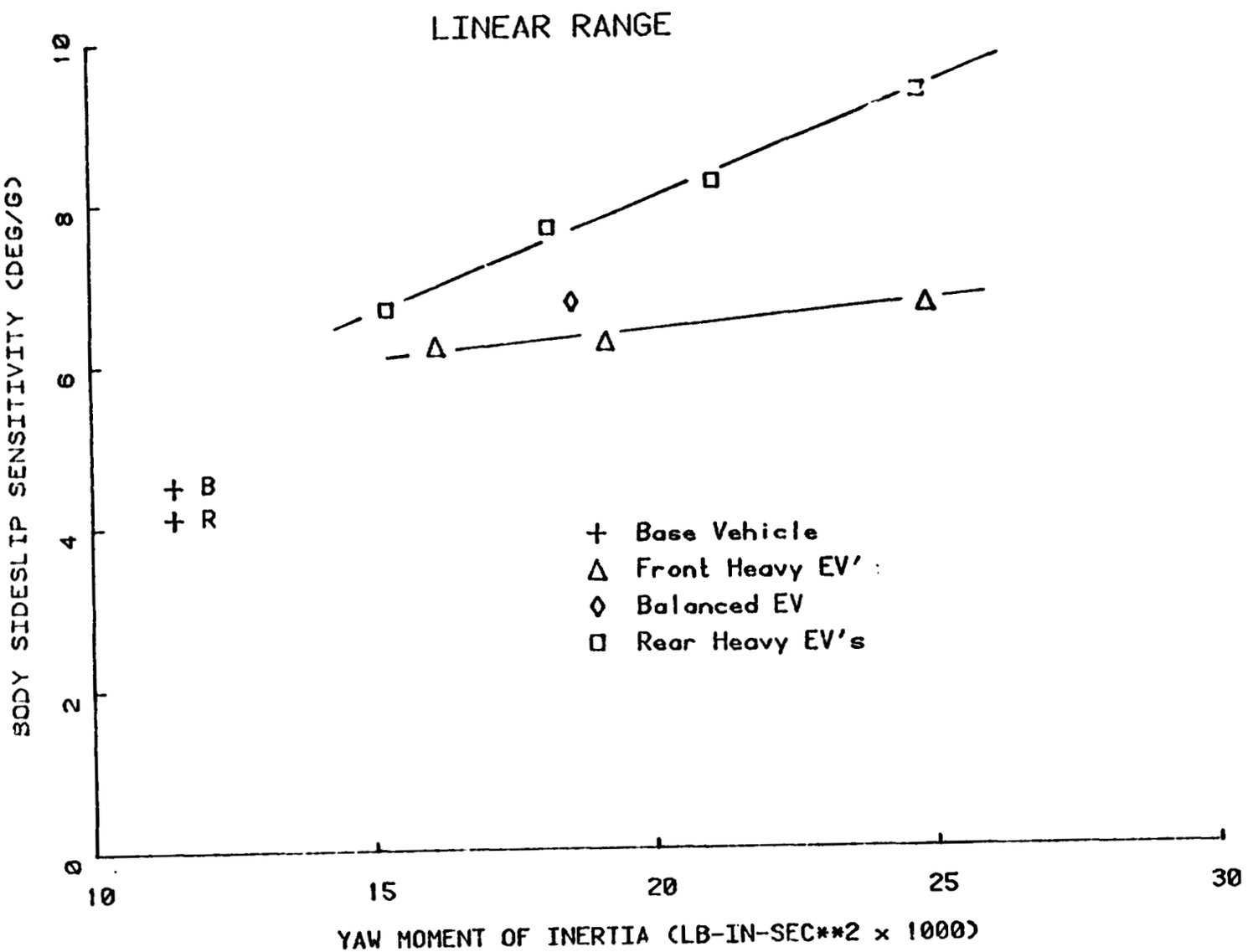

Figure 52 EFFECT OF INERTIA AND WEIGHT DISTRIBUTION ON SIDESLIP SENSITIVITY

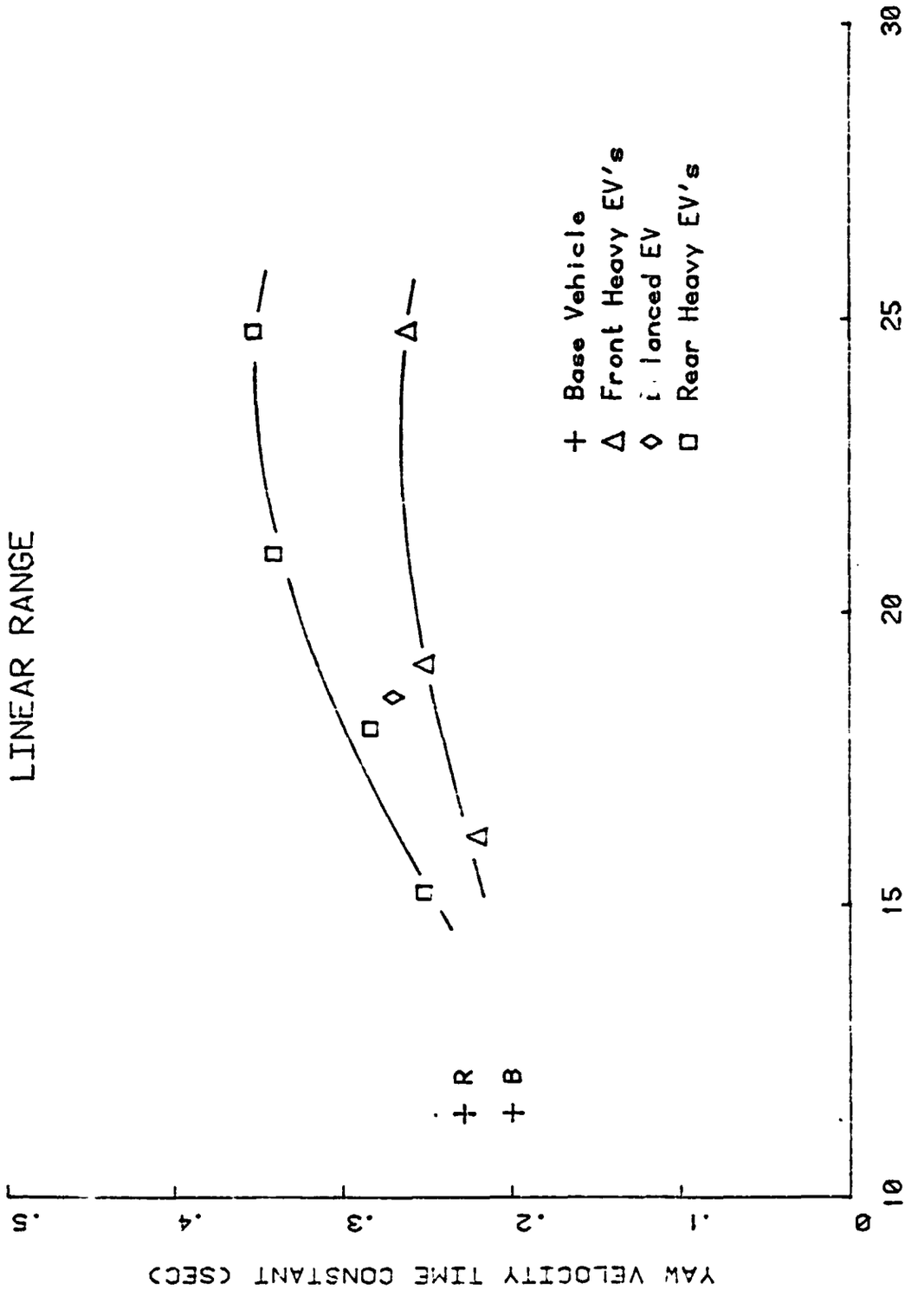

Figure 53 EFFECT OF INERTIA AND WEIGHT DISTRIBUTION ON YAW VELOCITY TIME CONSTANT

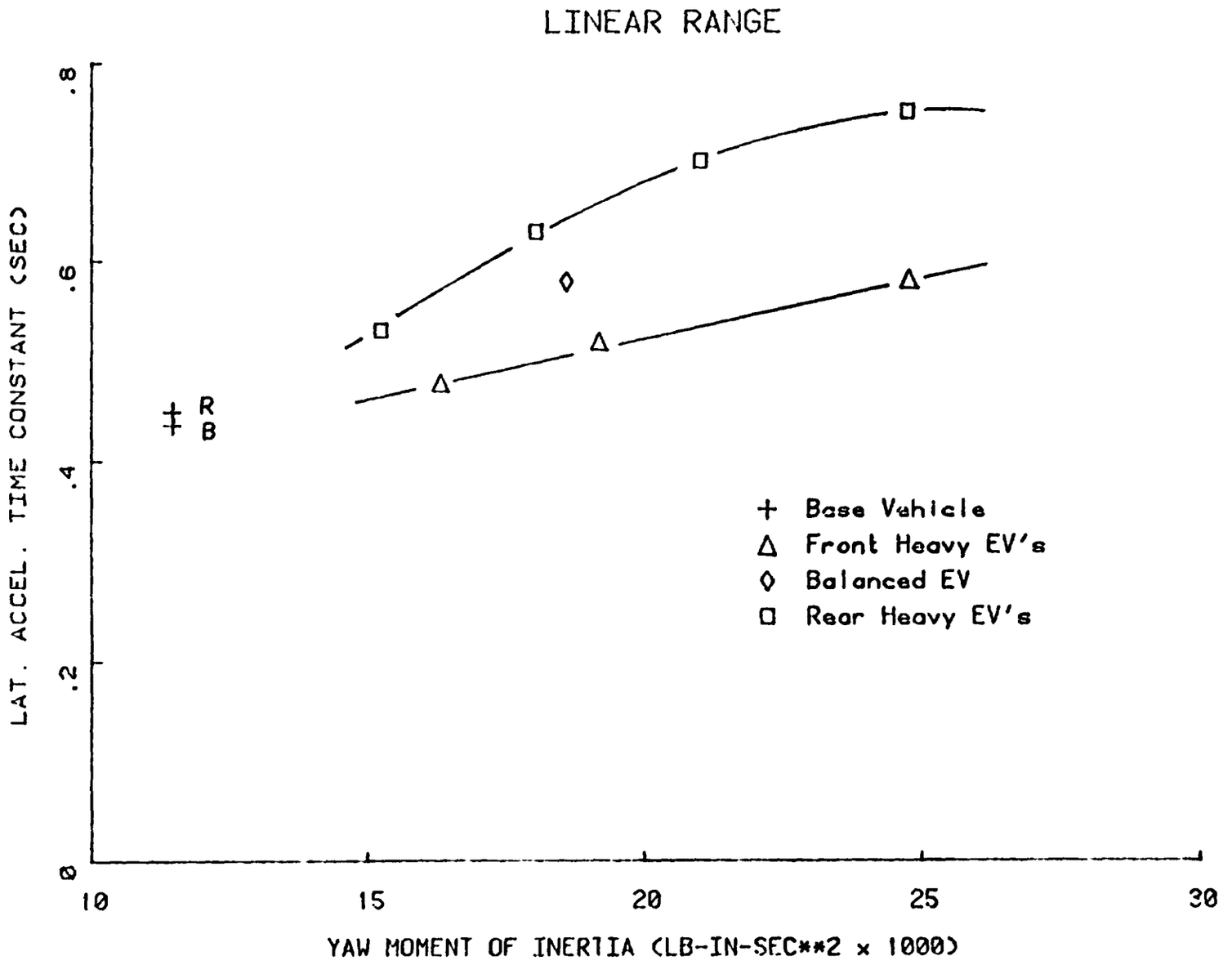

Figure 54 EFFECT OF INERTIA AND WEIGHT DISTRIBUTION ON LATERAL ACCELERATION TIME CONSTANT

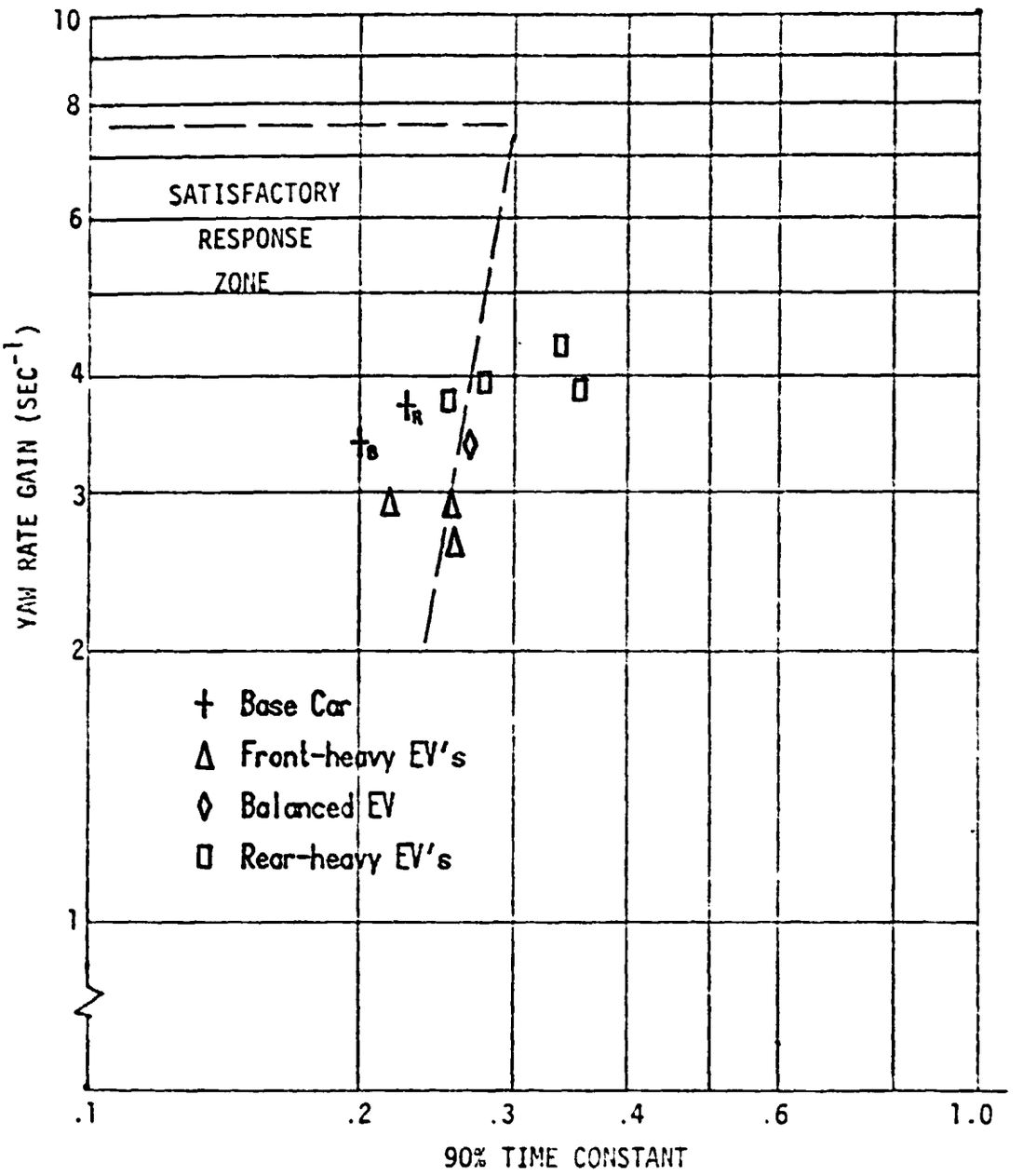

Figure 55 EFFECT OF WEIGHT DISTRIBUTION ON DIRECTIONAL RESPONSE OF VEHICLES

Although the boundaries are not considered to be exact, the trend again is for the front-heavy configurations to be favored over the rear-heavies.

Considering performance in the linear range of handling qualities, the evaluation of simulation results consistently points out a distinct advantage of designing a relatively high inertia vehicle so that the weight distribution is front-heavy. Since front/rear distributions beyond 55/45 in the front-heavy direction have not been explored, this conclusion is restricted to front axle loadings not exceeding 55% of the sprung weight. Balanced (50/50) distribution or even mildly rear-heavy weight distributions do not offer the advantages of a front-heavy distribution; rear-heavy configurations with a sprung mass yaw moment of inertia on the order of 20,000 lb-in-sec^2 or greater is believed to be particularly prone to severe handling problems.

Trapezoidal Steer Maneuver

This maneuver characterizes the directional response of a vehicle to a transient steer input, and is a standard handling test that is easy to perform and commonly used by the automotive industry and research organizations involved in handling studies. Results of the computer simulations of this maneuver for the case of a moderately severe steer input (normalized steer angle of 8°) will now be reviewed in the context of weight distribution effects. This amount of steer input produces steady-state (trim condition) lateral acceleration on the order of 0.5 to 0.6 g for the 95" wheelbase configurations, and is thus beyond the linear range of vehicle operation.

Peak body sideslip angles predicted for this maneuver are given in Figure 56 for the base vehicle (with bias-ply and radial tires) and the three categories of front/rear weight distribution. This figure indicates that the front-heavy EV's do not generate sideslip angles significantly above the base car, and are relatively invarient with respect to moment of inertia for the wide range considered. However, the peak sideslip angles for the rear-heavy

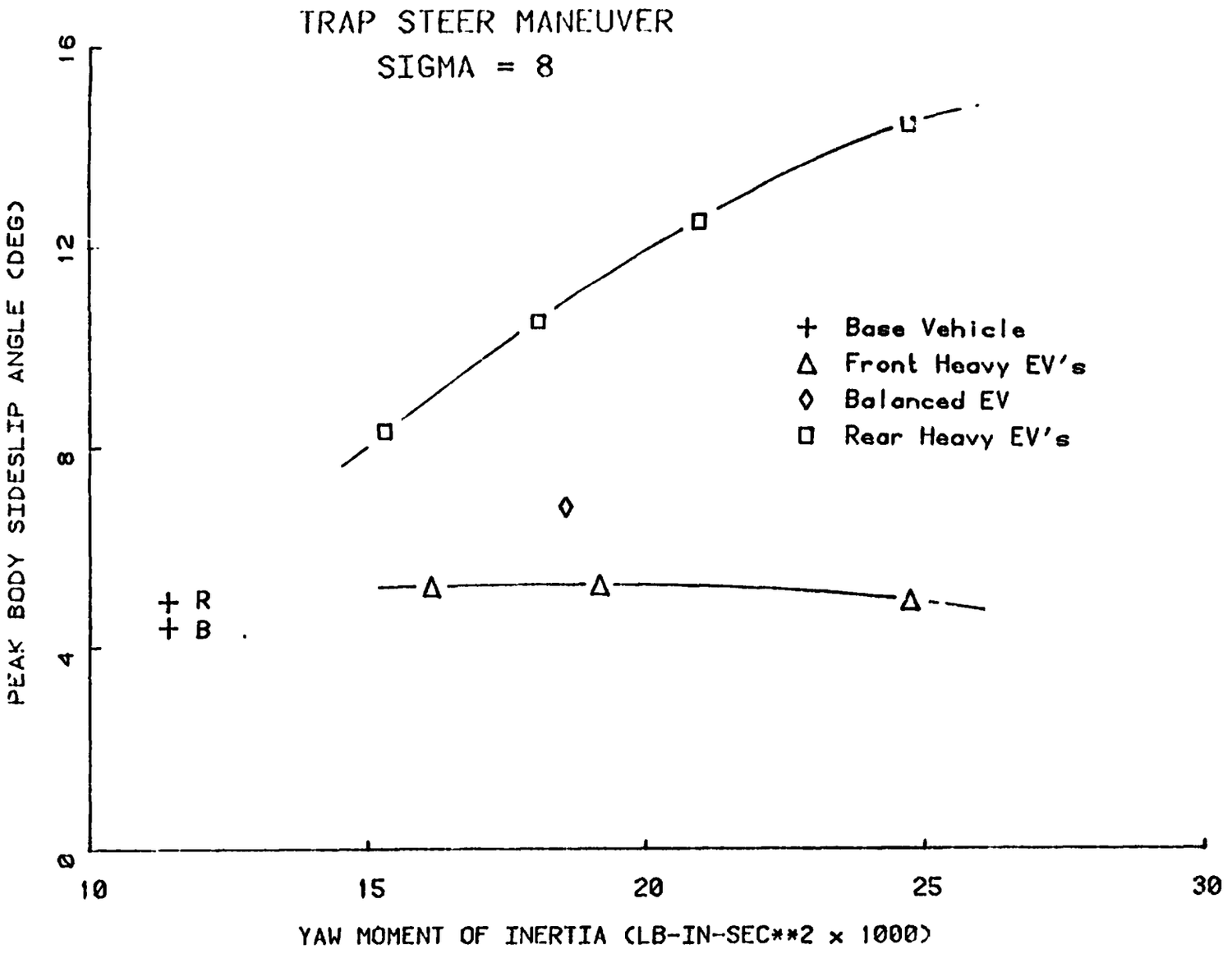

Figure 56 EFFECT OF INERTIA AND WEIGHT DISTRIBUTION ON PEAK SIDESLIP ANGLE

configurations are strong functions of rotational inertia and greatly exceed the base car sideslip response throughout the inertia range. The balanced configuration is seen to produce sideslip between that for the front and rear heavy distributions for the specific moment of inertia of this single balanced configuration.

Figure 57 presents yaw velocity response time as a function of moment of inertia for the same group of configurations. It is seen that response time constants tend to diverge when yaw moment of inertia reaches about 20,000 lb-in-sec^2. For the front-heavy EV's, the time constants remain relatively constant and of the same general magnitude as for the base car. But, the rear-heavy time constants increase dramatically for the higher range of inertia.

This trend is even more pronounced when considering the lateral acceleration time constants in Figure 58. Response times related to this variable (lateral responsiveness) are clearly excessive for the rear-heavy configurations with moment of inertia approaching (and exceeding) 20,000 lb-in-sec^2. The balanced and front-heavy EV's are, however, not strong functions of inertia and are in fact not substantially different than the base car with respect to this response measure.

Findings related to the trapezoidal steer maneuver in the non-linear performance regime are supportive of the trends noted in the linear response range. A clear advantage is again indicated for a front-heavy design approach, and a rear-heavy configuration is found to be much more susceptible to poor handling characteristics for the generic class of EV's being considered.

Sinusoidal Steer Maneuver

This is a transient response maneuver which involves a reversal of steer input necessary to produce a lateral displacement, such as required for a rapid lane change. As was the case for the above evaluation of trapezoidal steer, we will select a moderately severe condition, i.e., a peak normalized front wheel steer angle of $\pm$ 8° for analysis.

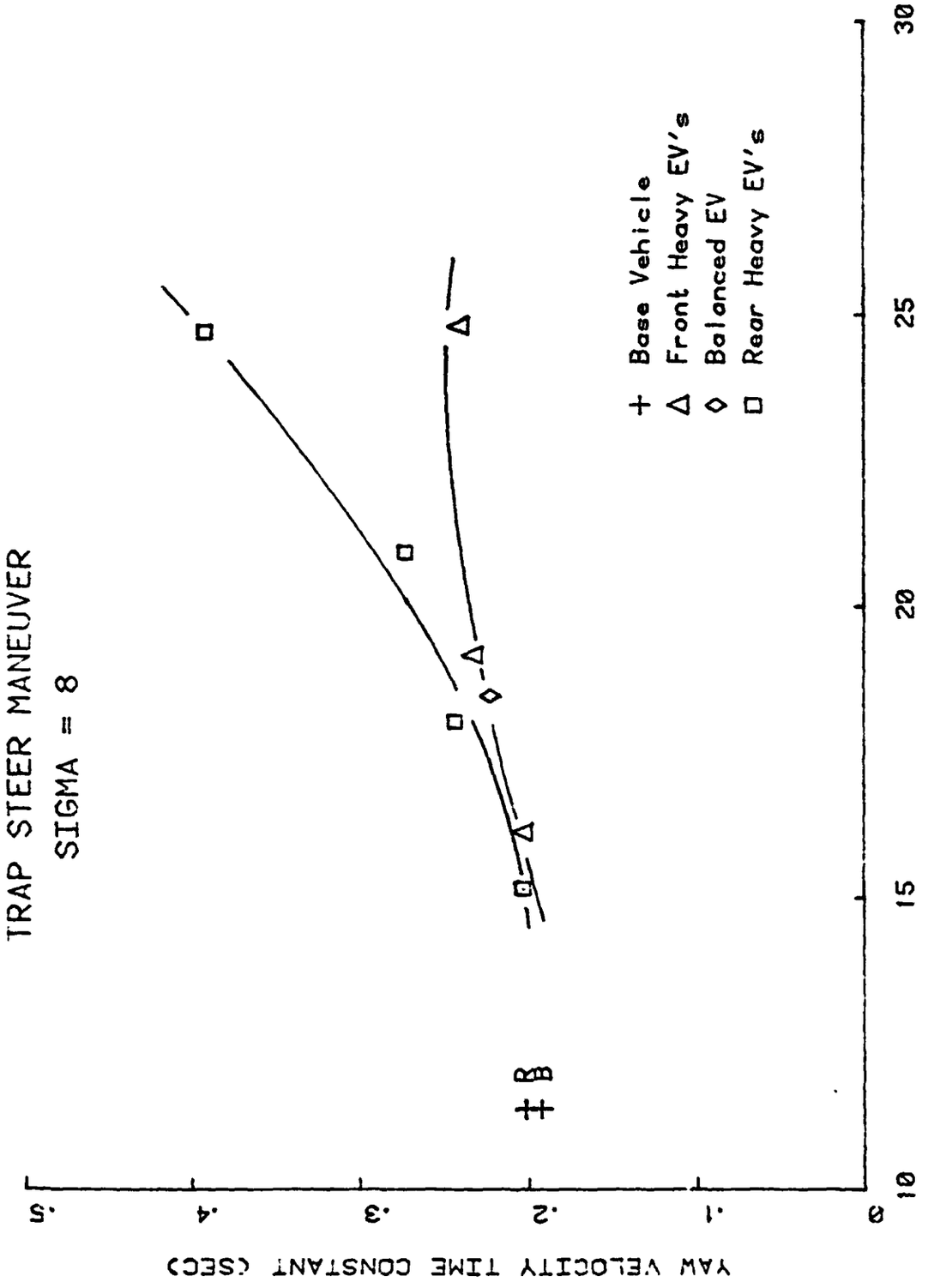

Figure 57 EFFECT OF INERTIA AND WEIGHT DISTRIBUTION ON YAW VELOCITY TIME CONSTANT

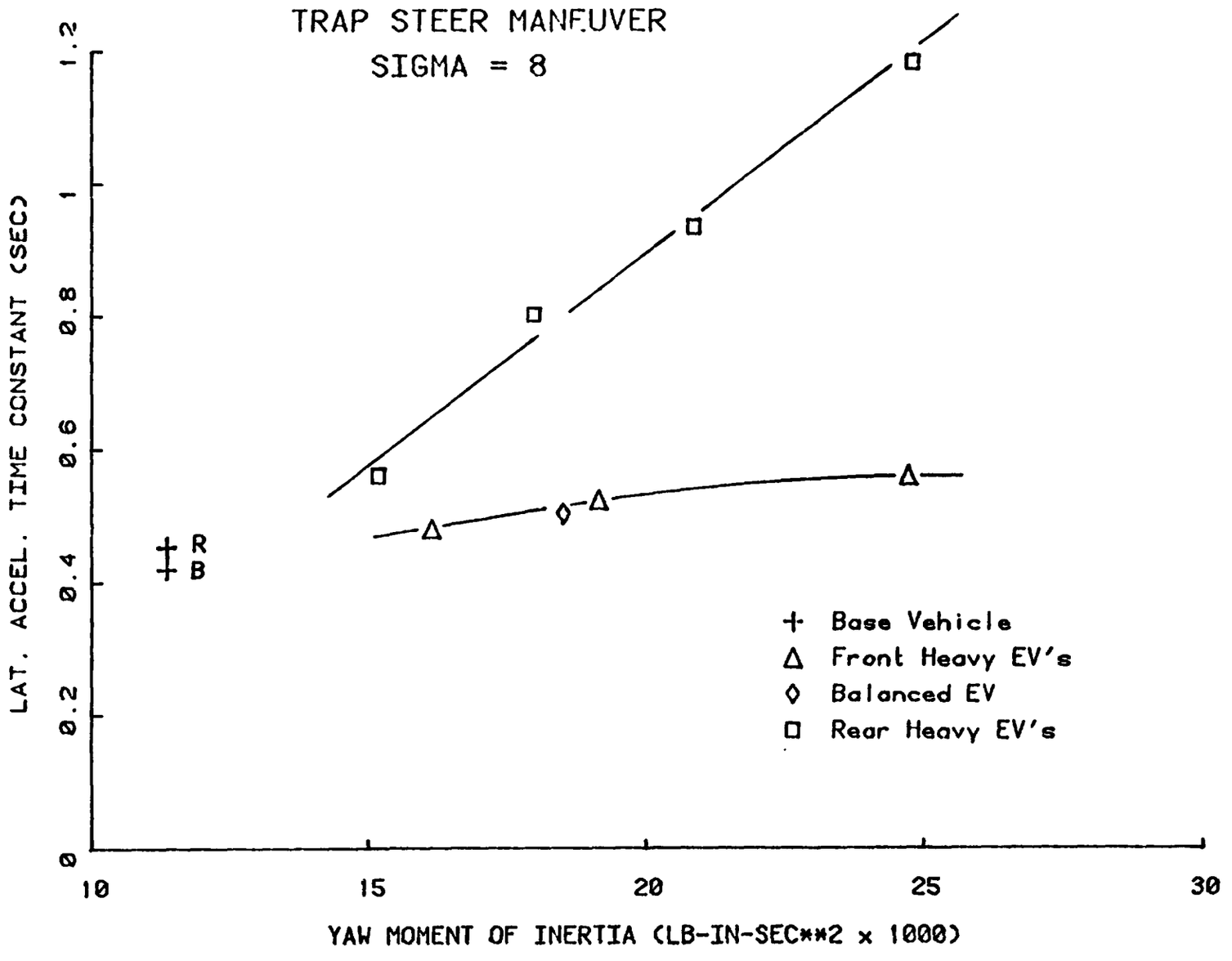

Figure 58 EFFECT OF INERTIA AND WEIGHT DISTRIBUTION ON LATERAL ACCELERATION TIME CONSTANT

Peak sideslip angles predicted by the simulation model are shown in Figure 59 for this transient condition. Although not strong functions of yaw moment of inertia, the rear-heavy configurations consistently produce higher sideslip than the front-heavy EV's. As has generally been the case, the balanced configuration gives a result between that of the two unbalanced weight distribution groups. The instabilities noted for the extreme limit condition are not apparent for this intermediate steer angle condition (refer back to Section 2.5 for limit performance results).

One important measure of the effectiveness of this maneuver is the lane change deviation from the "ideal" curvilinear path. Figure 60 shows lane change deviation (defined in Section 2.4) as a function of yaw moment of inertia. Since high deviations are undesirable, the front-heavy configurations again perform better than the rear-heavy configurations, at least in a relative sense.

The same trend is apparent when considering the magnitude of lateral displacement present at the end of the defined maneuver (at 3.4 sec.). Figure 61 illustrates that the front-heavy EV's are better behaved than the rear-heavies; recall that a lateral displacement of 12' represents the preferred response, and the front-heavy configurations respond very close to this desired magnitude of displacement.

Heading angle deviations (departure from a parallel path at the end of the maneuver) also favor the front-heavy approach. But, as shown in Figure 62, the two groups of unequal weight distribution EV's tend to show similar deviations at the higher levels of moment of inertia. Moment of inertia thus appears to have a stabilizing influence with respect to directional heading.

Yaw velocity response time lag and lateral acceleration response time lag is illustrated in Figures 63 and 64, respectively. Since high response times are known to be undesirable, the front-heavy configurations once again exhibit superiority over the rear-heavy and balanced weight distributions

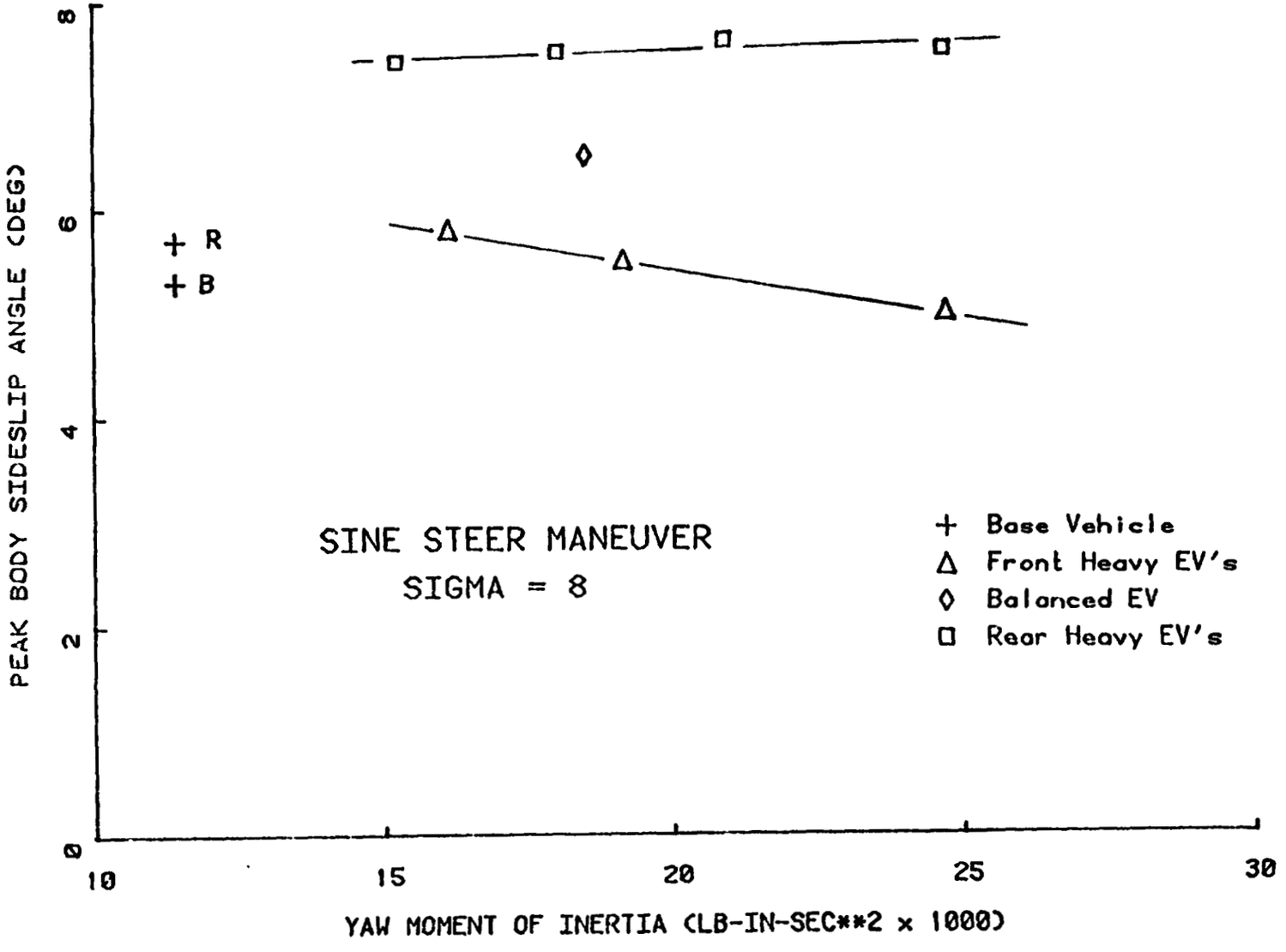

Figure 59 EFFECT OF INERTIA AND WEIGHT DISTRIBUTION ON PEAK SIDESLIP ANGLE

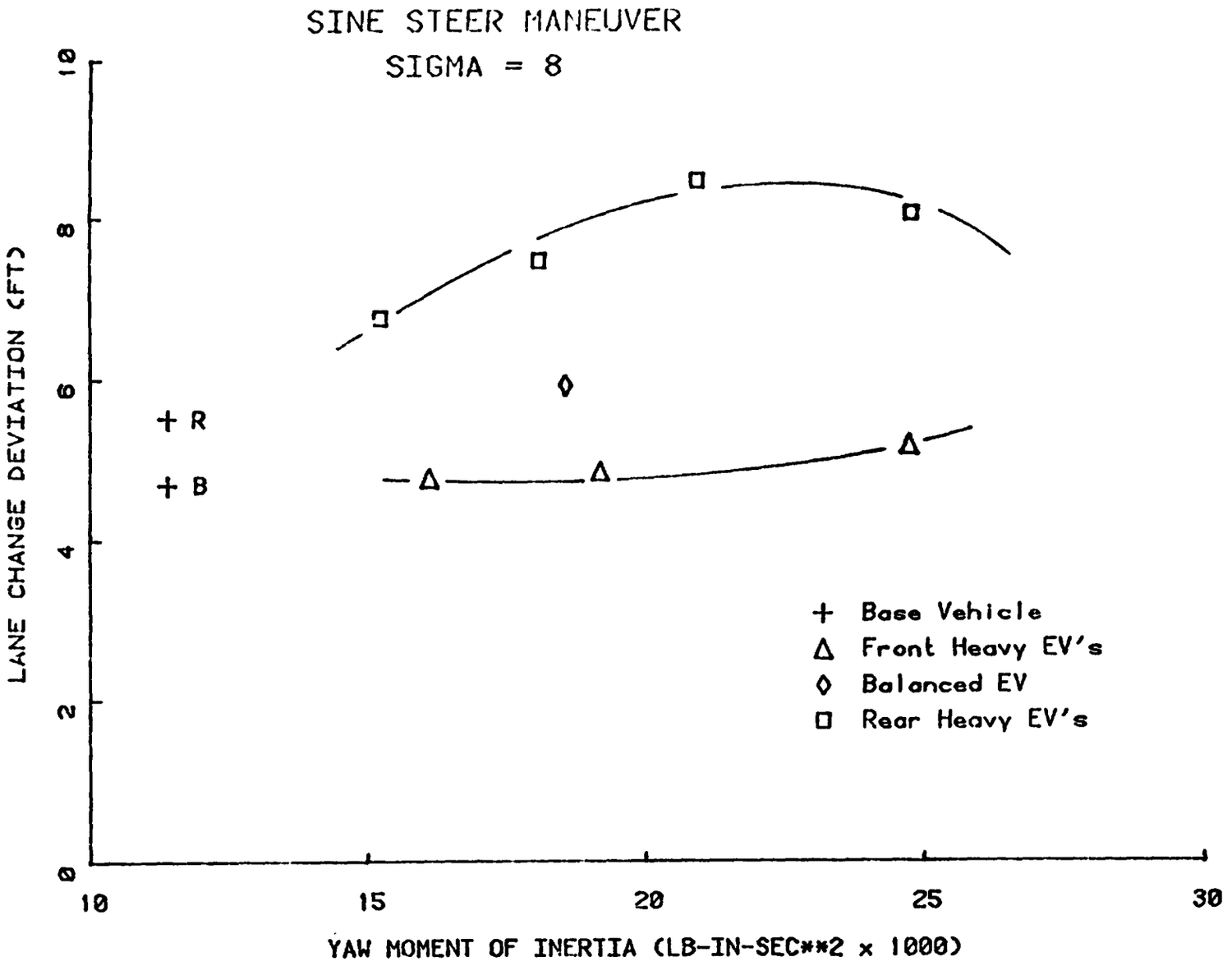

Figure 60 EFFECT OF INERTIA AND WEIGHT DISTRIBUTION ON LANE CHANGE DEVIATION

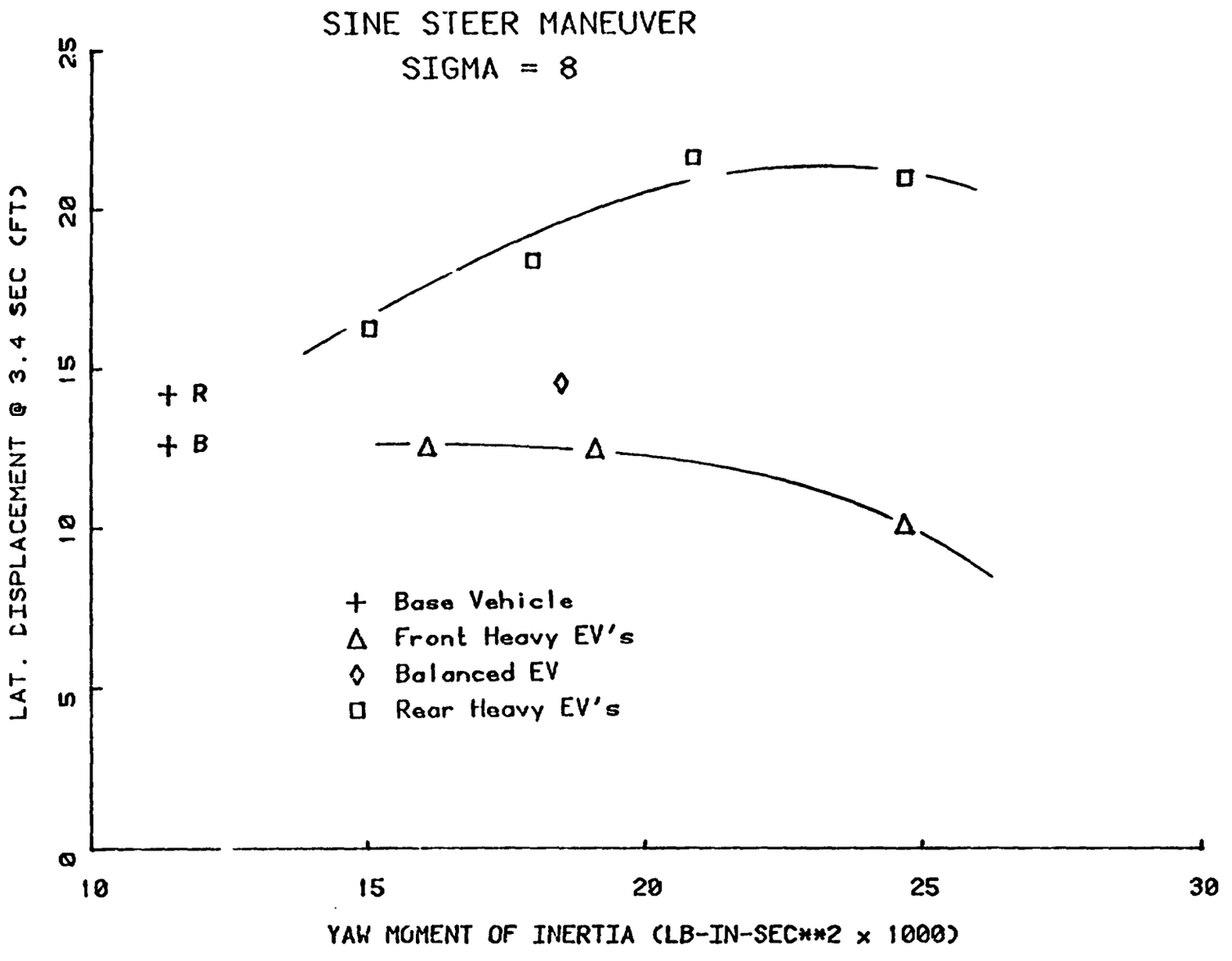

Figure 61 EFFECT OF INERTIA AND WEIGHT DISTRIBUTION ON FINAL LATERAL DISPLACEMENT

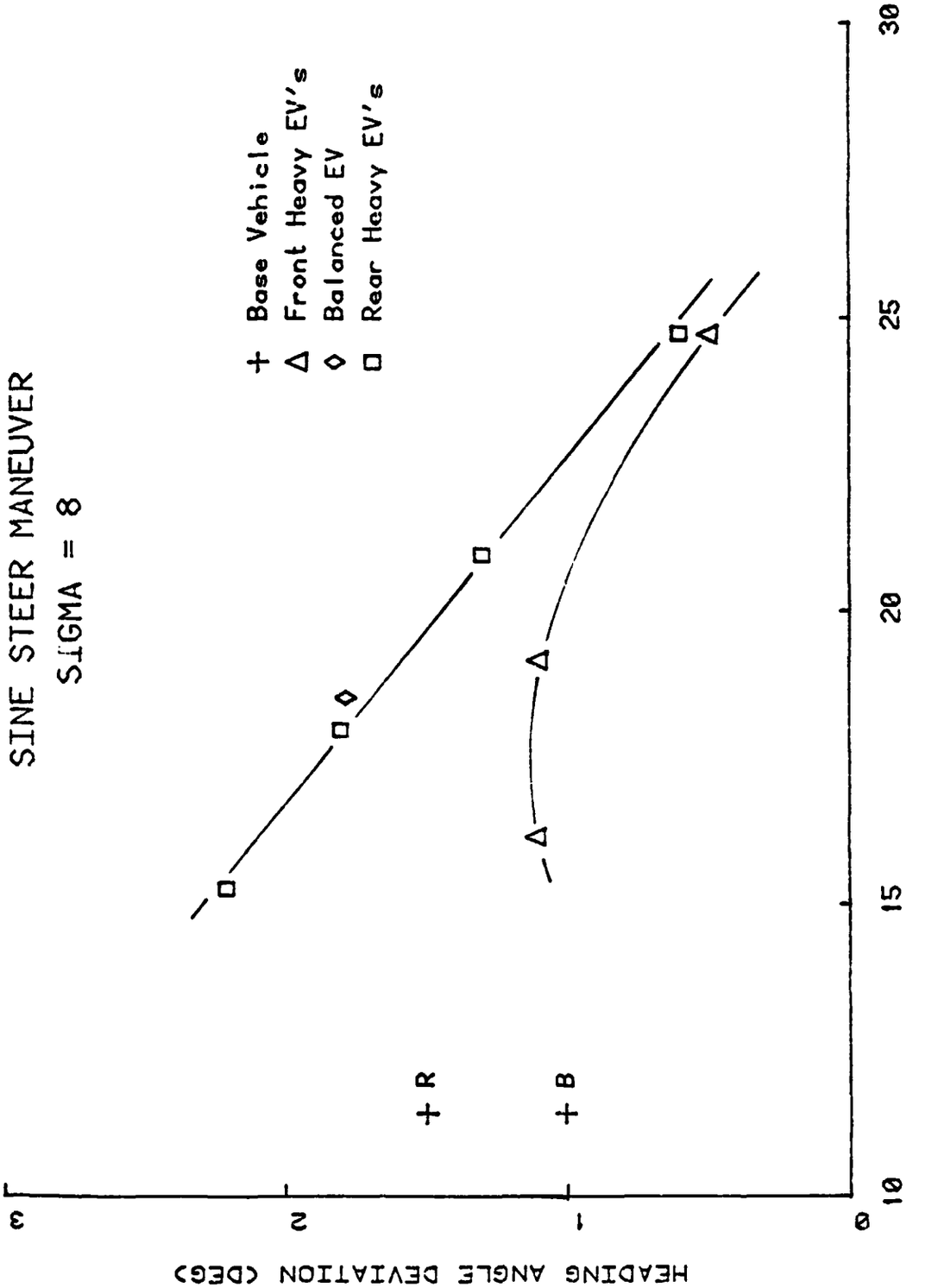

Figure 62 EFFECT OF INERTIA AND WEIGHT DISTRIBUTION ON HEADING ANGLE DEVIATION

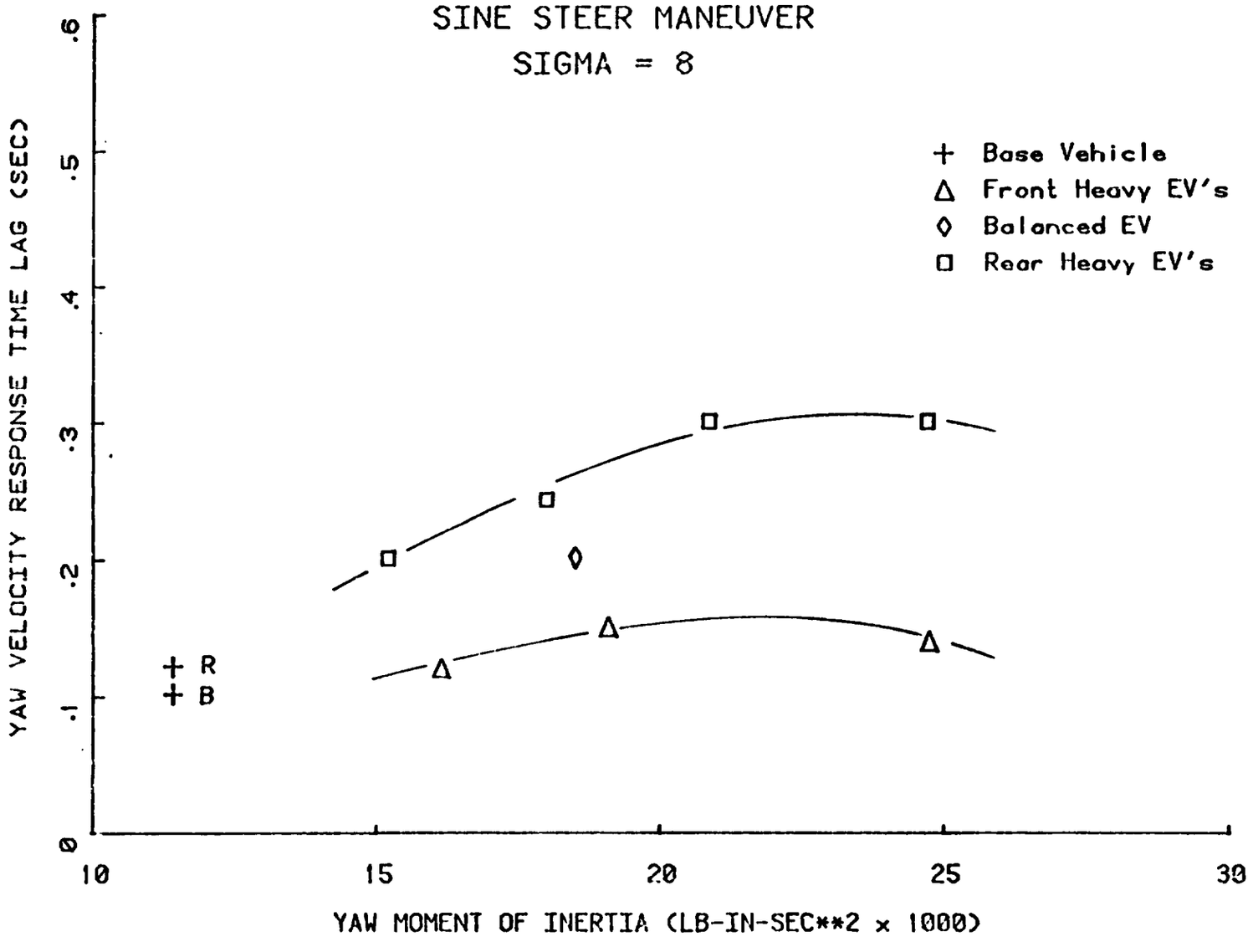

Figure 63 EFFECT OF INERTIA AND WEIGHT DISTRIBUTION ON YAW VELOCITY TIME LAG

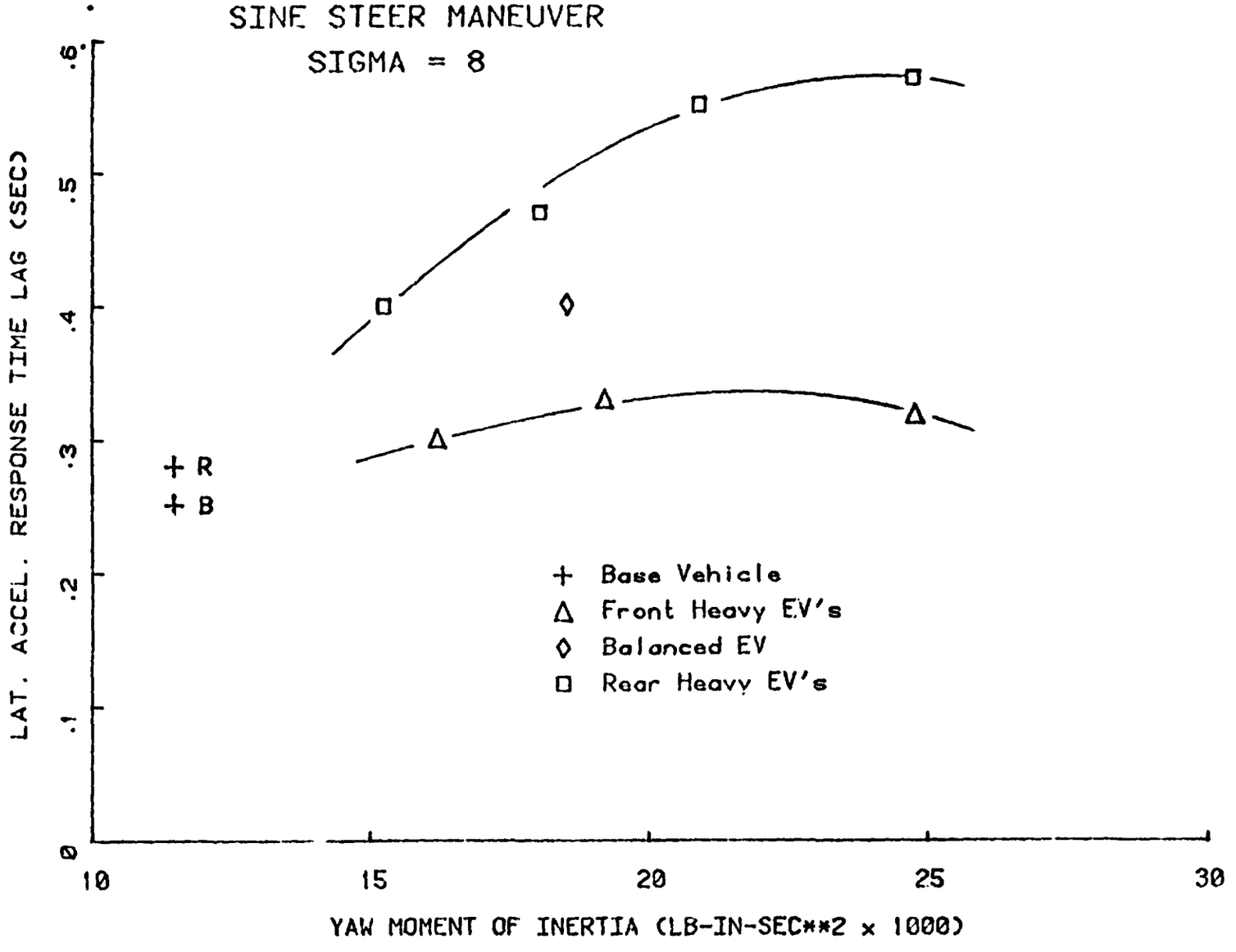

Figure 64 EFFECT OF INERTIA AND WEIGHT DISTRIBUTION ON LATERAL ACCELERATION TIME LAG

It is not possible to indicate limits of performance acceptability for the sinusoidal steer maneuver, since evaluation criteria are not well defined. Nevertheless, simulation results consistently indicate response trends which are in agreement with results of the steady-state steering analyses and the trapezoidal steer maneuver.

We will now evaluate a brief study of how tire and suspension properties can affect handling behavior.

2.9 Exploratory Study of Handling Performance Improvement

A limited study was conducted to give some insight into possible ways that electric vehicle handling might possibly be improved. The study focused on two important design areas--tire selection and suspension compliance adjustment.

It is recalled that properties of two different tires were used in the main part of the study. These were A78-13 bias-ply tires for the base car, and BR78-13 radial tires used on all EV configurations as well as the base car. From a design load standpoint, the A78-13 tires would be underrated for the EV's and the BR78-13 tires would be marginally acceptable, but a reasonable choice for the EV's with the possible exception of the heaviest vehicles. We have thus investigated the effect that larger (FR70-14) tires would have on handling performance. It is well known that larger (14 inch) tires would offer the advantage of improved boulevard ride characteristics and these tires also have higher cornering stiffness than the 13 inch tires considered previously.

Adjustment of suspension compliances is an important aspect of achieving acceptable handling qualities of an automobile in the design stage, and is widely practiced by manufacturers. It is again pointed out that compliance properties known for the base car were maintained constant for all of the EV derivatives. These compliances describe, in a quantitative

manner, the amount of flexibility existing in a given suspension system. Refer back to Section 2.3 for more details concerning compliance effects.

For the illustrative purposes of this study, we have selected three bounding conditions related to compliance adjustment:

- Zero front compliance and "standard" rear compliance
- "Standard" front compliance and zero rear compliance
- No front or rear compliance

During the remainder of this section, the "standard" suspension compliances denote those for the selected base car (Chevette) and the "standard" tires are BR78-13 radials.

Two electric vehicle configurations were chosen for this investigation, one a front-heavy design and the other a rear-heavy, both with moderately high yaw moments of inertia. These are (refer back to Table 2):

- Conv. Drive, 50/50 Batteries, 10" Outboard
  Front/rear weight distribution = 55/45
  Yaw moment of inertia = 19,140 lb-in-sec^2
- AiResearch Drive, 2/3-1/3 Battery Split Over Axles
  Front/rear weight distribution = 44/56
  Yaw moment of inertia = 20,906 lb-in-sec^2

Base car properties were varied in the same manner as the EV's for comparative purposes.

Because of the limited scope of this evaluation, only the steady-state properties (linear range) and trapezoidal steer properties (normalized steer angle = 8°) were obtained. Simulations results are discussed in the following.

Steady-State Steering Characteristics

The understeer gradient (K) varies as shown in the table below for the three vehicles simulated, as a function of the tire and compliance "adjustments" considered.

	UNDERSTEER GRADIENT (deg/g)				
	Standard*	14" Tires	No Frt. Comp.	No Rear Comp.	No Comp.
Base Car	4.9	3.7	1.0	5.1	1.5
Front-heavy EV	6.9	5.1	1.0	7.0	1.7
Rear-heavy EV	3.5	3.2	-1.1	4.7	0.1

The larger tires are seen to decrease understeer somewhat, particularly for the base car and front-heavy EV, but not to the extent of producing undesirable characteristics (these reductions may actually represent slight improvements). On the other hand, removing either the front compliances or all compliances produces a nearly neutral or, in one case, an oversteering condition ($K < 0$). This supports the finding based on linear theory (Section 2.3) that the rear-heavy EV's are inherently oversteering cars, but adjusted to understeer by suspension compliances. Eliminating only the rear suspension compliances results in a slight increase in understeer gradient, but not to an excessive magnitude.

Sideslip sensitivity ($\partial\beta/\partial a_y$), an undesirable phenomenon if excessive, is dramatically reduced by the use of 14" tires as shown below:

	SIDESLIP SENSITIVITY (deg/g)				
	Standard	14" Tires	No Frt. Comp.	No Rear Comp.	No Comp.
Base Car	4.1	1.6	4.3	3.4	3.7
Front-heavy EV	6.2	2.6	6.3	4.4	5.0
Rear-heavy EV	8.2	3.9	11.0	6.2	7.7

*Values for "standard" vehicle configurations taken from Table 7.

Note also that reducing the rear suspension compliances (or all compliances) can have a beneficial effect on sideslip sensitivity. But, eliminating front compliances only has an insignificant affect on the base car and front-heavy EV and actually aggravates the sideslip behavior of the rear-heavy EV.

With respect to Yaw Velocity Response Time Constant (T_r), increasing tire size results in a beneficial reduction for the rear-heavy EV, but has no discernable affect on the base car and front-heavy EV. The most interesting finding is that reduction in front suspension compliances can have a very deliterious effect on the response time. For instance, as indicated in the table that follows, the time constant is increased from 0.34 sec. to 1.42 sec. for the rear-heavy EV.*

YAW VELOCITY TIME CONSTANT (SEC)

	Standard	14" Tires	No Frt. Comp.	No Rear Comp.	No Comp.
Base Car	0.23	0.23	0.30	0.21	0.28
Front-heavy EV	0.25	0.25	0.42	0.24	0.34
Rear-heavy EV	0.34	0.26	1.42	0.28	0.67

Response time reductions are apparently achievable by compliance adjustment only for the condition where the rear compliances are reduced with the front compliances kept the same (or perhaps increased).

Lateral acceleration Time Constant (T_a) is affected by these changes in the same general trends:

* Highly excessive response time constants are characteristic of an oversteering car, which the rear-heavy configuration was previously shown to become with the front compliances removed.

	LATERAL ACCELERATION TIME CONSTANT (SEC)				
	Standard	14" Tires	No Frt. Comp.	No Rear Comp.	No Comp.
Base Car	0.45	0.36	0.61	0.43	0.54
Front-heavy EV	0.52	0.40	0.80	0.49	0.65
Rear-heavy EV	0.70	0.55	1.70	0.62	1.09

Increasing tire size results in a very pronounced decrease in time constant for each of the vehicles. Reducing rear compliances has a somewhat less dramatic effect, but nontheless, is beneficial. As with the yaw velocity time constant, reducing front compliances has a negative influence, as does reduction of all compliances.

In summary, linear response behavior can benefit by increasing tire size (increased cornering stiffness) and/or reducing the compliance (flexibility) of the rear suspension. A compliant front suspension appears to enhance linear performance, since this provides desirable understeer behavior and shorter response times.

Trapezoidal Steer Maneuver (σ = 8°)

As previously discussed in Sections 2.5 and 2.8, the numerics of particular concern for this maneuver are the peak sideslip angle, yaw velocity (rate) response time and lateral acceleration response time. Changes in these response variables resulting from the tire and compliance variations are evaluated in the remainder of this section.

Peak body sideslip angles predicted by the computer simulation are given in the table below:

	PEAK SIDESLIP ANGLE (DEG)				
	Standard	14" Tires	No Frt. Comp.	No Rear Comp.	No Comp.
Base Car	4.9	3.3	10.0	4.2	8.4
Front-heavy EV	5.2	3.5	11.0	4.2	8.5
Rear-heavy EV	12.5	7.6	30.0	8.0	21.2

The increased tire size has a very favorable effect on sideslip, especially for the rear-heavy EV. Reduction of rear compliance (without changing front compliance) also appears to have a positive influence. But, reducing front compliances (or all compliances) can severely degrade performance. Particularly note the extremely high sideslip angle associated with the rear-heavy EV when front compliances are eliminated.

Yaw velocity and lateral acceleration response times are given in the following table (lateral acceleration time constants in parentheses);

YAW VELOCITY RESPONSE TIMES (sec)
[LATERAL ACCELERATION RESPONSE TIMES (sec)]

	Standard	14" Tires	No Frt. Comp.	No Rear Comp.	No Comp.
Base Car	0.20 (0.45)	0.19 (0.37)	0.15 (0.50)	0.20 (0.44)	0.16 (0.40)
Front-heavy EV	0.23 (0.52)	0.21 (0.40)	0.19 (0.63)	0.22 (0.48)	0.19 (0.46)
Rear-heavy EV	0.27 (0.93)	0.24 (0.75)	0.35 (0.82)	0.22 (0.60)	0.32 (0.92)

Response time reductions are realized by increasing tire size. Decreasing rear compliance also gives beneficial reductions, but similar reductions in front compliance do not consistently provide reduced response times. The rear-heavy EV is seen to be most sensitive to the tire and compliance variations.

Results of the trapezoidal steer simulations are consistent with behavior in the linear range with respect to sideslip response and time constants. It is clear that increasing tire cornering stiffness (for instance by going to a high cornering stiffness 14" tire) has distinct advantages. Likewise, by prudent design of suspension compliances, i.e., minimizing rear suspension flexibility and properly selecting front suspension compliances, handling qualities can perhaps be improved. Thus, it may be possible to counteract some of the undesirable effects of high mass and yaw moment of inertia by tire and/or suspension modifications.

It is noted that using differential tire pressures (different pressures in the front and rear tires) can affect handling response since this, in effect, provides different cornering stiffnesses between the front and rear. Using different sizes or types of tires front and rear can also affect handling. However, handling "fixes" of this nature are believed to be poor practice. Proper handling qualities should be designed into the vehicle so that dependence on proper maintenance by the consumer is minimized.

This study is by no means a thorough treatment of the subject of effective suspension design, etc. There are many other vehicle parameters that can conceivably be investigated with respect to achieving handling performance improvements of electric vehicles (or any vehicle). Since a thorough study was beyond the scope of the present effort, our intent was only to point out the importance of addressing handling performance during the design stage of a vehicle. In addition, since many electric vehicle prototypes or production EV's are conversions of ICE cars, it is important to consider ramifications of maintaining original equipment suspension components and/or tires. Proper modification of these components can provide important handling improvements.

3. CONCLUSIONS

Main conclusions of the electric vehicle dynamics study are summarized here. It is recalled that the study focused on handling performance of hypothetical EV's with a wheelbase of approximately 95 inches, and these conclusions thus apply only to this size car in a strict sense. Nevertheless, we believe that generalization to larger or smaller cars is reasonable on a qualitative basis.

A Front-Heavy Weight Distribution is Advantageous

A most significant finding resulting from this study concerns the importance of maintaining a front heavy weight distribution on electric vehicles--whether they be conversions of conventional vehicles or totally new designs. We have examined EV configurations ranging from a 55/45 front/rear weight distribution to a 44/56 front/rear split and have characterized front heavy vehicles, balanced vehicles and rear heavy vehicles as having 55/45, 50/50, and 45/55 front/rear distributions, respectively.

Results presented in the previous sections consistently indicate that vehicles with a front-heavy weight distribution can tolerate a wide latitude of mass and yaw moment of inertia increases without severely compromising handling qualities. Rear-heavy configurations (and balanced configurations to a lesser extent), are much more susceptible to undesirable degradations in response metrics resulting in excessive body sideslip, long response times to steer inputs, and large phase lags between control inputs and directional responses as mass and inertia increase. These trends were uniformly evident for the linear range of performance as well as for the maneuvers simulated in the non-linear performance regime, i.e., trapezoidal steer inputs (severe cornering conditions) and sinusoidal steer inputs (quick lane change behavior).

It should be pointed out that front-heavy vehicles exhibited a trend that could be somewhat troublesome for extreme forward weight biases, i.e.,

lower yaw velocity and lateral acceleration response gains than were seen with the balanced or rear heavy vehicles. High steering torque requirements can also result from these configurations. But, these potential problems are more easily corrected (by steering system design or modification) than are the more fundamental lateral response problems associated with rear-heavy vehicles.

It is universally agreed that all passenger cars to be used by the general public should be "understeering". That is, steer angles must be increased to maintain a given radius of curvature as forward speed is increased. A basic attribute of a front-heavy car is that it will be intrinsically understeer. Rear-heavy vehicles can be made to understeer (even though they will possess intrinsic oversteering tendencies) by appropriate suspension design to provide counteracting compliance-steer and roll-steer properties, or by practices such as employing different front and rear tire pressures (which are not recommended for a vehicle to be used by the general public). But, even when a rear-heavy vehicle is designed to understeer, it will still be prone to excessive time constants and response lags when relatively high yaw moments of inertia are present.

Considering all results of this study, we strongly conclude that it is highly desirable to design electric vehicles so as to maintain a forward weight bias under all intended load conditions.

Moment of Inertia Limitations

This study has considered battery weight additions to a subcompact base car ranging between 1080 lbs. (18 sixty pound batteries) and 1840 lbs. (20 ninety-two pound batteries). Various packaging layouts of these batteries together with associated electric powertrain concepts resulted in sprung mass yaw inertias between about 15,000 and 25,000 lb-in-sec^2. The base car has a yaw moment of inertia of approximately 11,000 lb-in-sec^2. These magnitudes are for a two passenger loading condition.

Results of the study indicate that the front-heavy configurations maintain reasonable handling qualities (relative to base car performance) throughout the range of yaw inertia given above. Of course, some degradation of handling qualities was evident, as expected, for the extremely high inertia magnitude, but not to such an extent as to be grossly unacceptable. This conclusion appears to be tenable when it is realized that production passenger cars exist with comparable wheelbase, weight and yaw moment of inertia. For instance, the AMC Pacer has a wheelbase of approximately 100", weighs 3370 lbs., and has a yaw moment of inertia of about 22,400 lb-in-sec^2 (see Appendix A). Of course, as is the case for all recent model U.S. production cars, the AMC Pacer is front-heavy.

Conversely, the rear-heavy configurations possess fundamentally different handling qualities as yaw inertia is increased. The general tendency is for handling performance to severely degrade as yaw moment of inertia is increased beyond a magnitude on the order of 18,000 to 20,000 lb-in-sec^2. Although we cannot emphatically state that this is an absolute limit of acceptability, it is abundantly clear that a rear-heavy EV (or even a balanced configuration) cannot tolerate relatively high inertia properties nearly as well as a front-heavy weight distribution layout.

Proper Attention Must be Given to Tire Selection and Suspension System Design

Particularly when converting a conventional car to electric power, an analysis of proper tire selection may be ignored. The increase in weight associated with battery addition can obviously result in loadings beyond the OEM tire rated capacity. Proper load range tires must therefore be chosen for all electric vehicles. In addition, emphasis on selecting tires with proper cornering stiffness is equally important. Results discussed in Section 2.9 indicate that proper choice of tires can substantially improve handling qualities.

Another important aspect of EV design that is commonly overlooked relates to suspension characteristics. Adjustment of spring rates consistent with suspension loadings is obviously necessary, and generally practiced because the need is so evident. However, proper design of other (not obvious) suspension characteristics can be of great benefit to EV handling performance. For instance, this study has shown that suspension compliances (flexibility)--which are necessary for vibration and noise isolation--can have a critical (and sometimes dominant) effect on steering behavior, e.g., the understeering properties. Attention to overall suspension design can thus be very beneficial and, if properly implemented, can tend to counteract undesirable effects of relatively high mass and inertia.

Braking Systems Must be Designed Consistent with Weight Distribution

As illustrated in this study, the most important aspect of achieving reasonable braking performance is proper proportioning of braking torques between the front and rear wheels. Because of static front/rear weight distribution and forward weight transfer during braking, the torque must be applied so as to avoid undesirable behavior such as rear wheel lock-up before the front wheels lock, thereby causing yaw instability resulting from the loss of rear tire cornering power.

If braking systems are not properly designed (or modified) for a given EV configuration, which we believe is often the case when the conventional passenger car is converted to electric operation, performance problems can result which have severe safety implications. This is particularly true if the base vehicle weight distribution is substantially altered by the electric conversion, which is normally the case.

A Methodology to Support EV Handling Design Exists

Perhaps the most important result of this study is the demonstration that an analytical methodology presently exists which can be applied to the

design and development of electric vehicles having satisfactory handling qualities. Such a methodology can help avoid handling problems when an EV is designed from the ground up, or can indicate potential problems which may result from retrofitting an existing vehicle. If properly employed, handling performance analysis can also provide guidelines for EV design which can potentially offer handling improvements without unreasonable compromise of other design constraints. The prime example resulting from this study relates to front/rear weight distribution; it has been shown that packaging adjustments, which change a vehicle from a rear-heavy (or balanced) weight split to a moderately front-heavy configuration can offer distinct handling advantages.

The methodology that currently exists is not fully developed and validated at this time, since this study represents the first investigation of this subject, to our knowledge. Nevertheless, a strong technical foundation exists which can be of benefit to electric vehicle dynamics technology

4. RECOMMENDATIONS

Contained in the following are several recommendations that, in our opinion, are of a high priority nature and would effectively advance the state-of-the-art of electric vehicle technology related to handling performance.

Experimental Program

We recommend that a testing program be conducted that would (1) provide data for validating results of this analytical study, and (2) allow additional criteria to be developed for evaluating handling quality acceptability of EV's.

With respect to generating handling data for validation, a limited program would suffice utilizing a Chevette as the test vehicle; provision for altering weight distribution and moments of inertia would be required (controlled ballasting), as well as changing suspension spring rates.

A program for defining EV handling performance criteria would be more ambitious. Subjective and objective information would be required, and several actual EV prototypes would probably be the best test vehicles for this research (perhaps the GE/Chrysler and/or AiResearch prototype vehicles could be included in the sample) along with a suitable conventional car for comparison. The goal should be to establish ranges of handling response numerics (steady-state steering properties, time constants, limit maneuver response measures, etc) consistent with the intended mission of the electric vehicle. To our knowledge, no such project has ever been conducted, except for passenger cars where high speed performance has been stressed.

Vehicle Parameter Measurement Facility

In order to make maximum use of analytical methods for future research and investigating (predicting) handling performance of prototype

electric vehicles, a source for obtaining the necessary physical properties is required. Many of these properties can be measured with the Mobile Parametric Measuring Device (MPMD) under development by NHTSA. However, we know of no present plans to include suspension compliance measurement capability in this facility and no such capability currently exists outside of the automobile industry. In view of the importance of compliance effects, the treatment of these parameters in computer simulations is essential. As shown in Section 2.9, ignoring these effects can give a totally distorted evaluation (prediction) of handling performance.

Additional Basic Analytical Research

The present project represents the first investigation of electric vehicle handling performance using available analytical methods. It was necessarily limited in scope and therefore treated the subject in a relatively elementary manner. For instance, the project was concerned only with vehicles of a given size class (no wheelbase variation). Parameter variations were essentially limited to weight distribution, moments of inertia, tire characteristics, and suspension compliances. There are numerous other physical properties which affect handling qualities such as c.g. height, roll stiffness, suspension geometries, brake torque proportioning, shock absorber characteristics, and the like. Consequently, we recommend that an extended analytical investigation of EV handling be undertaken. We feel that this would be appropriate in parallel with an experimental program as recommended above.

Dissemination of Design Guidelines and Technical Assistance

Electric vehicle designers and manufacturers are in need of guidelines for properly incorporating handling qualities into their vehicles. This is particularly true for the small business manufacturer or entrepreneur. As this study suggests, fundamental information regarding desirable weight distribution and tire selection would perhaps help avoid many of the problems associated with vehicles having relatively high mass and moments of inertia.

It is not necessary or reasonable to provide detailed technical reports (such as this) to these individuals and companies. A brief digest, written in easily understood language without excessive technical content, would probably be the most effective approach for encouraging implementation of handling-related design concepts. Assistance in other areas could be offered by this approach as well, e.g., battery packaging, powerplant layout, crash safety, etc.

As a minimum, the electric vehicle community should be kept abreast of new technology and methodologies that could be applied to prototype and production vehicle design and evaluation. In addition, sources of assistance (either Governmental or commercial) should be made known to individuals and companies so that, if sufficient in-house capability is not available, outside consultation can be obtained in an expeditious manner. As in medicine, prevention or early diagnosis and treatment of a vehicle dynamics (or other) problem can be vitally important.

5. REFERENCES

1. Greene, J. E., "An Experimental Evaluation of the MARS II Electric Automobile," Calspan Corp. Report No. VJ-2623-K-1, February 1969.

2. Basso, G. L., "Functional Derivation of Vehicle Parameters for Dynamic Studies," National Aeronautical Establishment, National Research Council Canada, Report No. LTD-ST.747, September 1974.

3. Segal, D. J., "Highway-Vehicle-Object Simulation Model - 1976," (4 Volumes), Calspan Corp. Federal Highway Administration Report No. FHWA-RD-76-162, 163, 164, 165, February 1976.

4. Schuring, D. J., "Tire Parameter Determination," Vol. 1, Summary, Calspan Corp., Contract No. DOT-HS-4-00923, November 1976.

5. Milliken, W. F., et al., "Research in Automobile Stability and Control and in Tire Performance," published by the Institution of Mechanical Engineers, London. 1956.

6. Dell'Amico, F., "Steady-State Stability of the Automobile--An Approach Based on a Method of Tethered Vehicle Testing Using a Yaw Constraint," Cornell Aeronautical Laboratory Report No. YC-3004-K-1, August 1971.

7. Milliken, W. F., et al., "The Static Directional Stability and Control of the Automobile," SAE Paper No. 760712, October 1976.

8. Weir, D. H. and McRuer, D. T., "Review and Correlation of Driver/Vehicle Data," Systems Technology, Inc. (no number).

9. Ervin, R. D., et al., "Vehicle Handling Performance," Highway Safety Research Institute, The University of Michigan, Contract DOT-HS-031-1-159, November 1972.

10. Ervin, R. D., et al., "Refinement and Application of Open-Loop Limit-Maneuver Response Methods," Highway Safety Research Institute, The University of Michigan, SAE Paper 730491, May 1973.

11. Chiang, S. L. and Starr, D. C., "Using Computer Simulation to Evaluate and Improve Vehicle Handling," SAE Paper No. 780009, 1978.

12. Anon., "State-of-the-Art Assessment of Electric and Hybrid Vehicles," National Aeronautics and Space Administration, Lewis Research Center, Report No. HCP/M1011-01, February 1978.

APPENDIX A

VEHICLE PARAMETER MEASUREMENTS

Moments of inertia and related physical parameters were measured (under a purchase order arrangement) by Dynamic Science, Inc., Phoenix, Arizona, for the following vehicles:

- 1979 Chevrolet Chevette, 2-door model
- 1978 AMC Pacer Wagon
- EVA Pacer Electric Car*

Measurements were made using the Mobile Parametric Measurement Device (MPMD) developed under contract to the National Highway Traffic Safety Administration by Dynamic Science. Figure A-1 shows the EVA Pacer mounted on the measurement device. The device contains a platform supported by a hydraulically-lubricated, hemispherical bearing which allows nearly frictionless rotational motion about three orthogonal axes. The vehicle being measured is fixed to the platform and its suspension systems are constrained at static ride height by replacing the shock absorbers with rigid links. Calibrated reaction springs are then attached to the platform at known locations and small amplitude oscillations are induced about the desired axes of rotation. Measurement of the period of oscillation permits accurate calculation of the overall moments of inertia. The known moments of inertia of the supporting platform are then subtracted from the total inertias.

Once the moments of inertia are known for the total vehicle about specific axes of rotation, moments of inertia about the center of gravity of the vehicle can be calculated using appropriate transformation relationships This procedure has been validated by Dynamic Science and found to be accurate to within 2%.

*Produced by Electric Vehicle Associates, Inc., Cleveland, Ohio. A description of this vehicle is contained in Reference 12.

Figure A-1 EVA ELECTRIC MOUNTED ON MEASUREMENT DEVICE

Table A-1 contains results of the moment of inertia measurements for the three vehicles. Using these properties for the total vehicle, inertial properties for the sprung mass can be analytically obtained by assuming reasonable values for the unsprung masses and performing the necessary computations for subtracting the unsprung mass inertias and translating the center of gravity. Final parameters for the sprung masses are given in Table A-2.

Table A-1

PARAMETER MEASUREMENTS FOR TOTAL VEHICLES

Parameter	Chevette	AMC Pacer	EVA Pacer Electric
W_T (lbs)	2196 (57/43)*	3369 (55/45)	4488 (48/52)
a_T (in)	41.1	45.38	51.75
b_T (in)	53.4	55.06	48.44
ℓ (in)	94.5	100.44	100.19
h_{cgT} (in)	19.94	23.28	22.62
I_{xT} (lb-in-sec^2)	3462	5296	5758
I_{yT} (lb-in-sec^2)	13,421	22,696	34,337
I_{zT} (lb-in-sec^2)	13,817	26,210	37,914

*Front/rear weight distribution at the ground

Table A-2

CALCULATED PARAMETERS FOR SPRUNG MASS

Parameter	Chevette*	AMC Pacer**	EVA Pacer Electric**
W_s (lbs)	1848 (60/40)***	2859 (58/42)	3980 (50/50)
a_s (in)	37.89	42.38	50.43
b_s (in)	56.61	58.05	49.76
h_{cgs} (in)	21.63	25.24	23.94
I_s (lb-in-sec^2)	2975	5122	5681
I_{ys} (lb-in-sec^2)	11,124	18,942	29,261
I_{zs} (lb-in-sec^2)	11,206	22,408	34,630
I_{xzs} (lb-in-sec^2)	433	75	2468

* Calculations performed by MGA Research

** Calculations performed by Dynamic Science

*** Front/rear distribution of axle loading by sprung mass

APPENDIX B

SYNOPSIS OF COMPUTER MODEL

HIGHWAY/VEHICLE INTERACTION SIMULATION

Highway Vehicle Object Simulation Model (HVOSM) was developed under contract with the Federal Highway Administration by Calspan Corporation and other organizations to provide an analytical means of studying the interaction between an automobile and its environment. Two separate program versions are available, with each version having a specialized capability. The HVOSM-RD2 version was developed for evaluating roadside barriers, either of a rigid or deformable nature, and for detailed evaluations of roadway and roadside terrain geometrics such as those associated with railroad grade crossings, median earth berms and cut/fill slopes. The second program version, the HVOSM-VD2, was developed for the purpose of studying vehicle dynamics, particularly the effects of braking systems and the effects of driver control inputs in emergency and pre-collision situations.

The analytical representation of the vehicle (Figure 1) is an assembly of three, four, or five rigid bodies (depending on suspension options in use) consisting of the sprung mass (chassis and body) and unsprung masses (the wheels and/or axles) which move relative to the sprung mass. Since the sprung mass (M_s in the figure) is assumed to behave as a rigid body, six degrees of freedom (X'_c, Y'_c, Z'_c, $\emptyset$, θ, ψ) are required for its specification. If the independent front suspension is in use, the two front wheels (M_1, M_2) are assumed to move vertically with respect to the vehicle body and thus require one degree of freedom each (δ_1, δ_2). For a solid front axle (M_1), a vertical degree of freedom (δ_1) and a rotational degree of freedom ($\emptyset_F$) are required to describe its position and orientation. Similarly, for an independent rear suspension the wheels (M_3, M_4) have a degree of freedom each (δ_3,δ_4) and the solid rear axle (M_3) has a vertical (δ_3) and rotational ($\emptyset_R$) degree of freedom. The steer angle of the front wheels (ψ_f) is an optional degree of freedom which may be specified.

The Vehicle Dynamics Version includes rotational degrees of freedom for the four wheels. Thus, the effects on tire forces of rotational degrees of freedom are assumed to be isolated from the coupled differential equations of the

9950-297

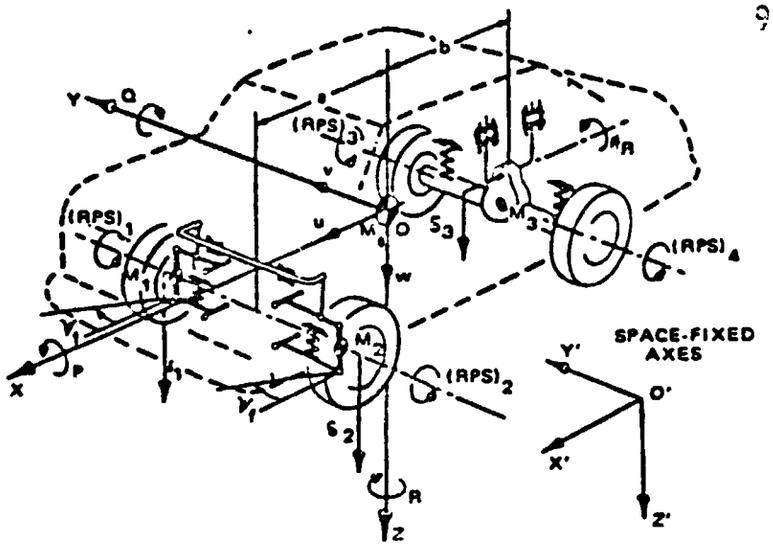

(a) INDEPENDENT FRONT - SOLID AXLE REAR SUSPENSION

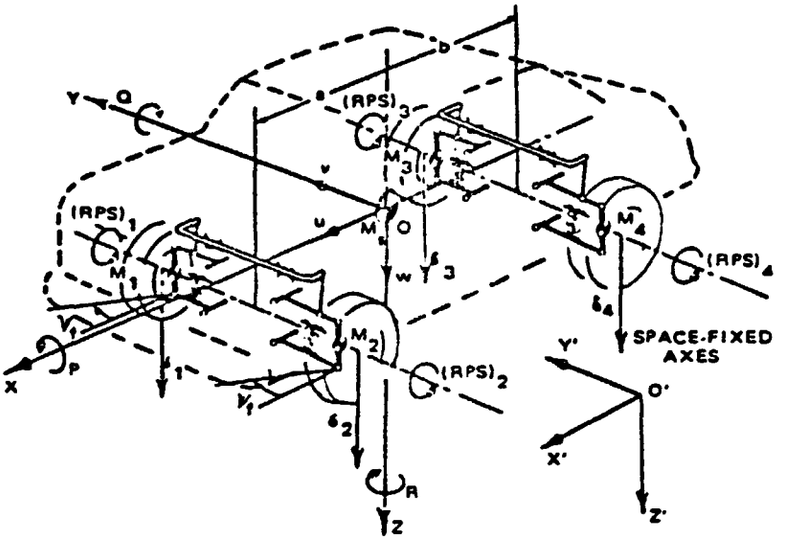

(b) INDEPENDENT FRONT AND REAR SUSPENSION

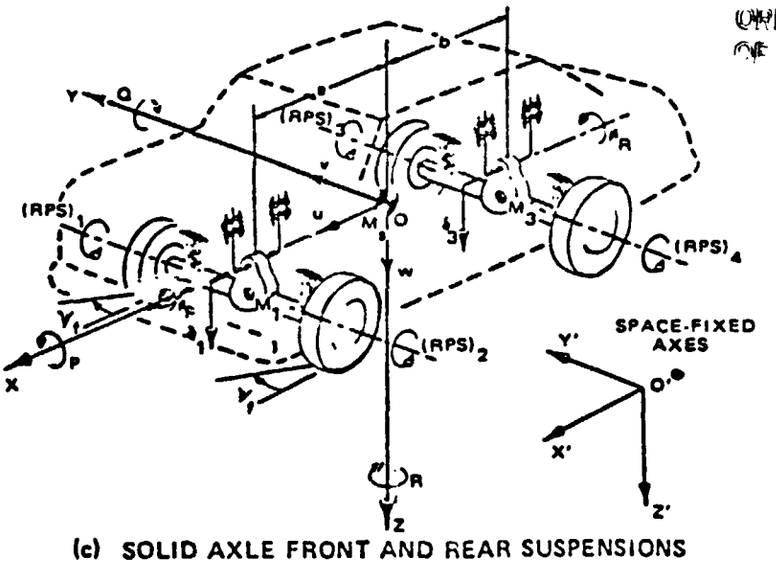

(c) SOLID AXLE FRONT AND REAR SUSPENSIONS

Figure 1 ANALYTICAL REPRESENTATION OF VEHICLES

sprung and unsprung masses but inertial coupling between the pair of drive wheels is included.

A description of features of the mathematical model appropriate for simulation of vehicle stability and performance follows.

Inertial Properties

Plane OXZ in Figure 1 is assumed to be a plane of mirror symmetry for the sprung mass.

The centers of gravity of independently suspended unsprung masses are assumed to coincide with the wheel centers. The wheels are treated as point masses, i.e., the fractional contribution of the suspension parts is approximated by a simple addition to the wheel mass.

The centers of gravity of solid axle unsprung masses are assumed to coincide with the geometric center of the axle. In the treatment of inertial coupling between the sprung mass and solid axle unsprung masses the axle is approximated by a thin rod.

Suspension Properties

Camber angles and half track change of independently suspended wheels relative to the vehicle are determined by interpolation of a tabular input of camber angle and track change as a function of suspension deflection. Camber angles are further modified to reflect suspension compliances.

Steer angles of the front wheels include a number of effects that are common in actual automobiles. A reference steer angle is determined at any point in time from either the steer equation of motion or a tabular interpolation procedure. This reference steer angle is defined as the average front wheel steer angle that would exist given a perfectly rigid steering system and no vehicle roll. This steer angle is then modified to include effects of Ackerman steering geometry, ride-steer, camber-steer and suspension compliances.

Rear axle roll steer is treated as a linear function of the angular degree of freedom of the rear axle, $\emptyset_R$ (see Figure 1). Inertial effects are neglected in the steer mode of rear axle motion. Independent rear suspension ride-steer is treated as a third order polynomial function of suspension position, and further modified to reflect effects of suspension compliances.

Anti-pitch effects of suspension geometry are simulated with tabular coefficients as a function of suspension deflection for the front and rear suspensions. Anti-roll effects (roll center height) may be included as a function of suspension ride position and tire lateral force.

The simulated suspensions bumper properties include progressively stiffening load-deflection rates and an adjustable amount of energy dissipation. Provision has also been incorporated for unsymmetrical placement of the jounce (compression) and rebound (extension) bumpers with respect to the design positions of the wheels. The combined spring and bumper forces are calculated in the manner depicted in Figure 2.

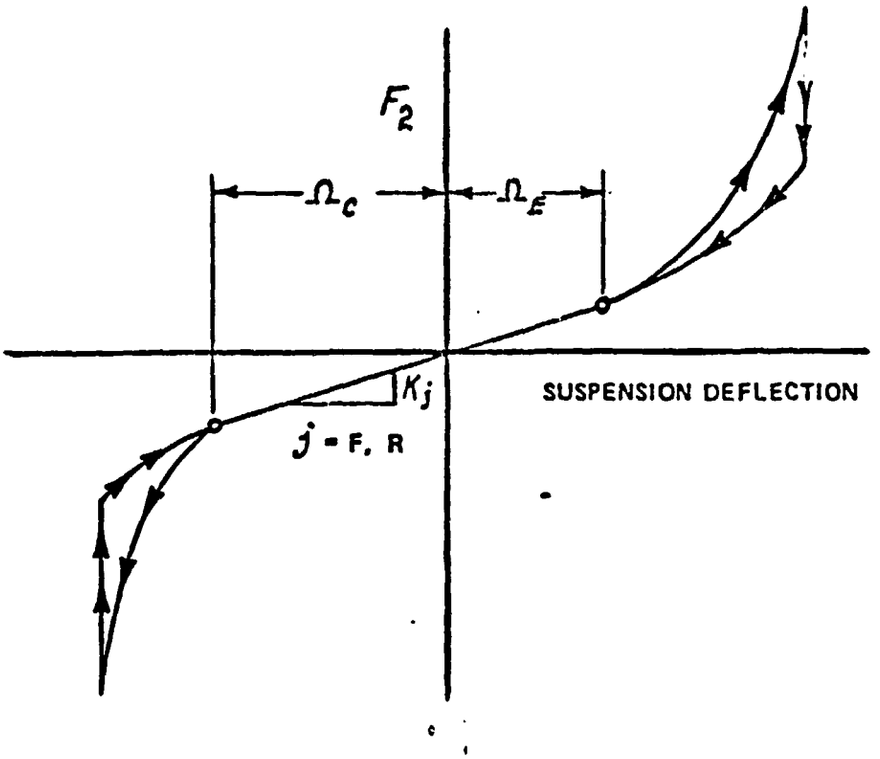

Figure 2 GENERAL FORM OF SIMULATED SUSPENSION BUMPER CHARACTERISTICS

The assumed form of damping is depicted in Figure 3. Velocity dependent damping is provided by a piecewise linear fit to known shock absorber data transformed to be effective at the wheel.

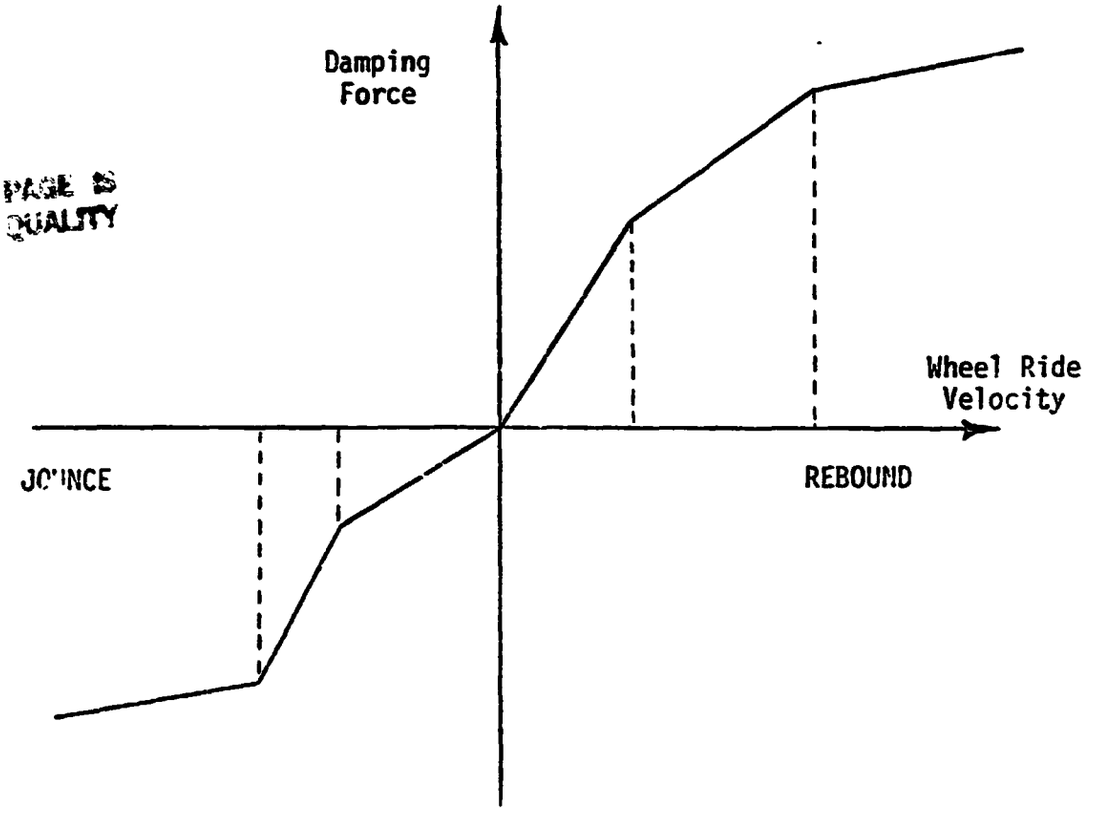

Figure 3 ASSUMED FORM OF DAMPING

Provision is made for the entry of auxiliary roll stiffness at both the front and the rear suspensions (i.e., roll stiffness in excess of that corresponding to the front suspension rates in ride and to the rear spring rates and spacing). While the anti-roll torsion bar which is frequently included in the independent front suspensions of conventional automobile designs constitutes an obvious form of auxiliary roll stiffness, it should be noted that torsional effects in the leaf springs of a conventional Hotchkiss rear suspension also produce a significant amount of auxiliary roll stiffness, as do increasingly common rear anti-roll torsion bars.

Tire Forces

The tire model is designed to handle the complete range of loading, from a loss of ground contact to extreme overload. Provision is made for up to four different sets of tire data, therefore, each tire on the vehicle may have different characteristics.

As a starting point in the tire force calculations, the radial loading of each tire, F_{R_i}, is first calculated from the position and orientation of the individual wheel in relation to the local terrain. At each point in time, the terrain elevations and slopes, at points directly under each wheel center, are obtained by interpolation of tabular input data for the terrain profile. Determination of the "ground contact point" is accomplished by passing a plane through the wheel center perpendicular to both the wheel and the local ground planes at the individual wheels. The point that lies in this plane, the wheel plane, and the ground plane is designated the "ground contact point". The distances between the individual wheel centers and the corresponding "ground contact points" are then calculated to determine the existence and the extent of radial tire deflections. A "hardening" spring characteristic is applied to generate corresponding radial loading for the individual tires.

The side, braking and traction forces are, of course, related to the tire load normal to the plane of the tire-terrain contact patch, F'_{R_i}, rather than the radial tire load, F_{R_i}. Therefore it is necessary to find the value of F'_{R_i} corresponding to the radial load, F_{R_i}, and the side force, F_s. The components of the external applied forces, F'_{R_i} and F_{s_i}, along the line of action of the radial tire force, F_{R_i}, are depicted in Figure 4. These force components must be in equilibrium with F_{R_i}, such that

$$F'_{R_i} \cos \phi_{CG_i} + F_{s_i} \sin \phi_{CG_i} = F_{R_i}.$$

Solution for F'_{R_i} yields

$$F'_{R_i} = F_{R_i} \sec \phi_{CG_i} - F_{s_i} \tan \phi_{CG_i}.$$

Since F'_{R_i} is required for the determination of F_{s_i}, an initial approximation of F_{s_i} is obtained by extrapolation from the previous time increment within the program. Following the calculation of F_{s_i} in the current time increment, an iterative procedure is employed to correct both F'_{R_i} and F_{s_i}.

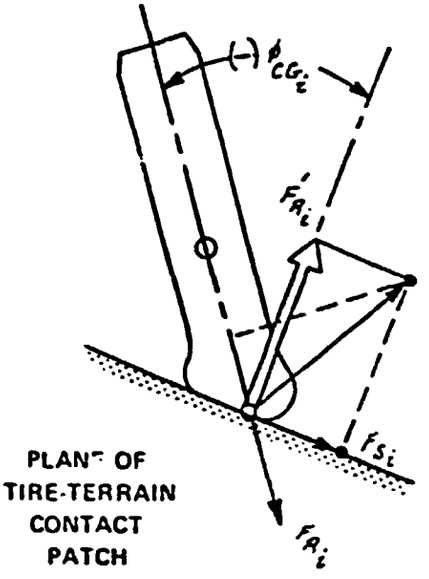

ϕ_{CG_i}	= CAMBER ANGLE RELATIVE TO TERRAIN (SHOWN NEGATIVE)
F_{s_i}	= SIDE FORCE PRODUCED BY COMBINATION OF SLIP ANGLE AND CAMBER ANGLE
i	= 1, 2, 3, 4

Figure 4 VECTOR SUMMATION OF FORCES WITH COMPONENTS ALONG THE LINE OF ACTION OF THE RADIAL TIRE FORCE (VIEWED FROM REAR)

The side force calculations are based on the small angle (slip and camber) properties of the tires which are saturated at large angles. Variations in the small-angle cornering and camber stiffnes .s produced by changes in tire loading are approximated by parabolic curves fitted to experimental data. The small-angle cornering stiffness is assumed to vary with load as:

$$C_{s0} = A_0 + A_1 F'_{R_i} - \frac{A_1}{A_2} (F'_{R_i})^2$$

and the camber stiffness is assumed to vary as:

$$C_{c0} = A_3 F'_{R_i} - \frac{A_3}{A_0} (F'_{R_i})^2$$

To permit the use of the nondimensional slip angle concept which saturates the side force at large slip angles, an "equivalent" slip angle (i.e., a slip angle which will produce the same value of side force as resulting from the camber angle) is defined to approximate camber effects.

With the above assumption, the resultant side force for small angles and the entire range of camber angles can be expressed as

$$F'_{S_i} = \left[\frac{A_1 F'_{R_i} (F'_{R_i} - A_2) - A_0 A_2}{A_2} \right] \left[\frac{V_{G_i}}{U_{G_i}} - \psi_i' + \beta_i' \right].$$

where β_i' is the "equivalent" slip angle for camber effects. Application of this equation to the nondimensional side force relationship (see Figure 5) yields

$$f(\bar{\beta}_i) = \frac{F_{S_i}}{(F_{S_i})_{max}} = \bar{\beta}_i - \frac{1}{3} \bar{\beta}_i \left| \bar{\beta}_i \right| + \frac{1}{27} \bar{\beta}_i^3$$

where F_{S_i} = resultant side force for entire range of slip and camber angles, and

$$\bar{\beta}_i = \frac{F'_{S_i}}{(F_{S_i})_{max}}$$

The tire model employed makes use of either the "friction circle" or the "friction ellipse" concept in establishing the relationship between side and circumferential forces. This choice allows the user to employ the most cost-effective tire representation consistent with the degree-of-detail required for any given application.

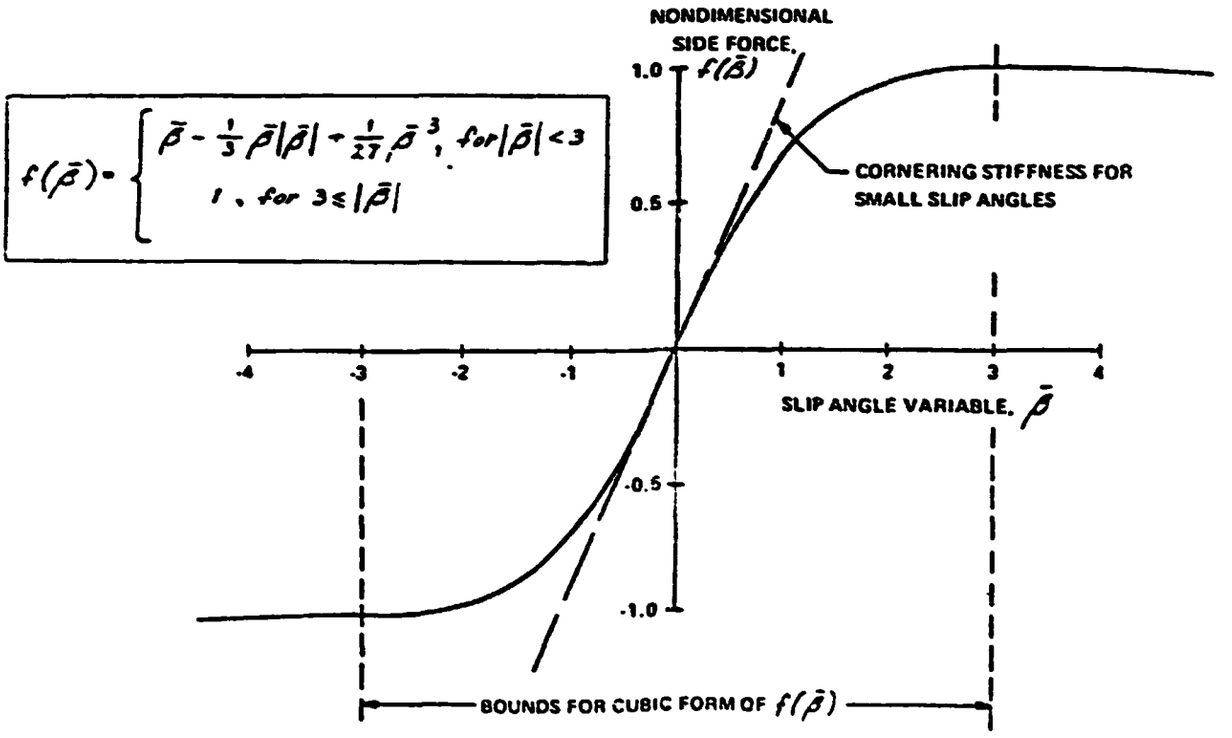

Figure 5 NONDIMENSIONAL TIRE SIDE-FORCE CURVE

APPENDIX C

BASE VEHICLE PHYSICAL PROPERTIES

BASE VEHICLE PHYSICAL PROPERTIES (HVOSM INPUT)

SPRUNG MASS	XMS	=	5.560	LB-SEC**2/IN
FRONT UNSPRUNG MASS	XMUF	=	0.346	LB-SEC**2/IN
REAR UNSPRUNG MASS	XMUR	=	0.553	LB-SEC**2/IN
X MOMENT OF INERTIA	XIX	=	3104.000	LB-SEC**2-IN
Y MOMENT OF INERTIA	XIY	=	11199.000	LB-SEC**2-IN
Z MOMENT OF INERTIA	XIZ	=	11376.000	LB-SEC**2-IN
XZ PRODUCT OF INERTIA	XIXZ	=	464.000	LB-SEC**2-IN
FRONT AXLE MOMENT OF INERTIA	XIF	=	0.0	NOT USED
REAR AXLE MOMENT OF INERTIA	XIR	=	185.000	LB-SEC**2-IN
GRAVITY	G	=	386.400	IN/SEC**2

FRONT WHEEL X LOCATION	A	=	39.200	INCHES
REAR WHEEL X LOCATION	B	=	55.300	INCHES
FRONT WHEEL Z LOCATION	ZF	=	11.515	INCHES
REAR WHEEL Z LOCATION	ZR	=	13.850	INCHES
FRONT WHEEL TRACK	TF	=	51.000	INCHES
REAR WHEEL TRACK	TR	=	51.750	INCHES
FRONT ROLL AXIS	RHOF	=	0.0	NOT USED
REAR ROLL AXIS	RHO	=	-2.460	INCHES
FRONT SPRING TRACK	TSF	=	0.0	NOT USED
REAR SPRING TRACK	TS	=	36.000	INCHES
FRONT AUX ROLL STIFFNESS	RF	=	126500.00	LB-IN/RAD
REAR AUX ROLL STIFFNESS	RR	=	52880.00	LB-IN/RAD

	FRONT SUSPENSION				REAR SUSPENSION			
SUSPENSION RATE	AKF	=	170.250	LB/IN	AKR	=	123.000	LB/IN
COMPRESSION STOP COEFS.	AKFC	=	156.800	LB/IN	AKRC	=	156.800	LB/IN
	AKFCP	=	283.000	LB/IN**3	AKRCP	=	283.000	LB/IN**3
EXTENSION STOP COEFS.	AKFE	=	824.400	LB/IN	AKRE	=	824.400	LB/IN
	AKFEP	=	313.400	LB/IN**3	AKREP	=	313.400	LB/IN**3
COMPRESSION STOP LOCATION	OMEGFC	=	-2.400	INCHES	OMEGRC	=	-2.300	INCHES
EXTENSION STOP LOCATION	OMEGFE	=	1.900	INCHES	OMEGRE	=	2.500	INCHES
STOP ENERGY DISSIPATION FACTOR	XLAMF	=	0.500		XLAMR	=	0.500	
VISCOUS DAMPING COEFS.	CFJ1	=	6.680	LB-SEC/IN	CRJ1	=	8.590	LB-SEC/IN
	CFJ2	=	13.290	LB-SEC/IN	CRJ2	=	3.050	LB-SEC/IN
	CFJ3	=	5.180	LB-SEC/IN	CRJ3	=	3.050	LB-SEC/IN
	CFR1	=	4.990	LB-SEC/IN	CRR1	=	2.010	LB-SEC/IN
	CFR2	=	2.110	LB-SEC/IN	CRR2	=	2.010	LB-SEC/IN
	CFR3	=	2.110	LB-SEC/IN	CRR3	=	2.010	LB-SEC/IN
DAMPING COEF. CHANGE VELOCITIES	DDFJ1	=	-12.600	IN/SEC	DDRJ1	=	-19.100	IN/SEC
	DDFJ2	=	-16.500	IN/SEC	DDRJ2	=	-1000.000	IN/SEC
	DDFR1	=	12.000	IN/SEC	DDRR1	=	1000.000	IN/SEC
	DDFR2	=	1000.000	IN/SEC	DDRR2	=	2000.000	IN/SEC
COULOMB FRICTION	CFP	=	45.000	LB	CRP	=	20.000	LB
FRICTION LAG	EPSF	=	0.100	IN/SEC	EPSR	=	0.100	IN/SEC

FRONT WHEEL CAMBER
VS
SUSPENSION DEFLECTION

DELTAF INCHES	PHIC DEGREES
-2.50	-1.07
-2.00	-0.59
-1.50	-0.21
-1.00	0.05
-0.50	0.21
0.0	0.25
0.50	0.10
1.00	-0.20
1.50	-0.67
2.00	-1.42

9950-297

BASE VEHICLE SUSPENSION SYSTEM MECHANICAL PROPERTIES (HVOSM INPUT)

BASE VEHICLE SUSPENSION GEOMETRIC AND COMPLIANCE PROPERTIES (HVOSM INPUT)

SUSPENSION COEFFICIENTS		FRONT	REAR
ANTI ROLL COEFFICIENTS	CR0	= 0.142000E+00 ($\frac{lb}{lb}$)	0.0
	CR1	= 0.0	0.0
	CR2	= 0.0	0.0
STEER-STEER COEFFICIENTS	CPSIST1	= 0.0	0.0
	CPSIST2	= 0.0	0.0
	CPSIST3	= 0.0	0.0
CAMBER-STEER COEFFICIENTS	CPHIST1	= 0.0	0.0
	CPHIST2	= 0.0	0.0
RIDE-STEER COEFFICIENTS	CPSIDZ1	= -.479900E-02(rad)	0.0
	CPSIDZ2	= -.386300E-02(rad/in)	0.0
	CPSIDZ3	= -.705600E-03(rad/in^2)	0.0
LONGITUDINAL FORCE COMPLIANCE STEER COEF.S	CPSIFX1	= 0.0	0.0
	CPSIFX2	= 0.0	0.0
LATERAL FORCE COMPLIANCE STEER COEF.S	CPSIFY1	= -.363029E-04 ($\frac{rad}{lb}$)	-.209440E-05 ($\frac{rad}{lb}$ [illegible]
	CPSIFY2	= 0.0	0.0
OVERTURNING MOMENT COMPLIANCE STEER COEF.S	CPSIMX1	= 0.0	0.0 [illegible]
	CPSIMX2	= 0.0	0.0
ALIGNING TORQUE COMPLIANCE STEER COEF.S	CPSIMZ1	= 0.223402E-03($\frac{rad}{lb\text{-}ft}$)	0.593412E-04($\frac{rad}{lb}$- [illegible]
	CPSIMZ2	= 0.0	0.0
LONGITUDINAL FORCE COMPLIANCE CAMBER COEF.S	CPHIFX1	= 0.0	0.0 [illegible]
	CPHIFX2	= 0.0	0.0
LATERAL FORCE COMPLIANCE CAMBER COEF.S	CPHIFY1	= -.645772E-04 ($\frac{rad}{lb}$)	-.495674E-04 ($\frac{rad}{lb}$ [illegible]
	CPHIFY2	= 0.0	0.0
OVERTURNING MOMENT COMPLIANCE CAMBER COEF.S	CPHIMX1	= 0.0	0.0 [illegible]
	CPHIMX2	= 0.0	0.0
ALIGNING TORQUE COMPLIANCE CAMBER COEF.S	CPHIMZ1	= 0.279253E-04($\frac{rad}{lb\text{-}ft}$)	0.174533E-05($\frac{rad}{lb}$- [illegible]
	CPHIMZ2	= 0.0	0.0

BASE VEHICLE TIRE PROPERTIES (HVOSM)

			TIRE DATA RF	LF	RR	LR	
TIRE LINEAR SPRING RATE	AKT	=	1150.000	1150.000	1150.000	1150.000	LB/IN
DEFL. FOR INCREASED RATE	SIGT	=	10.000	10.000	10.000	10.000	INCHES
SPRING RATE INCREASING FACTOR	XLAMT	=	10.000	10.000	10.000	10.000	
	A0	=	1671.840	1671.840	1671.840	1671.840	
	A1	=	10.410	10.410	10.410	10.410	
SIDE FORCE COEFFICIENTS	A2	=	2049.720	2049.720	2049.720	2049.720	
	A3	=	2.152	2.152	2.152	2.152	
	A4	=	2614.290	2614.290	2614.290	2614.290	
TIRE OVERLOAD FACTOR	OMEGT	=	1.000	1.000	1.000	1.000	
TIRE UNDEFLECTED RADIUS	RW	=	11.420	11.420	11.420	11.420	INCHES
TIRE / GROUND FRICTION COEF.	AMU	=	0.750	0.750	0.750	0.750	
	CAT1	=	-.2300E-03	-.2300E-03	-.2300E-03	-.2300E-03	
ALIGNING TORQUE COEFFICIENTS	CAT2	=	0.1851E-03	0.1851E-03	0.1851E-03	0.1851E-03	
	CAT3	=	0.9700E-01	0.9700E-01	0.9700E-01	0.9700E-01	
	COM0	=	0.0	0.0	0.0	0.0	
OVERTURNING MOMENT COEF.S	COM1	=	-.1350E-03	-.1350E-03	-.1350E-03	-.1350E-03	
	COM2	=	-.5330E-04	-.5330E-04	-.5330E-04	-.5330E-04	
	COM3	=	-.4710E+00	-.4710E+00	-.4710E+00	-.4710E+00	

APPENDIX D

SAMPLE RESULTS OF TRAPEZOIDAL STEER COMPUTER SIMULATIONS

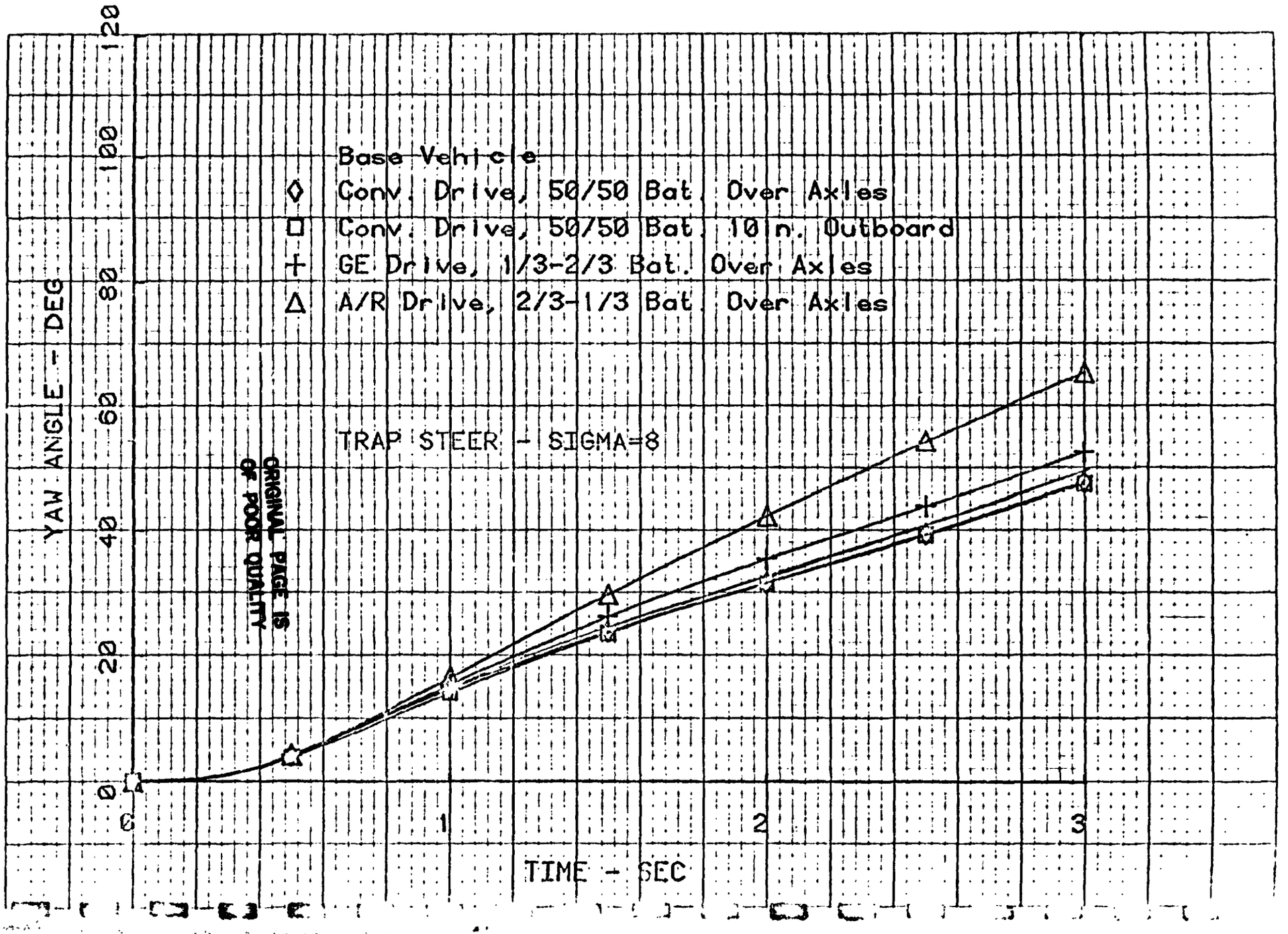
Base Vehicle
◇ Conv. Drive, 50/50 Bat. Over Axles
□ Conv. Drive, 50/50 Bat. 10 in. Outboard
+ GE Drive, 1/3-2/3 Bat. Over Axles
Δ A/R Drive, 2/3-1/3 Bat. Over Axles
TRAP STEER - SIGMA=8
YAW ANGLE - DEG
TIME - SEC
0
20
40
60
80
100
120
1
2
3
ORIGINAL PAGE IS
OF POOR QUALITY

9950-297

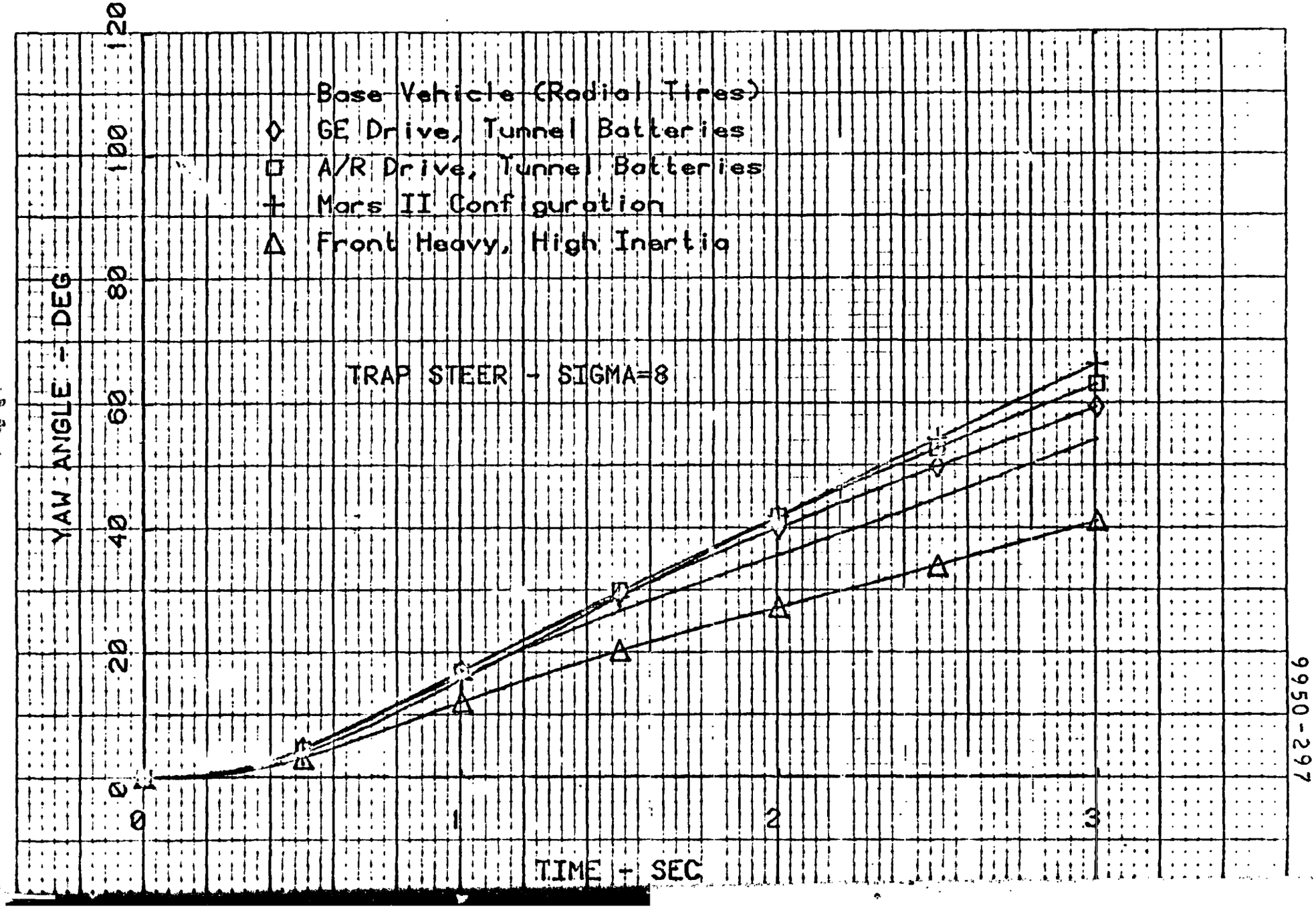
Base Vehicle (Radial Tires)
GE Drive, Tunnel Batteries
A/R Drive, Tunnel Batteries
Mars II Configuration
Front Heavy, High Inertia
TRAP STEER → SIGMA=8
YAW ANGLE - DEG
TIME - SEC
0
20
40
60
80
100
120
1
2
3
9950-297

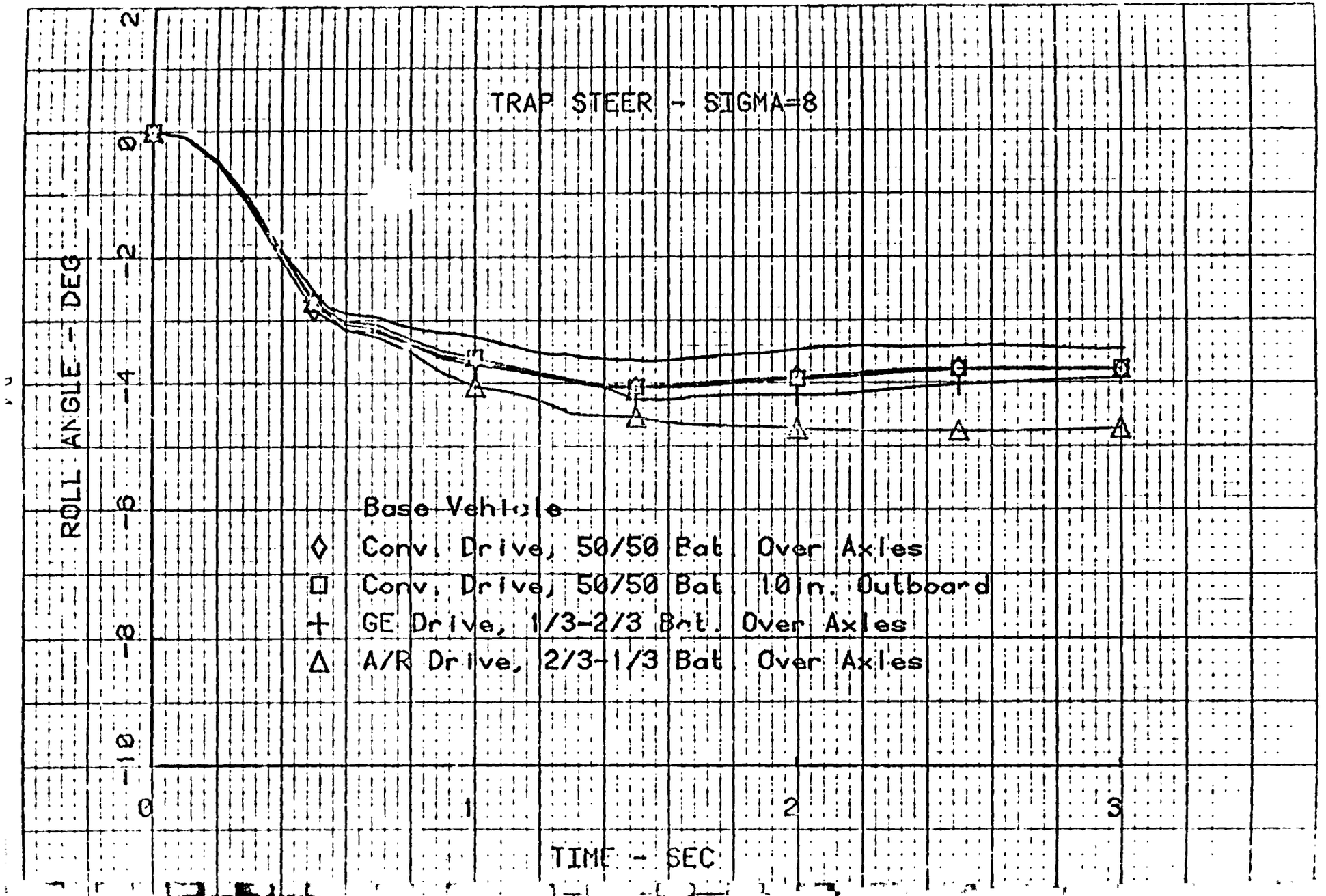
TRAP STEER - SIGMA=8
ROLL ANGLE - DEG
2
0
-2
-4
-6
-8
-10
0
1
2
3
TIME - SEC
Base Vehicle
Conv. Drive, 50/50 Bat. Over Axles
Conv. Drive, 50/50 Bat. 10in. Outboard
GE Drive, 1/3-2/3 Bat. Over Axles
A/R Drive, 2/3-1/3 Bat. Over Axles

9950-277

9950-247

9950-297

TRAP STEER - SIGMA#8
VEH SLIP ANG-DEG
TIME - SEC
0
-5
-10
-15
-20
-25
1
2
3
Base Vehicle
◇ Conv. Drive, 50/50 Bat., Over Axles
□ Conv. Drive, 50/50 Bat., 10In. Outboard
+ GE Drive, 1/3-2/3 Bat., Over Axles
△ A/R Drive, 2/3-1/3 Bat., Over Axles

9950-207
TRAP STEER - SIGMA=8
VEH SLIP ANG-DEG
5
0
-5
-10
-15
-20
-25
0
1
2
3
TIME - SEC
Base Vehicle (Radial Tires)
GE Drive, Tunnel Batteries
A/R Drive, Tunnel Batteries
Mars TI Configuration
Front Heavy, High Inertia

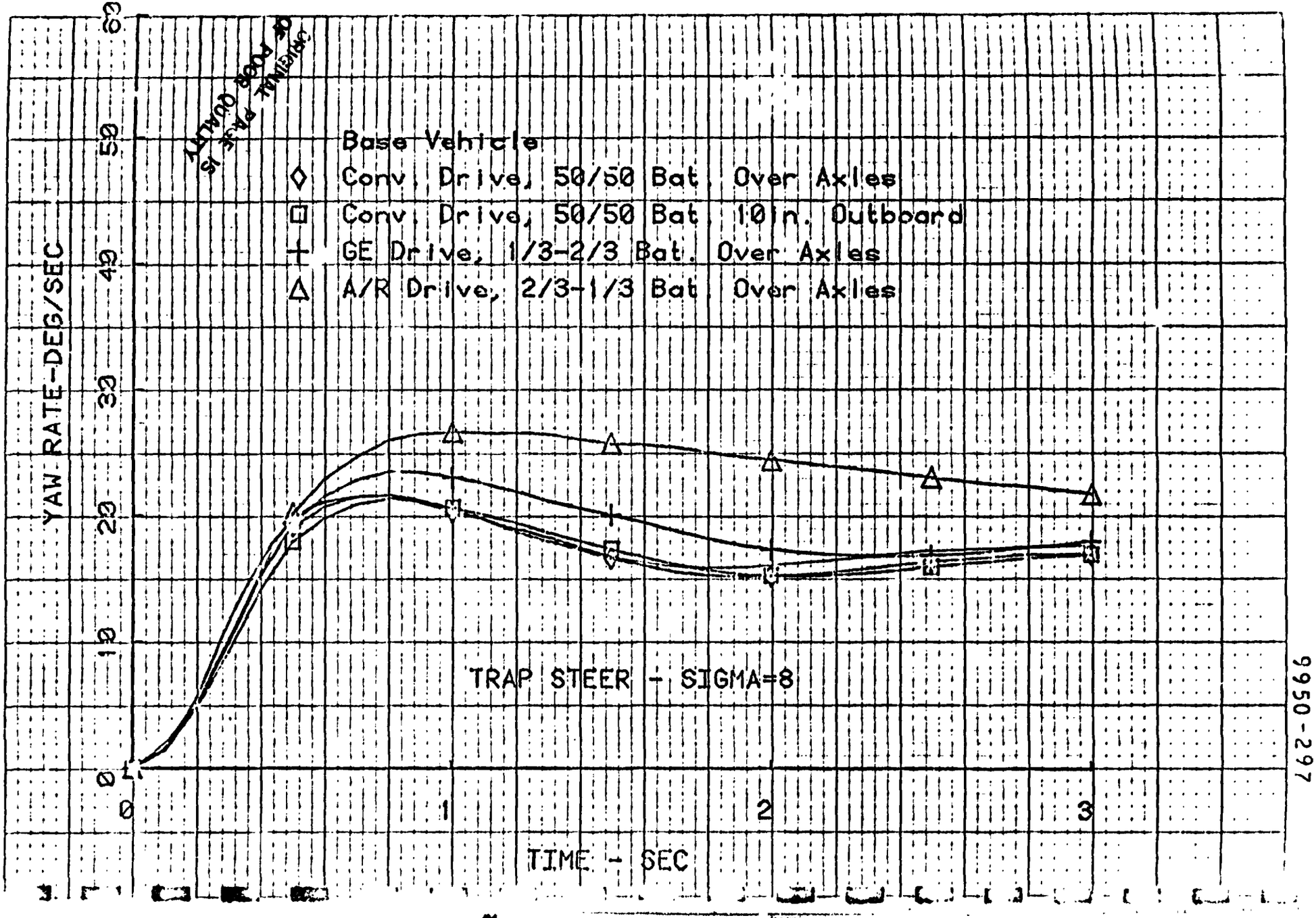
ORIGINAL PAGE QUALITY IS POOR
Base Vehicle
◇ Conv. Drive, 50/50 Bat. Over Axles
□ Conv. Drive, 50/50 Bat. 10in. Outboard
+ GE Drive, 1/3-2/3 Bat. Over Axles
△ A/R Drive, 2/3-1/3 Bat. Over Axles
YAW RATE-DEG/SEC
0
10
20
30
40
50
60
TRAP STEER - SIGMA=8
0
1
2
3
TIME - SEC

9950-297

9950-297

Base Vehicle (Radial Tires)
◇ GE Drive, Tunnel Batteries
□ A/R Drive, Tunnel Batteries
+ Mars II Configuration
△ Front Heavy, High Inertia
TRAP STEER - SIGMA=8
YAW RATE-DEG/SEC
TIME - SEC
0
10
20
30
40
50
60
1
2
3

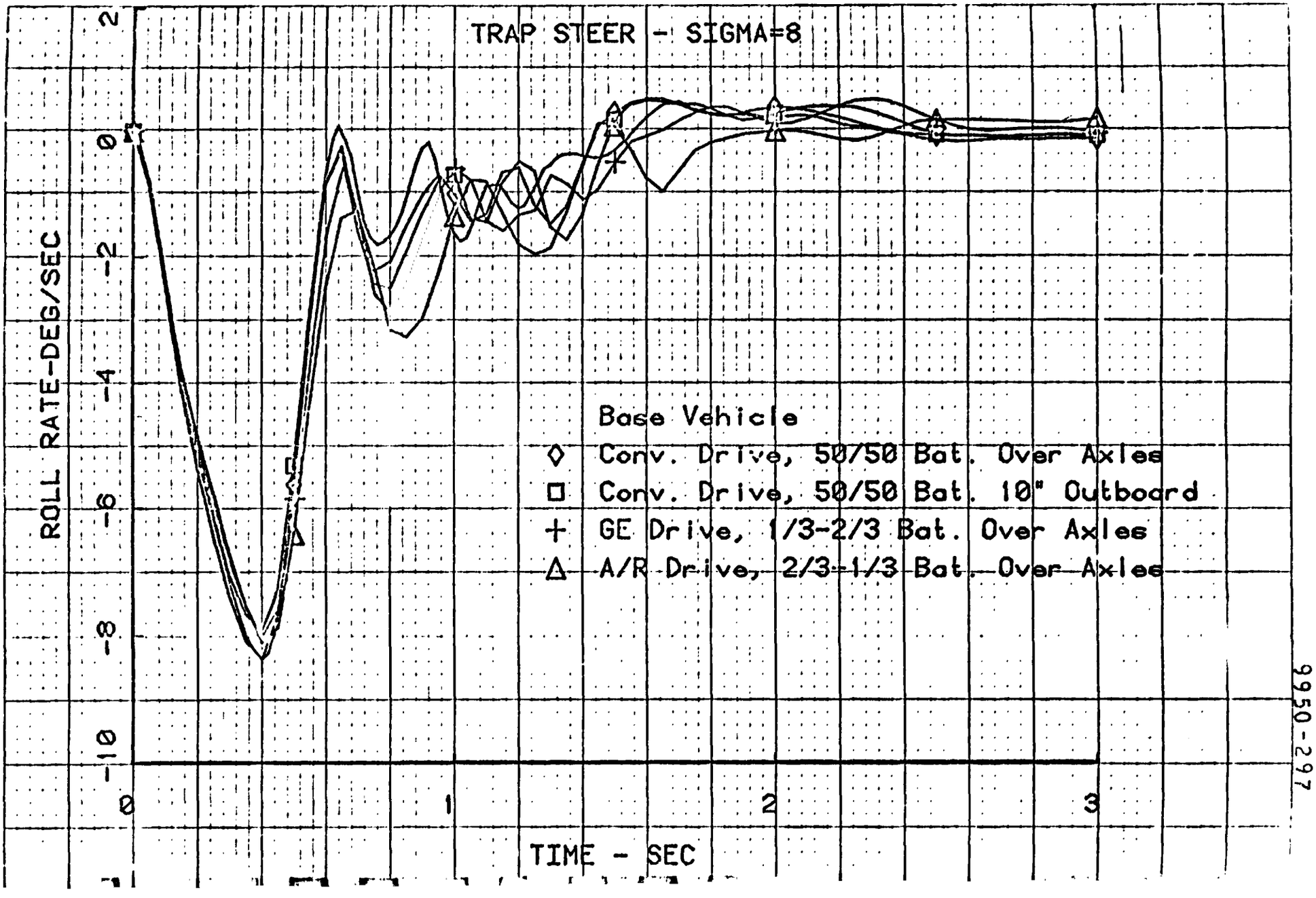
TRAP STEER - SIGMA=8
ROLL RATE-DEG/SEC
2
0
-2
-4
-6
-8
-10
0
1
2
3
TIME - SEC
Base Vehicle
◇ Conv. Drive, 50/50 Bat. Over Axles
□ Conv. Drive, 50/50 Bat. 10" Outboard
+ GE Drive, 1/3-2/3 Bat. Over Axles
△ A/R Drive, 2/3-1/3 Bat. Over Axles

9950-297

9950-297

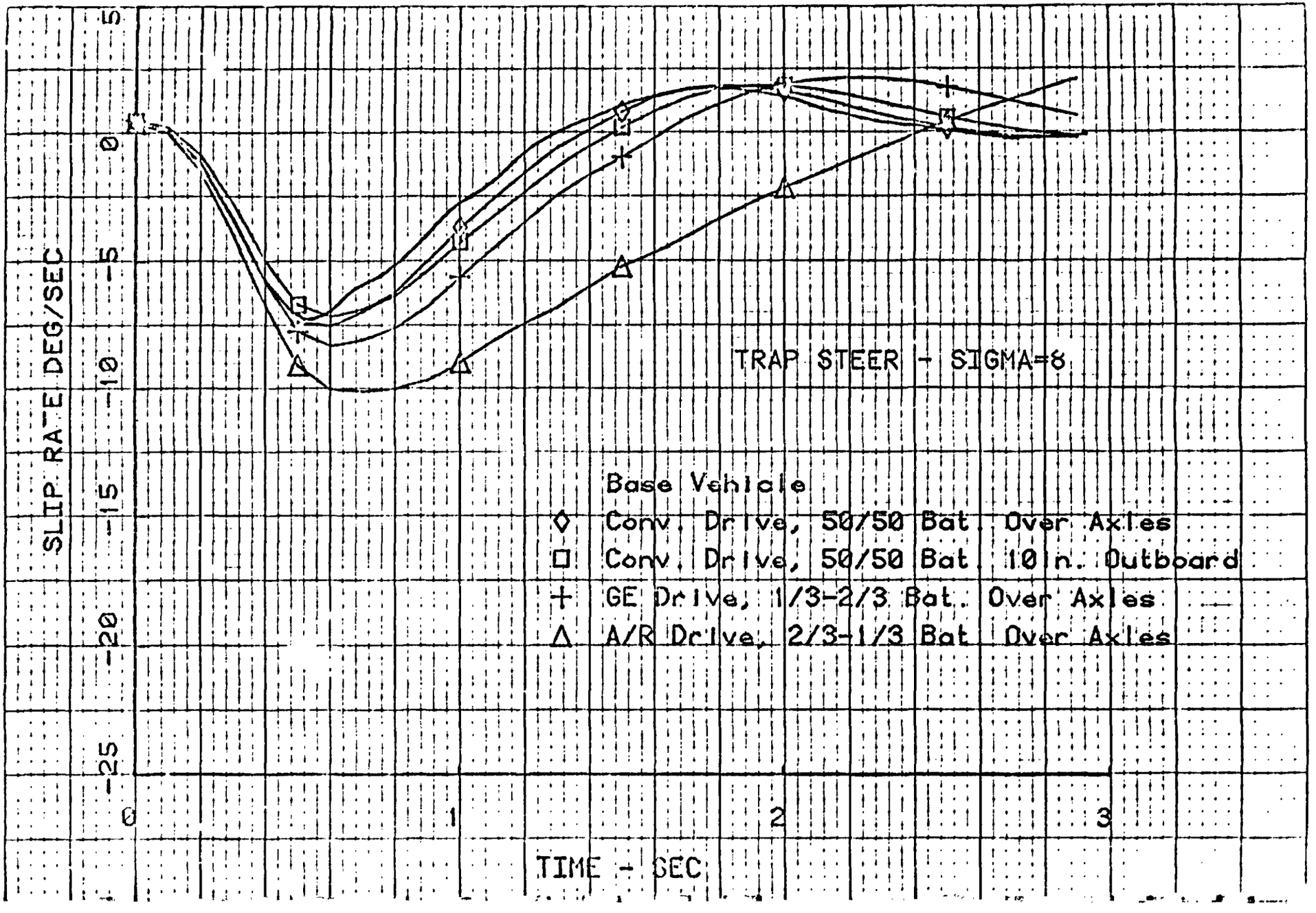
SLIP RATE DEG/SEC
5
0
-5
-10
-15
-20
-25
0
1
2
3
TIME - SEC
TRAP STEER - SIGMA=8
Base Vehicle
◇ Conv. Drive, 50/50 Bat. Over Axles
□ Conv. Drive, 50/50 Bat. 10 in. Outboard
+ GE Drive, 1/3-2/3 Bat. Over Axles
Δ A/R Drive, 2/3-1/3 Bat. Over Axles

9950-237

9950-297

VEH SLIP RATE - DEG/SEC
5
0
-5
-10
-15
-20
-25
0
1
2
3
TIME - SEC
TRAP STEER - SIGMA=8
◇ Base Vehicle (Radial Tires)
□ GE Drive, Tunnel Batteries
+ A/R Drive, Tunnel Batteries
△ Mars II Configuration
Front Heavy, High Inertia

9950-297

Base Vehicle
◇ Conv. Drive, 50/50 Bat. Over Axles
□ Conv. Drive, 50/50 Bat. 10 in. Outboard
+ GE Drive, 1/3-2/3 Bat. Over Axles
Δ A/R Drive, 2/3-1/3 Bat. Over Axles
TRAP STEER - SIGMA=8
LAT ACCEL-G's
TIME - SEC
.2
.4
.6
.8
1
2
3

9950-297

Base Vehicle (Radial Tires)
◇ GE Drive, Tunnel Batteries
□ A/R Drive, Tunnel Batteries
+ Mars II Configuration
△ Front Heavy, High Inertia
TRAP STEER - SIGMA=8
LAT ACCEL-G's
TIME - SEC
0
0.2
0.4
0.6
0.8
1
1.2
1
2
3
ORIGINAL PAGE IS
OF POOR QUALITY

APPENDIX E

SAMPLE RESULTS OF SINUSOIDAL STEER COMPUTER SIMULATIONS

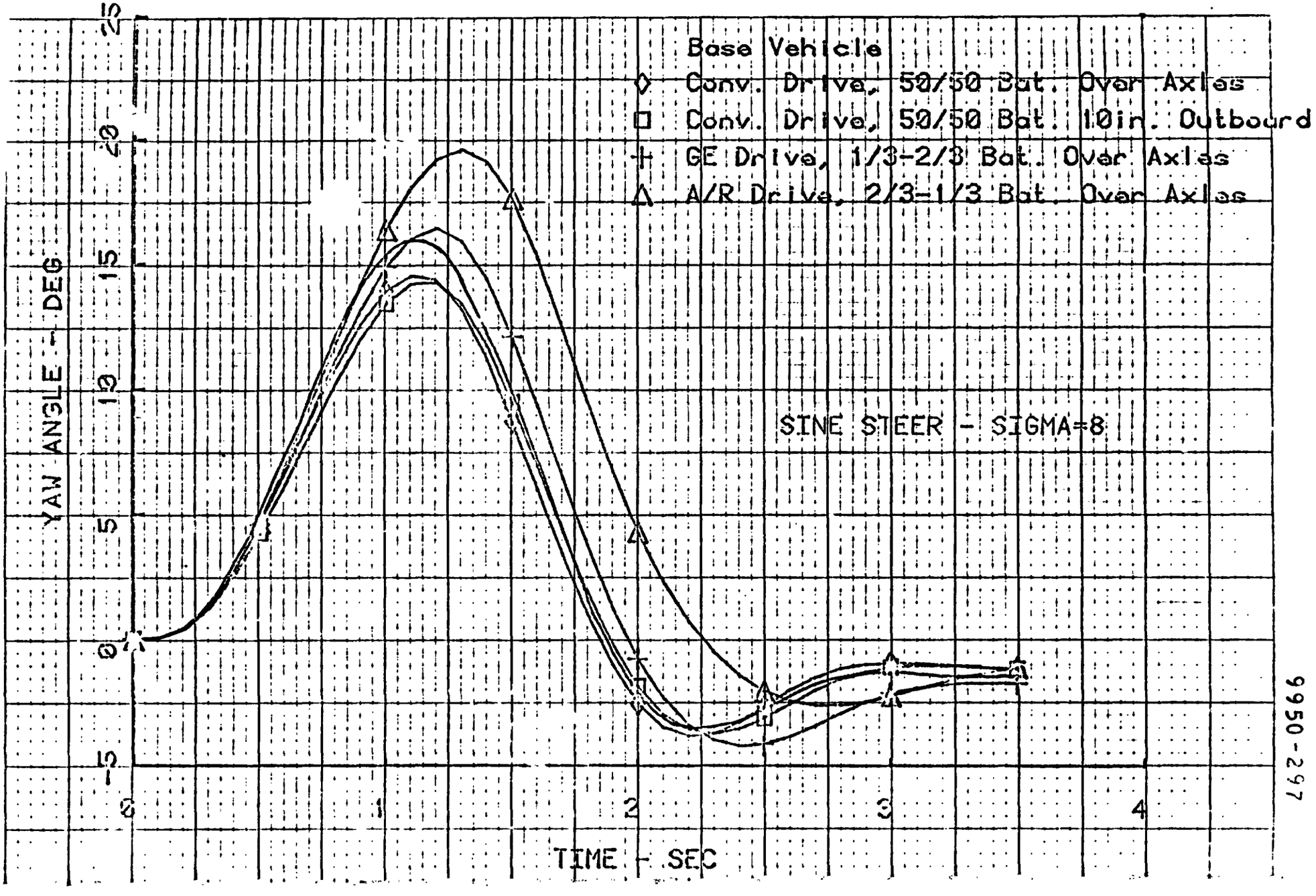
Base Vehicle
Conv. Drive, 50/50 Bat. Over Axles
Conv. Drive, 50/50 Bat. 10in. Outboard
GE Drive, 1/3-2/3 Bat. Over Axles
A/R Drive, 2/3-1/3 Bat. Over Axles
SINE STEER - SIGMA=8
YAW ANGLE - DEG
TIME - SEC
25
20
15
10
5
0
-5
0
1
2
3
4

9950-297

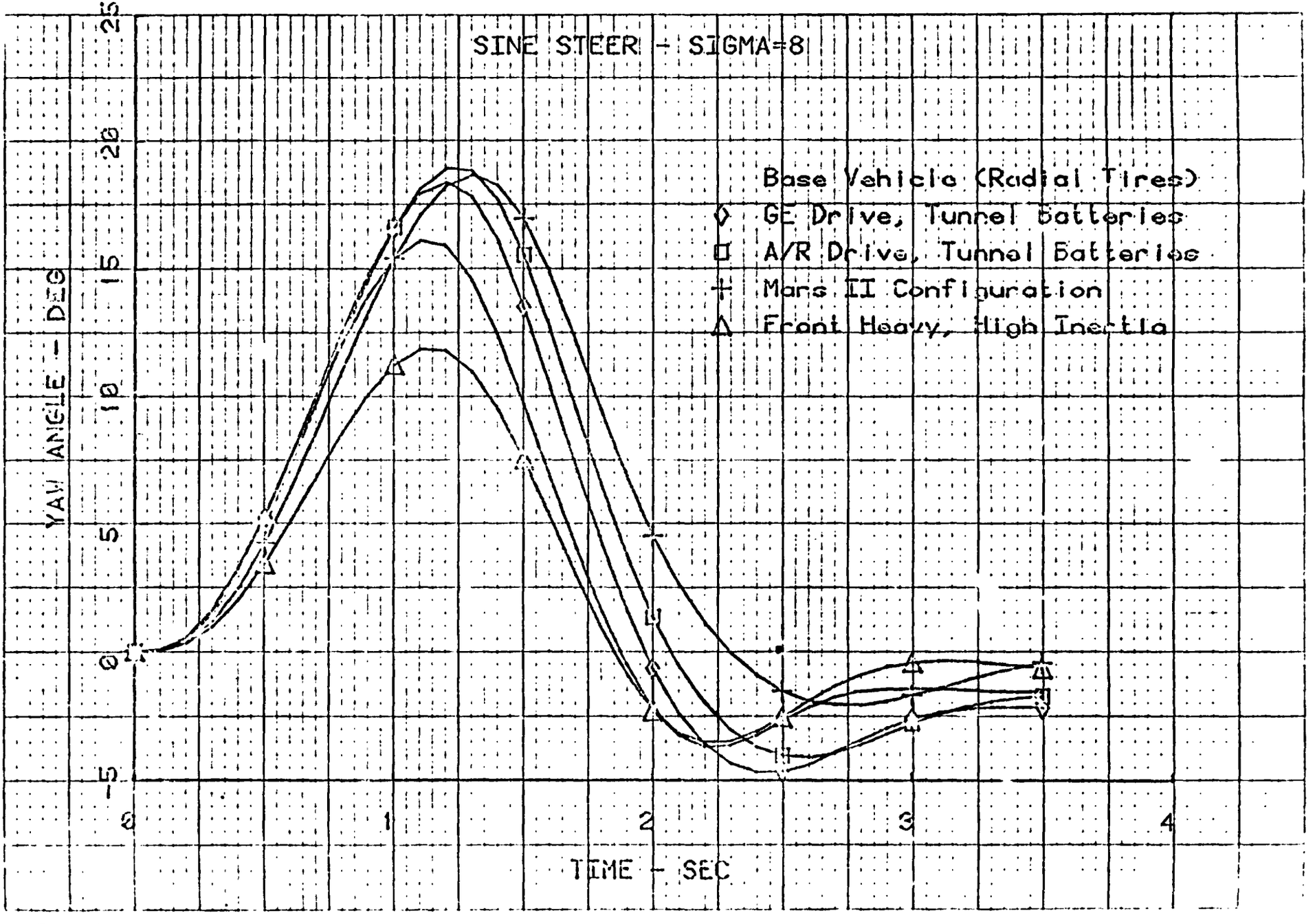
SINE STEER - SIGMA=8
Base Vehicle (Radial Tires)
◇ GE Drive, Tunnel Batteries
□ A/R Drive, Tunnel Batteries
+ Mars II Configuration
△ Front Heavy, High Inertia
YAW ANGLE - DEG
25
20
15
10
5
0
-5
0
1
2
3
4
TIME - SEC

9950-277

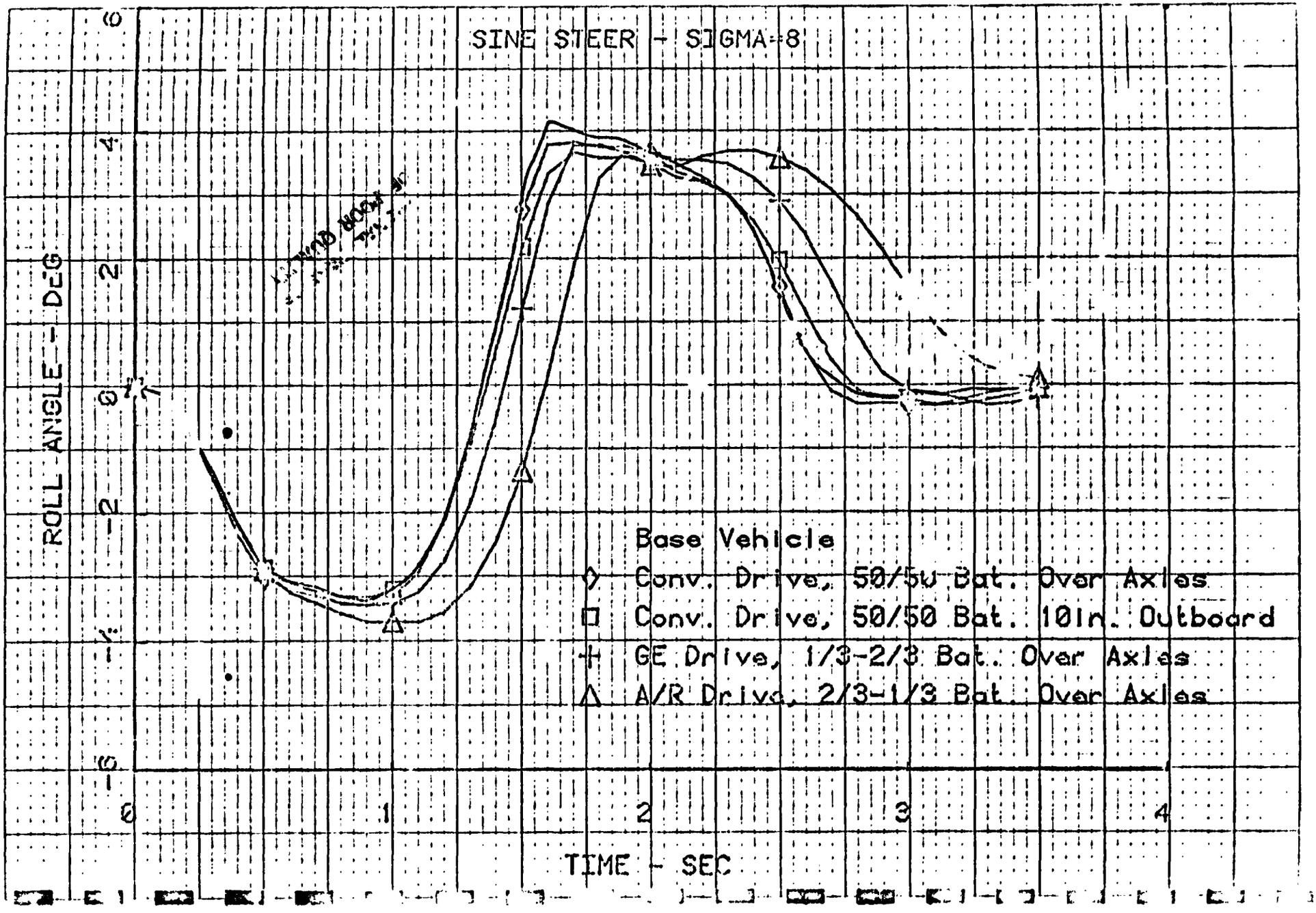
SINE STEER - SIGMA=8
ROLL ANGLE - DEG
TIME - SEC
6
4
2
0
-2
-4
-6
1
2
3
4
Base Vehicle
Conv. Drive, 50/50 Bat. Over Axles
Conv. Drive, 50/50 Bat. 10in. Outboard
GE Drive, 1/3-2/3 Bat. Over Axles
A/R Drive, 2/3-1/3 Bat. Over Axles

9950-297

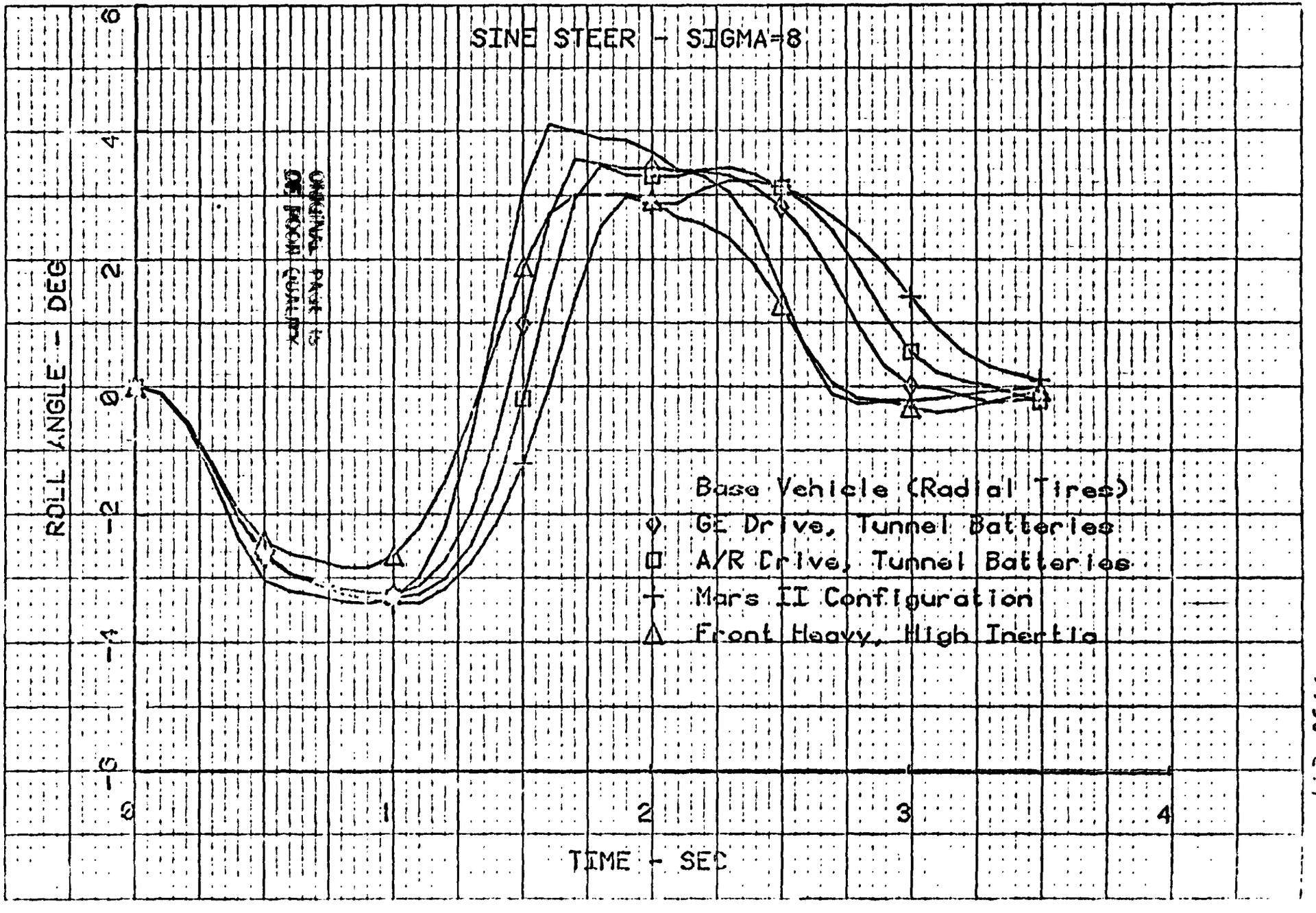
SINE STEER - SIGMA=8
ROLL ANGLE - DEG
6
4
2
0
-2
-4
-6
0
1
2
3
4
TIME - SEC
Base Vehicle (Radial Tires)
GE Drive, Tunnel Batteries
A/R Drive, Tunnel Batteries
Mars II Configuration
Front Heavy, High Inertia

9950-297

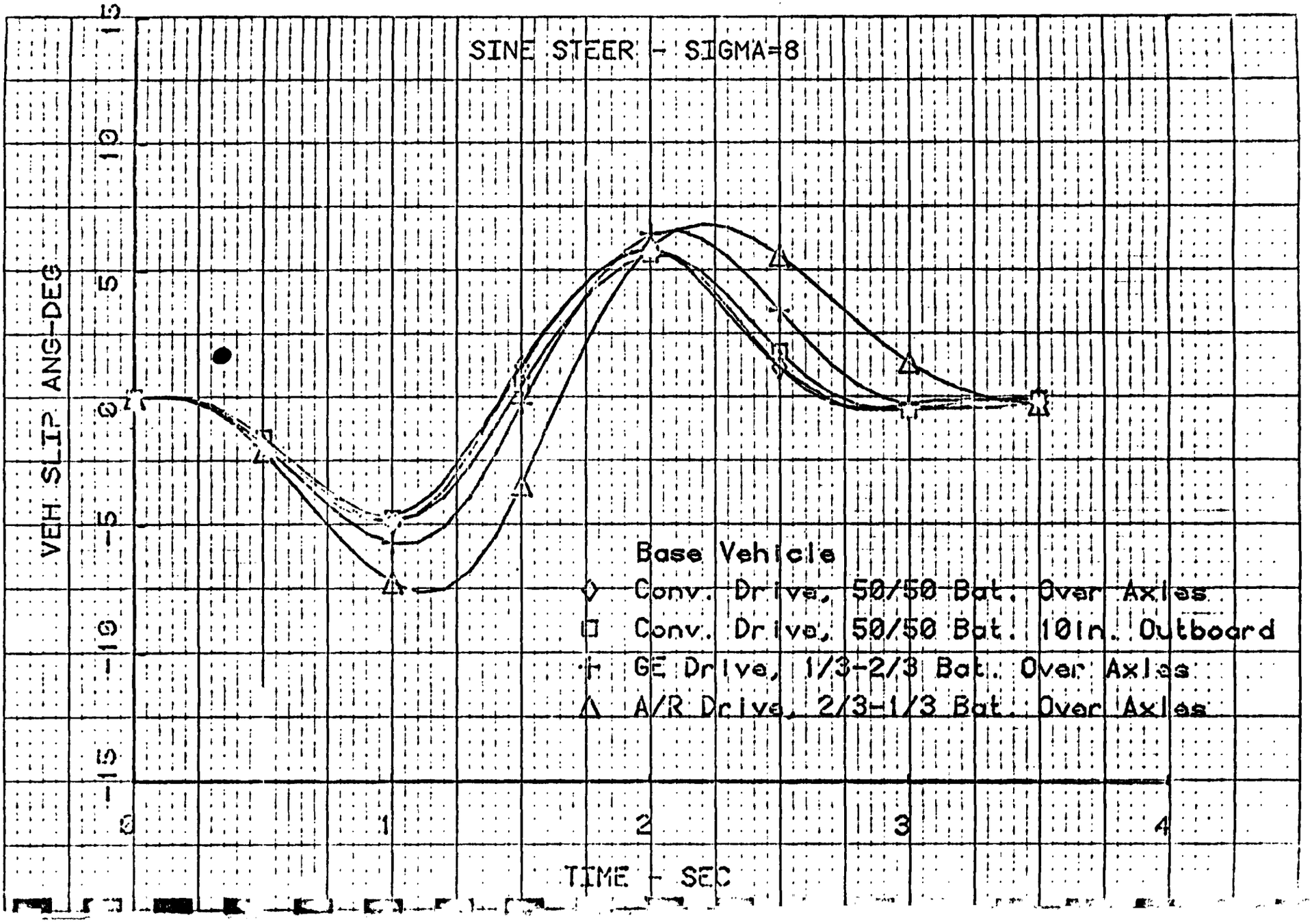
SINE STEER - SIGMA=8
VEH SLIP ANG-DEG
15
10
5
0
-5
-10
-15
0
1
2
3
4
TIME - SEC
Base Vehicle
◇ Conv. Drive, 50/50 Bat. Over Axles
□ Conv. Drive, 50/50 Bat. 10in. Outboard
+ GE Drive, 1/3-2/3 Bat. Over Axles
△ A/R Drive, 2/3-1/3 Bat. Over Axles

9950-297

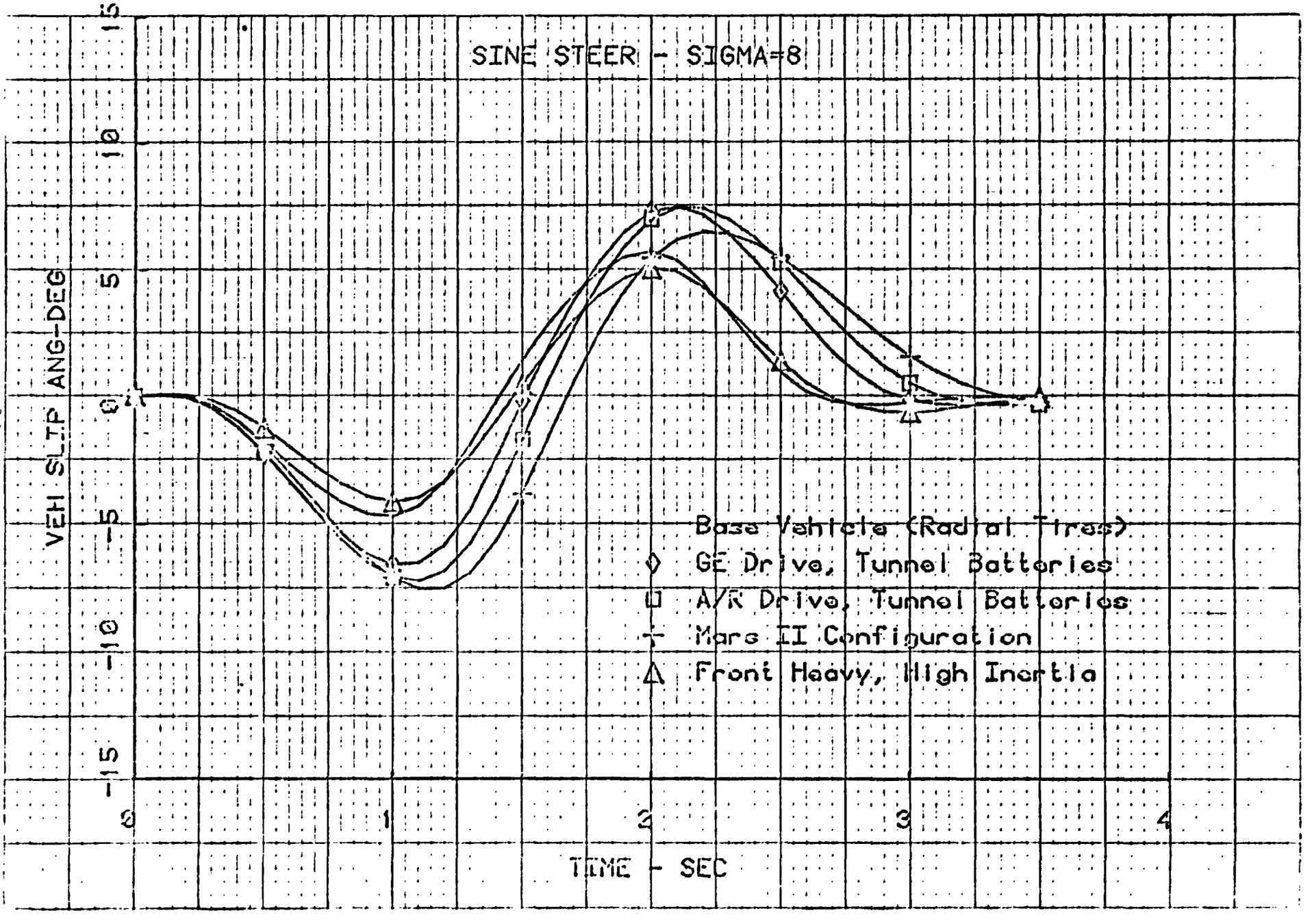
SINE STEER - SIGMA=8
VEH SLIP ANG-DEG
15
10
5
0
-5
-10
-15
0
1
2
3
4
TIME - SEC
Base Vehicle (Radial Tires)
GE Drive, Tunnel Batteries
A/R Drive, Tunnel Batteries
Mars II Configuration
Front Heavy, High Inertia

77-0550

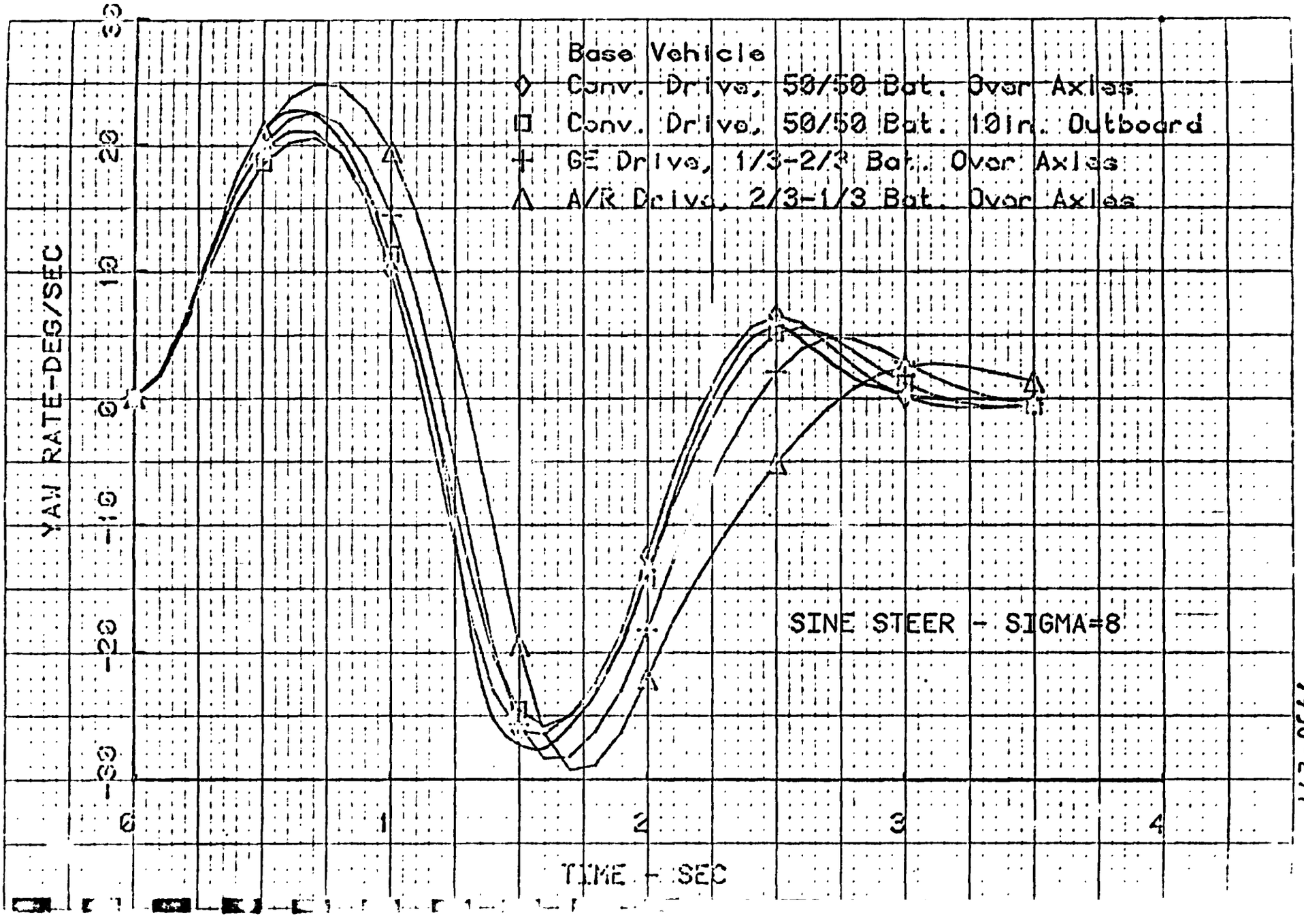
Base Vehicle
Conv. Drive, 50/50 Bat. Over Axles
Conv. Drive, 50/50 Bat. 10in. Outboard
GE Drive, 1/3-2/3 Bat. Over Axles
A/R Drive, 2/3-1/3 Bat. Over Axles
SINE STEER - SIGMA=8
YAW RATE-DEG/SEC
TIME - SEC
30
20
10
0
-10
-20
-30
0
1
2
3
4
9950-297

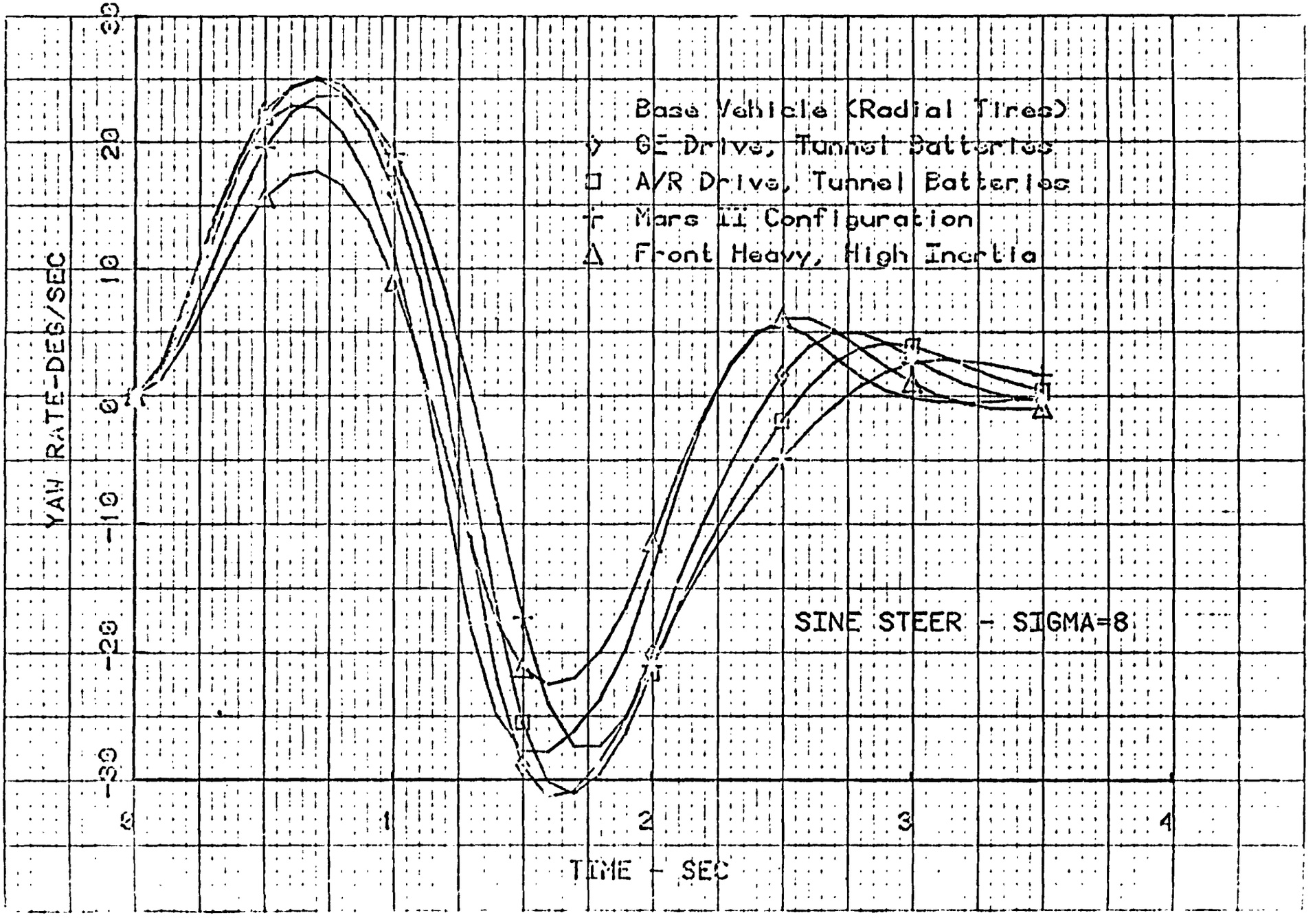
Base Vehicle (Radial Tires)
GE Drive, Tunnel Batteries
A/R Drive, Tunnel Batteries
Mars III Configuration
Front Heavy, High Inertia
SINE STEER - SIGMA=8
YAW RATE-DEG/SEC
TIME - SEC
30
20
10
0
-10
-20
-30
0
1
2
3
4

9950-297

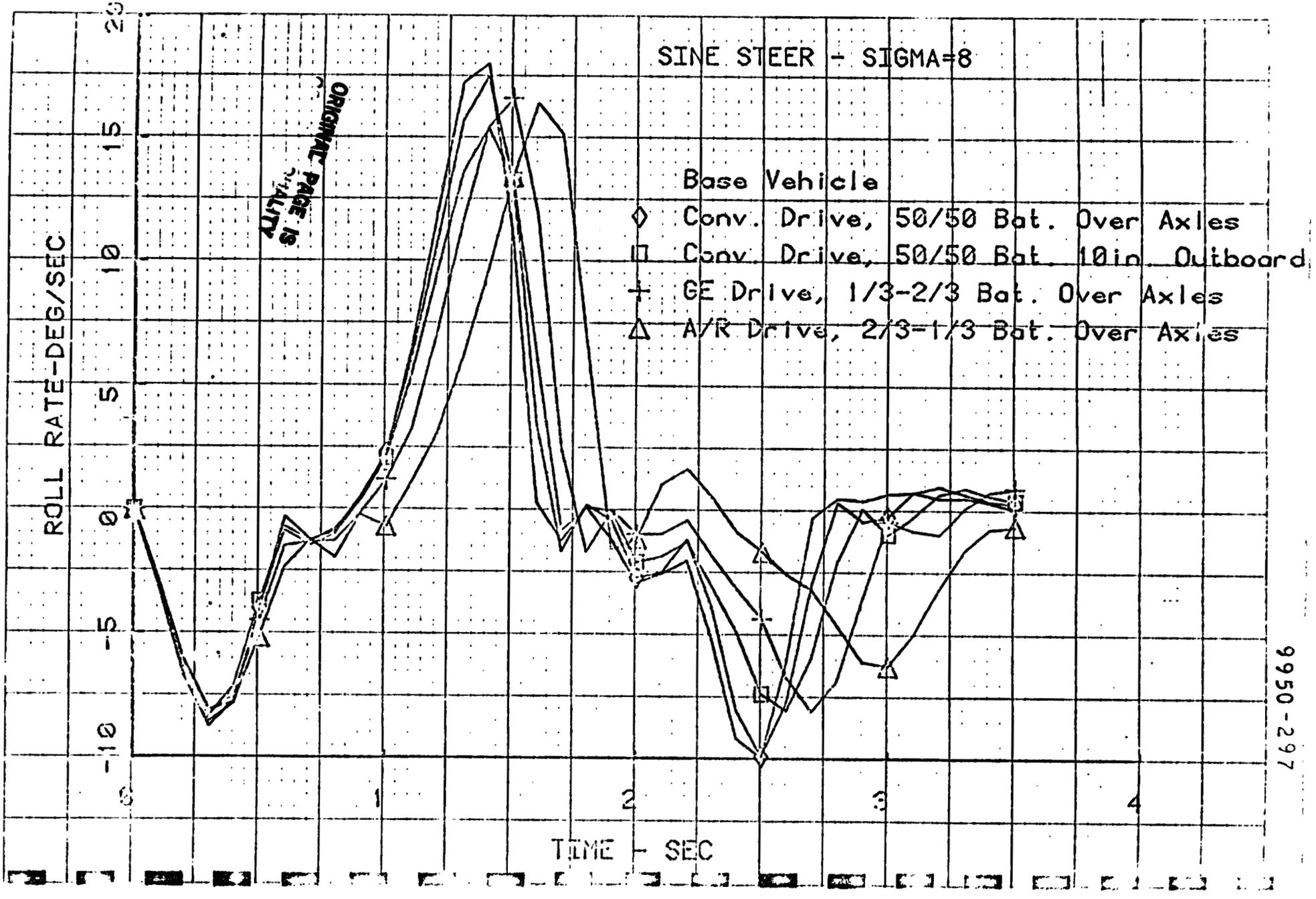
SINE STEER - SIGMA=8
Base Vehicle
◇ Conv. Drive, 50/50 Bat. Over Axles
□ Conv. Drive, 50/50 Bat. 10in. Outboard
+ GE Drive, 1/3-2/3 Bat. Over Axles
△ A/R Drive, 2/3-1/3 Bat. Over Axles
ROLL RATE-DEG/SEC
TIME - SEC
20
15
10
5
0
-5
-10
0
1
2
3
4
9950-297
ORIGINAL PAGE IS OF POOR QUALITY

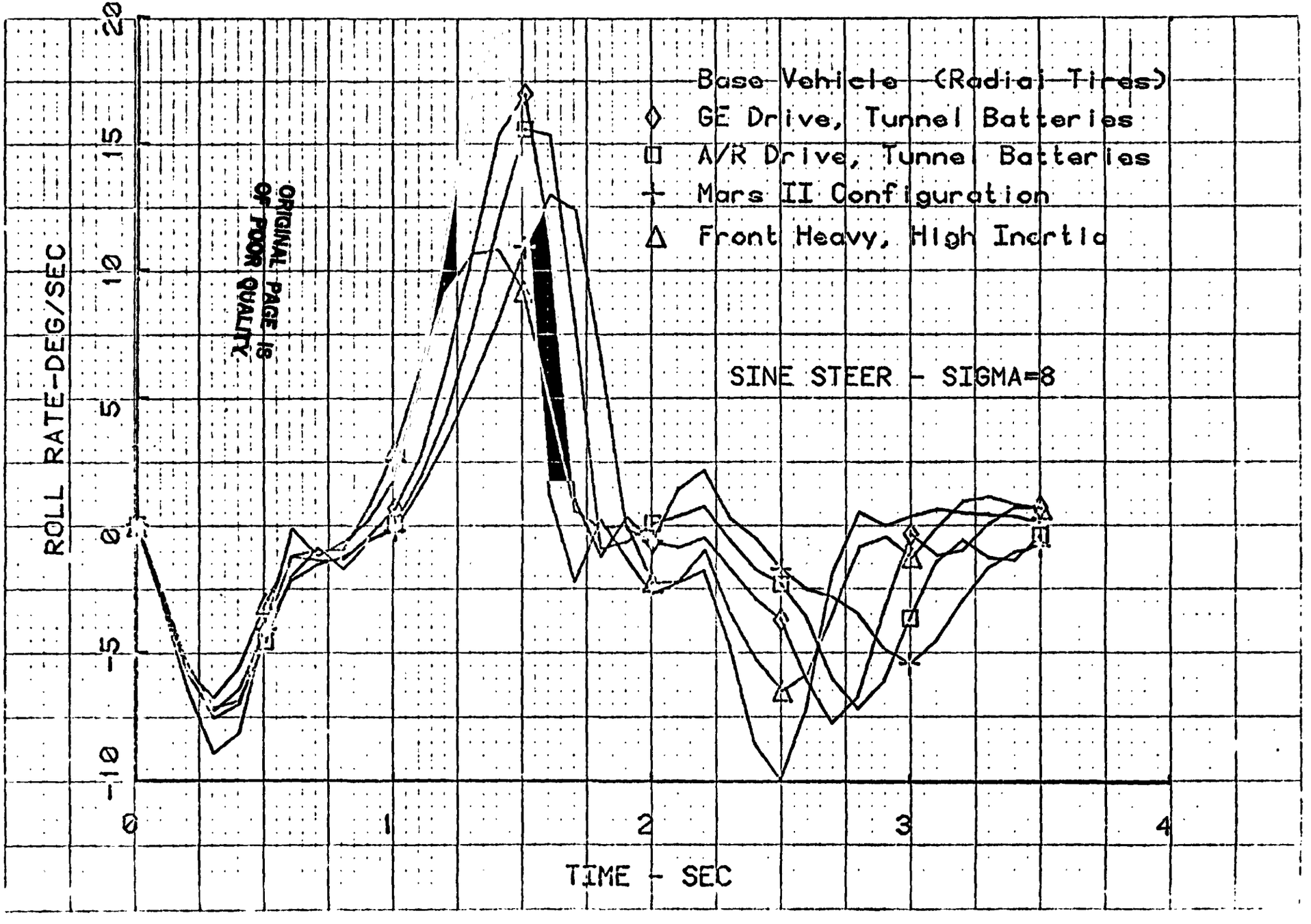

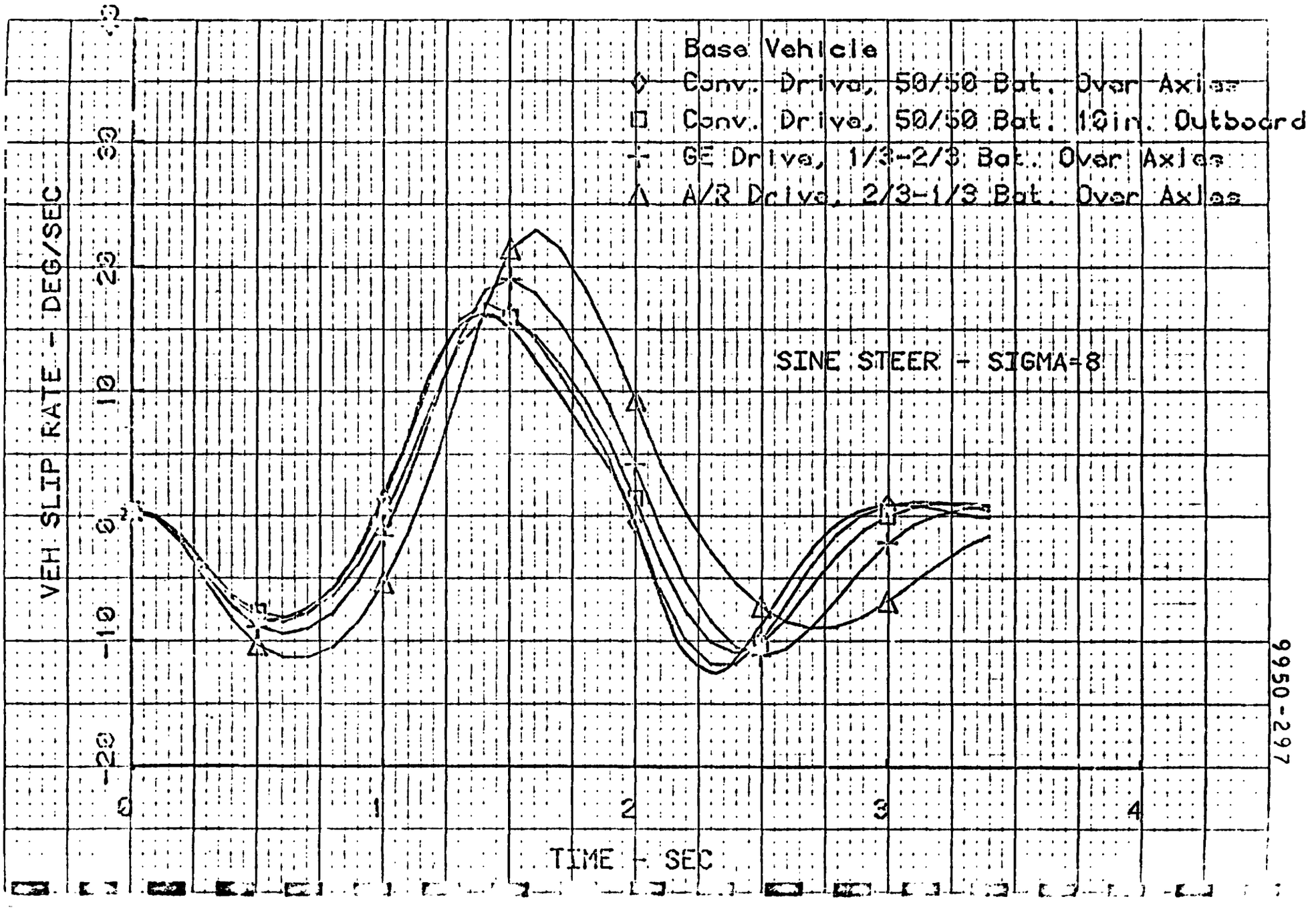
Base Vehicle
Conv. Drive, 50/50 Bat. Over Axles
Conv. Drive, 50/50 Bat. 10in. Outboard
GE Drive, 1/3-2/3 Bat. Over Axles
A/R Drive, 2/3-1/3 Bat. Over Axles
SINE STEER + SIGMA=8
VEH SLIP RATE - DEG/SEC
30
20
10
0
-10
-20
0
1
2
3
4
TIME - SEC
9950-297

Base Vehicle (Radial Tires)
◇ GE Drive, Tunnel Batteries
□ A/R Drive, Tunnel Batteries
+ Mars II Configuration
△ Front Heavy, High Inertia
SLIP RATE DEG/SEC
30
20
10
0
-10
-20
1
2
3
4
5
TIME - SEC

Base Vehicle
◇ Conv. Drive, 50/50 Bat. Over Axles
□ Conv. Drive, 50/50 Bat. 10in. Outboard
+ GE Drive, 1/3-2/3 Bat. Over Axles
Δ A/R Drive, 2/3-1/3 Bat. Over Axles
SINE STEER - SIGMA=8
LAT ACCEL-G's (X10**-1)
TIME - SEC
ORIGINAL PAGE IS OF POOR QUALITY

9950-297

Base Vehicle (Radial Tires)
◇ GE Drive, Tunnel Batteries
□ A/R Drive, Tunnel Batteries
+ Mars II Configuration
△ Front Heavy, High Inertia
SINE STEER - SIGMA=8
LAT ACCEL-G's (X10^-1)
TIME - SEC

APPENDIX F

SAMPLE RESULTS OF BRAKING-IN-A-TURN COMPUTER SIMULATIONS

9950-297

Base Vehicle
◇ Conv. Drive, 50/50 Bat. Over Axles
□ Conv. Drive, 50/50 Bat. 10in. Outboard
+ GE Drive, 1/3-2/3 Bat. Over Axles
△ A/R Drive, 2/3-1/3 Bat. Over Axles
BIT - 75% LOCK
YAW ANGLE - DEG
TIME - SEC
0
50
100
150
200
250
300
1
2
3
4

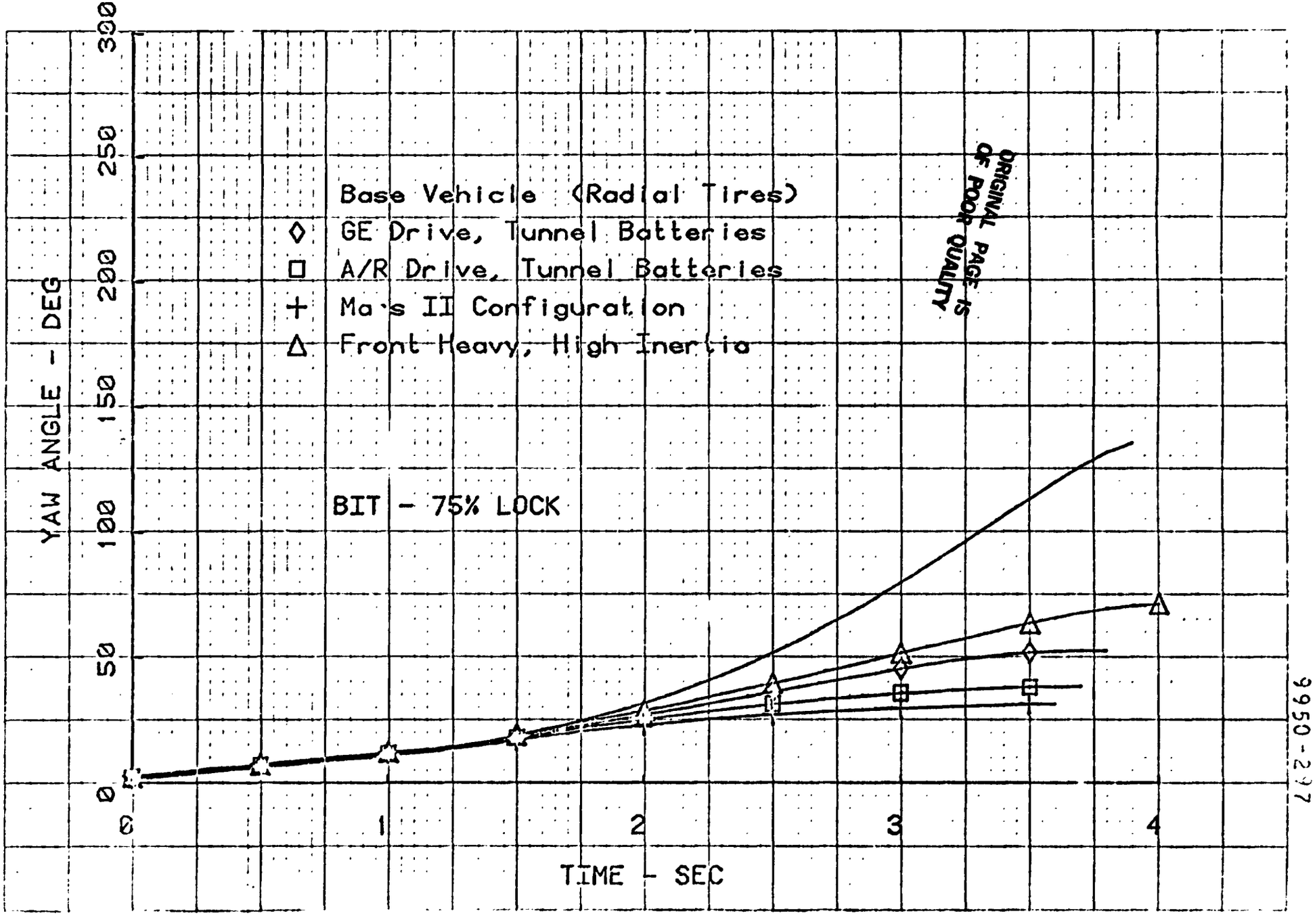
YAW ANGLE - DEG
0
50
100
150
200
250
300
0
1
2
3
4
TIME - SEC
Base Vehicle (Radial Tires)
◊ GE Drive, Tunnel Batteries
□ A/R Drive, Tunnel Batteries
+ Mass II Configuration
Δ Front Heavy, High Inertia
BIT - 75% LOCK
ORIGINAL PAGE IS OF POOR QUALITY
9950-277

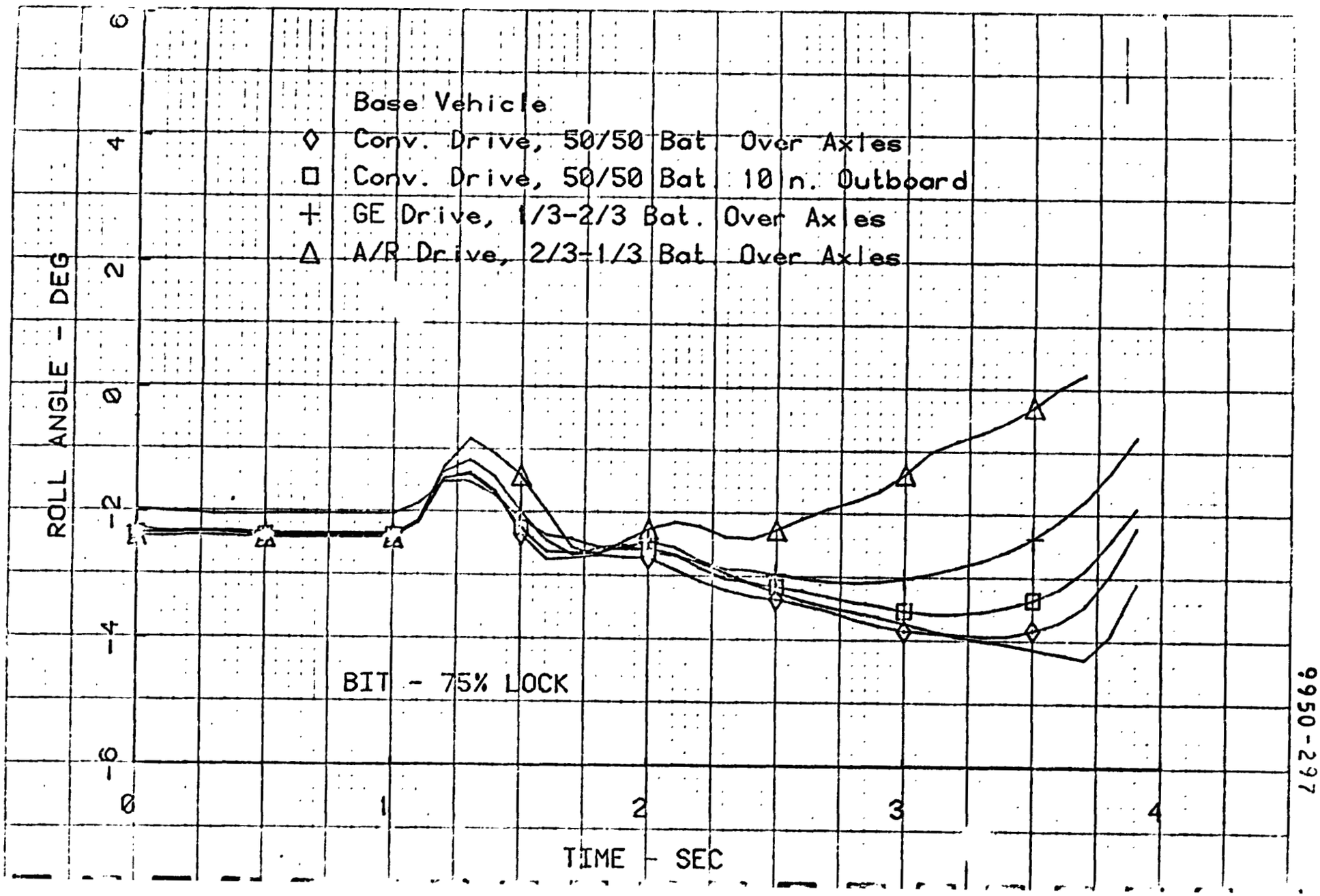
Base Vehicle
Conv. Drive, 50/50 Bat. Over Axles
Conv. Drive, 50/50 Bat. 10 n. Outboard
GE Drive, 1/3-2/3 Bat. Over Axles
A/R Drive, 2/3-1/3 Bat. Over Axles
BIT - 75% LOCK
ROLL ANGLE - DEG
TIME - SEC
6
4
2
0
-2
-4
-6
0
1
2
3
4
9950-297

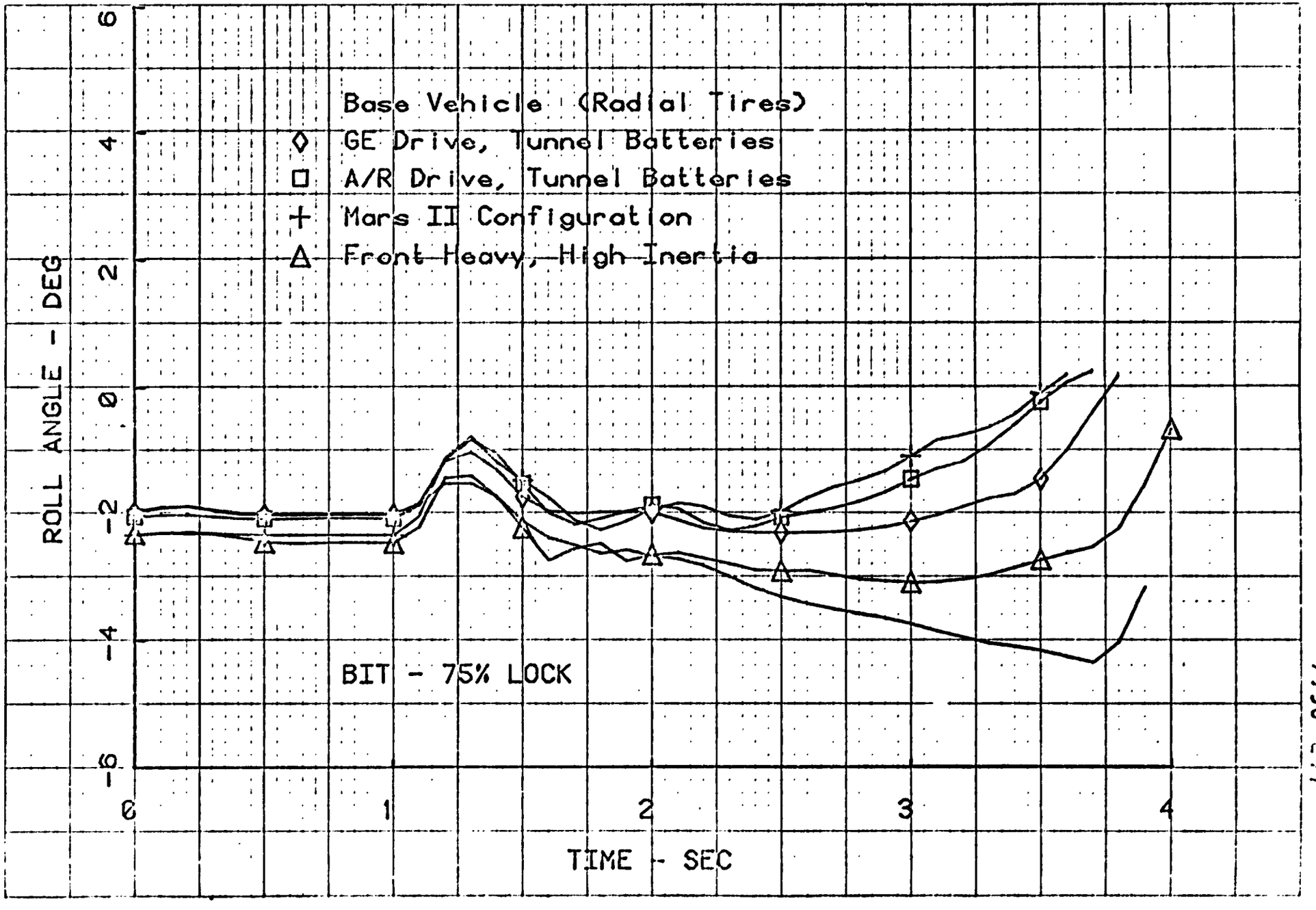
Base Vehicle (Radial Tires)
GE Drive, Tunnel Batteries
A/R Drive, Tunnel Batteries
Mars II Configuration
Front Heavy, High Inertia
BIT - 75% LOCK
ROLL ANGLE - DEG
TIME - SEC
6
4
2
0
-2
-4
-6
0
1
2
3
4

9950-297

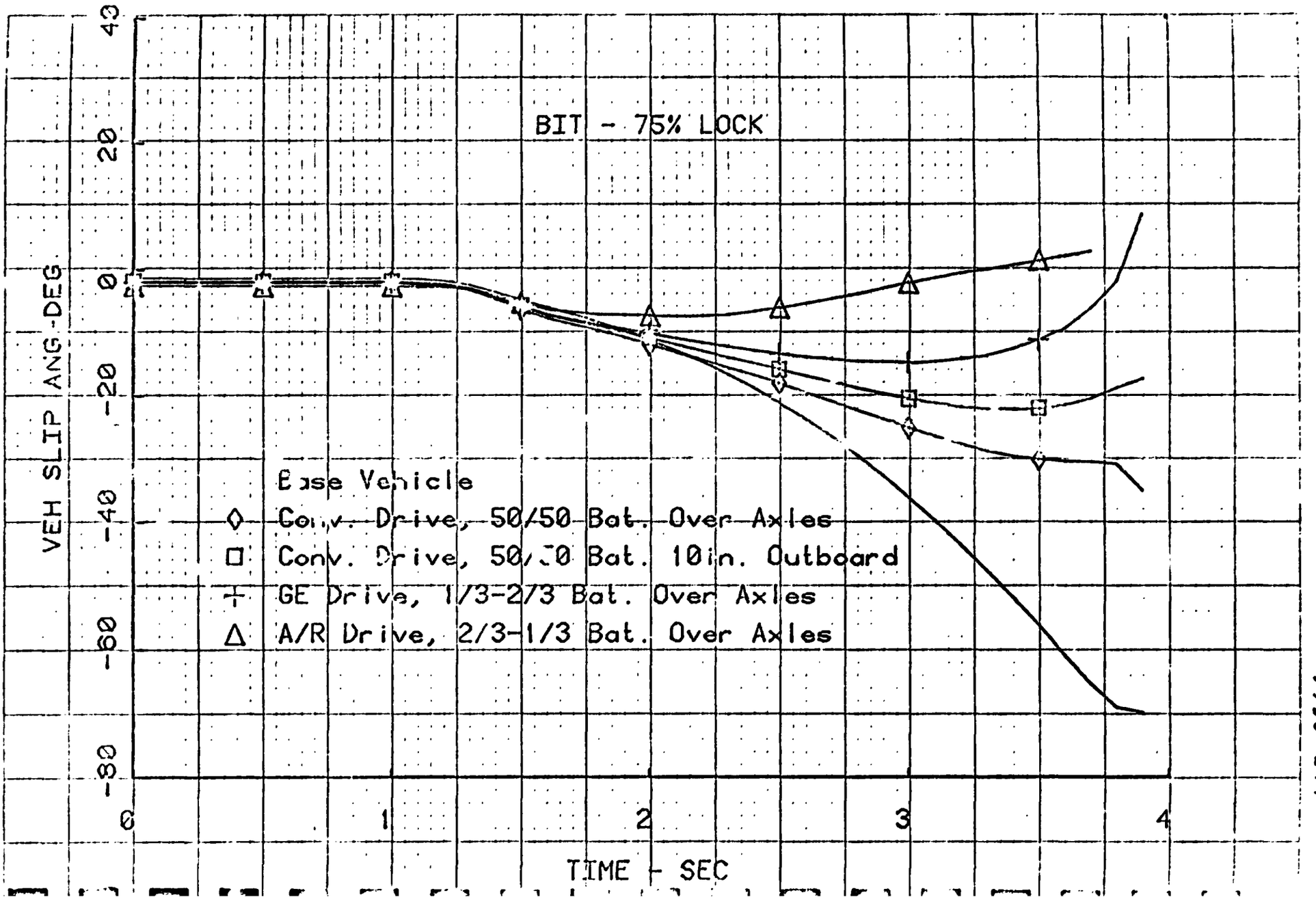
BIT - 75% LOCK
VEH SLIP ANG-DEG
40
20
0
-20
-40
-60
-80
0
1
2
3
4
TIME - SEC
Base Vehicle
Conv. Drive, 50/50 Bat. Over Axles
Conv. Drive, 50/50 Bat. 10in. Outboard
GE Drive, 1/3-2/3 Bat. Over Axles
A/R Drive, 2/3-1/3 Bat. Over Axles

9950-277

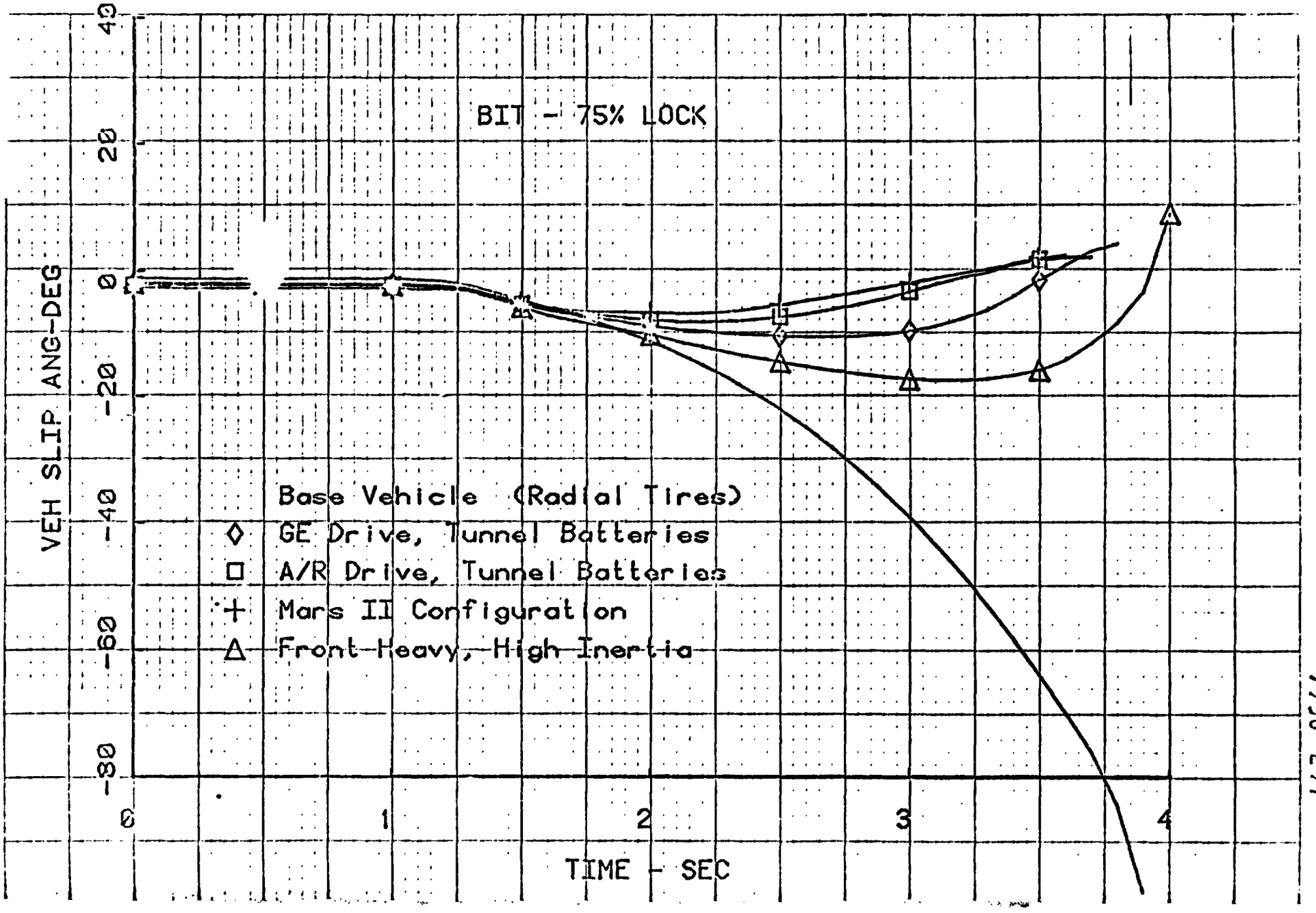
BIT - 75% LOCK
VEH SLIP ANG-DEG
40
20
0
-20
-40
-60
-80
0
1
2
3
4
TIME - SEC
Base Vehicle (Radial Tires)
GE Drive, Tunnel Batteries
A/R Drive, Tunnel Batteries
Mars II Configuration
Front Heavy, High Inertia
9950-297

9950-297

ORIGINAL PAGE IS
OF POOR QUALITY
Base Vehicle
◇ Conv. Drive, 50/50 Bat. Over Axles
□ Conv. Drive, 50/50 Bat. 10in. Outboard
+ GE Drive, 1/3-2/3 Bat. Over Axles
△ A/R Drive, 2/3-1/3 Bat. Over Axles
BIT - 75% LOCK
YAW RATE-DEG/SEC
TIME - SEC
0
20
40
60
80
100
120
1
2
3
4

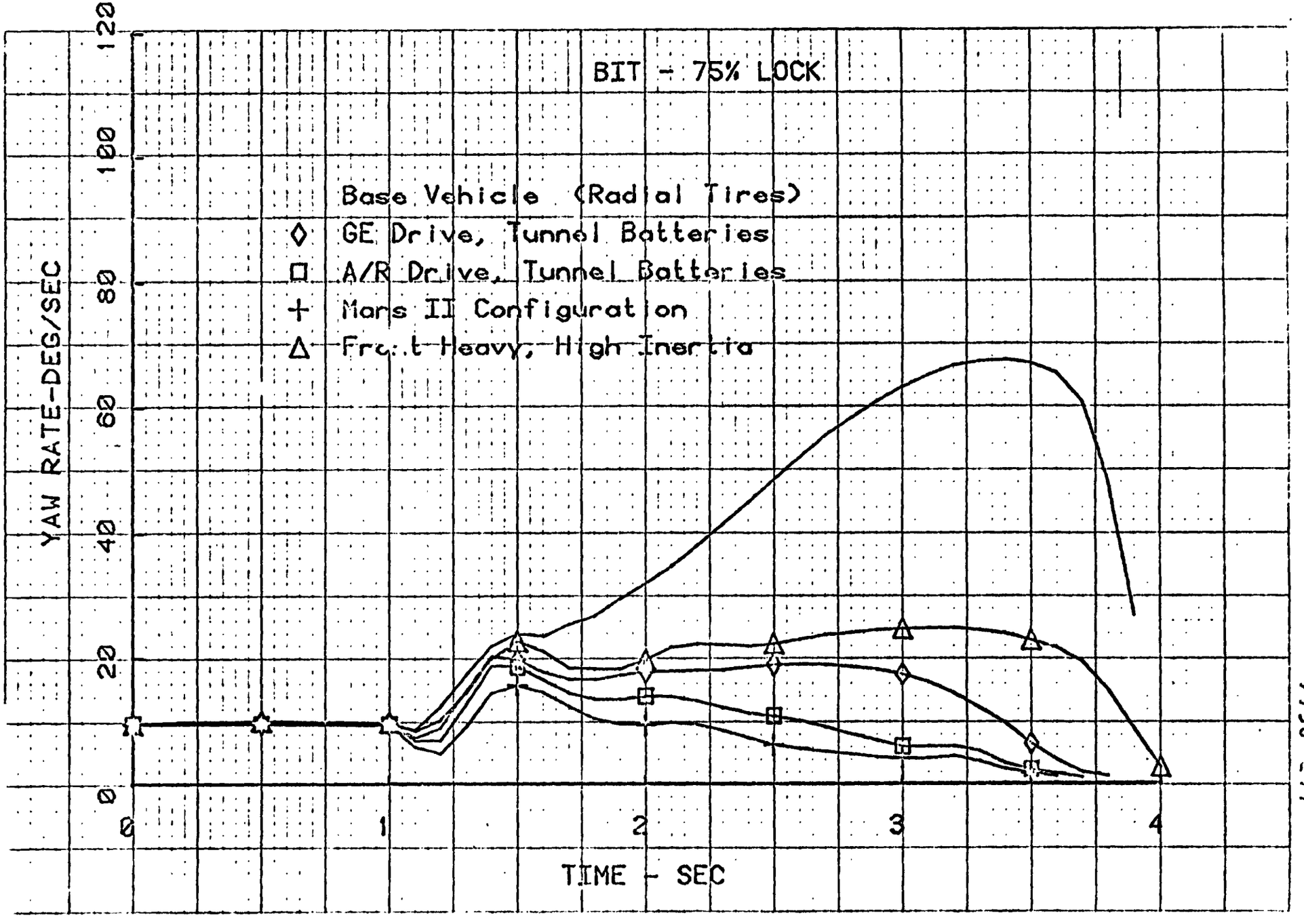
BIT - 75% LOCK
Base Vehicle (Radial Tires)
◇ GE Drive, Tunnel Batteries
□ A/R Drive, Tunnel Batteries
+ Mars II Configuration
△ Front Heavy, High Inertia
YAW RATE-DEG/SEC
0
20
40
60
80
100
120
0
1
2
3
4
TIME - SEC

9950-297

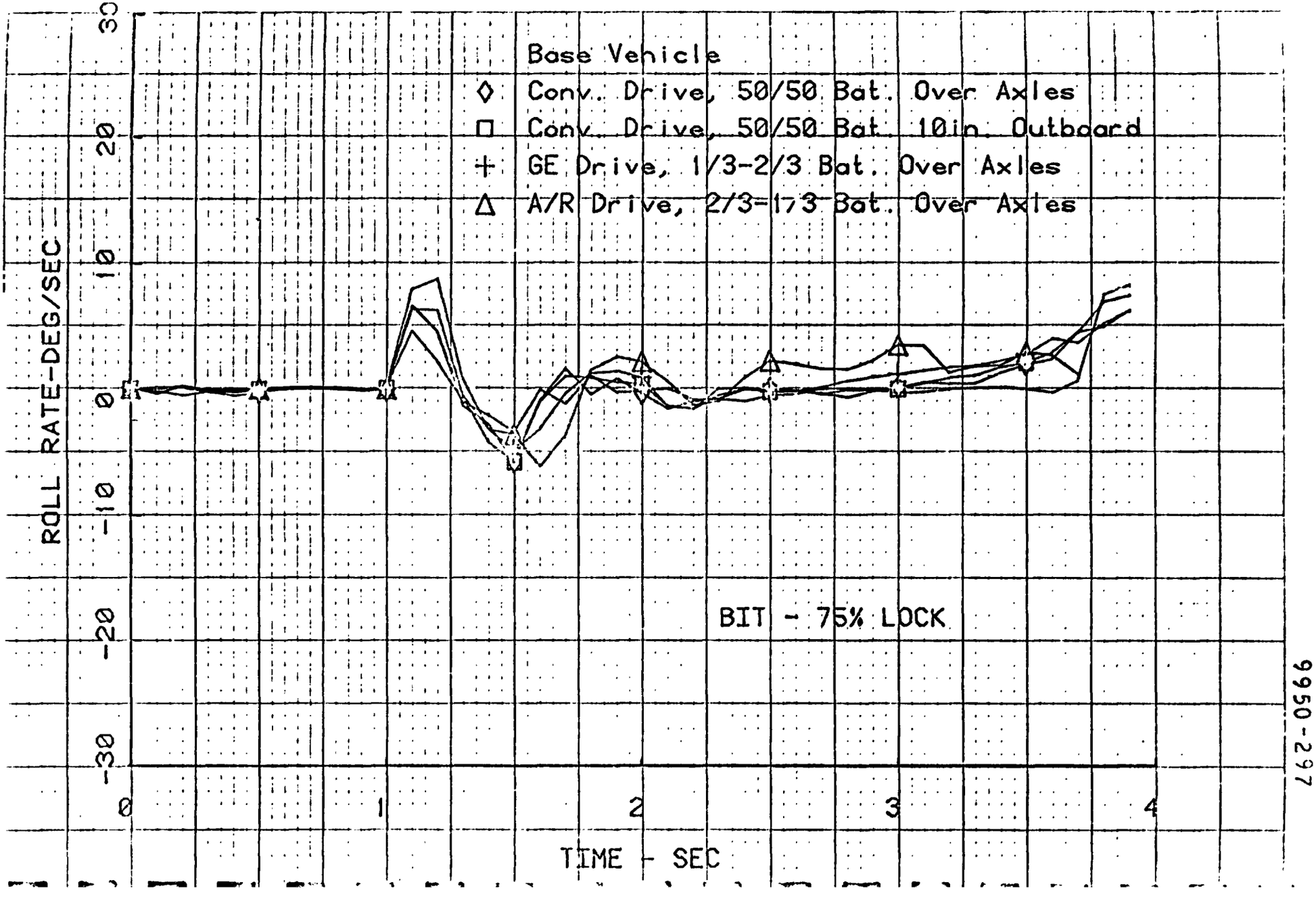
Base Vehicle
◇ Conv. Drive, 50/50 Bat. Over Axles
□ Conv. Drive, 50/50 Bat. 10in. Outboard
+ GE Drive, 1/3-2/3 Bat. Over Axles
△ A/R Drive, 2/3-1/3 Bat. Over Axles
BIT - 75% LOCK
ROLL RATE-DEG/SEC
30
20
10
0
-10
-20
-30
0
1
2
3
4
TIME - SEC
9950-297

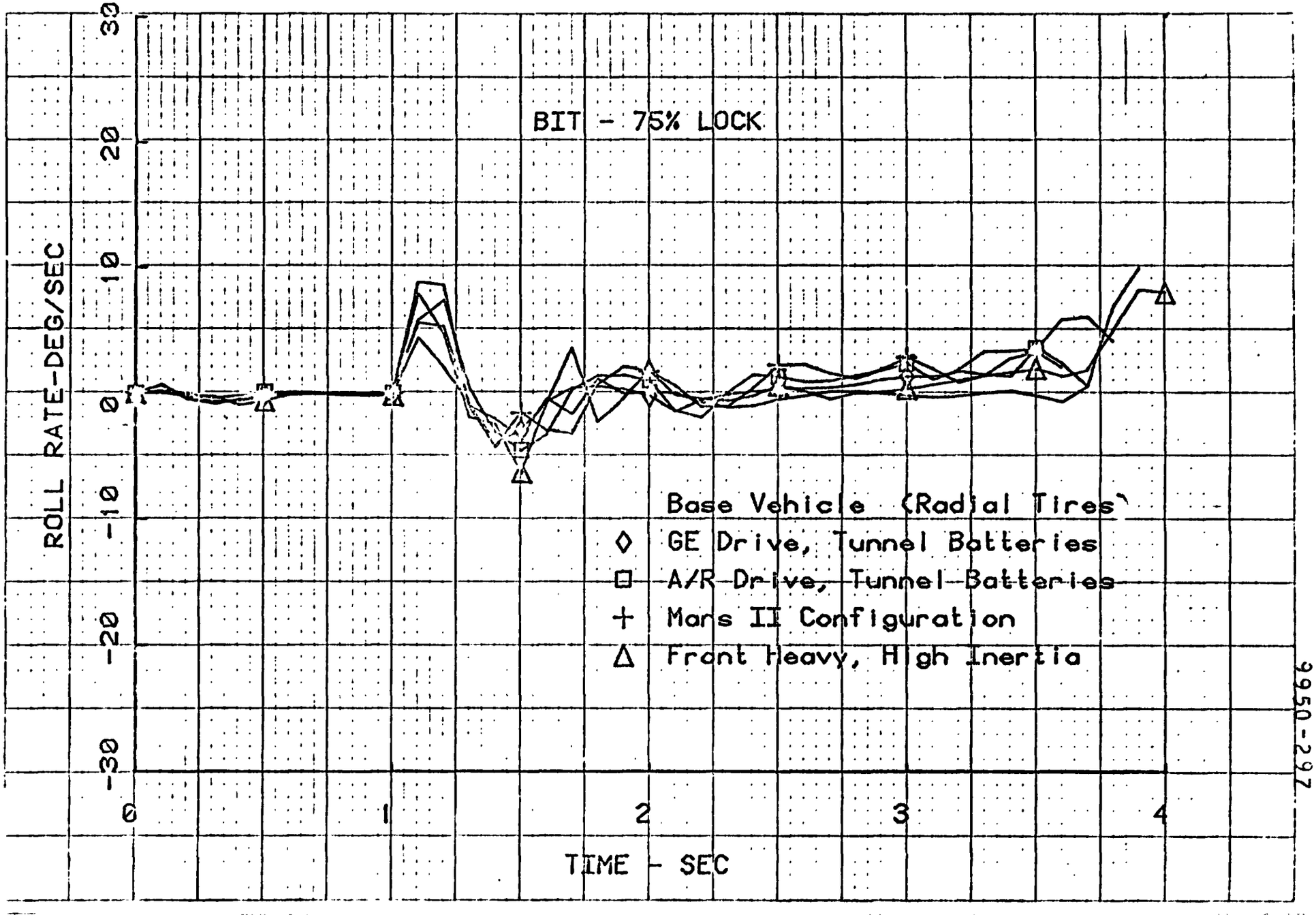
BIT - 75% LOCK
ROLL RATE-DEG/SEC
30
20
10
0
-10
-20
-30
0
1
2
3
4
TIME - SEC
Base Vehicle (Radial Tires)
◊ GE Drive, Tunnel Batteries
□ A/R Drive, Tunnel Batteries
+ Mars II Configuration
Δ Front Heavy, High Inertia
9950-297

Base Vehicle
◇ Conv. Drive, 50/50 Bat. Over Axles
□ Conv. Drive, 50/50 Bat. 10in. Outboard
+ GE Drive, 1/3-2/3 Bat. Over Axles
△ A/R Drive, 2/3-1/3 Bat. Over Axles
BIT - 75% LOCK
VEH SLIP RATE DEG/SEC
150
100
50
0
-50
-100
-150
0
1
2
3
4
TIME - SEC

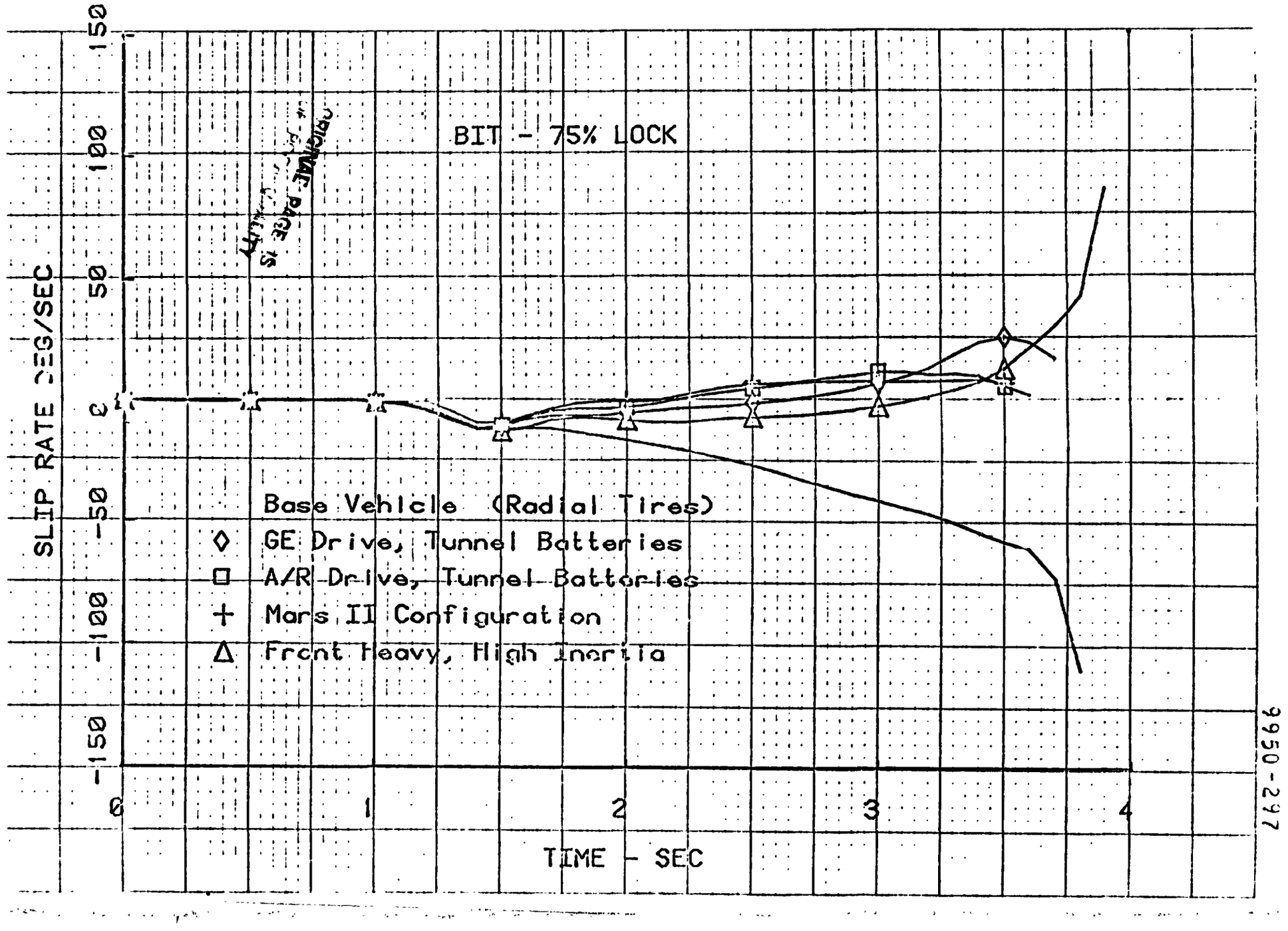
BIT - 75% LOCK
SLIP RATE DEG/SEC
150
100
50
0
-50
-100
-150
0
1
2
3
4
TIME - SEC
Base Vehicle (Radial Tires)
◇ GE Drive, Tunnel Batteries
□ A/R Drive, Tunnel Batteries
+ Mars II Configuration
△ Front Heavy, High Inertia
9950-297

9950-277

Base Vehicle
Conv. Drive, 50/50 Bat. Over Axles
Conv. Drive, 50/50 Bat. 10in. Outboard
GE Drive, 1/3-2/3 Bat. Over Axles
A/R Drive, 2/3-1/3 Bat. Over Axles
BIT - 75% LOCK
LONG ACCEL-G'S
TIME - SEC
1.5
1
0.5
0
-0.5
-1
-1.5
0
1
2
3
4
ORIGINAL PAGE IS OF POOR QUALITY

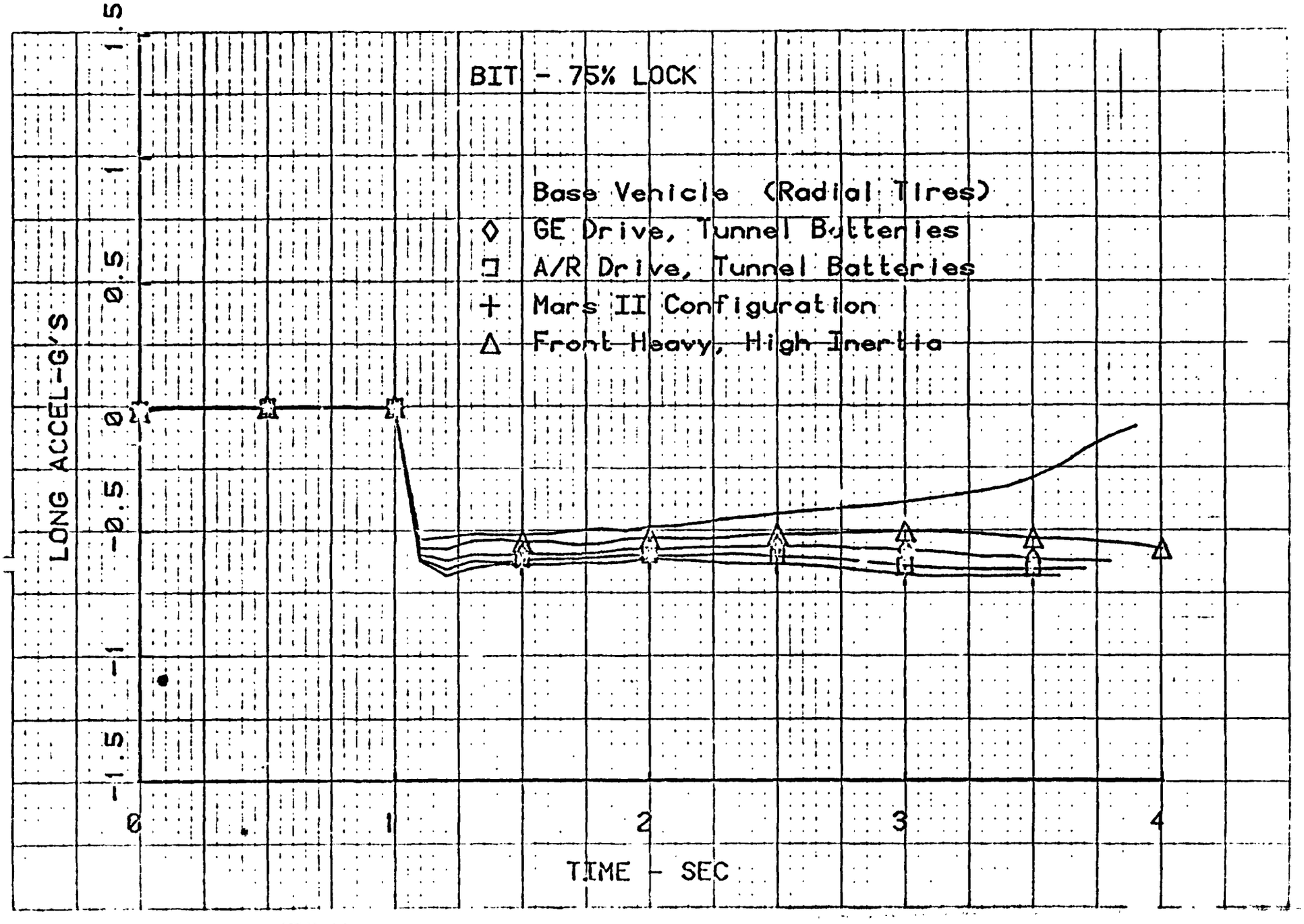
BIT - 75% LOCK
Base Vehicle (Radial Tires)
◊ GE Drive, Tunnel Batteries
□ A/R Drive, Tunnel Batteries
+ Mars II Configuration
△ Front Heavy, High Inertia
LONG ACCEL-G'S
1.5
1
0.5
0
-0.5
-1
-1.5
0
1
2
3
4
TIME - SEC

9950-277

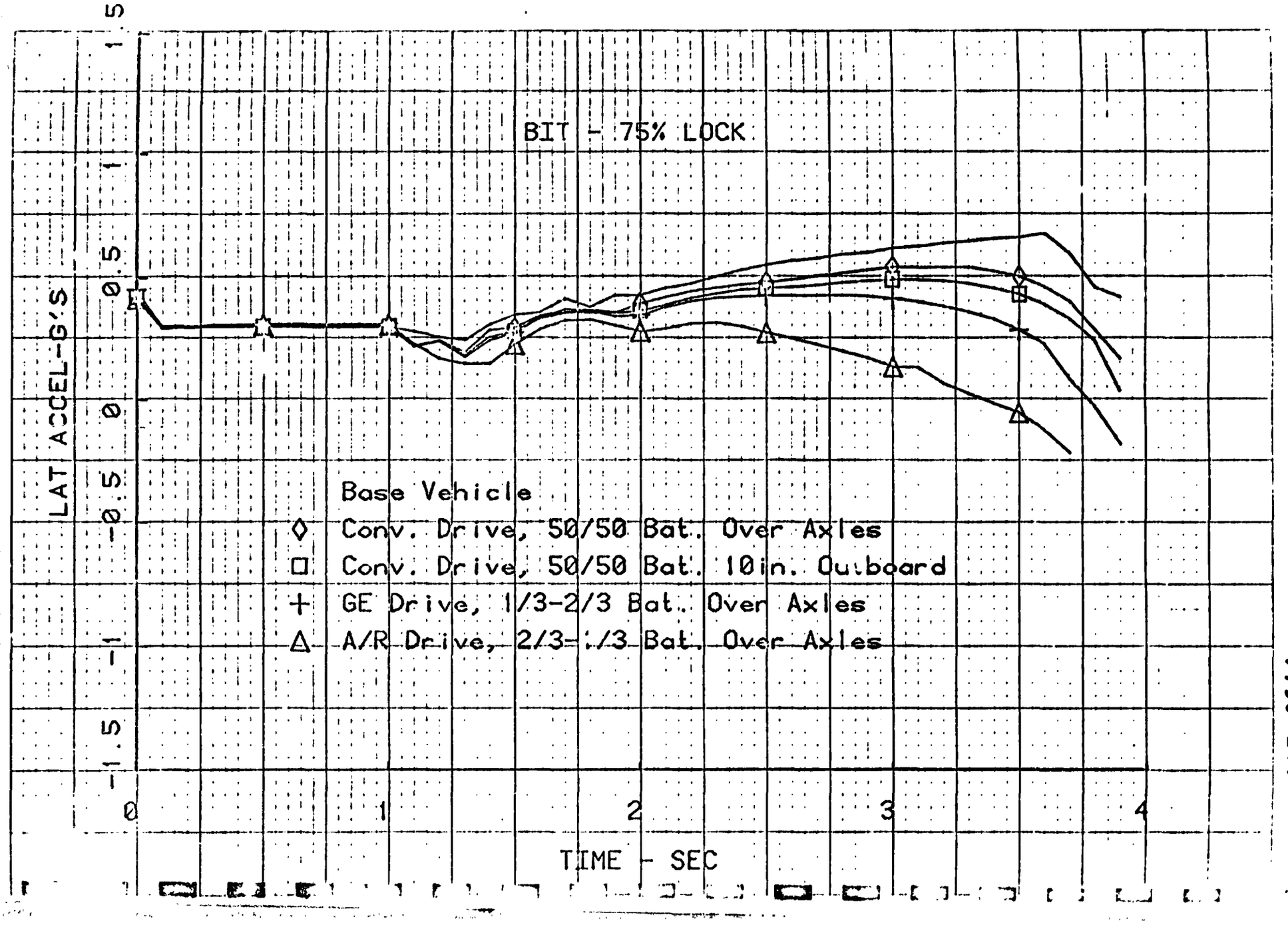
BIT - 75% LOCK
LAT ACCEL-G'S
1.5
1
0.5
0
-0.5
-1
-1.5
0
1
2
3
4
TIME - SEC
Base Vehicle
◊ Conv. Drive, 50/50 Bat. Over Axles
□ Conv. Drive, 50/50 Bat. 10in. Outboard
+ GE Drive, 1/3-2/3 Bat. Over Axles
△ A/R Drive, 2/3-1/3 Bat. Over Axles

9950-297

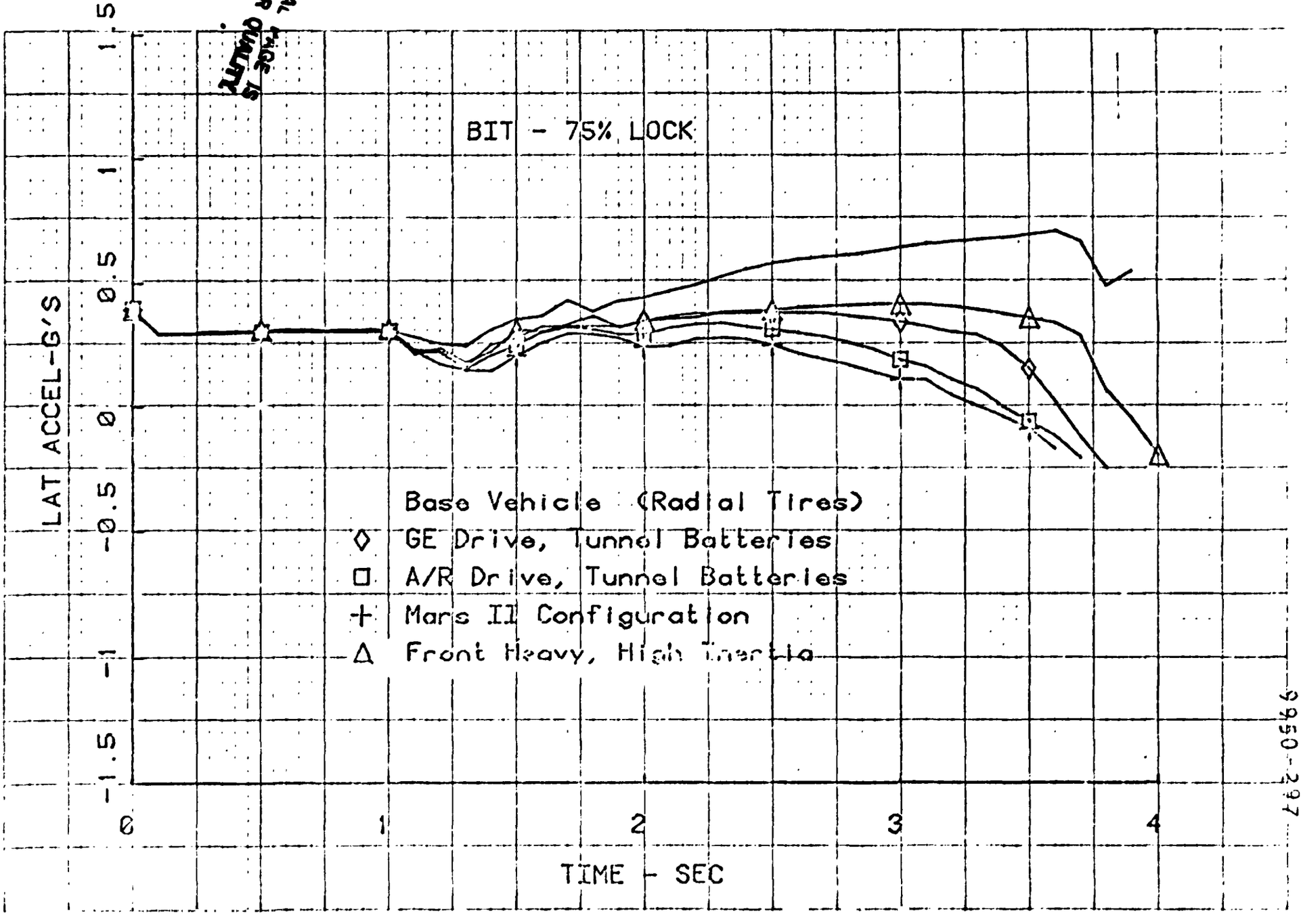
BIT - 75% LOCK
LAT ACCEL-G'S
1.5
1
0.5
0
-0.5
-1
-1.5
0
1
2
3
4
TIME - SEC
Base Vehicle (Radial Tires)
◇ GE Drive, Tunnel Batteries
□ A/R Drive, Tunnel Batteries
+ Mars II Configuration
△ Front Heavy, High Inertia
9950-297